UNIVERSITY OF BIRMINGHAM

birmingham archaeology

Analysis of the Effectiveness of Airborne Lidar Intensity for Predicting Organic Preservation Potential of Waterlogged Deposits

Stage 1 Report

Project Manager
Keith Challis, HP Vista Centre, Birmingham Archaeology,
University of Birmingham, Edgbaston, Birmingham, B15 2TT
(0121 414 5563, k.challis@bham.ac.uk)

Report Prepared by

Keith Challis, HP Vista Centre, Birmingham Archaeology,
Dr Andy J Howard, Institute of Archaeology and Antiquity,
Mark Kincey, HP Vista Centre, Birmingham Archaeology
Dr Chris Carey, HP Vista Centre, Birmingham Archaeology
Derek Moscrop, HP Vista Centre, Birmingham Archaeology
Dr Tom Hill, Birmingham ArchaeoEnvironmental, University of Birmingham

Revision 1: March 2008

PNUM 4782

Analysis of the Effectiveness of Airborne Lidar Intensity for Predicting Organic Preservation Potential of Waterlogged Deposits

Stage 1 Report

Project Manager
Keith Challis, HP Vista Centre, Birmingham Archaeology,
University of Birmingham, Edgbaston, Birmingham, B15 2TT
(0121 414 5563, k.challis@bham.ac.uk)

Report Prepared by

Keith Challis, HP Vista Centre, Birmingham Archaeology,
Dr Andy J Howard, Institute of Archaeology and Antiquity,
Mark Kincey, HP Vista Centre, Birmingham Archaeology
Dr Chris Carey, HP Vista Centre, Birmingham Archaeology
Derek Moscrop, HP Vista Centre, Birmingham Archaeology
Dr Tom Hill, Birmingham ArchaeoEnvironmental, University of Birmingham

Revision 1: March 2008

PNUM 4782

LIST OF CONTENTS

LIST OF FIGURES

LIST OF TABLES

1 INTRODUCTION

1 INTRODUCTION

1.1 PREAMBLE

This document is a report on the first stage of work for the English Heritage ALSF funded project Analysis of the Effectiveness of Airborne Lidar Backscattered Laser Intensity for Predicting Organic Preservation Potential of Waterlogged Deposits (PN4782). The report comprises a brief review of the project aims and objectives (section 1: précised from the original PD), a discussion of the laboratory analysis of the relationship between NIR spectral reflectance and sediment properties (Section 2), discussion of the use of ground based laser scanning as an analogue for airborne lidar (section 3) a discussion of the analysis of airborne lidar intensity (section 4) and some general discussion and conclusions (section 5). A list of references cited is provided in section 6

1.2 PROJECT RATIONALE

Airborne remote sensing techniques have traditionally been employed to great effect in mapping cultural archaeology and to a lesser extent the geomorphology of valley floor landscapes. Archaeologists have largely focused their attention on the comprehensive mapping of cropmarks and other features of the archaeological landscape revealed from aerial photographs (eg. Riley 1980; Whimster 1989), and large areas of England have been comprehensively mapped as part of the National Mapping Programme undertaken by English Heritage (Bewley 2003). Aerial photographs have also been employed in mapping geomorphology in alluvial landscapes, for example in extensive studies of the valleys of the Rivers Trent (Baker 2003; Garton and Malone 1998) and Thames (Lambrick 1992; Robinson and Lambrick 1994).

Such mapping of fluvial geomorphology provides a context for past cultural landscapes and assists in identifying topographical features of high archaeological potential (for example relict river channels) and isolating areas of past river erosion where little in the way of archaeological material might be expected to survive (*cf* Brown 1997). The systematic reconnaissance, mapping and classification of aggregate bearing valley floor landscapes in this way has played a significant role in the strategic management of the geoarchaeological resource and intimately associated archaeological remains (e.g. fishweirs, bridges, platforms, trackways, etc.) in the face of growing impacts from aggregate extraction and other development pressures (Bishop 2003). More recently, such information relating to former fluvial regimes is also being increasingly used in understanding wider issues of floodplain management, particularly with respect to assessing the impacts of changing flood frequency and magnitude with respect to future climate (Thompson and Clayton, 2002).

While the two dimensional record of air-photography provides an approach to mapping the quantity of archaeological material (both cultural and geoarchaeological) within aggregate bearing landscapes, it provides no indication of the state of preservation of that material or the associated cultural evidence. In particular, aerial photography provides no indication of the moisture level and the potential for the

preservation of organic sediments. This is a significant shortfall in the usefulness of the data, since the presence of moist, organic-rich sediments may greatly increase the archaeological value of deposits.

The generic potential of this research are:

- It will create a tool to allow the rapid assessment of valley floor corridors to provide baseline information on the environmental potential of organic sediments, usually preserved within palaeochannels. Such information may prevent the need for costly environmental investigations of potential extraction areas prior to the submission of planning proposals.

- It may provide information on the hydrological condition of valley floor sediments prior to aggregate extraction, an important issue in the consideration of the effects of artificial pumping and draw-down on the water table.

In addition to the benefits this work may provide for the aggregates industry in their consideration of the archaeological record, this study may also produce important data that can be used in wider environmental management themes, for example, consideration of catchment management with respect to changing flood frequency and magnitude associated with future climate change, the Water Frameworks Directive.

Airborne Laser Altimetry provides access to high resolution, high accuracy terrain information and as a secondary output a laser "image" of the land surface derived from measurements of the intensity of reflection of each backscattered laser pulse. A detailed description of Lidar is provided in Wehr and Lohr (1999). Archaeological applications of Lidar have focused largely on its ability to provide a high resolution record of terrain variation, allowing the detection and mapping of subtle archaeological features (Bewley *et al*, 2005), mapping of fluvial geomorphology (Challis 2005b and in press) and its unique ability to penetrate vegetation cover to map underlying archaeological earthworks (Devereux, *et al*, 2005).

Backscattered laser intensity measurements have largely escaped attention, and indeed do not form a part of the standard data product supplied by EA (although intensity data is collected on each EA flight and can be accessed by reprocessing original flight data). The lidar system used by EA, NERC and many UK-based commercial lidar providers (an Optech Airborne Laser Terrain Mapper) operates in the near infra-red (NIR: 1047nm) and so backscattered intensity is in-effect a record of the reflectance of earth surface materials at this wavelength.

While it is recognised that other airborne remote sensing techniques (ATM, CASI, etc. *cf* Figure 1) may be equally or more effective than lidar at detecting geoarchaeological and anthropogenic features, this study focuses on lidar for a number of reasons. Principally lidar has been chosen as the basis of this study because it is an emerging technology, still poorly understood within the archaeological community. There is a growing demand for and supply of commercial lidar providers. National agencies such as EA already operate lidar, while Ordnance Survey are actively investigating a move into ownership of a lidar system for data acquisition to assist national mapping. Some good work has been done in understanding the parameters of lidar terrain mapping required for archaeological

purposes (Challis 2005, Crutchley, pers comm) and so archaeologists are equipped to specify such work when commissioning survey. However, little or no work has been undertaken to investigate intensity, which until now has been largely ignored both by archaeologists and by the lidar industry as a whole.

1.3 REVIEW OF ORIGINAL PROJECT AIMS AND OBJECTIVES

This project emerged from the applicants own work with lidar (EH PNUM 3357, 3850, 3307) and through helpful discussion with colleagues at English Heritage (principally, Dr David Earle Robinson, Peter Horne, Simon Crutchley and Dr Jim Williams). The project seeks to address the ALSF objective two criteria:

- research to enhance understanding of the scale and character of the historic environment in aggregate producing areas in order to provide the baseline information necessary for effective future catchment management.
- support for the development of management and conservation strategies for the historic environment in aggregate producing areas.

It also seeks to address two of the additional ALSF criteria outlined by English Heritage in the *Science Coordinator's Review of Land-Based ALSF Research in England, 2002 – 2005* (Thompson 2005, 31) namely:

- Increased use of 'lidar imagery to enhance/upgrade Historic Environment Records'.
- Continued development of prediction, evaluation, and mitigation techniques (continual improvement of methods and techniques is of paramount importance).

1.4 STUDY AREAS

The underlying control on the evolution of river valley floors and floodplain development is the contrasting geomorphological settings of the upland, piedmont and lowland landscape zones (see Howard and Macklin, 1999). In order to assess the effectiveness of this methodology, it is essential that river systems from these contrasting geomorphological contexts are assessed. The study areas selected for the research were chosen since they represent contrasting styles of floodplain evolution.

1.4.1 Study Area 1, The Trent Valley around the Trent – Soar confluence

Upland and piedmont river systems have been characterised by high rates of lateral channel mobility throughout the Holocene, leaving a series of abandoned palaeochannels across the valley floor. The Middle Trent between Tamworth and Newark is characteristic of a high-energy upland / piedmont system.

The Trent Valley has been the focus of intensive geoarchaeological study as part of a number of components of the ALSF *Trent Valley Geoarchaeology* 2002 (PNUM 3307). In addition, the evolution of its major tributaries, the Dove and the Idle are currently the focus of a further ALSF study (*The Trent Tributaries Project*, PNUM 3850). In the middle Trent Valley, further collaborative research by the Universities

of Birmingham and Exeter, funded by the ALSF (PNUM 3357) has resulted in a detailed archaeological investigation of the landscape and underlying deposits around the confluence of the River's Trent and Soar. Stage 1 of this project involved the collation and dovetailing of datasets collected using a combination of aerial (lidar, IFSAR) and ground-based remote sensing techniques (ground penetrating radar); this information allowed the construction of a preliminary model of confluence evolution. Stage 2 of the project refined this model by dating key stratigraphic units, including palaeochannels, which in turn are being assessed for their environmental potential and consideration of taphonomic issues. Ground penetrating radar proved excellent in identifying structures within the terrace sediments, but poor in determining the internal structure of waterlogged, fine grained fills of palaeochannels; therefore, during Stage 2, further geoprospection techniques investigated palaeochannel stratigraphy using ERGI (Fig. 1).

1.4.2 Study Area 2, The Thames Valley around Port Meadow, Oxford

The River Thames around Port Meadow, a few kilometres north of the City Centre is a rich archaeological landscape. Although the archaeological remains identified at Port Meadow itself form part of a Scheduled Ancient Monument, the area to the north has been the focus of significant aggregate extraction, archaeological survey and excavation (notably, the Yarnton project undertaken by Oxford Archaeology and funded by English Heritage: (http://www.oxfordarch.co.uk/micro_ sites/yarnton/index.htm). The Thames around Port Meadow is also a lowland river, but in contrast to the Idle, it vertically accreted sediments are less organic than the peatlands of the River Idle. Historic map evidence suggests greater lateral channel migration, which may explain this contrast between these two lowland river systems (Fig. 2).

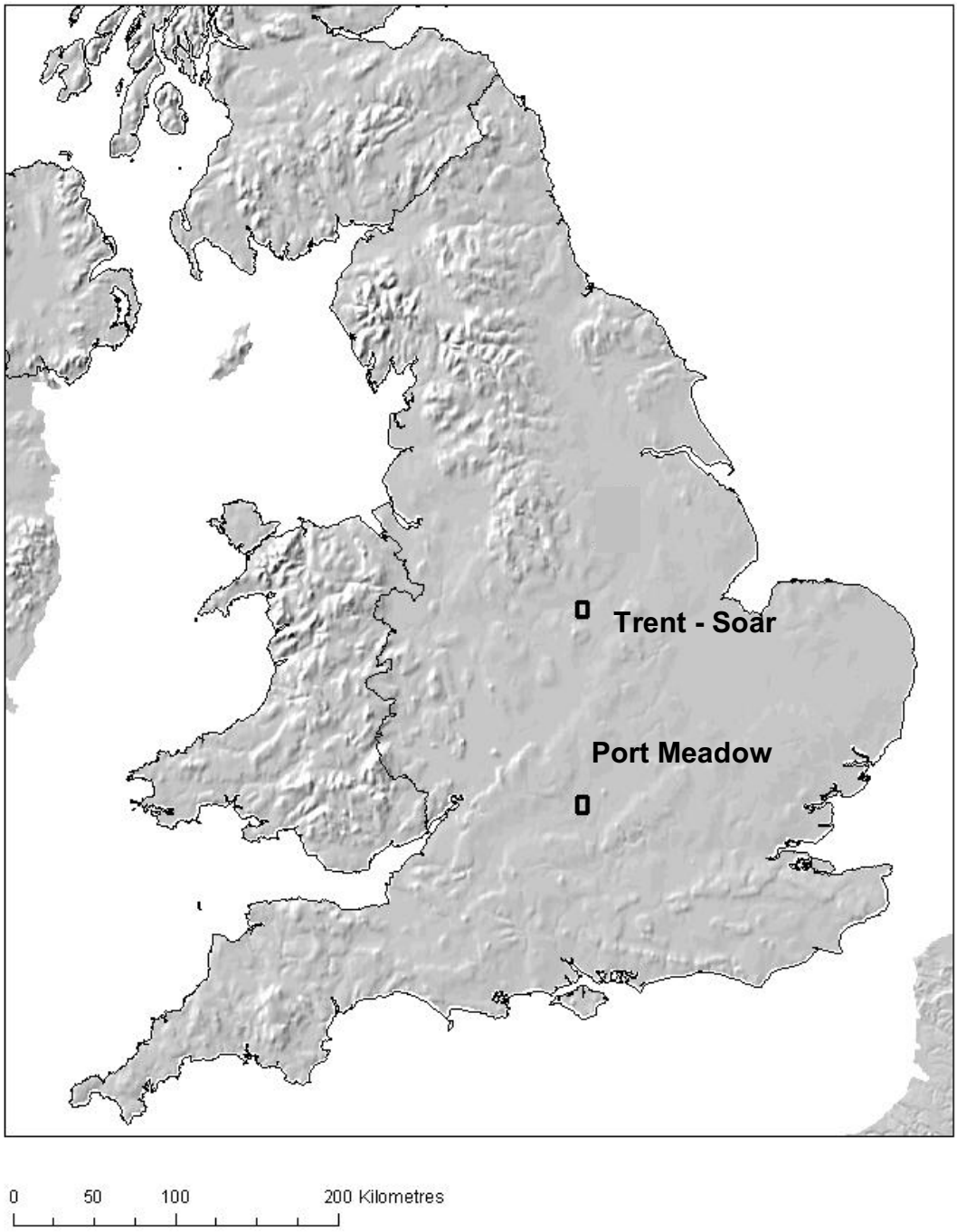

Fig 1: Location of the Trent/Soar and Port Meadow study areas.

2 LABORATORY ANALYSIS OF SEDIMENTS

2 LABORATORY ANALYSIS OF SEDIMENTS

2.1 INTRODUCTION

The relationship of lidar intensity to soil sediment architecture and soil organic content is investigated in this project through both air borne and ground based laser scanning. Both approaches aim to investigate the complex relationships in between NIR reflectance to sediment architecture.

The air borne and ground based prospection surveys were undertaken in real world conditions, where variance was introduced into the data due to the conditions of a survey location on a given day, e.g. vegetation, surface moisture, cloud, etc. Therefore, it was decided to create a laboratory data set, investigating a series of cores retrieved from palaeochannels in the confluence zone of the rivers Trent and Soar using NIR spectroscopy,. This allows the creation of clean data set, free from variance introduced by 'field conditions'. The laboratory analysis of cores also held several other advantages, namely, reflectance in multiple data bands could be recorded and related to spatially precise sampling of sediment for soil organic content and other parmeters. The laboratory data set in effect acts as an independent control for the ground based and air borne NIR data sets.

2.2 METHODS STATEMENT

2.2.1 Sample collection

A series of palaeochannels were sampled from the Trent Soar confluence study area (Fig. 3) for the analysis of the lidar intensity against other soil parameters. Palaeochannels were initially cored using a thin 2cm gouge, to assess the sediment stratigraphy. After assessment the section of palaeochannel was either abandoned or sample collection proceeded using an 8cm diameter gouge core. Retrieved samples were wrapped in cling film and placed in plastic guttering lengths of 1m each. Sample labels and depths were recorded on each gutter before wrapping in silver foil. In the laboratory the samples were cleaned back and visually examined. Their colour was described using a Munsel Chart and their stratigraphy recorded using a modified Troel-Smith key (Fig. 4).

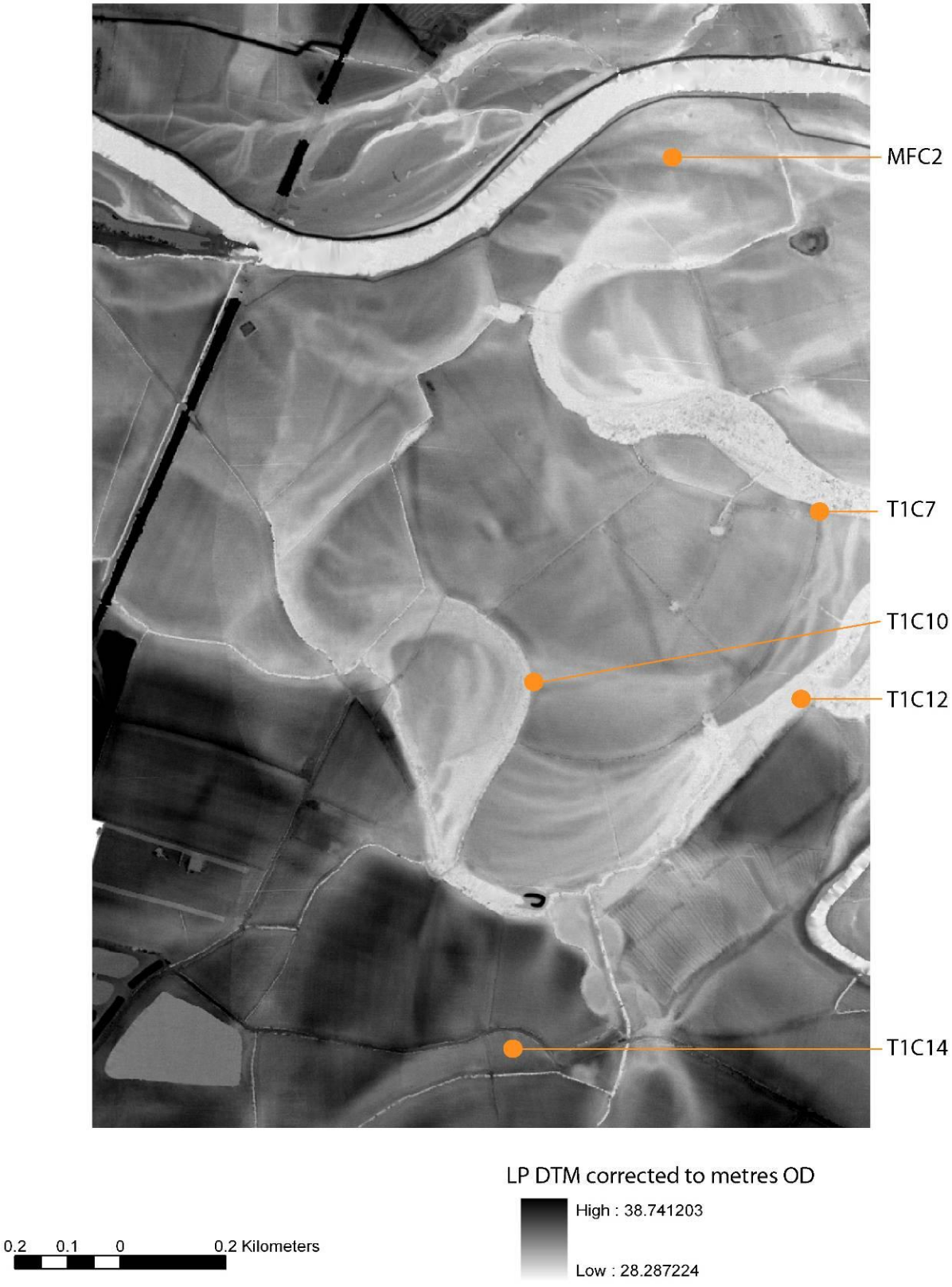

Fig 3: The core sample locations that were subject to NIR analysis in the Trent/Soar confluence.

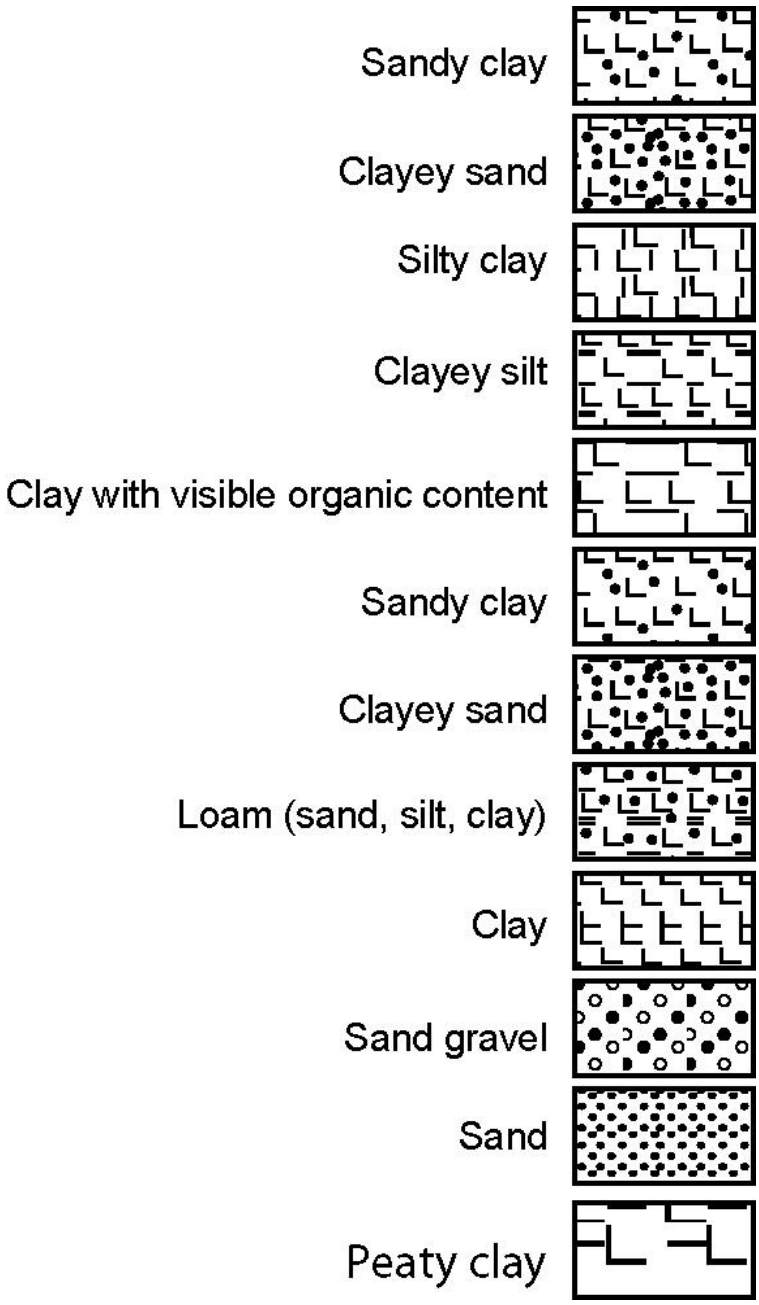

Fig 4: Modified Troel Smith key for sediment descriptions.

2.2.2 Organic content

All cores were sampled at 1cm contiguous intervals along their entire length. Sediment from each sample was transferred to a labelled sample bag and freeze dried. After freeze drying samples were sieved in a 2mm stainless steel sieve. Crucibles were dried overnight at 109^{O}C to remove any excess moisture. The crucibles were weighed (a) and then approximately 1g of the $\leq$2mm soil fraction was added to each crucible. The crucibles were again dried overnight at 109^{O}C to remove any moisture from the sediment. The crucibles and samples were weighed (b) and then placed in a muffle furnace at 450^{O}C for 4 hours. The crucibles and soil sample were then

weighed again (c). The % organic mater of the soil was then calculated using the formula:

$$\% \text{ Organic matter} = \frac{(a - c)}{(a - b) * 100}$$

2.2.3 Carbonate content

After the organic content had been burned off the samples, the crucibles were returned to the muffle furnace at 800^{O}C for a further hour. The crucibles were again weighed (d). The carbonate content of the sample was calculated through the formula:

$$\% \text{ carbonate content} = \frac{(c - d)}{(b - a) * 100}$$

2.2.4 pH

The pH of the samples was measured using an Alpha 500 contact probe. The instrument was switched on for 30 minutes to warm up. The contact probe was calibrated through immersion in a series of standard buffers at pH 4 and pH 7, whilst measuring the temperature of the buffer solution. pH readings were made at 5cm intervals along the cores and tins through placing the probe into the sediment. The contact probe was washed thoroughly between readings.

2.2.5 Magnetic susceptibility

The magnetic susceptibility of the samples was measured through a Bartington MSII. A 10ml pot was then weighed (d), filled with the $\leq$2mm of sediment, then reweighed (e). The Bartington MSII was switched on for 30 minutes to warm up. Each sample was measured three times in the following sequence: Measurement of air (a), measurement of sample (b), measurement of air (c). The timing for each sample measurement was set at 30 seconds. The measurement of air samples allowed for the calibration of drift of the instrument. From this data the average of the three readings was calculated for each sample via the formulae:

$$e - d = f$$

$$b1 - (a1 + c1) = g1$$
$$b2 - (a2 + c2) = g2$$
$$b3 - (a3 + c3) = g3$$

$$\frac{(g1 + g2 + g3)}{3} = h$$

$$\frac{h}{f} = \text{magnetic susceptibility units } (10^{-8} m^3 Kg^{-1})$$

2.2.6 NIR analysis

NIR data was collected using the LabSpec 2500 spectrometer, manufactured by Analytical Spectral Devices. Data was collected between 350nm – 2500nm using a hand held contact probe (Fig. 5). The contact probe was zeroed before each sample location through placing on a white disc of 100% reflective capacity to zero the spectrometer. Each sample location then had five sequential readings taken. The data was exported as text files and imported into Microsoft Excel. An average was then made of the five readings at each sample location. In all of the stratigraphic diagrams in this chapter the green line represents 1047nm the same wavelength of Optech airborne lidar and the blue line represents 950nm the wavelength of the ground based Measurement Devices Ltd (MDL) LaserAce scanner used in the terrestrial lidar surveys.

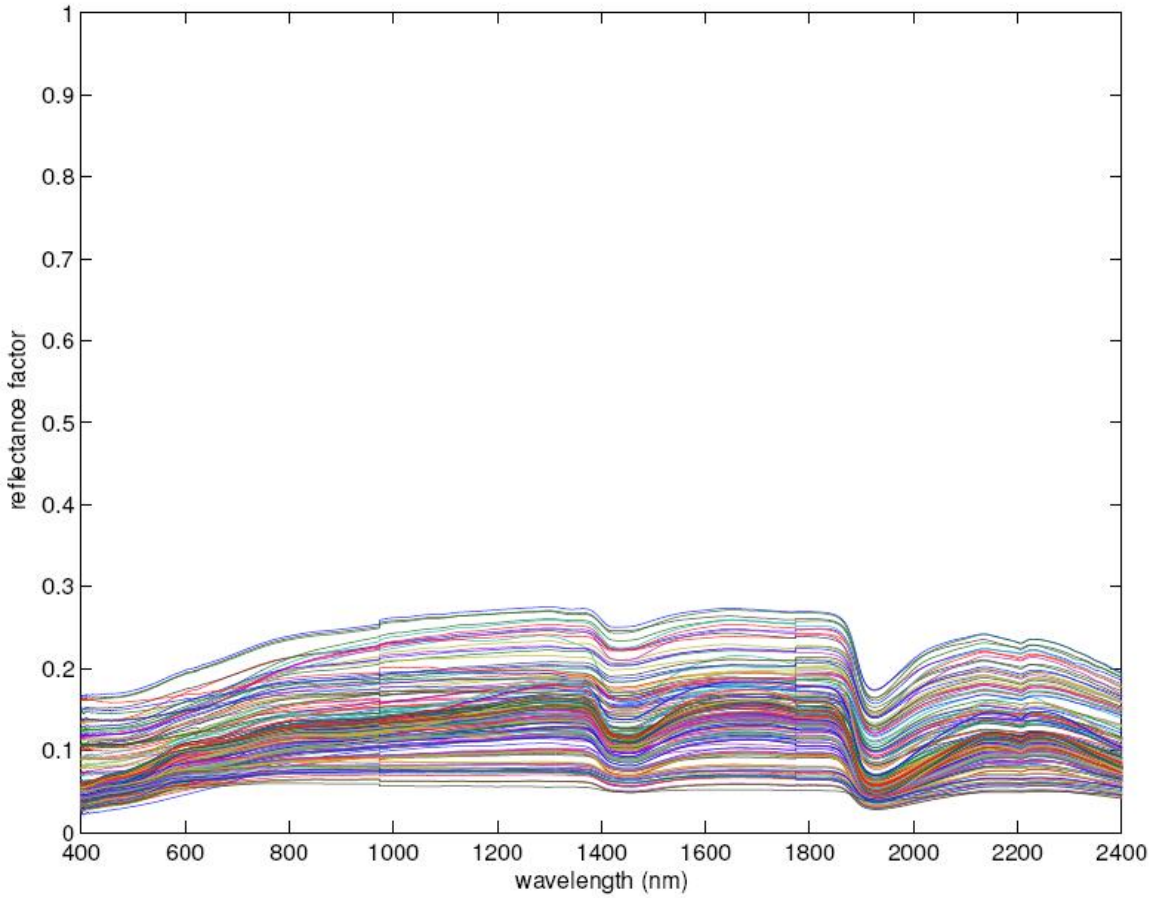

Fig 5: All data from the NIR analysis of core MFC2 (each line represents one measurement on the core).

2.2.7 Statistical procedure

Statistical analysis of the data followed a simple prescribed route. Primarily data was examined using line graphs to assess 1047nm reflectance change against sediment stratigraphy from the palaeocores. Secondly, scattergraphs were used to look at the relationship between 1047nm reflectance and various soil parameters. Correlation coefficients were computed to quantify these relationships between 1047nm reflectance and the soil parameters, using a Pearson correlation coefficient. Such a bivariate measure assumes that neither variable is dependant on the other, although in this instance, it was not clear whether dependency between variables existed. Lastly,

some analysis was undertaken on the between core variation using ANOVA's, with Duncan's multiple range *post-hoc* testing.

2.3 RESULTS: NEAR INFRA RED INTENSITY AND QUALITATIVE COMPARISON TO SEDIMENT STRATIGRAPHY

The stratigraphy of the sediment cores was recorded through a modified Troel-Smith key, with descriptions of their elasticity, colour, etc. This qualitative data was then drawn into scaled sediment stratigraphy diagrams of the palaeochannel. The 1047nm and 950nm reflectance graphs are shown against these stratigraphies as recorded in the laboratories. The sediment architecture was logged before any treatment had been undertaken on the palaeo-cores, e.g. sampling, allowing NIR measurement of the cores in their 'field state'. This first section of the results qualitatively evaluates whether NIR can be used to identify changes in sediment composition, recorded through sediment stratigraphy.

2.3.1 Core MFC2: 1047nm reflectance and sediment stratigraphy

This core was sampled in a palaeochannel on the modern floodplain (Fig. 4). The precise stratigraphy of the core is given through the quantification of soil organic content, soil carbonate content and magnetic susceptibility on a 1cm sample interval (Fig. 6). MFC2 has a dark red brown clayey silt A horizon underlain by a reddish brown silty clay. Below this between 56 – 82cm is dark grey/black silty clay, which shows elevated organic and carbonate contents and a higher magnetic susceptibility. Below this between 82 – 116cm is a red brown silty clay, underlain by a reduced grey brown silty clay. A grey brown silty sandy clay is between 151 – 163, with a black clayey sand at 163 – 172cm and a grey brown coarse sand at the base. The unit between 56 – 82cm stands out as having a higher organic content. There was no sand within this unit suggesting a very low energy depositional environment. It is also a notable break between two units of red brown clay and appears to reflect a change is depositional history.

The core MFC2 was de-sampled on a 5cm sample interval to coincide with the spectroscopy sampling interval (Fig. 7). The change between the A horizon and the red brown silty clay beneath it (10 – 56cm) is evident as an area of elevated 1047nm reflectance and lower soil organic content. The dark grey black silty clay at 56 – 82cm is evident as an area of higher organic content and although the 1047nm reflectance data is spiky in this unit, a general area of lower reflectance is seen compared to the unit above. The next two units of red brown silty clay (82 – 116cm) and grey brown silty clay are relatively constant in 1047nm reflectance and this correlates with relatively constant organic soil content for these units. The last three sediment units (grey brown silty clay 151 – 163cm, black clayey sand 163 – 172cm and grey brown coarse sand 172 – 185cm) all show an overall decrease in 1047nm reflectance and organic content.

Overall the reflectance in the NIR shows variance along the cores, with changes that can be related to the sediment composition of the core. In particular the dry silty clay unit at 10 – 56cm is evident as a unit of lower reflectance at 1047nm and this may

well be related to lower sediment moisture content. Likewise, the basal sand units also show lower reflectance at 1047nm and this again could be related to a lower sediment moisture content.

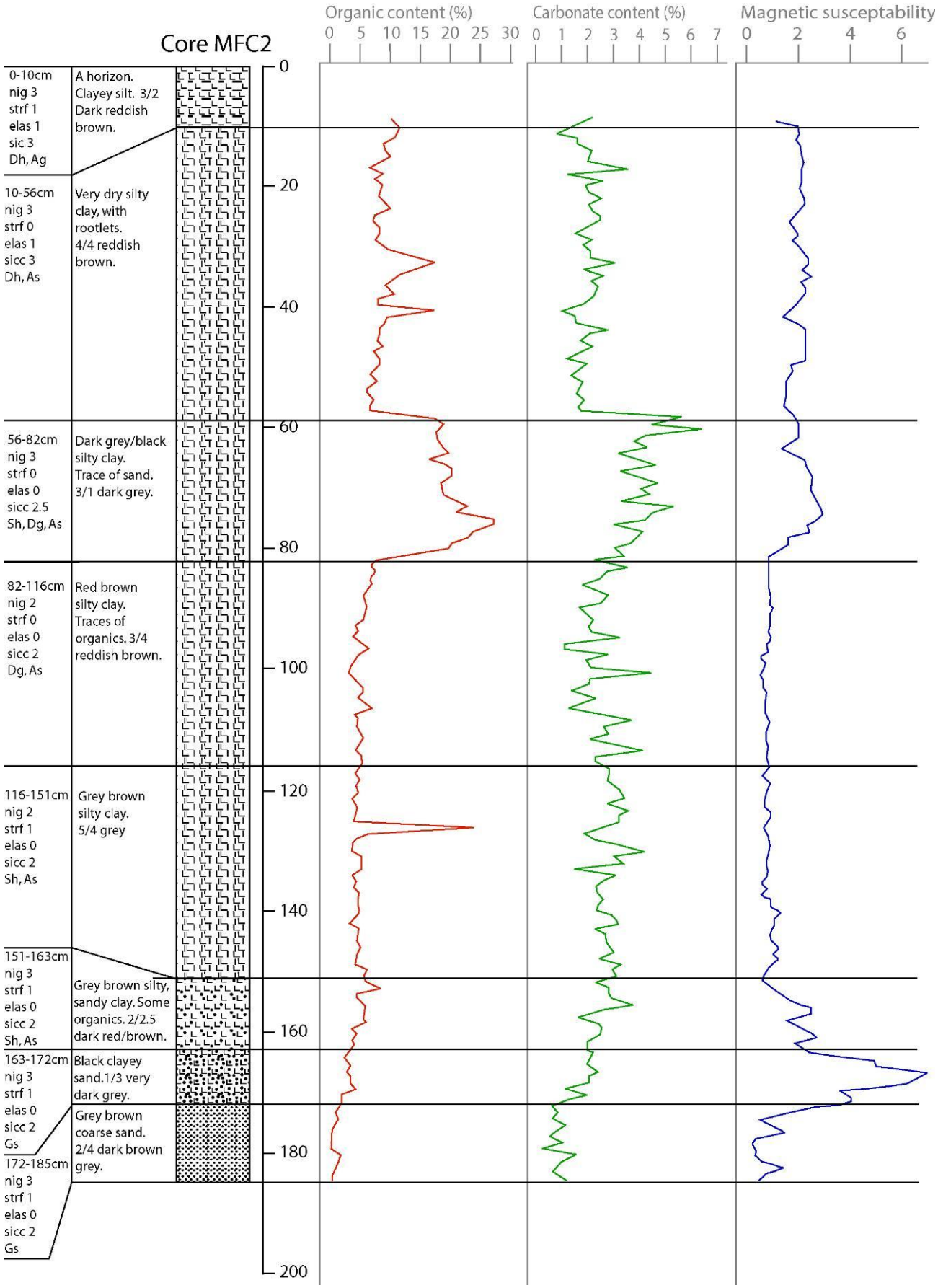

Fig 6: The stratigraphy of core MFC2 compared to soil organic content, soil carbonate content and magnetic susceptibility.

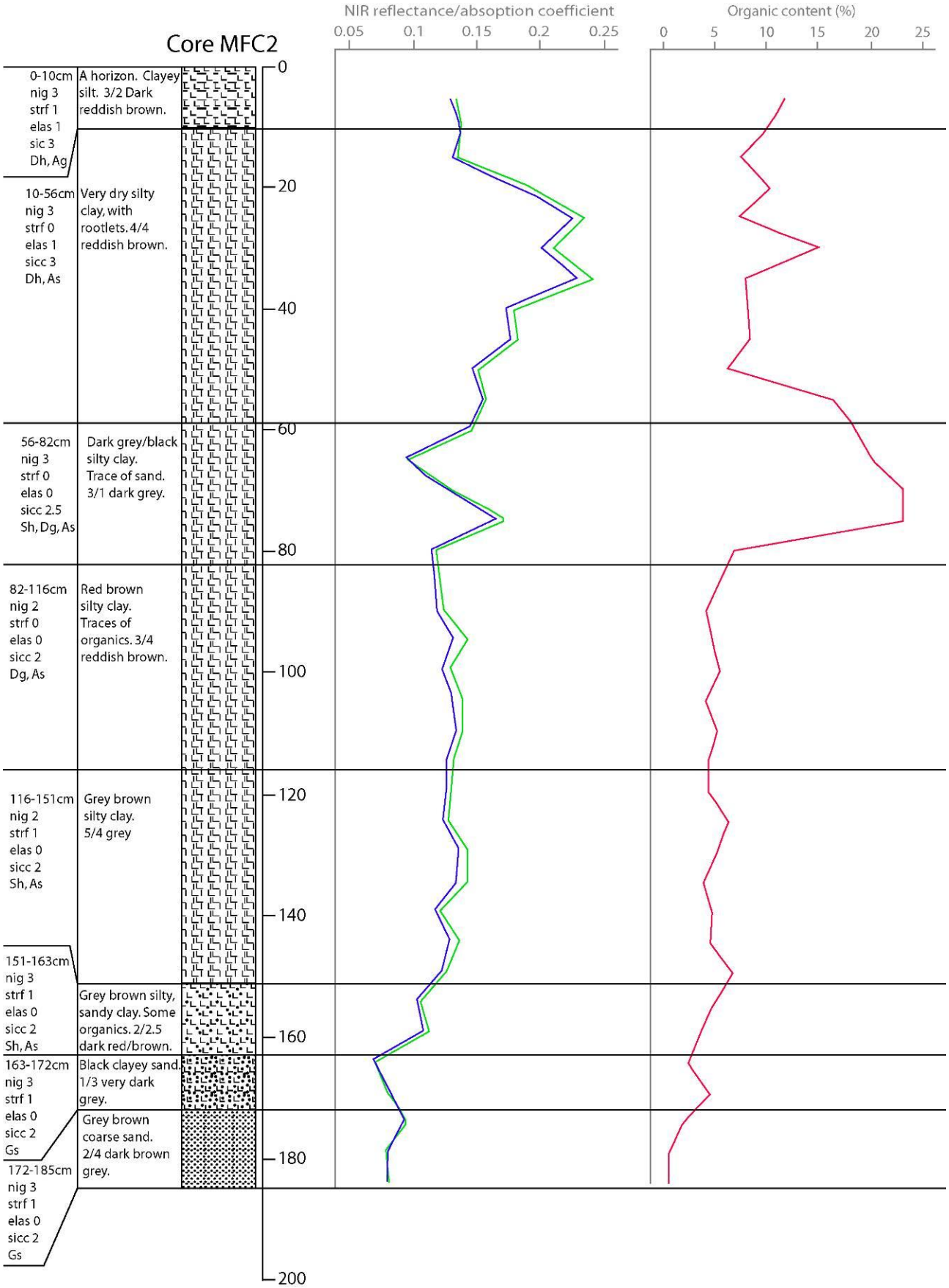

Fig 7: Core MFC2 de-sampled to a 5cm ample interval showing stratigraphy against 1047nm reflectance and soil organic content.

2.3.2 Core T1C7: 1047nm reflectance and sediment stratigraphy

This core was sampled in a palaeochannel of the river Soar, located on terrace 1 (Fig. 4). Core T1C7 has an A horizon between 0 – 6 cm, underlain between 6 – 45cm by a brown silty clay. After this point (45cm) the core is dominated by two main sediment units. Firstly, there is an upper blue grey with Fe inclusions between 45 – 140cm. Below this between 140 – 225cm is a blue grey clay with visible organic fragments. The organic content is relatively high throughout the core and shows a good relationship to the sediment stratigraphy. The magnetic susceptibility shows a notable peak in the blue grey unit between 45 – 140cm, but this does not correspond with a recognised change in sediment composition (Fig. 8).

The core T1C7 was de-sampled on a 5cm sample interval to coincide with the spectroscopy sample spacing (Fig. 9). The dark brown silty clay is seen as an area of decreasing reflectance at 1047nm, whilst the organic content of this unit is relatively high. The blue grey clay unit between 45 – 140cm is seen as an area of increased reflectance at 1047nm, except for the low values at 50cm and 55cm. Conversely, the organic content shows an inverse relationship with a lower organic content within this unit. The blue grey clay with organics between 140 – 225cm shows a gradual decrease in reflectance with the organic content remaining relatively homogeneous. The stratigraphy of the core T1C7 shows a good relationship to soil organic content at both the 1cm and the 5cm sample interval. Likewise, the reflectance data reveals distinct changes that correspond with changes in the sediment architecture of the core.

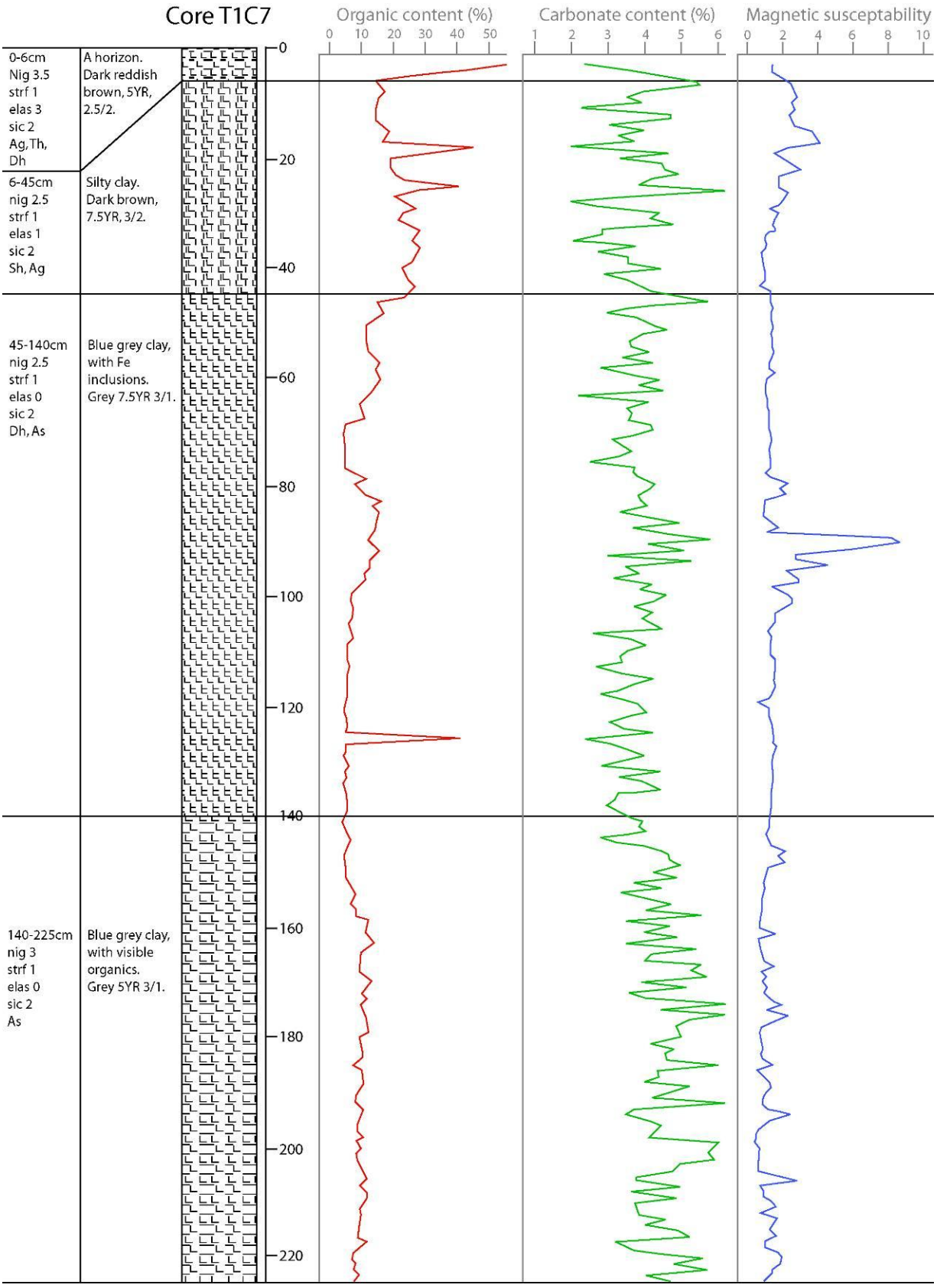

Fig 8: Core T1C7 with soil organic content, soil carbonate content and magnetic susceptibility measurements at a 1cm interval.

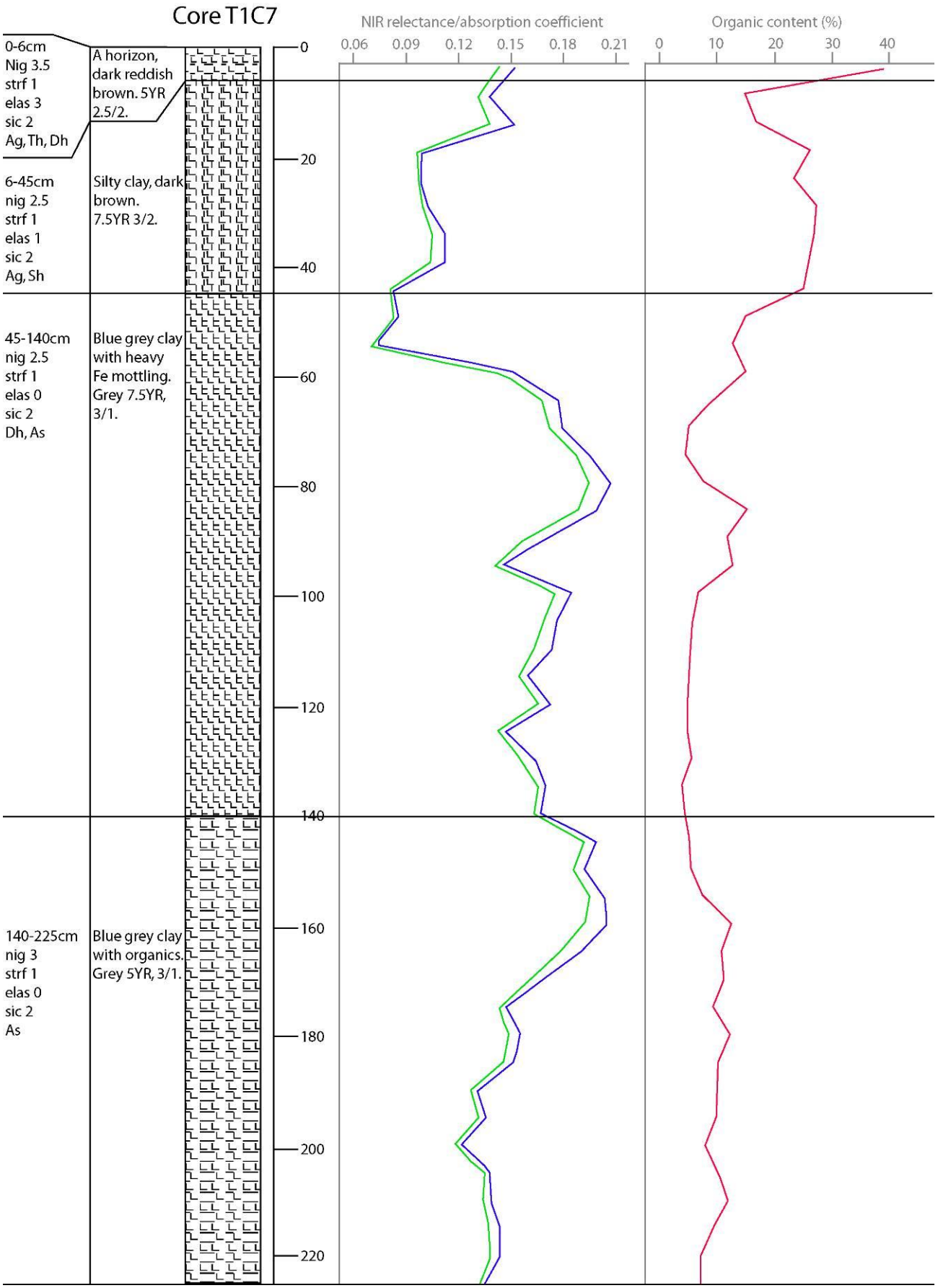

Fig 9: Core T1C7 de-sampled to a 5cm sample interval showing 1047nm reflectance against soil organic content.

2.3.3 Core T1C10: 1047nm reflectance and sediment stratigraphy

This core was taken from a palaeochannel that runs east/west through an area of terrace 1 (Fig. 4). This core has a brown silty clay A horizon between 0 – 22cm, underlain by a red brown loam (silt, clay with sand) between 22 – 58cm. Below this a unit extends past the redox boundary, between 58 – 142cm. The upper 58 – 100cm is red brown increasingly gleyed clay with depth. From 100 – 142cm, this unit is grey clay. Between 142 – 158cm is a dark grey clayey silt, with fine sand and heavy Fe and Mn staining. At the base is a dark grey clay with a trace of sand between 158 – 185cm. Overall the organic content through the core is low, with the carbonate content showing no systematic variation with stratigraphy. The organic content is slightly elevated in the basal dark grey clay until between 158 – 185cm. Magnetic susceptibility shows little variation, except an elevation in the A horizon and elevation in the dark grey clay basal unit (Fig. 10).

The core T1C10 was de-sampled on a 5cm sample interval to coincide with the spectroscopy sampling interval (Fig. 11). The overall 1047nm reflectance plot is interesting due to the spikiness of the data compared to other cores. The soil organic content on the 5cm sample interval also displays this same spiky distribution, in both the 1cm and 5cm sampling diagrams. The brown stiff silty clay between 0 – 22cm has a high soil organic content, with a generally low level of reflectance at 1047nm this does display a notable peak at 15cm. The red brown loam at 22 – 58cm is marked by its relatively high reflectance at 1047nm, with falling soil organic content.

The red brown – grey clay unit (diffuse boundary) between 58 – 142cm has an erratic pattern of reflectance at 1047nm, with spiky data that is mirrored in the soil organic content. The unit below is a dark grey clayey silt at 142 – 158cm that follows this same pattern of spiky data, whilst the dark grey clay with a trace of sand at 158 – 185cm shows decreasing reflectance at 1047nm, with the soil organic content showing elevated values at the base of the core. Overall the reflectance at 1047nm identifies the top two units on the core, with less distinction between units further down the core. The soil organic content follows a similar pattern. Neither the reflectance at 1047nm nor soil organic content define specific stratigraphic variation within the bottom three units of core T1C10.

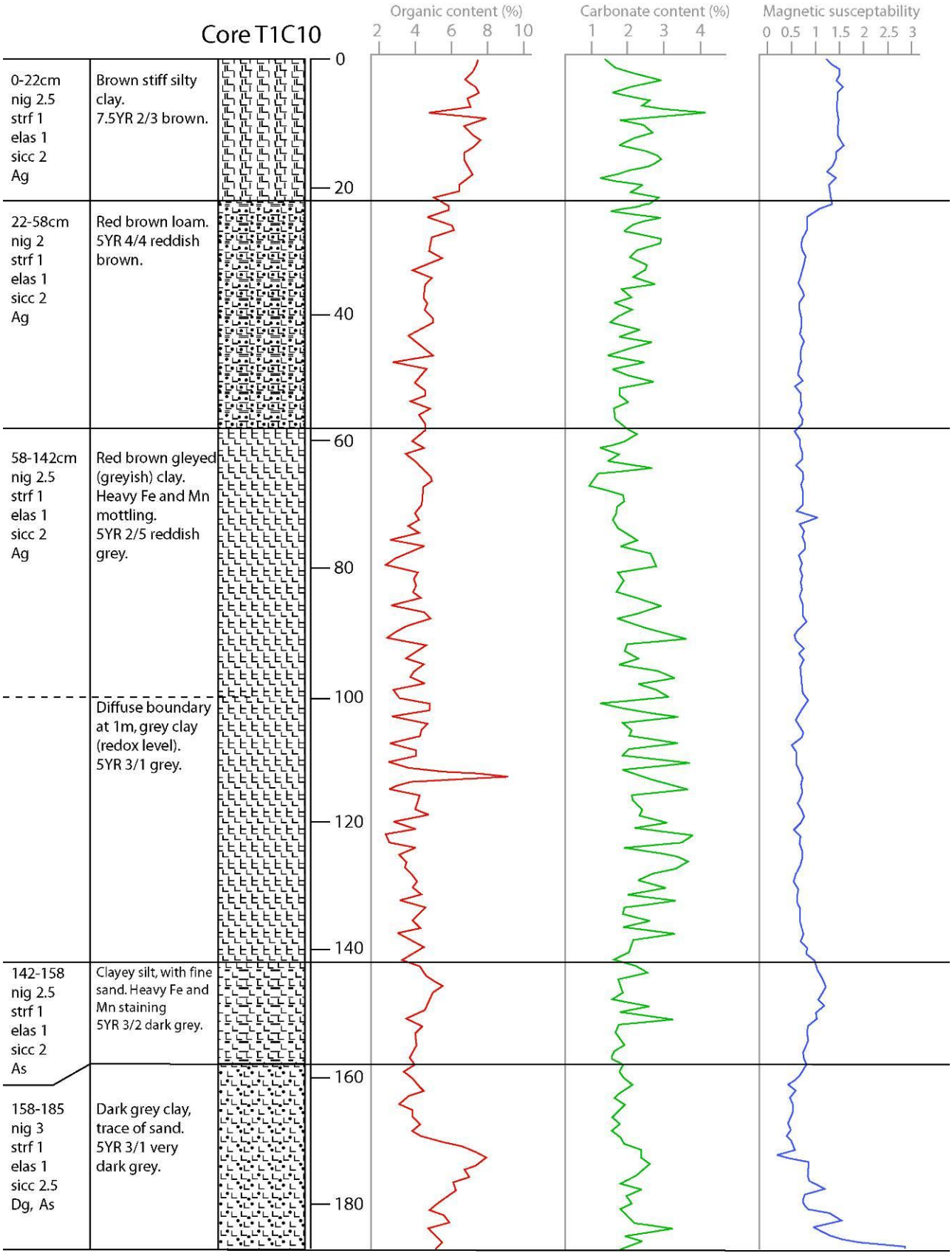

Fig 10: Core T1C10 with soil organic content, soil carbonate content and magnetic susceptibility measurements at a 1cm interval.

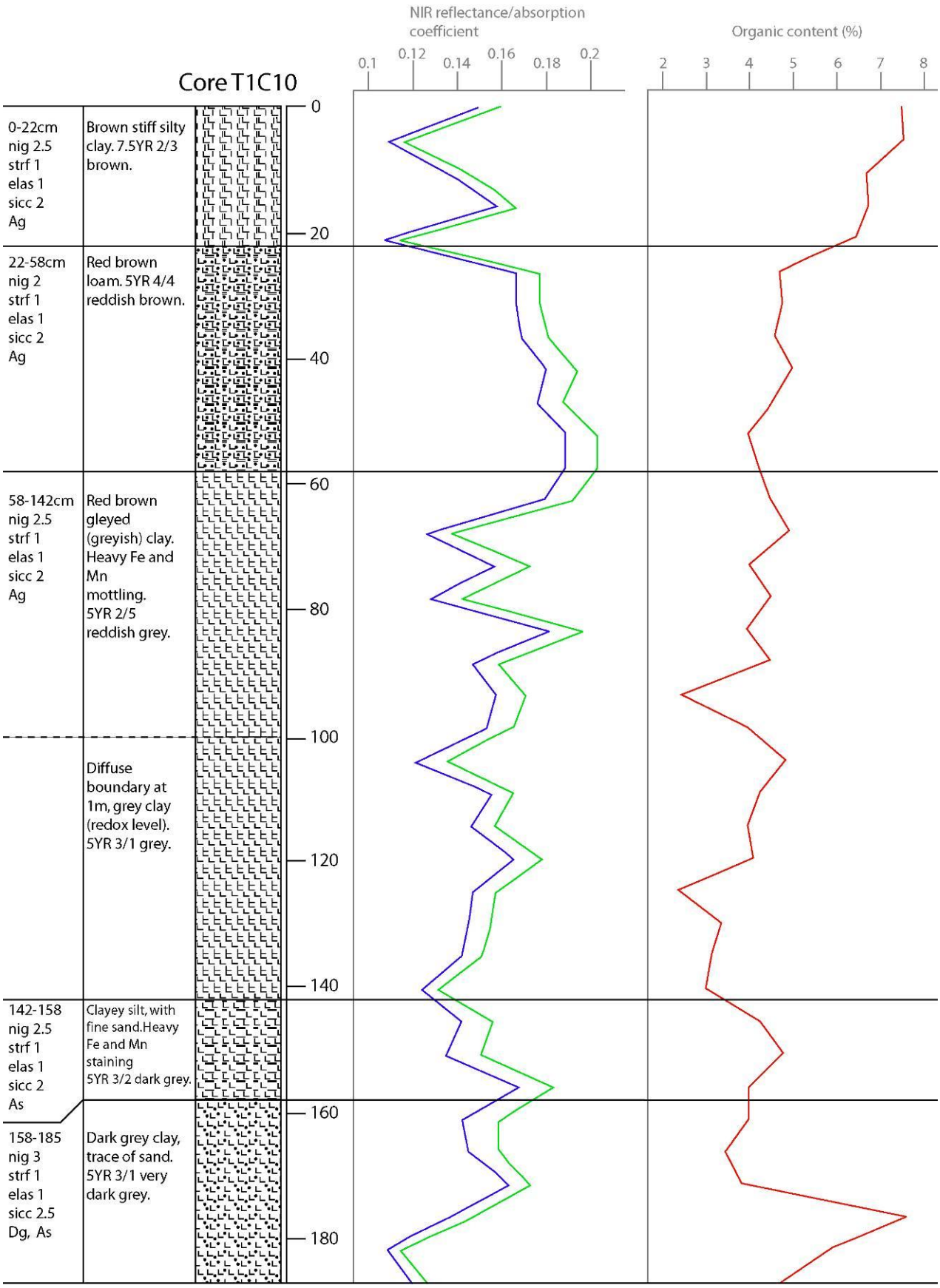

Fig 11: Core T1C10 de-sampled to a 5cm sample interval showing reflectance at 1047nm against soil organic content.

2.3.4 Core T1C12: 1047nm reflectance and sediment stratigraphy

This core was located in the palaeochannel that denotes the boundary between terrace 2 and terrace 1 (Fig. 4). The core stratigraphy has a 10cm A horizon of red brown clayey silty, underlain between 10 – 29cm by an organic brown black silty clay. A thin unit of reddish brown silty clay is located between 29 – 37cm. Below this is a large unit of red brown silty clay, stretching from 37 – 139cm. At 139 –183cm a dark grey clay is encountered, with a basal unit of black grey clay between 183 – 214cm. The organic content is consistently high throughout the core, with elevated levels seen between 10 – 37cm. Magnetic susceptibility also shows elevate values between 10 – 37cm (Fig. 12).

The 1047nm reflectance values relate well to the overall stratigraphic composition of T1C12, as defined through its sediment composition (Fig. 13). The orange brown black silty clay between 10 – 29cm has decreasing reflectance values and an erratic soil organic content distribution. The red brown silty clay unit at 29 – 37cm has low reflectance at 1047nm and falling soil organic content. The large red brown silty clay unit below this at 37 – 139cm has elevated reflectance values, which marginally increase in depth. Conversely, the same unit has low soil organic content values, which marginally decrease with depth. The grey clay unit at 139 – 183cm shows an appreciable rise in reflectance at 1047nm, whilst the soil organic content of the soil also rises in this unit. Lastly, the black grey clay with visible organic remains at 183 – 214cm shows lower reflectance values, which rise slightly to the base of the core. In contrast the soil organic content shows lower values in this unit, with a rise in organic content to the base of this core.

Overall the reflectance at 1047nm reflects the major changes in sediment architecture well, with the main units being identifiable on the NIR graph. The relationship of the soil organic content to the sediment stratigraphy is less obvious. The relationship between the reflectance values and the soil organic content is often opposite in this core, with increases in reflectance often coinciding with lower soil organic content values.

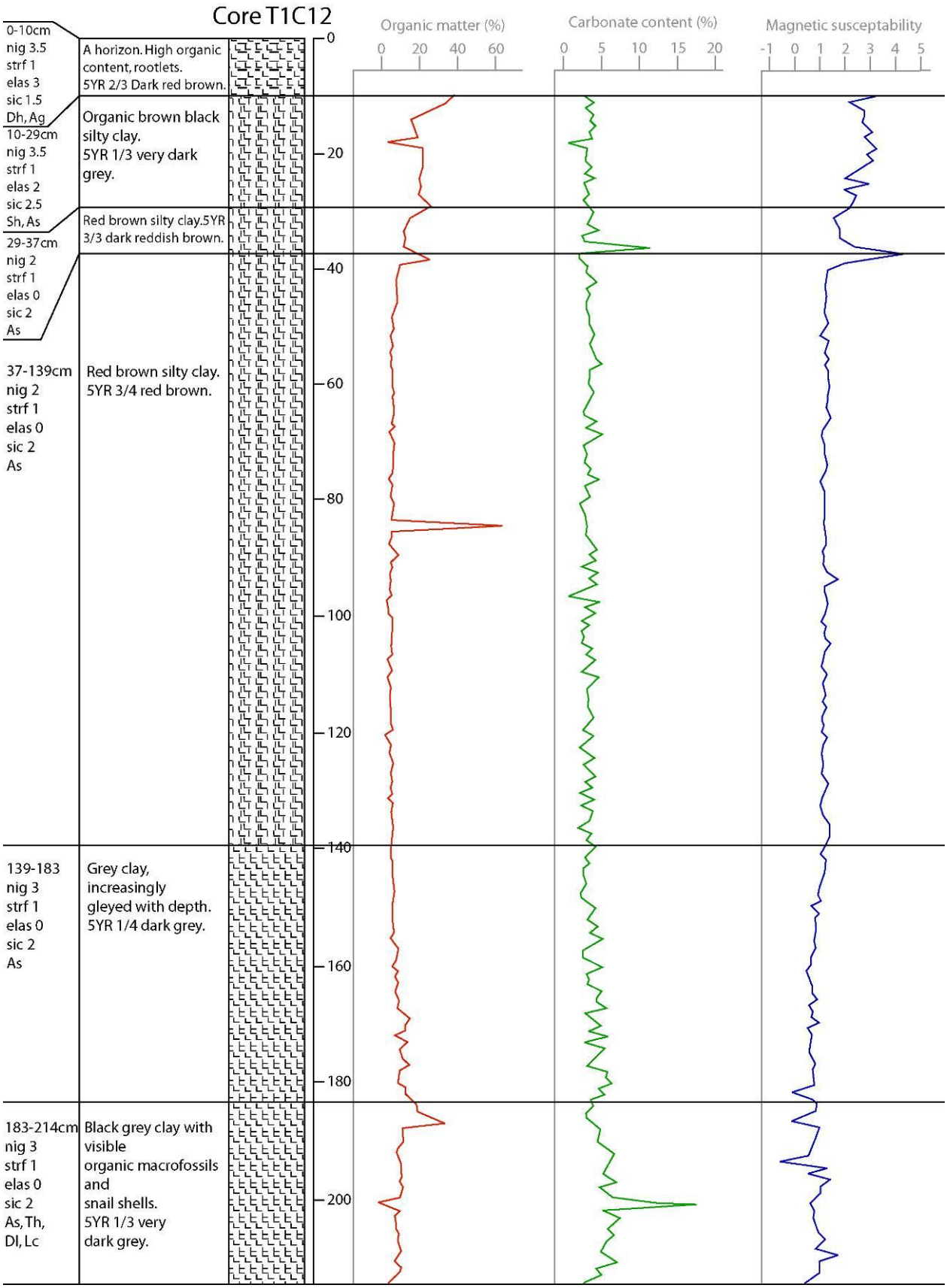

Fig 12: Core T1C12 with soil organic content, soil carbonate content and magnetic susceptibility measurements at a 1cm interval.

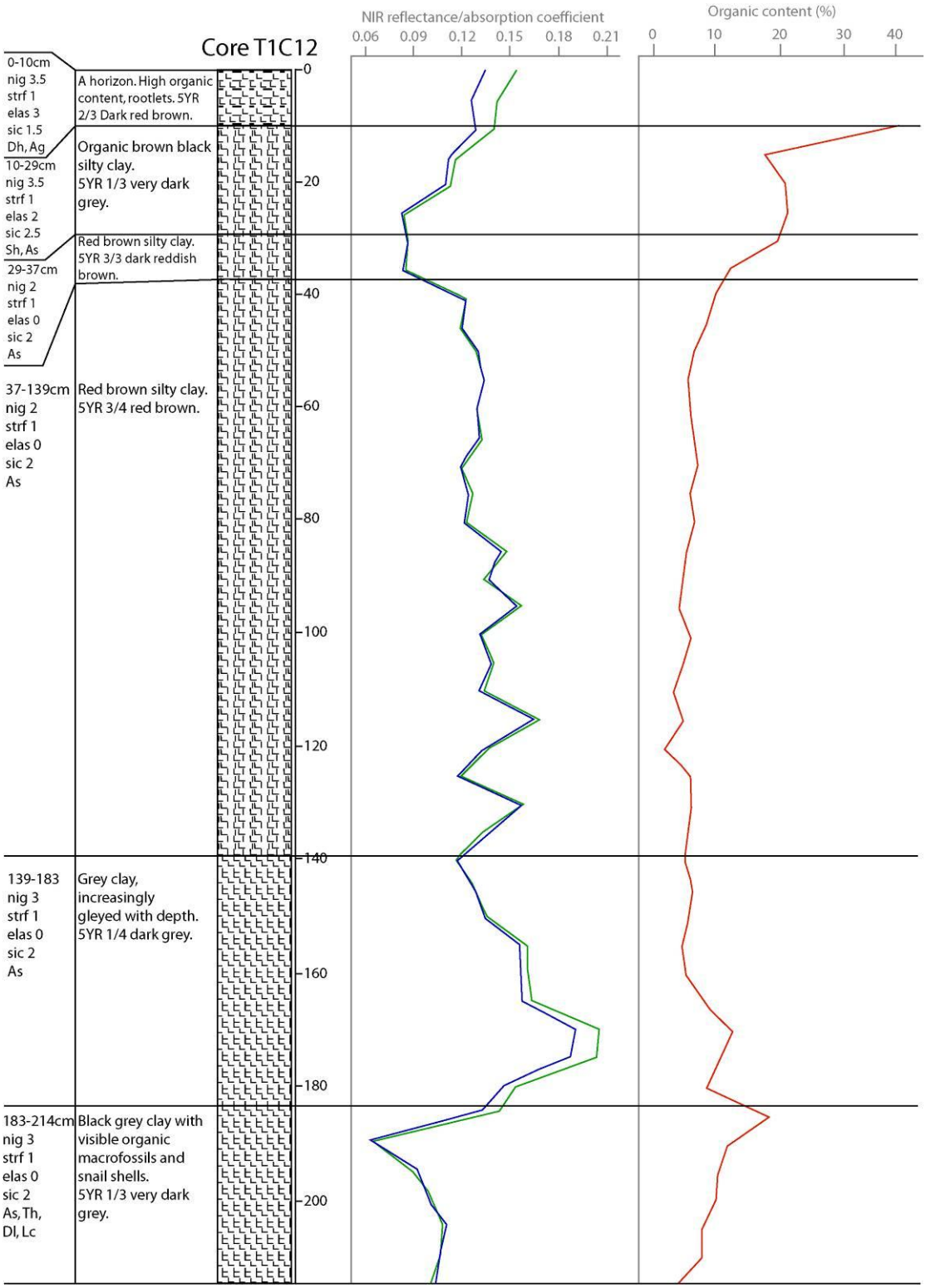

Fig 13: Core T1C12 de-sampled to a 5cm sample interval showing 1047nm reflectance against soil organic content. Changes in 1047nm reflectance relate well to the stratigraphic changes recorded in the core.

2.3.5 Core T1C14: 1047nm reflectance and sediment stratigraphy

Core T1C14 was located in a palaeochannel located on terrace 2 (Fig. 4). Core T1C14 is relatively short at 90cm, with a dark red brown AP horizon between 0 – 5cm. Below this is a dark red brown silty clay with a trace of sand between 5 – 28cm. A red brown silty clay unit is located between 28 – 54cm, with a basal blue grey clay with a trace of silt and sand, and Fe and Mn mottling between 54 – 90cm. The organic content is low throughout the core. The upper two units (0 – 5cm and 5 – 28cm) both show relatively elevated organic and magnetic susceptibility contents (Fig. 14).

The reflectance values at 1047nm relate well to the general core stratigraphy (Fig. 15). The dark red brown silty clay unit between 5 – 28cm shows low reflectance values, whilst the soil organic content declines appreciably in this unit. The red brown silty clay unit at 28 – 54cm is well defined by high reflectance values, except for the reading at 30cm, whilst the soil organic content continues to decline in this unit. The blue grey clay with a trace of silt and sand between 54 – 90cm also shows elevated reflectance values, which marginally increase with increasing depth. Conversely, the soil organic content in this bottom unit is relatively low.

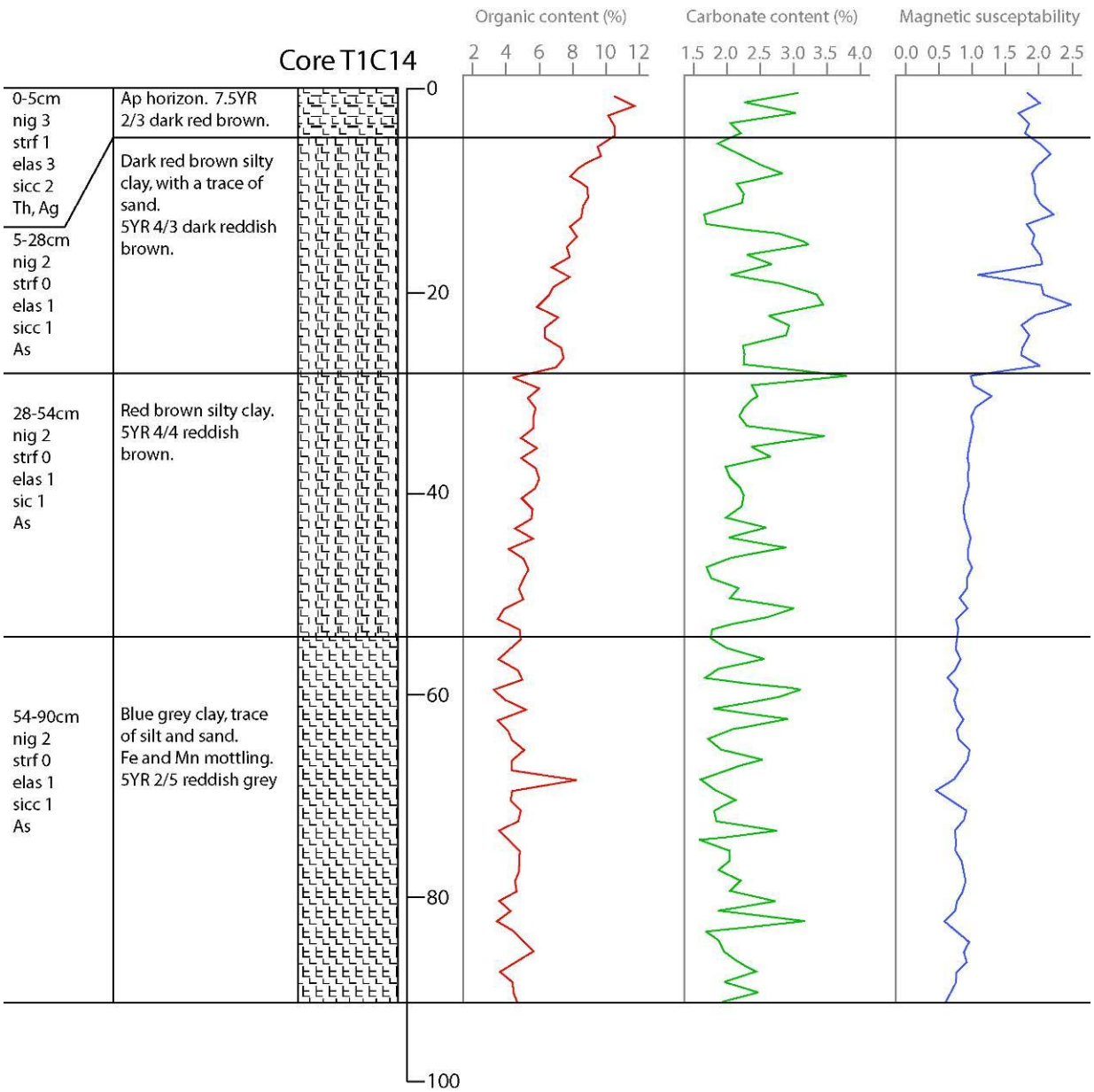

Fig 14: Core T1C14 with soil organic content, soil carbonate content and magnetic susceptibility measurements at a 1cm interval.

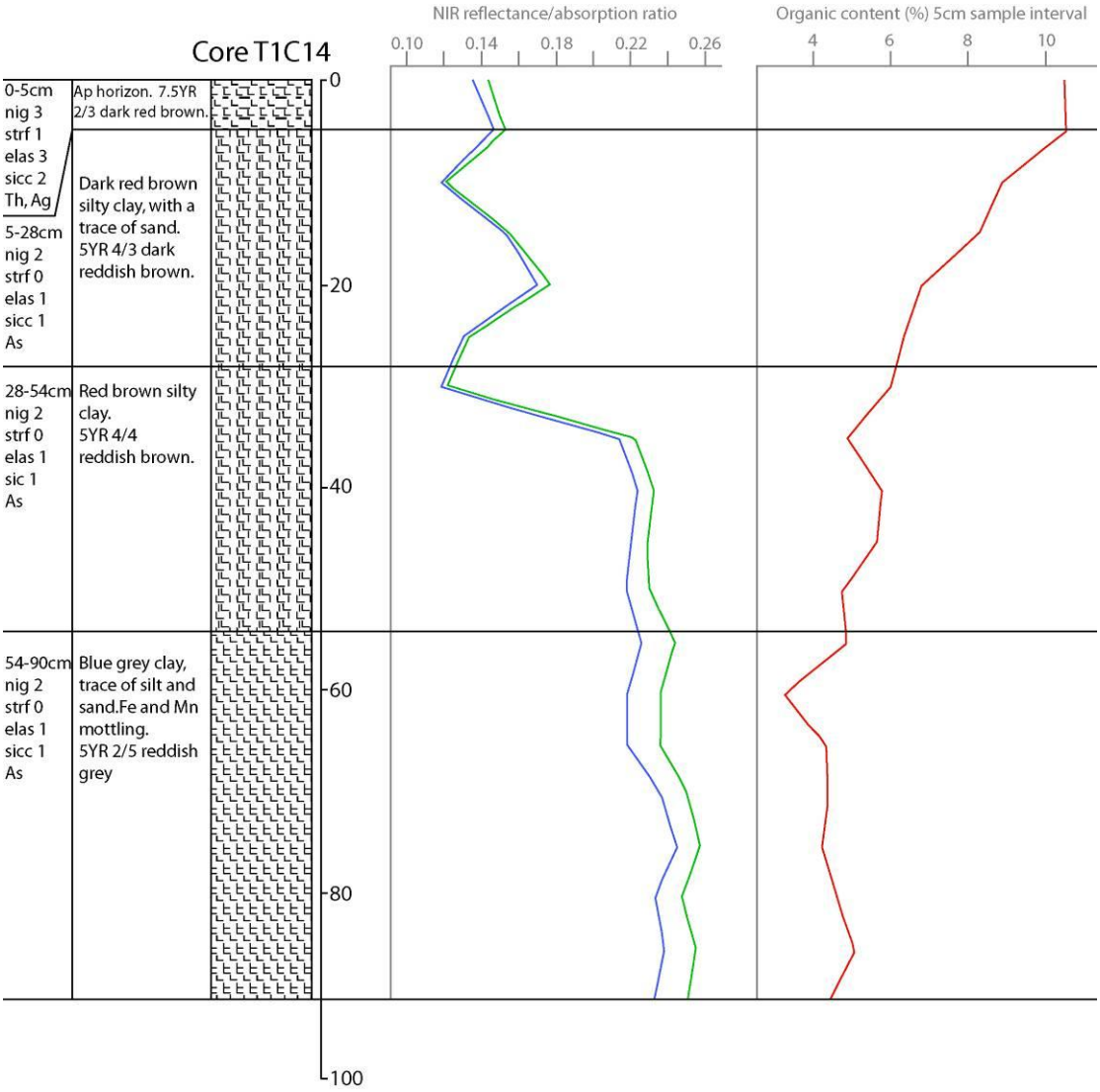

Fig 15: Core T1C14 de-sampled to a 5cm sample interval showing 1047nm reflectance against soil organic content. Changes in 1047nm reflectance relate well to the stratigraphic changes recorded in the core.

2.3.6 Overall summary: 1047nm reflectance and qualitative comparison to sediment stratigraphy

The 1047nm reflectancealues have a visual relationship to sediment architecture, with stratigraphic changes in some of the cores relating to changes in reflectance. As a qualitative visual assessment it is possible to state that reflectance at 1047nm does reflect changes in core stratigraphy. However, the changes in reflectance are not always exact with the recorded changes in sediment architecture, nor are they consistent. Some cores showed very clear correspondence between reflectance and changes in sediment structure, such as T1C12, whilst other cores such as T1C10 displayed variation in sediment composition not depicted clearly by changes in reflectance.

Likewise, the soil organic content displayed variation that coincided with the changes in sediment composition along the cores. Like the reflectance values these changes were not always coincident with changes in sediment composition. Some units

displayed a strong relationship between sediment structure and organic content, such as the unit at 56 – 82cm on core MFC2, whilst other changes in sediment composition were not reflected in soil organic content, such as the lower units on core T110.

The relationship between soil organic content and reflectance is harder to qualify. Both displayed variation that reflected changes in sediment composition, but the variation between soil organic content reflectance was not consistent. Generally, when the organic content of the soil increased, the reflectance values decreased and vice versa. However, this relationship was not constant, with some sediment units displaying a rise in both reflectance and soil organic content, whilst other units displayed a decrease in both. Therefore, whilst the qualitative assessment recognises a relationship between the two variables, this relationship may be indirect, i.e. neither variable is dependant on the other, but both are reflecting changes in one or more other variables, e.g. grain size, soil moisture content, etc.

The data set may suffer from a form of *equi-finality*, whereby different variables in soil composition give the same result in one variable, but a different response in another. Take a hypothetical example of two units, one being a black grey clay and the other a fine orange water logged sand. Conceivably both may have a high organic content, but one may produce a high reflectance and the other a low reflectance value response due to changes in grain size, colour, etc.

The qualitative examination of the sediment stratigraphy of cores has shown that changes in sediment composition can be mirrored in variations in reflectance at 1047nm. The nature of the underlying reasons for the relationship between changes in sediment structure and reflectance are less clear, with two competing models. Firstly, reflectance maybe the product of multi-variables, such as organic content, particle size, moisture content, carbonate content, etc (Fig. 16). Although these variables have a strong relationship to each other it is the sum of the components that dictate the sediments spectral properties, and it is not possible to extract significant univariable relationships to reflectance, although a qualitative relationship to sediment architecture is apparent. A competing model is a variation of Fig. 16, which although the sum of the sediment properties dictate the spectral reflectance at 1047nm, significant univariable relationships are visible, through specific variables having a dominant influence on spectral reflectance at 1047nm (Fig. 17). The next sections (2.4 – 2.8) look at single variable relationships between sediment properties and reflectance at 1047nm.

2.4 RESULTS: 1047NM REFLECTANCE AND QUANTIFICATION OF RELATIONSHIP TO SEDIMENT ORGANIC CONTENT

The relationship of soil organic content to reflectance at 1047nm is undertaken on a core-by-core basis and then through analysis of the all core data set. This methodology allows variation within cores and variation between cores to be tested. The scattergraphs of 1047nm reflectance dependant on organic content all show weak relationships between the two variables. Core MFC2 revealed a weak positive relationship between the two variables (Fig. 18), whilst cores T1C7 (Fig. 19), T1C10 (Fig. 20), T1C12 (Fig. 21) and T1C14 (Fig. 22) all revealed negative correlations.

Core T1C14 displays the strongest relationship between the two variables, with a linear R squared value of 61%.

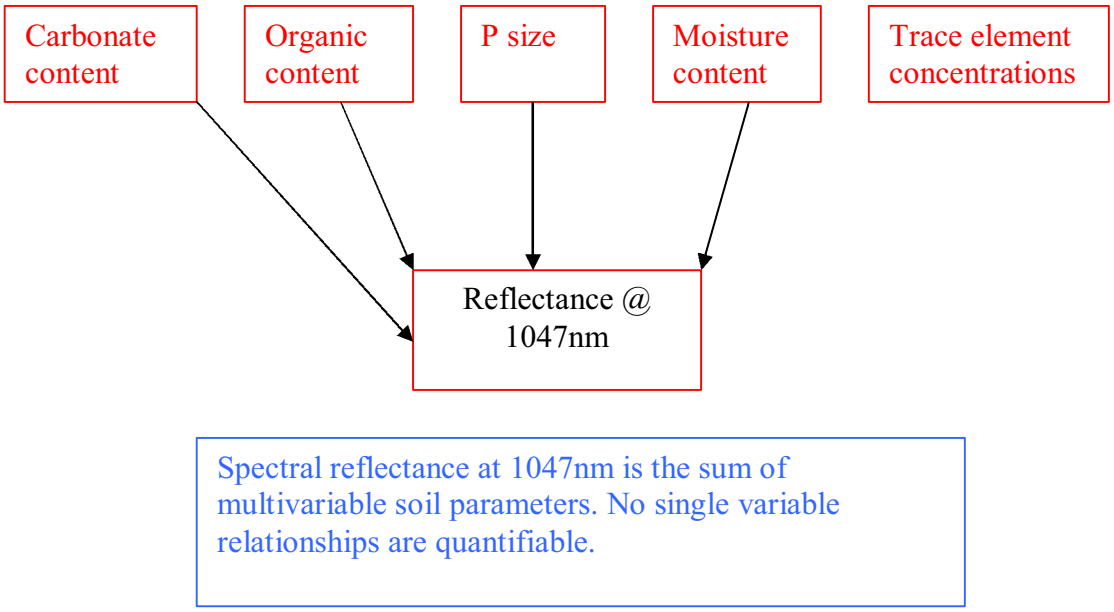

Fig 16: Model A: Spectral reflectance at 1047nm is the sum of multivariable soil parameters, with no single variable having a quantifiable relationship to 1047nm.

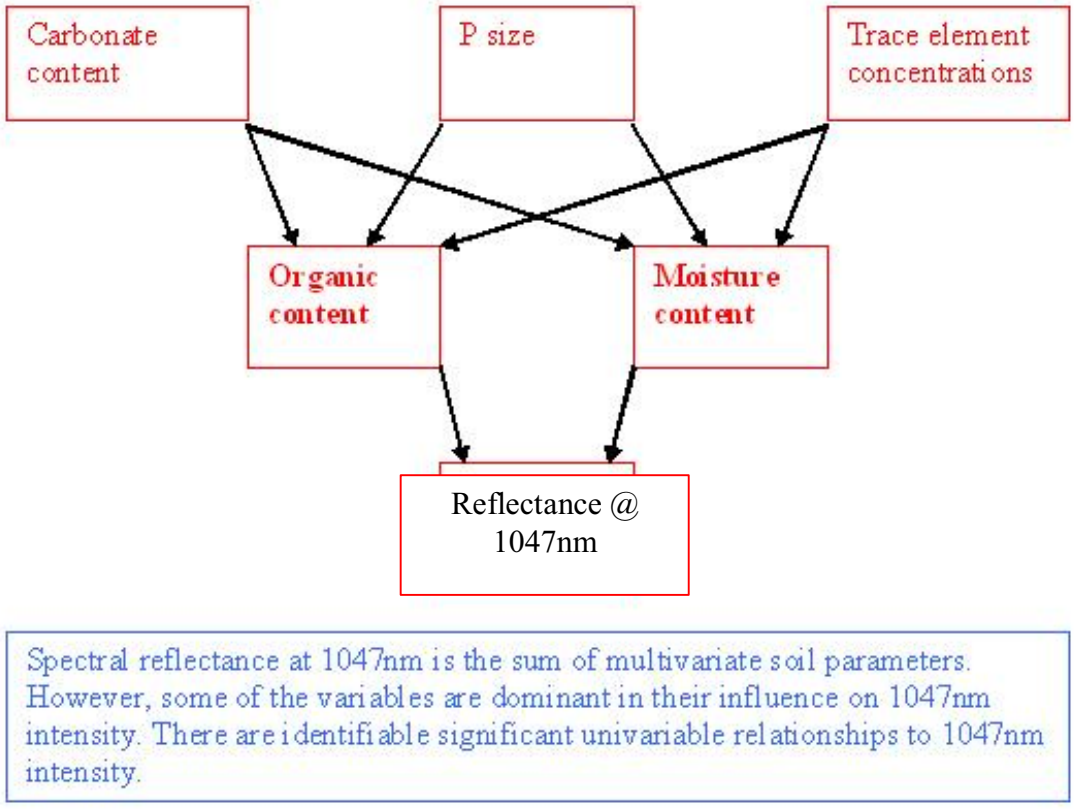

Fig 17: Model B: Although spectral reflectance at 1047nm is the product of multivariable soil parameters, single univariable relationships to 1047nm are identifiable.

However, the 'all core' data set reveals a very weak relationship between the two variables, with 5.8% of the variance within the data set explained by the relationship of the two variables (Fig. 23). This is confusing, as generally the negative correlations between variables produced stronger relationships. It is also clear through visual examination of the scattergraphs that outliers within the data set are having a strong leverage on the results. It is entirely possible that with a larger data set, both in terms of data points, and also in terms of a greater spectrum of alluvial sediment types, the effect of these outlying values would decrease. This is potentially a cause of the positive correlation on core MFC2.

Although the visual examination of the data suggested a weak negative relationship between the two variables, a Pearson correlation coefficient was computed, testing the null hypothesis that there is no significant relationship between 1047nm reflectance and organic content. The correlation coefficient showed a highly significant relationship between two variables at the 0.01 level (two tailed), with a negative relationship (Fig. 24). This produces a strange aspect to the data set that cannot be satisfactorily explained through the visual examination of the linear relationship of the two variables through scattergraphs. Therefore, the null hypothesis is rejected and the alternative hypothesis is accepted that is a significant relationship between the two variables at the 0.01 level (there is a 1% chance of making a type one error at this level).

At this stage of analysis a model is put forward accepting the alternative hypothesis. Although there is significant relationship between the two variables this relationship cannot be viewed graphically as a linear relationship and therefore another form of relationship must exist, such as quadratic or cubic. To test this 1047nm reflectance responses and organic matter contents were placed on a log scale (Fig. 25), which has the ability to turn quadratic responses into linear responses. The results showed that a log of 1047nm reflectance dependant on organic matter still had a weak negative relationship.

In summary it can be seen that the computed correlation coefficient shows a highly significant negative relationship between the two variables. However, this relationship between the two variables cannot be visualised in linear or quadratic forms. It is postulated that the relationship between the two variables is indirect or incidental, i.e. 1047nm reflectance is not dependant on soil organic content, but both vary in a systematic way dependant on one or more other soil variables. It is interpreted that both are reflecting changes in sediment architecture, thus residual variance in the two variables caused through sediment architecture shows a highly significant correlation when 1047nm reflectance and organic content are analysed in isolation. The fact that the relationship between the two variables is not linear or quadratic, means that the predictive capacity of 1047nm reflectance in identifying organic contents is limited. Thus the predictive capacity of 1047nm reflectance for the identification of organic rich sediments may have to occur on a more qualitative subjective basis, rather than a quantifiable mathematically predictive model.

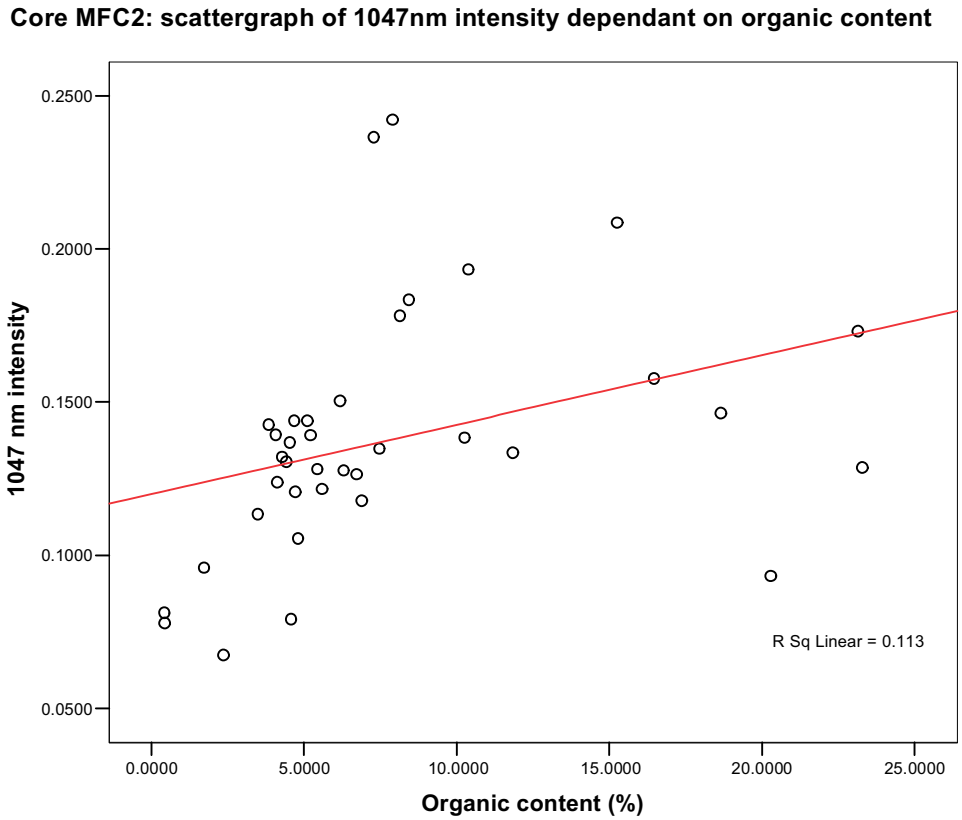

Fig 18: Core MFC2: 1047nm reflectance dependant on organic content.

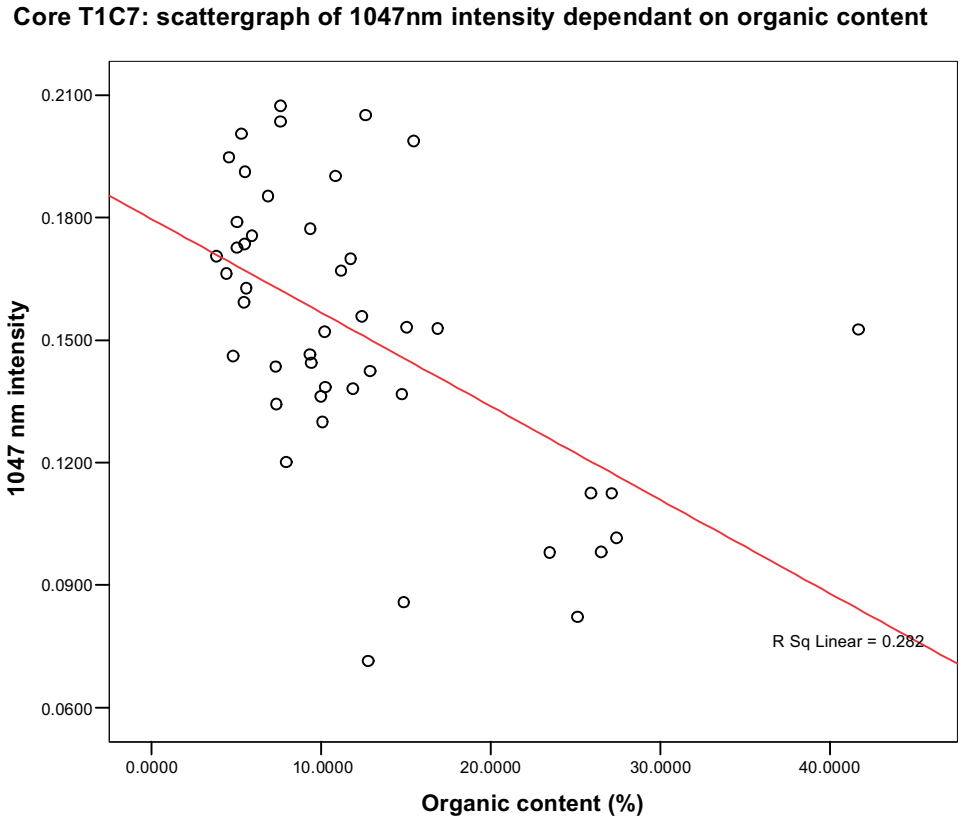

Fig 19: Core T1C7: 1047nm reflectance dependant on organic content.

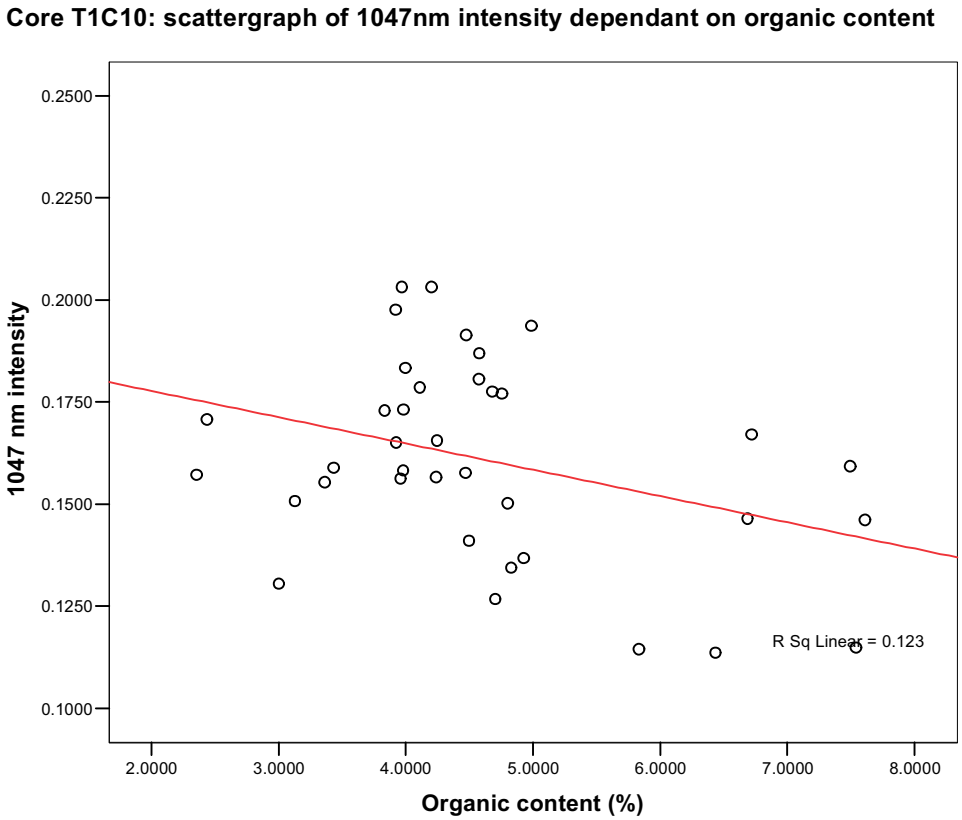

Fig 20: Core T1C10: 1047nm reflectance dependant on organic content.

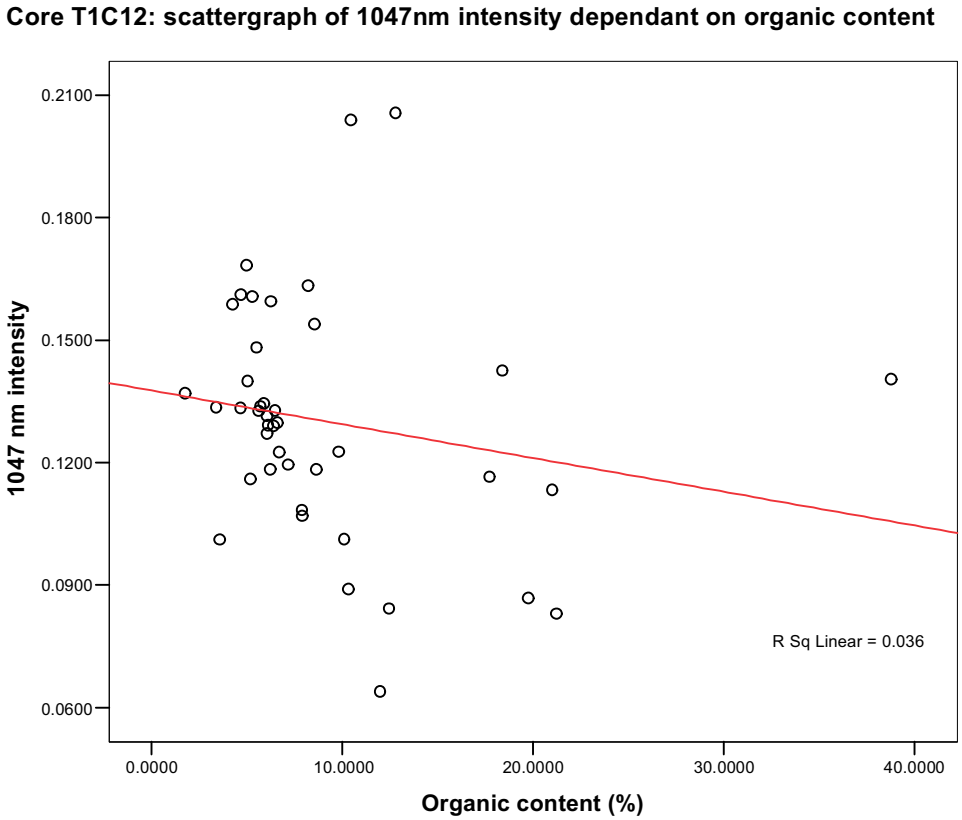

Fig 21: Core T1C12: 1047nm reflectance dependant on organic content.

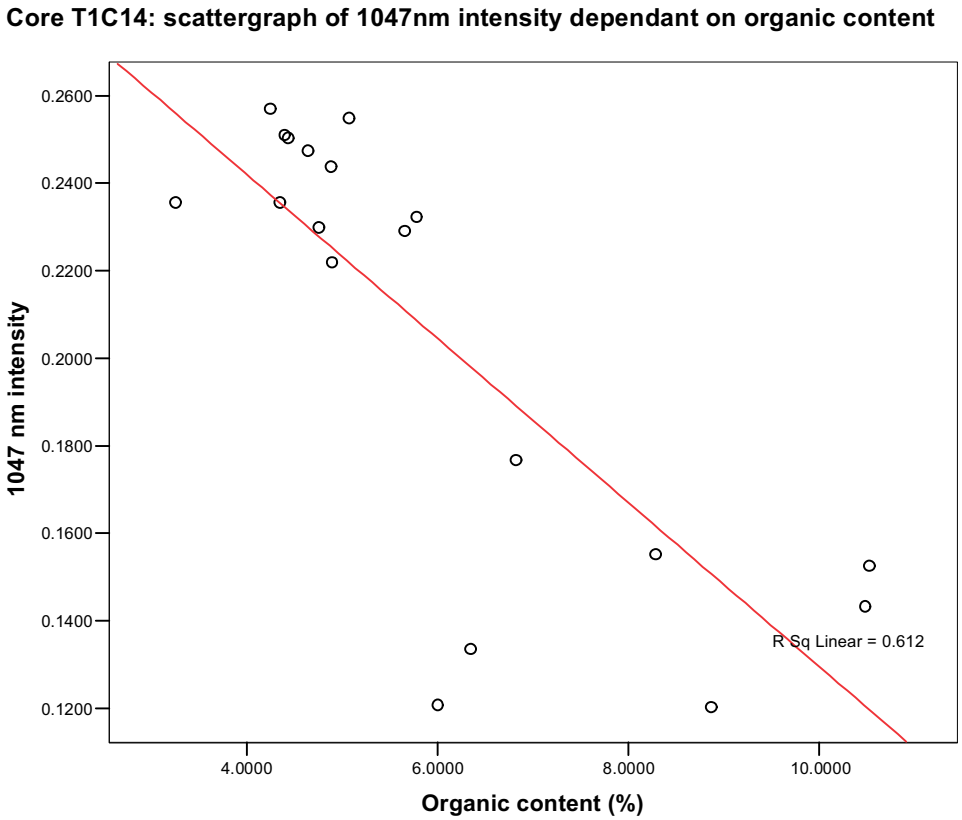

Fig 22: Core T1C14: 1047nm reflectance dependant on organic content.

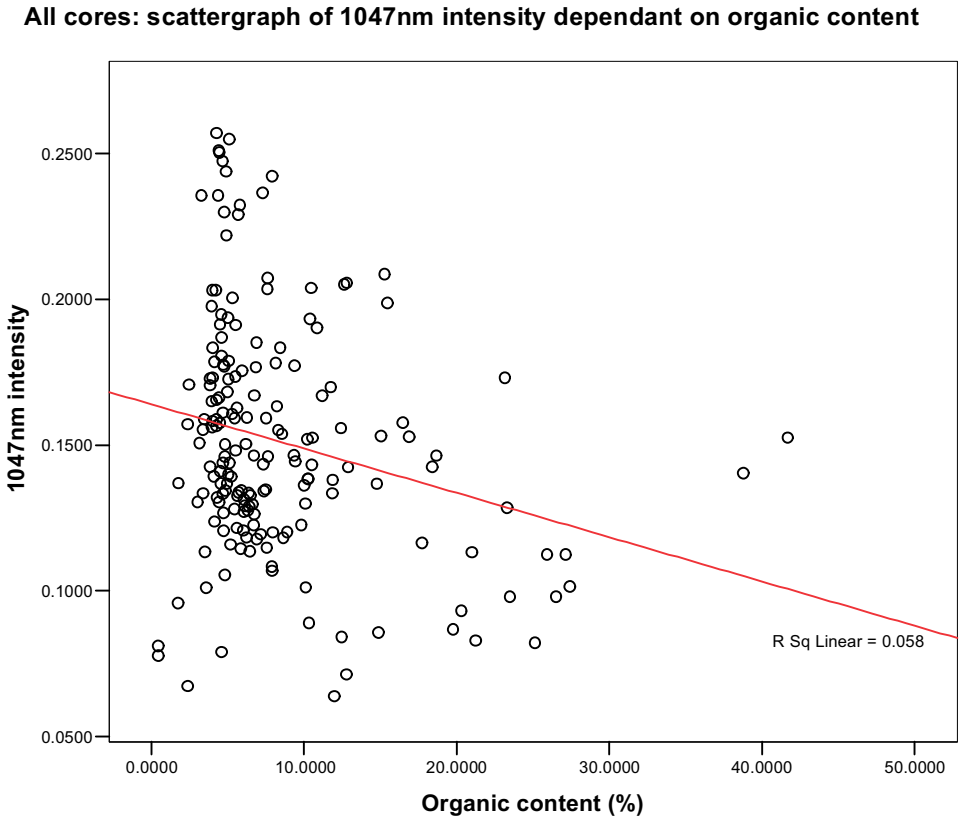

Fig 23: All core data set. 1047nm reflectance dependant on organic content.

Correlations

		Organic content coefficient	1047nm
Organic content coefficient	Pearson Correlation	1	-.240**
	Sig. (2-tailed)		.001
	N	180	180
1047nm	Pearson Correlation	-.240**	1
	Sig. (2-tailed)	.001	
	N	180	180

**. Correlation is significant at the 0.01 level (2-tailed).

Fig 24: All core data set. There is a highly significant relationship between the two variables at the 0.01 level, although this relationship is not visible as a linear function between the two variables.

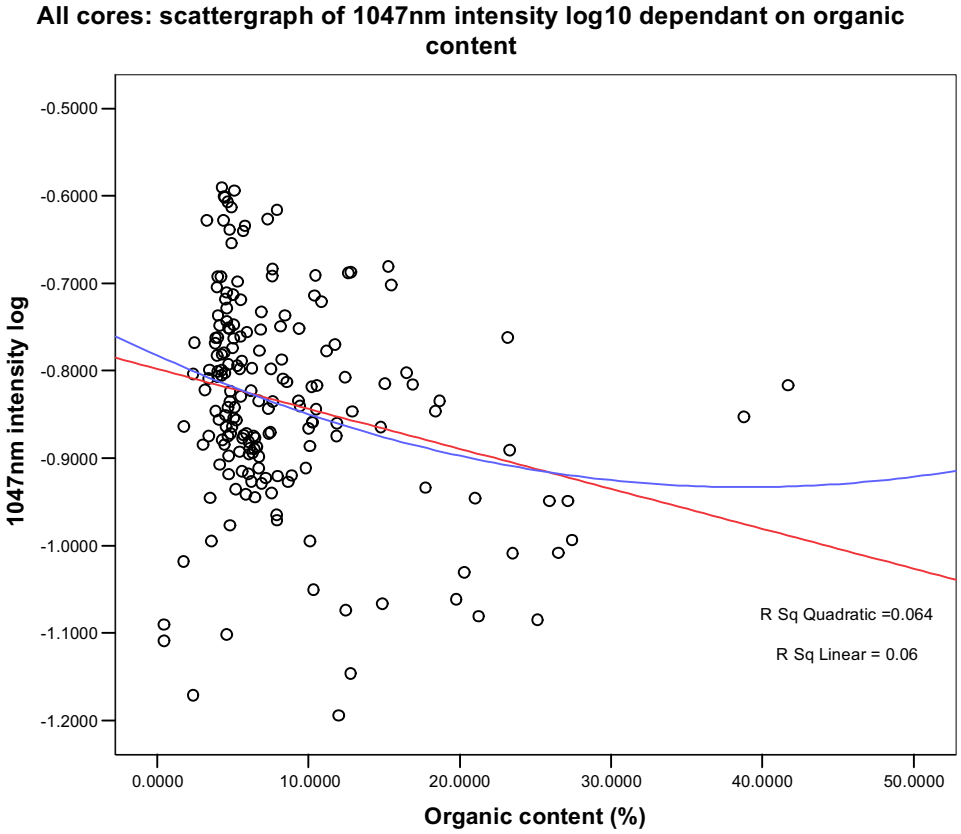

Fig 25: All core data set, log 1047nm reflectance. Even though a log response is used, there is still no obvious linear or quadratic relationship between the two variables.

2.5 RESULTS: 1047NM REFLECTANCE AND QUANTIFICATION OF RELATIONSHIP TO SEDIMENT CARBONATE CONTENT

This section again considers the analysis of the data occurs on a core-by-core basis and then through an all core data set. The linear relationship between carbonate content and 1047nm reflectance is extremely weak in all of the cores (Figs. 26 – 30), with a mixture of weak positive relationships (MFC2, T1C7, T1C12) and weak negative relationships (T1C10 and T1C14). The all core data revealed an overall weak negative correlation between 1047nm reflectance and carbonate content (Fig. 31).

A Pearson correlation coefficient was computed between the two variables and a significant relationship is seen at the 0.05 level (two tailed; Fig. 32). This is again surprising due to the inability to visualise the linear relationship between the two variables. A log 10 response of 1047nm reflectance was plotted against carbonate content and again no relationship between the two variables was visible in linear or quadratic forms (Fig. 33).

Again a strong relationship is described between 1047nm reflectance and a soil variable, this time carbonate content, but this relationship is not visualised. It is postulated that this relationship between 1047nm reflectance and carbonate content is indirect or incidental, i.e. 1047nm reflectance is not dependant on carbonate content, but both vary in a systematic way dependant on one or more other soil variables. It is interpreted that both are reflecting changes in sediment architecture, thus residual variance in the two variables caused through sediment architecture shows a highly significant correlation when 1047nm reflectance and carbonate content are analysed in isolation.

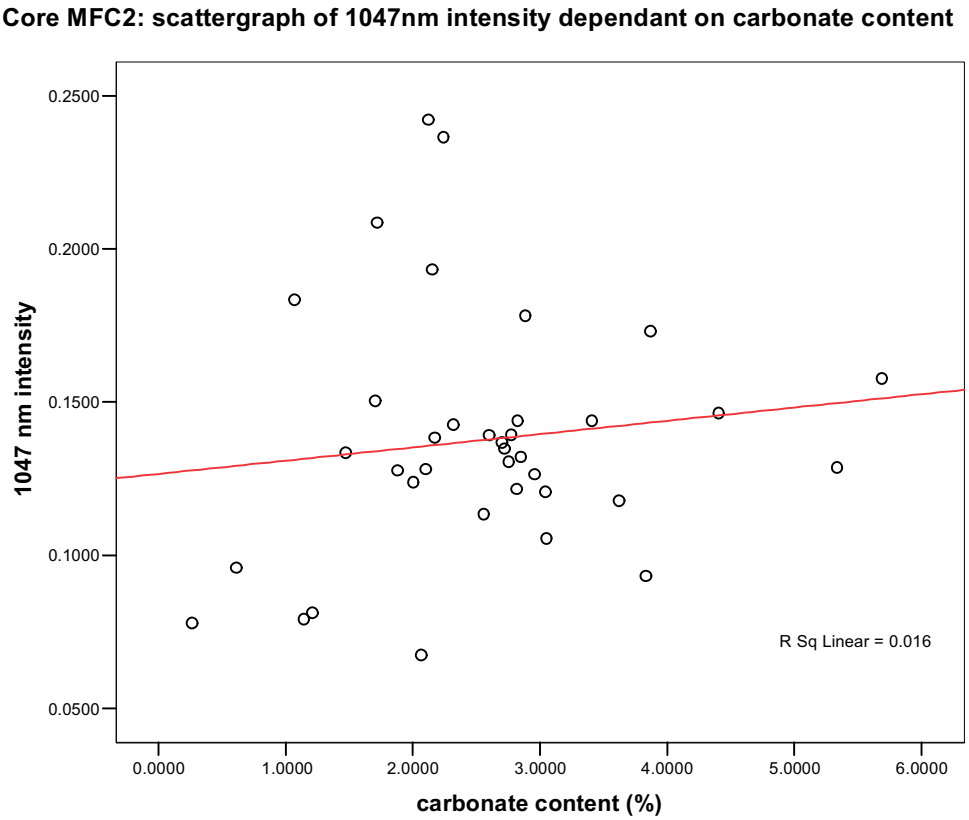

Fig 26: Core MFC2: 1047nm reflectance dependant on carbonate content.

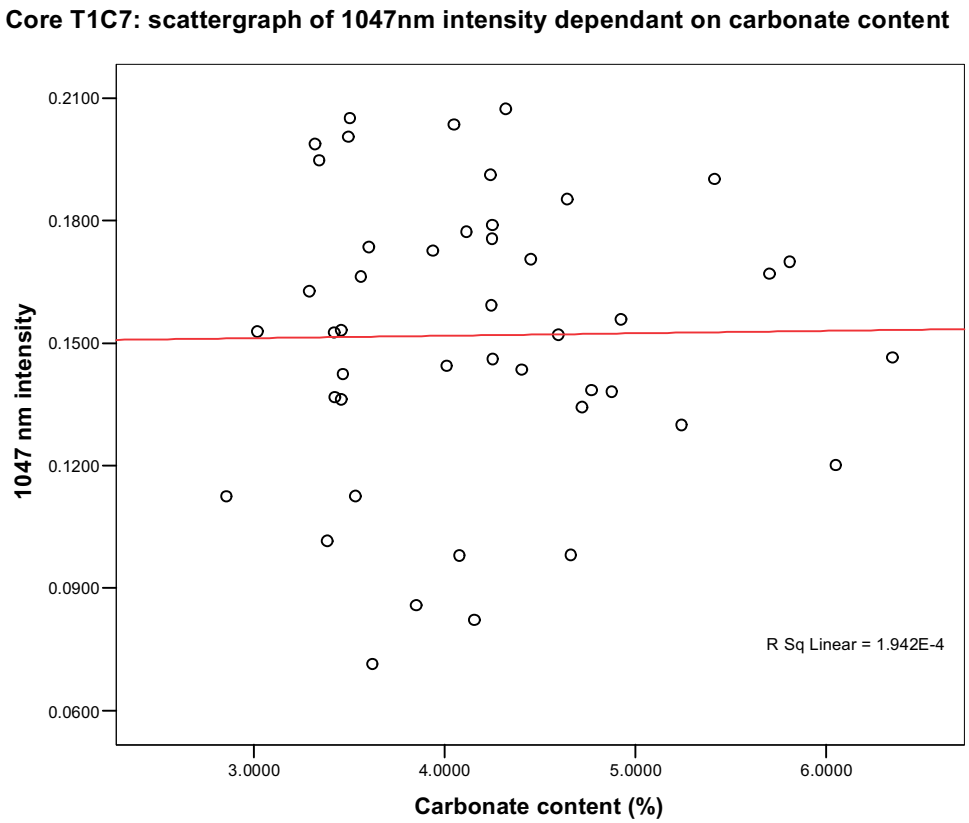

Fig 27: Core T1C7: 1047nm reflectance dependant on carbonate content.

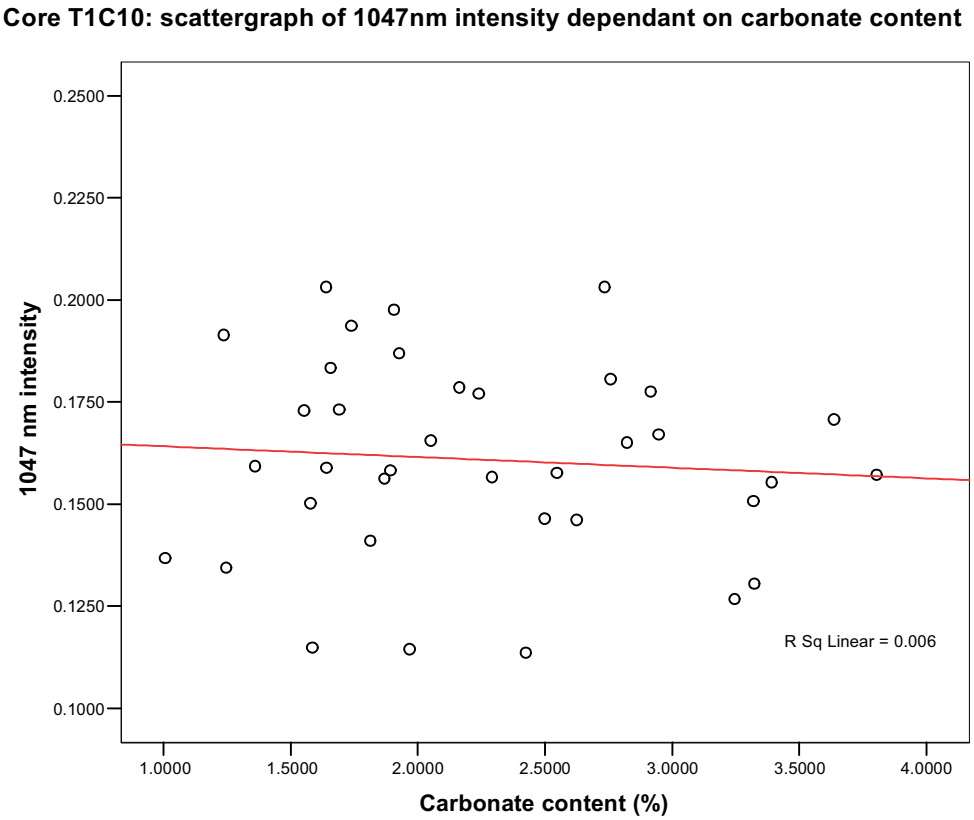

Fig 28: Core T1C10: 1047nm reflectance dependant on carbonate content.

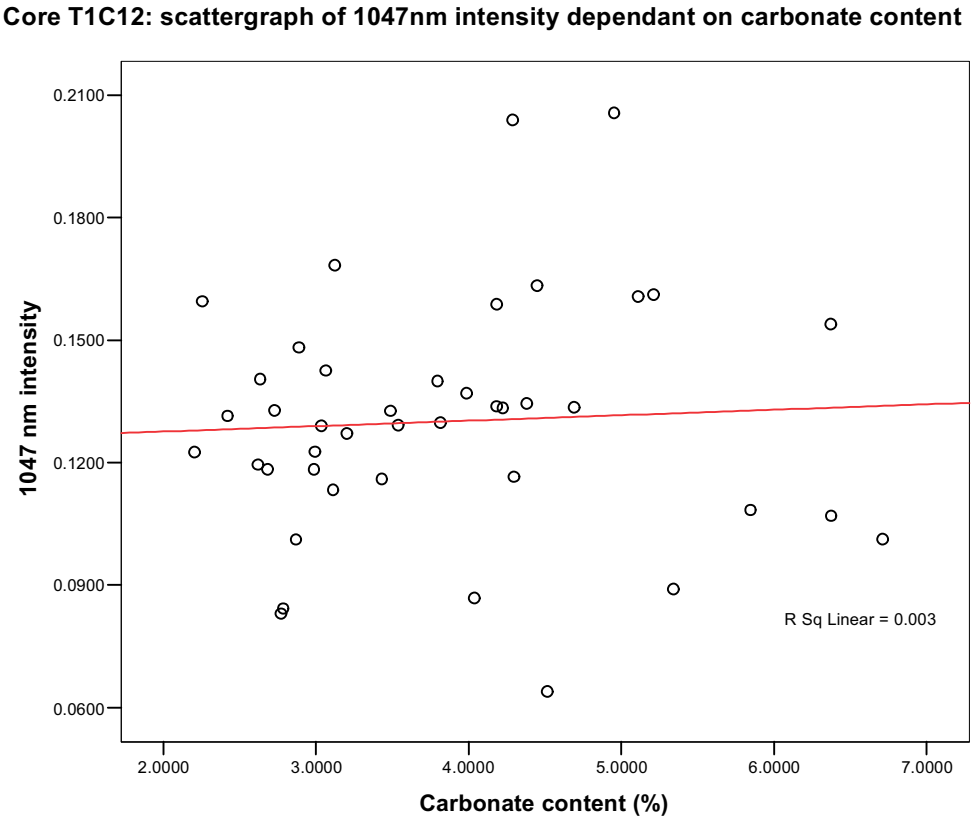

Fig 29: Core T1C12: 1047nm reflectance dependant on carbonate content.

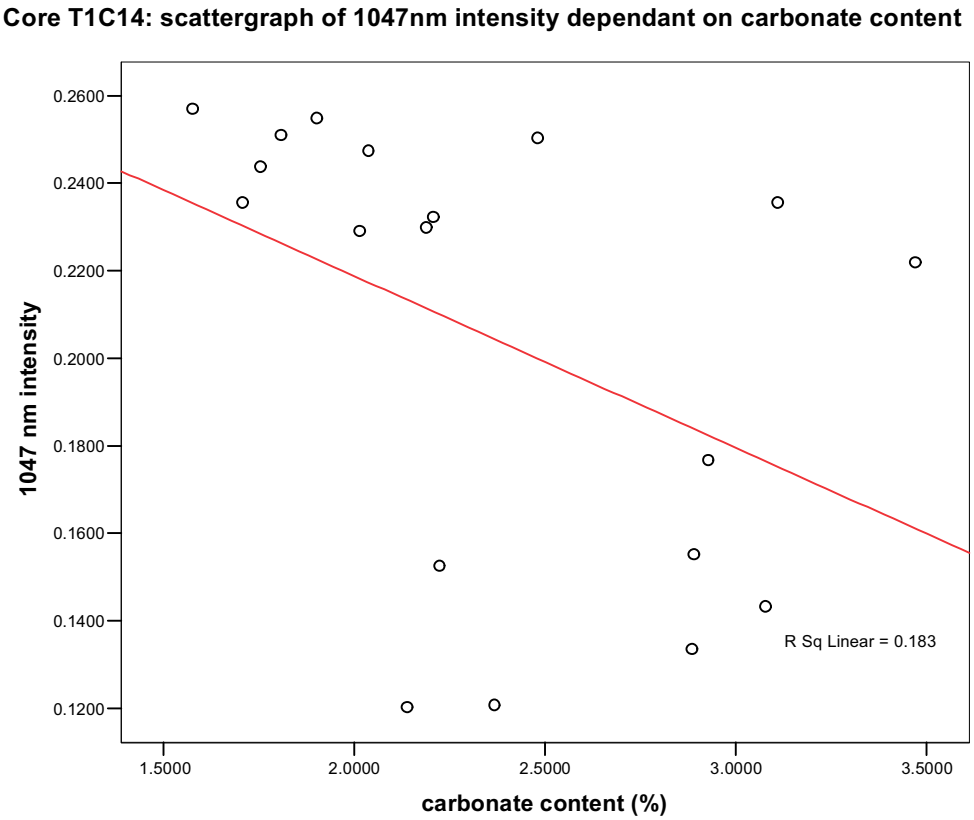

Fig 30: Core T1C14: 1047nm reflectance dependant on carbonate content.

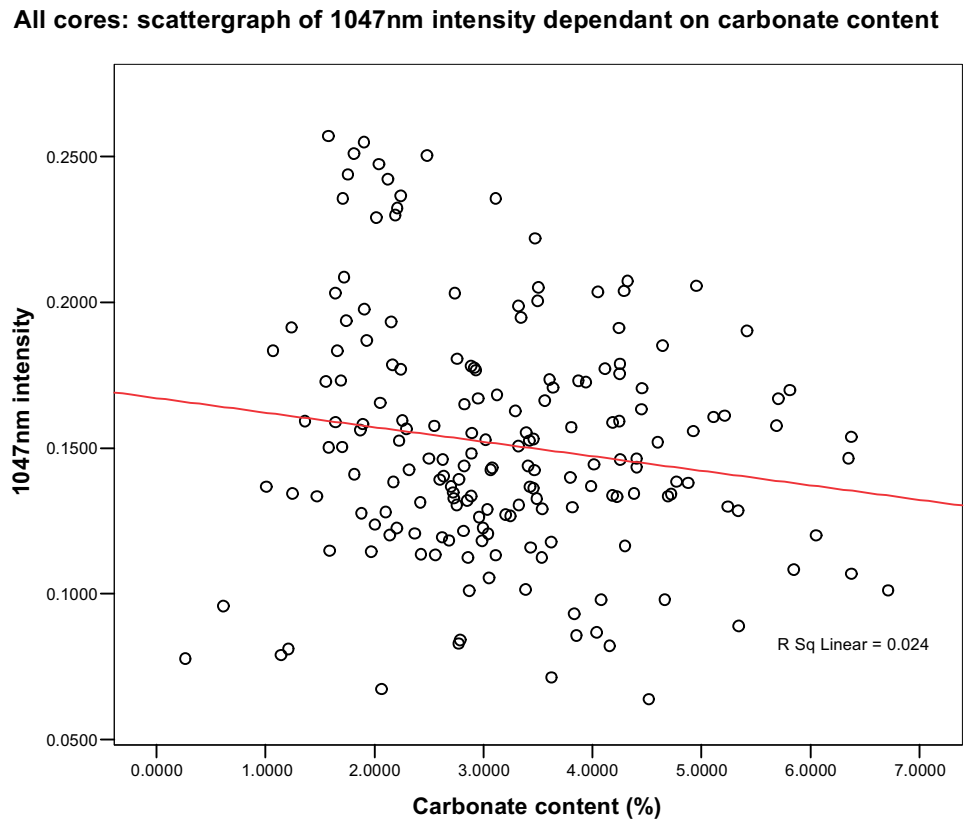

Fig 31: All core data set: 1047nm reflectance dependant on carbonate content.

Correlations

		1047nm	Carbonate content (%)
1047nm	Pearson Correlation	1	-.154*
	Sig. (2-tailed)		.040
	N	180	180
Carbonate content (%)	Pearson Correlation	-.154*	1
	Sig. (2-tailed)	.040	
	N	180	180

*. Correlation is significant at the 0.05 level (2-tailed).

Fig 32: All core data set. There is a significant relationship between the two variables at the 0.05 level, although this relationship is not visible as a linear function between the two variables.

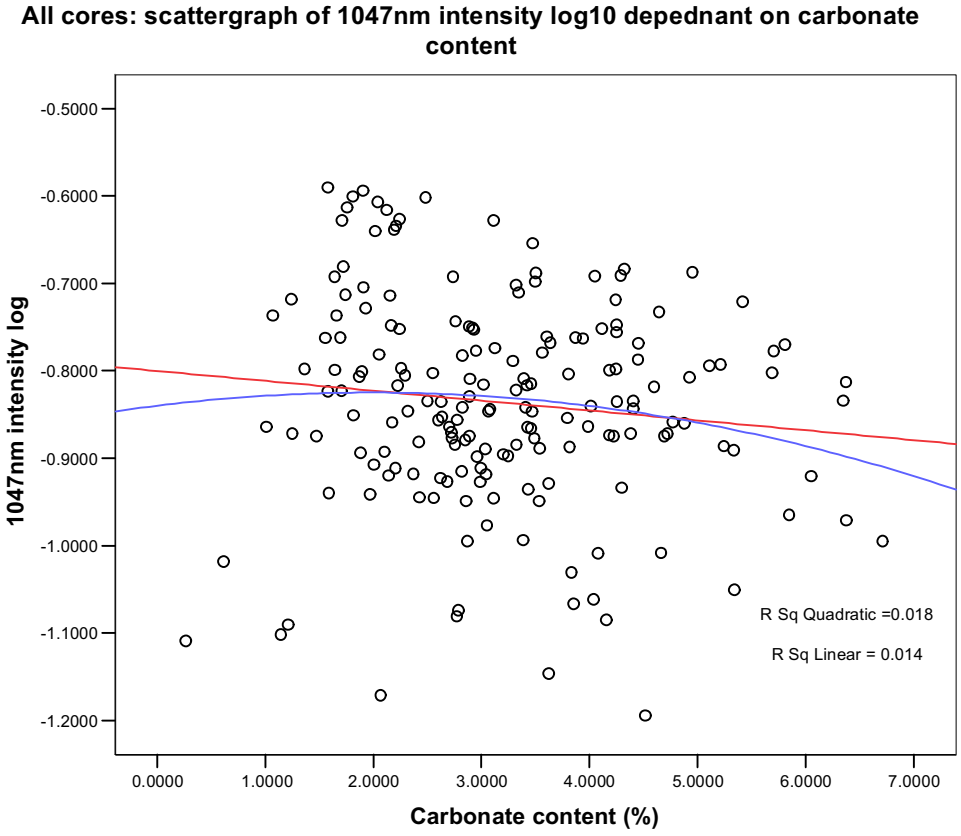

Fig 33: All core data set, log 10 1047nm reflectance dependant on carbonate content. Even though a log response is used, there is still no obvious linear or quadratic relationship between the two variables.

2.6 RESULTS: 1047NM REFLECTANCE AND QUANTIFICATION OF RELATIONSHIP TO SEDIMENT MAGNETIC SUSCEPTIBILITY

This section again considers the analysis of the data occurs on a core-by-core basis and then through an all core data set. The linear relationship between magnetic susceptibility and 1047nm reflectance again varies throughout the cores. Cores MFC2 and T1C7 both have an extremely low residual r squared value, showing virtually no systematic relationship between the two variables (Figs. 34 and 35). T1C10 has a slightly stronger negative relationship (Fig. 36), as does T1C12 (Fig. 37), with T1C14 having the strongest relationship between the two variables, with a residual r squared of 69% (Fig. 38). The all core data set shows the same general trend of a weak negative relationship between magnetic susceptibility and 1047nm reflectance (Fig. 39).

However, a Pearson correlation coefficient between the two variables again shows significance at the 0.05 level (two tailed, Fig. 40). This is again surprising due to the inability to visualise the relationship between the two variables. A log 10 response of 1047nm reflectance was plotted against magnetic susceptibility and again no relationship between the two variables was visible in linear or quadratic forms (Fig. 41).

Again a strong relationship is described between 1047nm reflectance and a soil variable, this time magnetic susceptibility, but this relationship is not visualised. It is postulated that this relationship between 1047nm reflectance and magnetic susceptibility is indirect or incidental, i.e. 1047nm reflectance is not dependant on magnetic susceptibility, but both vary in a systematic way dependant on one or more other soil variables. It is interpreted that both are reflecting changes in sediment architecture, thus residual variance in the two variables caused through sediment architecture is showing a highly significant correlation when 1047nm reflectance and magnetic susceptibility are analysed in isolation.

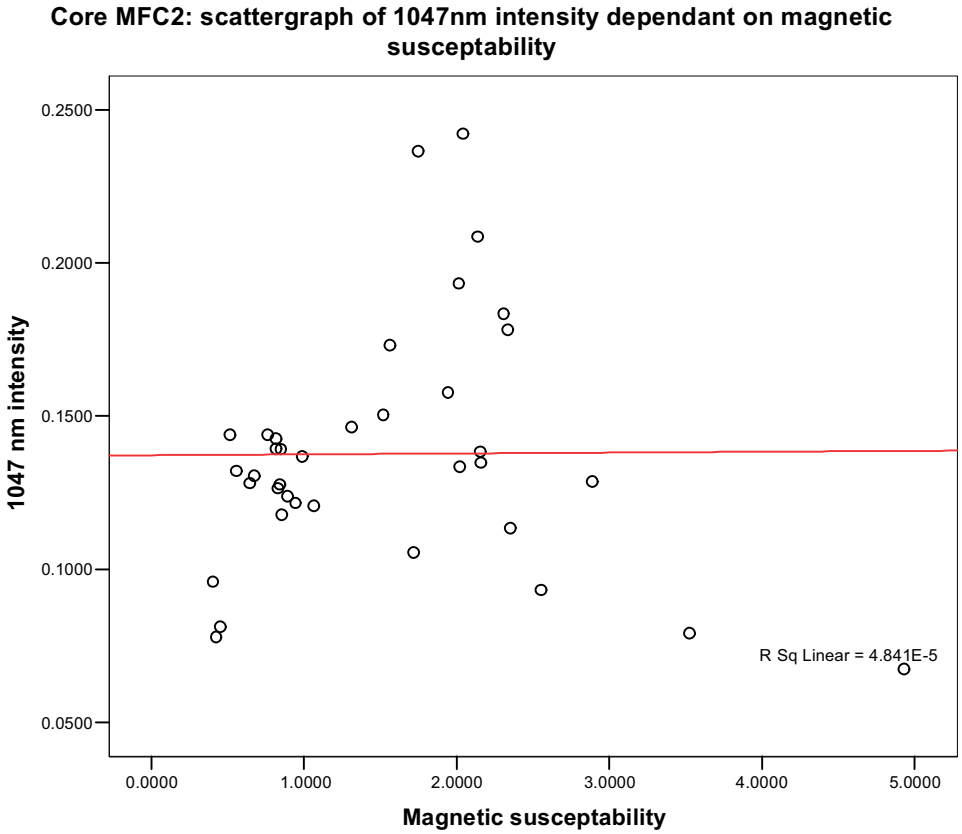

Fig 34: Core MFC2: 1047nm reflectance dependant on magnetic susceptibility.

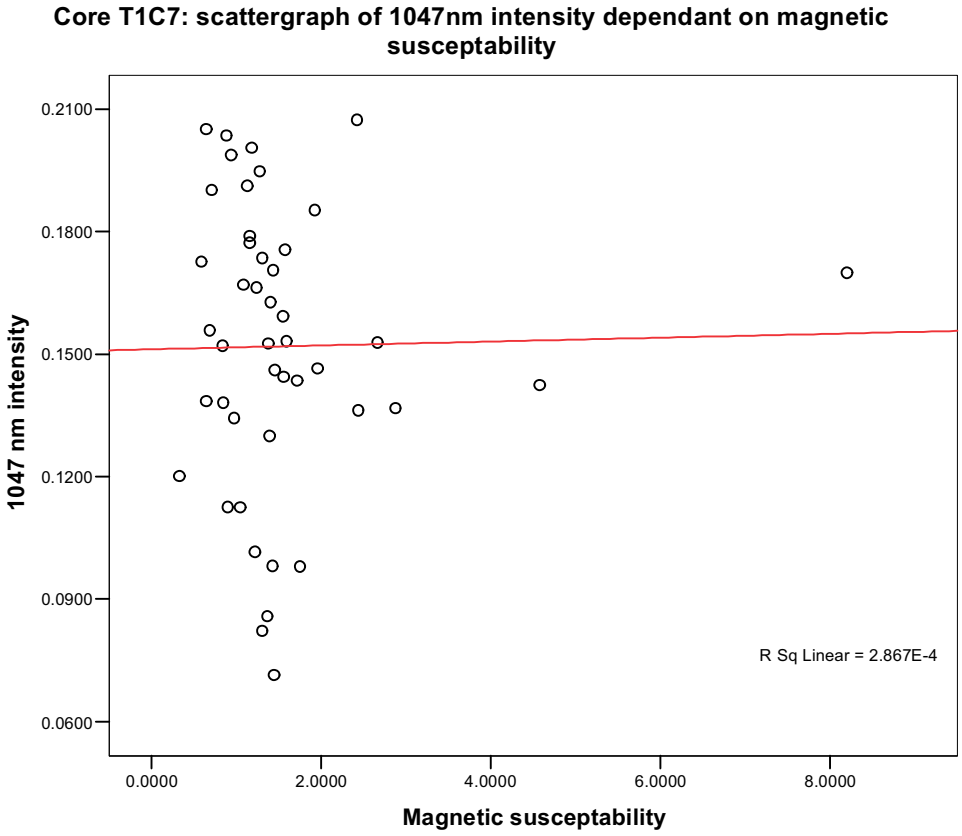

Fig 35: Core T1C7: 1047nm reflectance dependant on magnetic susceptibility.

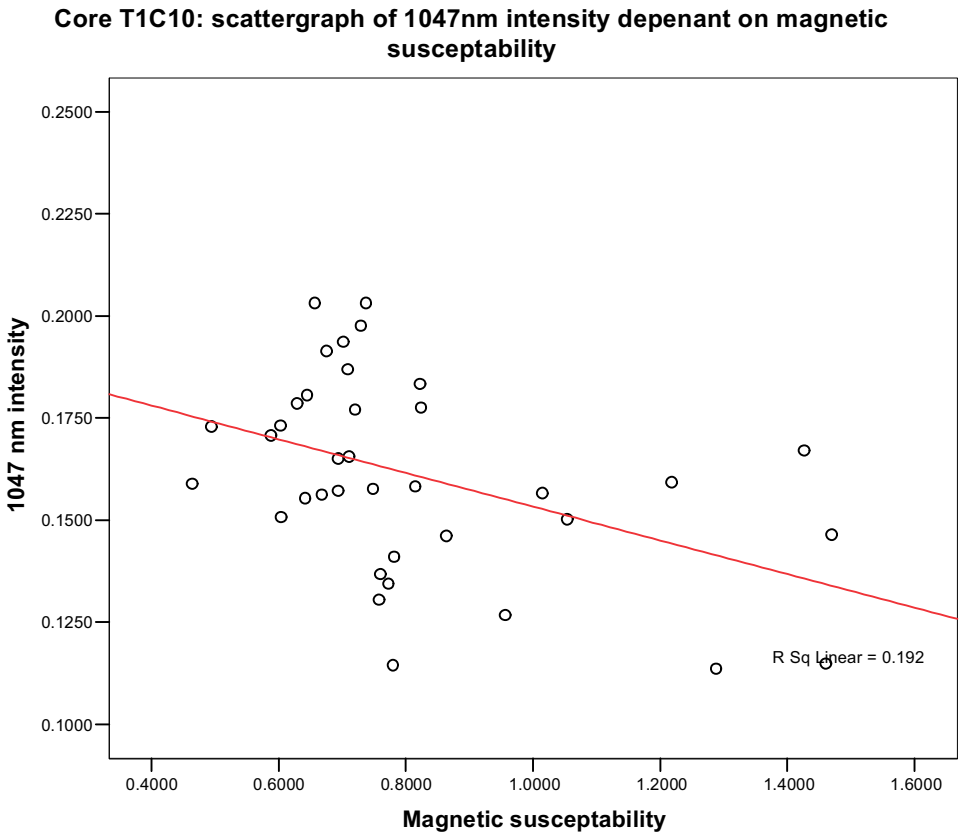

Fig 36: Core T1C10: 1047nm reflectance dependant on magnetic susceptibility.

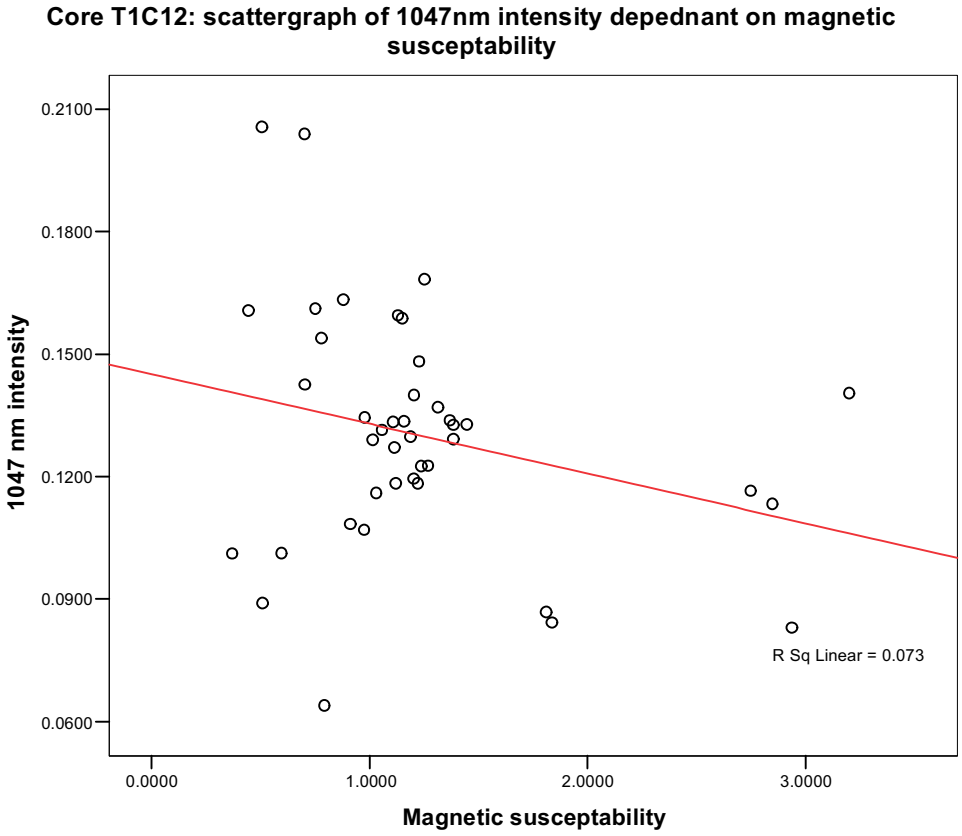

Fig 37: Core T1C12: 1047nm reflectance dependant on magnetic susceptibility.

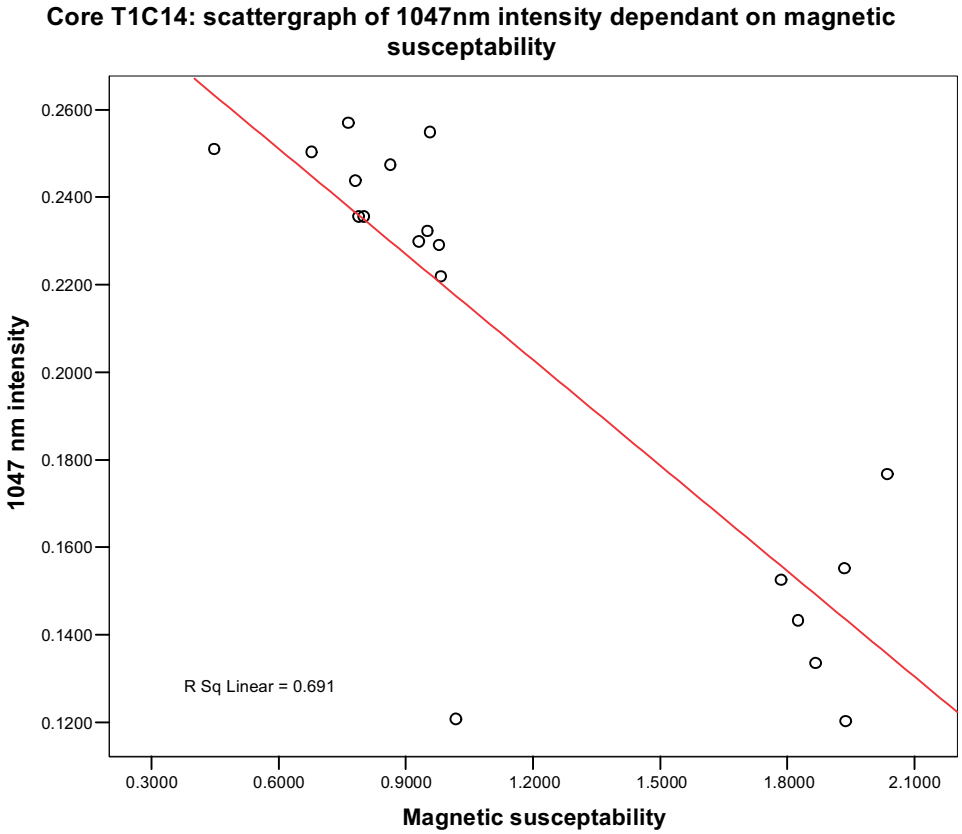

Fig 38: Core T1C14: 1047nm reflectance dependant on magnetic susceptibility.

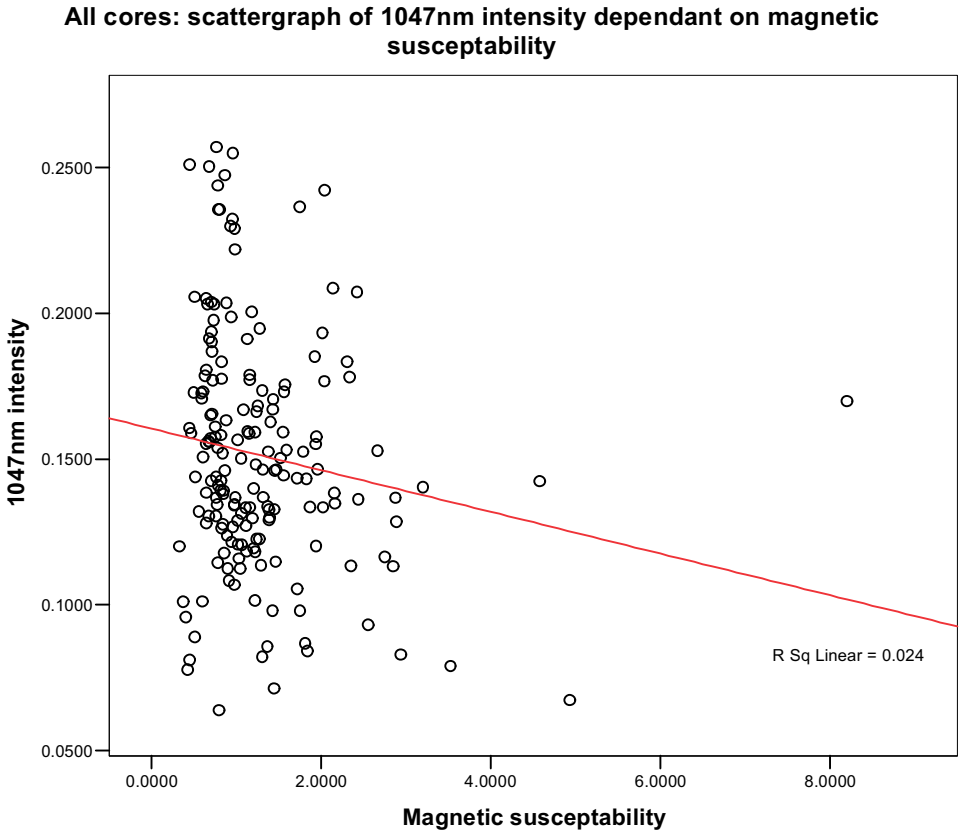

Fig 39: All core data set: 1047nm reflectance dependant on magnetic susceptibility.

Correlations

		1047nm	Magnetic susceptability
1047nm	Pearson Correlation	1	-.156*
	Sig. (2-tailed)		.037
	N	180	180
Magnetic susceptability	Pearson Correlation	-.156*	1
	Sig. (2-tailed)	.037	
	N	180	180

*. Correlation is significant at the 0.05 level (2-tailed).

Fig 40: All core data set. There is a significant relationship between the two variables at the 0.05 level, although this relationship is not visible as a linear function between the two variables.

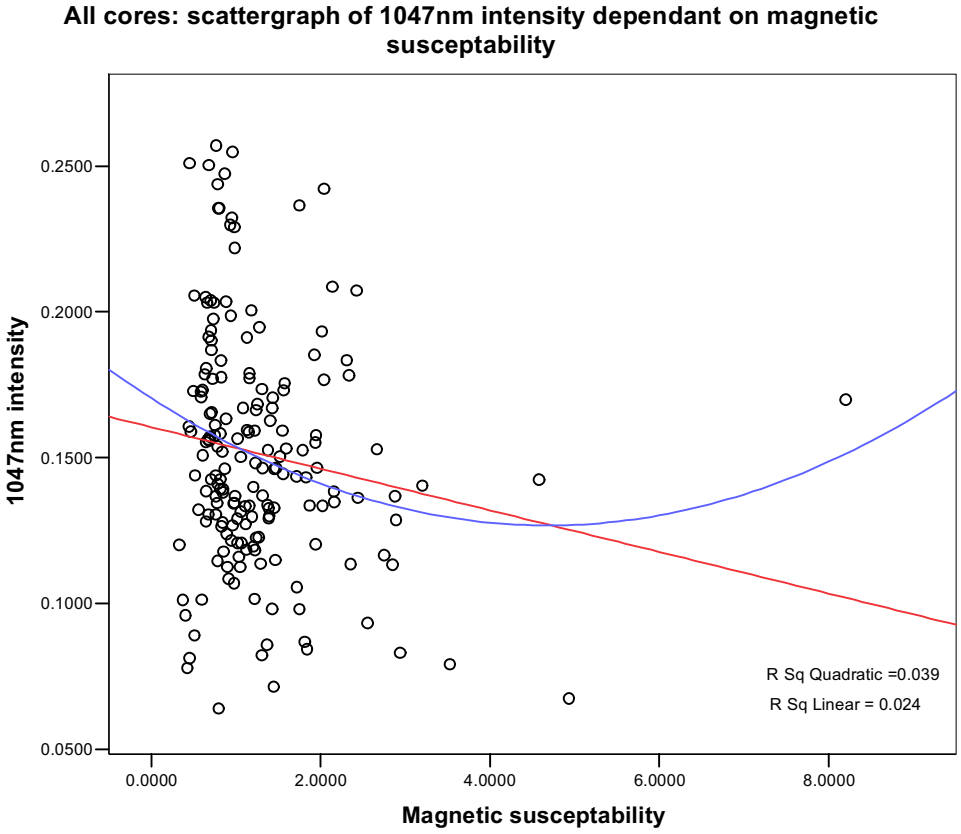

Fig 41: All core data set, log 10 1047nm reflectance dependant on organic content. Even though a log response is used, there is still no obvious linear or quadratic relationship between the two variables.

2.7 RESULTS: 1047NM REFLECTANCE AND QUANTIFICATION OF RELATIONSHIP TO SEDIMENT PH

The analysis of the data occurs on a core-by-core basis and then through an all core data set. The linear relationship between pH and 1047nm reflectance again varies throughout the cores. Again there is a mixture of positive and negative relationships within the data set. MFC2 has a weak negative relationship between 1047nm reflectance and pH (Fig. 42), T1C7 has no systematic relationship between the two variables (Fig. 43) and T1C10 has a weak negative relationship between the two variables (Fig. 44). Core T1C12 reveals a stronger positive relationship between the two, with a residual r squared value of 15.3% (Fig. 45), whilst T1C14 has a negative relationship between the two variables, with a residual r squared value of 34.3% (Fig. 46). The all core data set showed a very weak negative relationship between 1047nm reflectance and pH (Fig. 47), which the Pearson correlation coefficient agreed with (Fig. 48), accepting the null hypothesis that there is no significant relationship between the two variables at the 0.05 level.

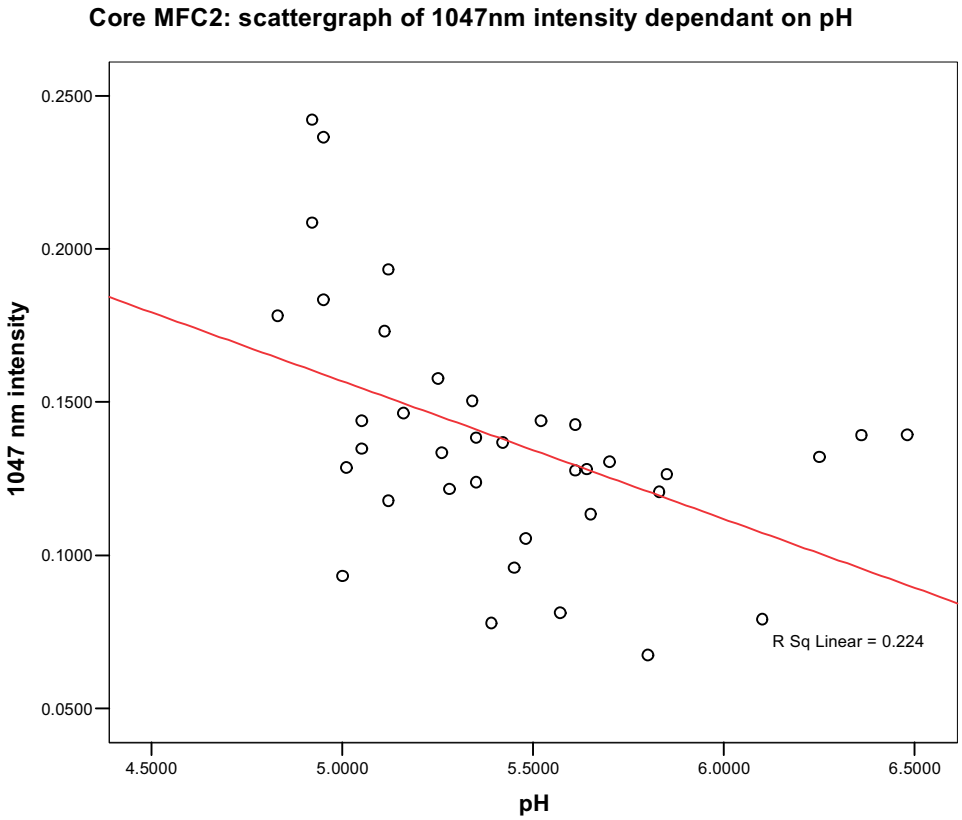

Fig 42: Core MFC2: 1047nm reflectance dependant on pH.

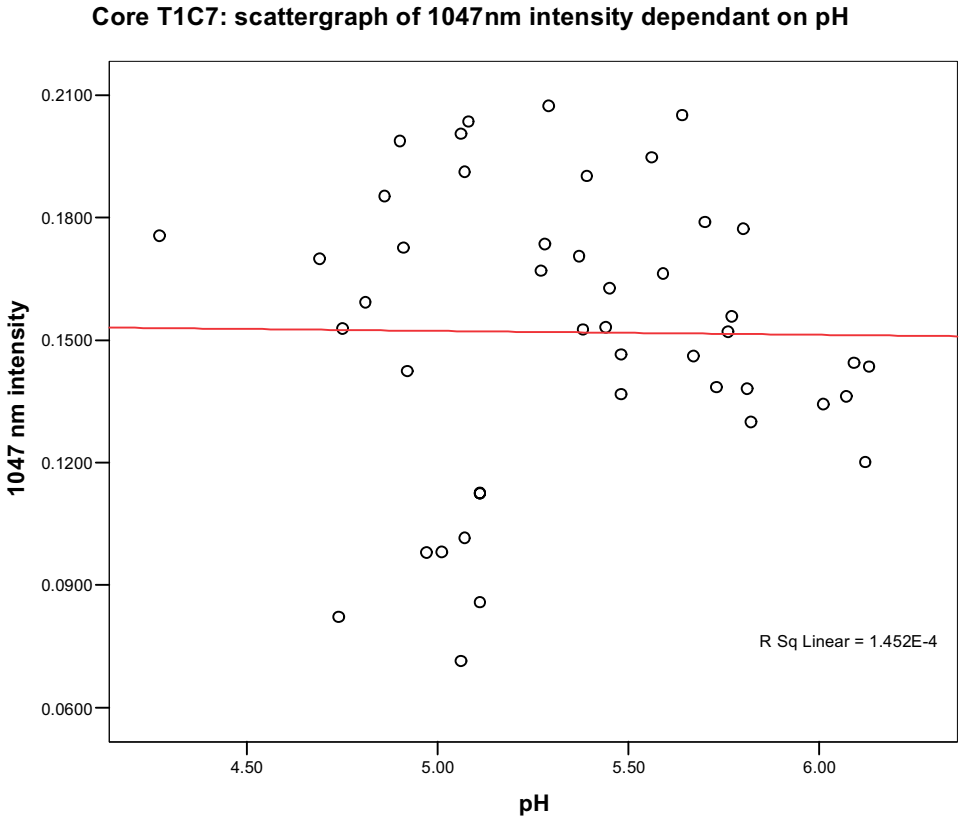

Fig 43: Core T1C7: 1047nm reflectance dependant on pH.

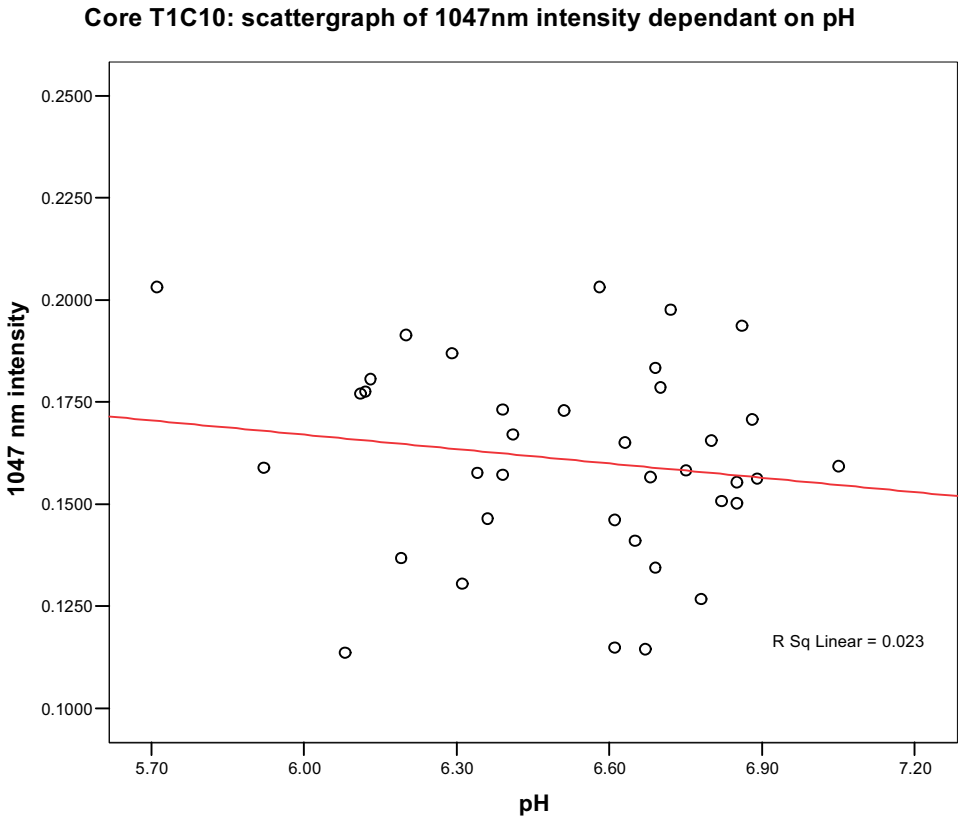

Fig 44: Core T1C10: 1047nm reflectance dependant on pH.

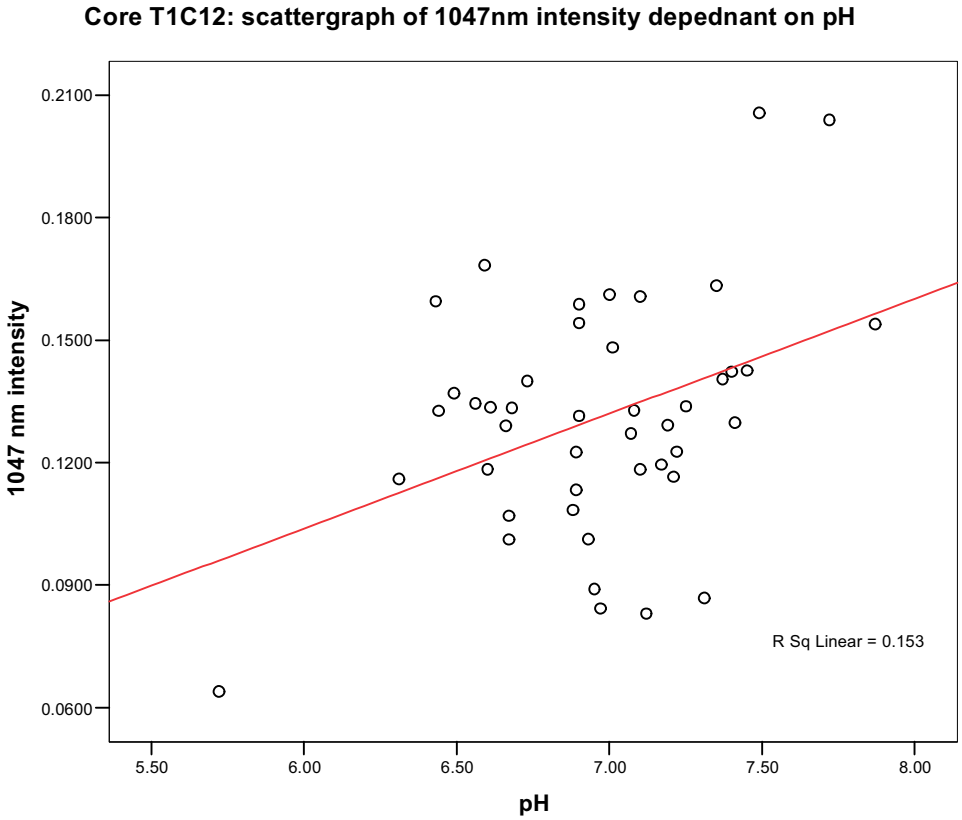

Fig 45: Core T1C12: 1047nm reflectance dependant on pH.

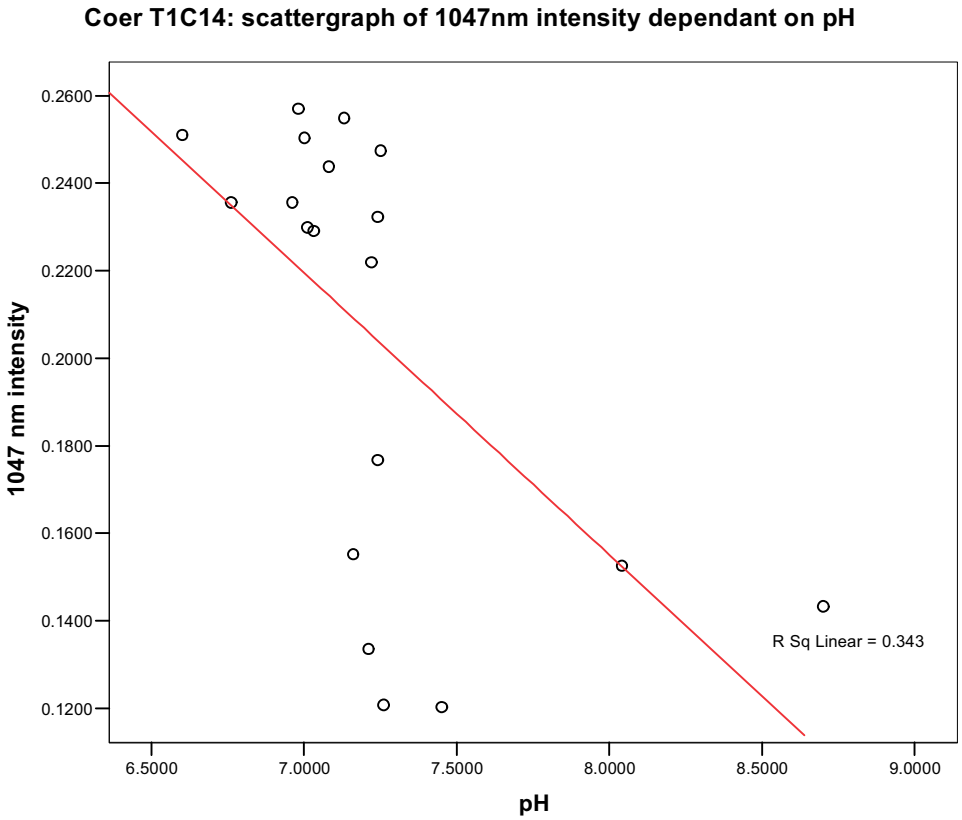

Fig 46: Core T1C14: 1047nm reflectance dependant on pH.

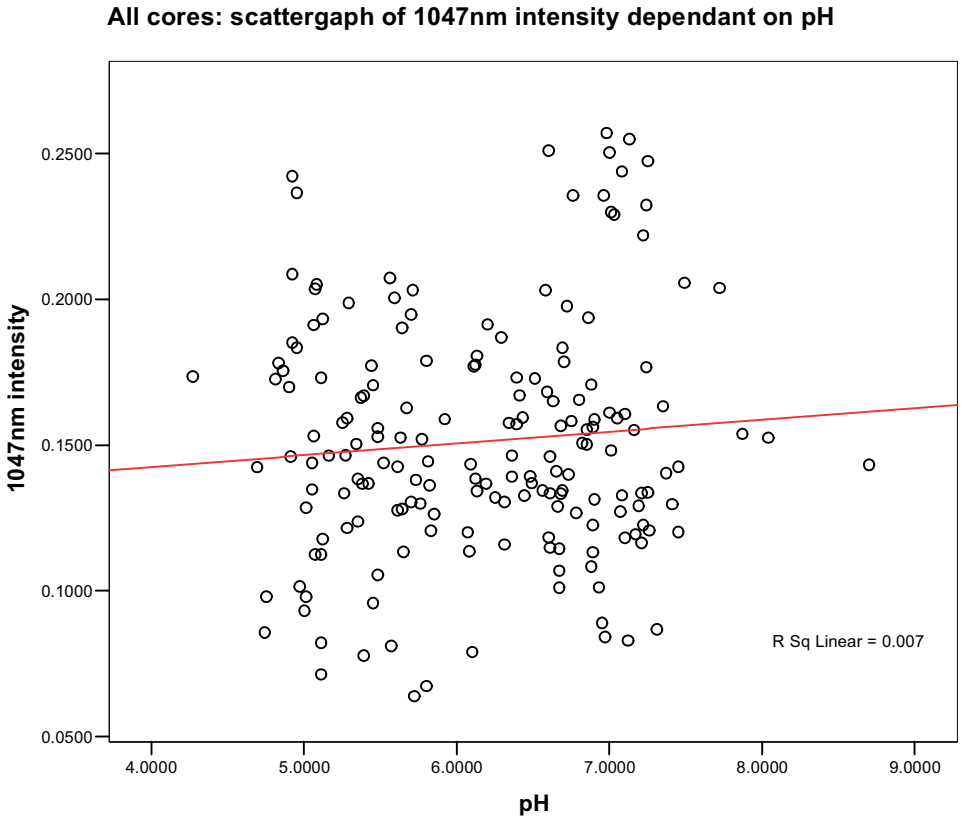

Fig 47: All cores data set: 1047nm reflectance dependant on pH.

Correlations

		1047nm	pH
1047nm	Pearson Correlation	1	.085
	Sig. (2-tailed)		.255
	N	180	180
pH	Pearson Correlation	.085	1
	Sig. (2-tailed)	.255	
	N	180	180

Fig 48: All core data set. There is no significant relationship between the two variables at the 0.05 level.

2.8 RESULTS: ANALYSIS OF THE ALL CORE POPULATION

The qualitative and quantitative analyses of the individual cores and all core data sets against univariable soil parameters had significant findings, summarised as:

- 1047nm reflectance has been qualitatively shown to reflect changes in sediment architecture.
- There are statistically significant relationships between 1047nm reflectance and organic content, carbonate content and magnetic susceptibility.
- These relationships were non linear and were not visualised through scattergraphs.
- The variation between cores does potentially exhibit *equi-finality*, in that different cores can show different relationships in 1047nm reflectance to the same variable, i.e. 1047nm reflectance dependant on organic matter had both positive and negative relationships in different cores.

Further work has already been conducted on the palaeoecological potential of these cores, as part of the project Predictive Modelling of Multi-period geoarchaeological resources at a river confluence phase II (Brown *et al.* 2007). From that analysis it is known that T1C7 and T1C12 had the highest preservation potential, then MFC2, with both T1C14 and T1C10 having low preservation potential. This simple grouping should be borne in mind for the analysis of the all core population.

2.8.1 Summary statistics of the cores

It was also clear that there was more information that could be extracted from this data set, other than simple univariable correlations with 1047nm dependant on a single soil parameter. Of importance is the between core variance. The between core variance allows the cores to be ordered by factors such as organic content, and this allows a comparison with the 1047nm response.

This approach feeds directly back into the assessment of remote sensed Lidar data. The between core evaluation using 1047nm reflectance is the same as using Lidar intensity to identify areas of high geoarchaeological potential, as different cores or sample locations are assessed based on 1047nm intensity. A summary of the cores 1047nm reflectance data gives the minimum, maximum, mean and top values and also the within core variance (Tab. 1). The cores show a large range in minimum values

ranging from T1C7 at 71.5% through to MFC2 at 6.8%. In contrast the maximum value shows limited between core variation, ranging from T1C14 at 25.7% through to T1C10 at 20.3%. The range shows T1C7 to have the highest range, T1C12 the second highest range, MFC2 to have the third highest range, T1C14 to have the fourth highest range and T1C10 to have the lowest range.

The mean values show T1C14 to have the highest mean, then T1C10, T1C7, T1C12 and lastly MFC2. Of the within core variance T1C14 has the highest level of variance (based on the sums of squares), then MFC2, with T1C7, T1C10 and T1C12 all being the same. It is interesting that T1C14 provides the highest level of within core variance and the highest mean value, as this is the core that demonstrated the strongest relationship between 1047nm reflectance and organic matter, carbonate content and magnetic susceptibility. It is possible that the larger variance, within a smaller data set, allowed a greater contrast in 1047nm reflectance on the T1C14 core, allowing relationships to be visualised.

The top value is especially important in this analysis as it allows the comparison of cores, based on the intensity reading at the top of each core. This reading is analogous to what would be seen based on the remote sensed 1047nm backscatter data, if the terrain was in a bare earth condition with all vegetation removed. Of these T1C10 has the highest value, then T1C7, then T1C14, then T1C12 and lastly MFC2. This would effectively be the order of these sample locations based on intensity. Thus is there a relationship between these surface readings and the sub-surface sediment architecture and hence geoarchaeological potential?

Core	Min value	Max value	Range	Mean value	Top value	Within population variance	Sample population
MFC2	.0675	0.2423	0.1748	0.1377	0.1366	0.002	37
T1C7	0.7150	0.2074	0.5076	0.1520	0.1527	0.001	45
T1C10	0.1137	0.2032	0.0895	0.1609	0.1594	0.001	37
T1C12	0.640	0.2057	0.4343	0.1301	0.1405	0.001	42
T1C14	0.1204	0.2571	0.1367	0.2049	0.1434	0.003	19

Tab 1: Summary statistics of the between cores analysis. The top value is particularly useful in this comparison as it allows a qualification of the surface intensity values against within core variation. This effectively summarises the surface to sub surface relationship of the sediments.

2.8.2 Mean organic content and mean 1047nm reflectance of the cores

The cores are shown with mean 1047nm reflectance and mean organic content (converted from a percentage to a coefficient through dividing by 100; Fig. 49). The data shows that although T1C14 has the highest mean intensity value it does not have the lowest mean organic value. T1C7 has the highest mean organic content, but the third highest mean intensity value. Thus the negative relationship between 1047nm and organic content does not hold true on a mean value basis for each core. This may not be surprising as each core was composed of a variety of different sediment units.

Through looking at the within core variance this distribution within the data is further detailed and there is a clear disparity within the data set (Fig. 50). T1C10 displays a low degree of variance of in both 1047nm reflectance and organic content, but has

more variance in the 1047nm reflectance data than the organic content. Conversely, T1C7 shows a high degree of variance in the organic content but a low degree of variance in 1047nm intensity, as does T1C12 and to a lesser degree MFC2. T1C14 is more unusual in that it has a higher degree of 1047nm intensity, with a much lower level of organic content variance. The variance of 1047nm reflectance compared to variance of organic content does highlight T1C10 and T1C14 as being substantially different to T1C7, T1C12 and MFC2. This demonstrates that there is not a predictable pattern between the mean organic content and the mean 1047nm reflectance of the cores.

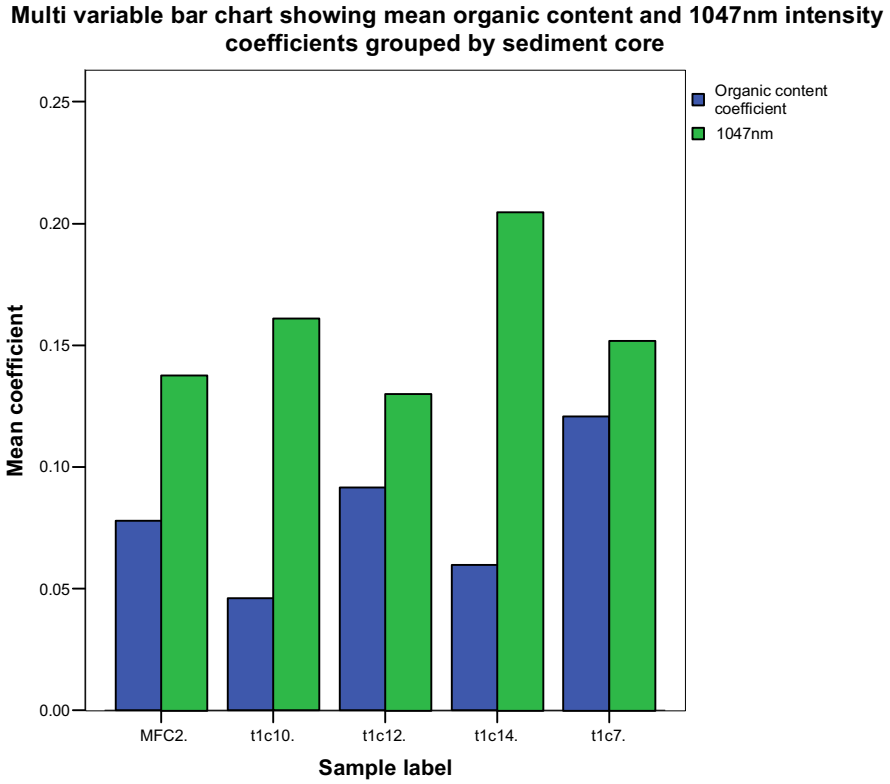

Fig 49: The between core analysis of 1047nm reflectance and organic content based on core means.

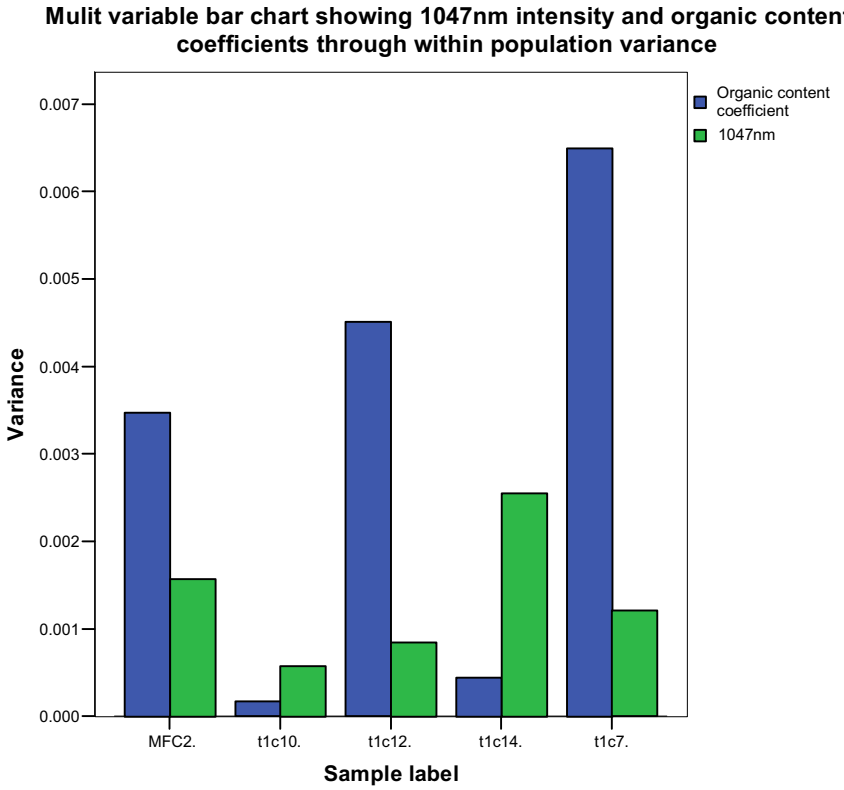

Fig 50: The between core analysis of 1047nm reflectance and organic content based on core variance.

2.8.3 Surface 1047nm reflectance and surface organic content of the cores

The top intensity values (Fig. 51) and the top organic values (Fig. 52) for each core are shown, which are effectively the ground surface from where the core was sampled. T1C10 has the highest intensity value and the lowest organic content value, which is consistent with a negative relationship between the two variables. However, T1C7 has the next highest surface intensity reading and the highest surface organic content. T1C14 has the fourth highest organic content and third highest intensity reading. Again it appears there is little predictive capacity between the 1047nm reflectance response and the organic content. From this simple analysis of the top of core sediment samples it would be easier to predict that cores T1C7 and TC12 have a higher geoarchaeological potential due to their higher organic content, rather than their intensity readings.

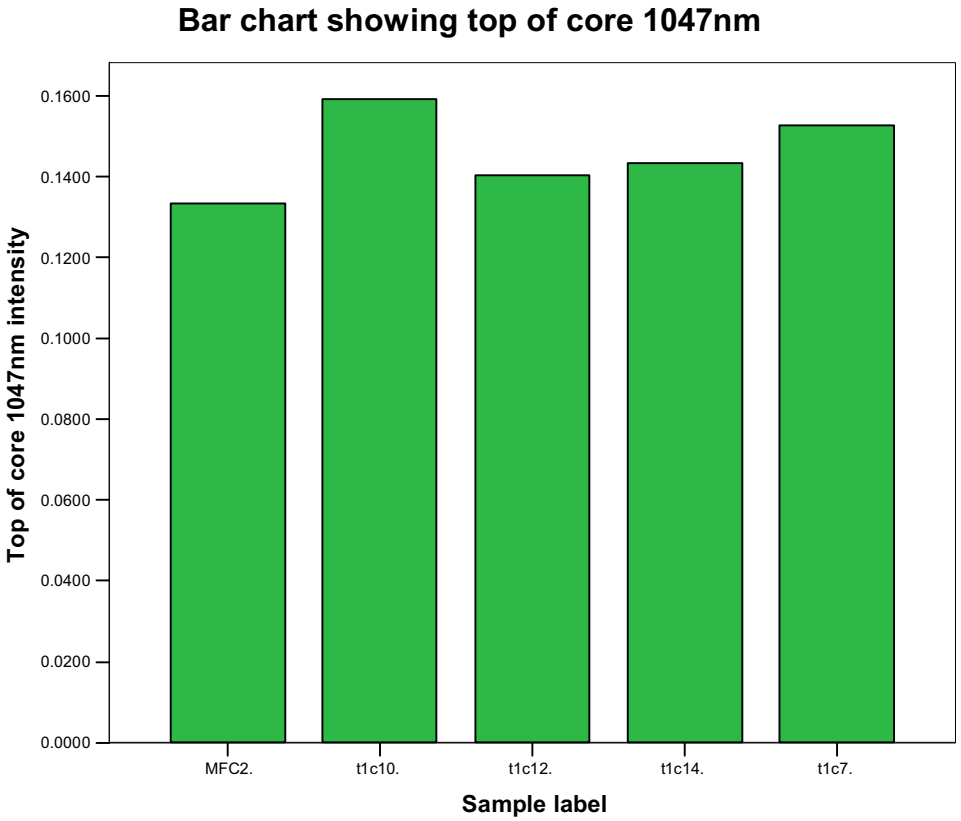

Fig 51: The top value of 1047nm reflectance for each of the cores.

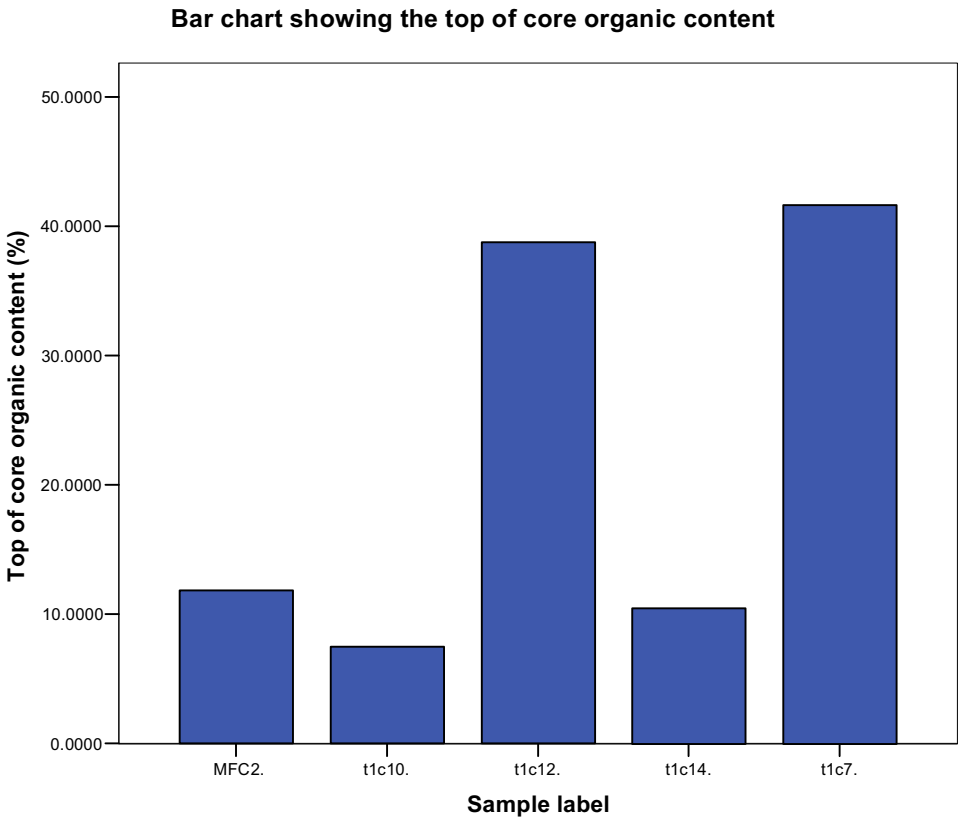

Fig 52: The top value of organic content for each of the cores.

2.8.4 Surface to sub surface relationships of the cores

To compare the surface 1047nm reflectance readings with the subsurface sediment architecture, the palaeochannels were ranked by surface intensity, mean organic core content and number of stratigraphic units (Tab. 2). As can be seen MFC2 has the most complex below sediment architecture (most recorded stratigraphic units) and has the lowest surface 1047nm reflectance reading. T1C12 has the next lowest 1047nm reflectance reading and has the second highest number of stratigraphic units. T1C14 and T1C7 both have four sediment units and have the third and fourth lowest intensity readings. T1C10 has the highest intensity reading and 5 stratigraphic units.

Whilst care must be taken in making generalisations from the ranking of the surface 1047nm reflectance and number of stratigraphic units, due to the small population size (the sample population = 5), it does appear that increasing complexity in stratigraphy produces lower surface 1047nm reflectance values. However, the relationship between surface intensity, number of stratigraphic units and mean core organic content is not clear, with seemingly no relationship between mean organic content and the other two variables.

Core	Surface intensity rank	Number of core stratigraphic units	Mean core organic content rank
MFC2	5 (lowest)	8	3
T1C7	2	4	1 (highest)
T1C10	1 (highest)	5	5 (lowest)
T1C12	4	6	2
T1C14	3	4	4

Tab 2: Relationship of surface 1047nm reflectance values and sub surface sediment architecture.

2.8.5 Creation of homogenous subsets of the cores

As a final means of analysis the mean organic content and the mean 1047nm reflectance was compared between the cores, to look at any similarity in pattern. The means were compared using a one way ANOVA, with a Duncan's multiple range *post-hoc* test, to create homogeneous subsets. All testing was done at the 0.05 level. There are uneven sample sizes and this can exert leverage on the different sample populations, thus care must be taken in the interpretation of the results.

The ANOVA for the organic content showed there was significant differences between the five cores, T1C7 with the highest organic content, MFC2 and T1C12 as the second highest subset, MFC2 and T1C14 as the third highest subset and T1C14 and T1C10 as the lowest subset (Figs. 53 and 54). For contrast the ANOVA for the 1047nm reflectance also showed significant differences between the cores. T1C14 was the highest subset, then T1C14 and T1C10, then T1C10 and T1C7, then the subset of T1C7 and MFC2 and the lowest subset of MFC2 and T1C12 (Figs. 55 and 56).

The comparison of means is interesting as it shows a broad general pattern that is almost exactly reversed between the two analyses. The order is slightly different, but T1C10 and T1C14 are the bottom organic subset and top intensity subset. In contrast T1C12 has the second highest organic content but has the lowest 1047nm reflectance

ranking, and so forth. However, the pattern is not exact, with T1C7 having the highest mean organic content but third lowest intensity mean.

The pattern can be interpreted through sorting the cores into two fairly homogeneous groups. Firstly there is the first homogeneous grouping of T1C14 and T1C10. This group has low organic content, high 1047nm reflectance values. There is a second homogeneous grouping consisting of T1C7, T1C12 and MFC2, both of which have higher mean organic contents and therefore have a much higher potential for the preservation of palaeoecological remains, but lower 1047nm reflectance values. This pattern is interesting as it closely corresponds with the summary statistics of the cores (Tab. 1), with T1C7 having the highest range in 1047nm intensity, then T1C12, then MFC2, then T1C14 and lastly T1C10.

ANOVA

Organic content (%)

	Sum of Squares	df	Mean Square	F	Sig.
Between Groups	1293.891	4	323.473	9.279	.000
Within Groups	6100.720	175	34.861		
Total	7394.611	179			

Fig 53: ANOVA analyses of the organic content between the cores. There are significant differences between the cores.

Organic content (%)

	Core	N	Subset for alpha = .05			
			1	2	3	4
Duncan[a,b]	T1C10	37	4.609997			
	T1C14	19	5.980169	5.980169		
	MFC2	37		7.790369	7.790369	
	T1C12	42			9.161667	
	T1C7	45				12.092844
	Sig.		.349	.216	.349	1.000

Means for groups in homogeneous subsets are displayed.

a. Uses Harmonic Mean Sample Size = 32.740.

b. The group sizes are unequal. The harmonic mean of the group sizes is used. Type I error levels are not guaranteed.

Fig 54: Duncan's multiple range test of the organic content ANOVA, showing a spread of homogeneous subsets, with T1C7 highest and T1C10 lowest.

ANOVA

1047nm

	Sum of Squares	df	Mean Square	F	Sig.
Between Groups	.084	4	.021	17.297	.000
Within Groups	.212	175	.001		
Total	.295	179			

Fig 55: ANOVA analyses of the 1047nm reflectance between the cores. There are significant differences between the cores.

1047nm

	Core	N	Subset for alpha = .05			
			1	2	3	4
Duncan[a,b]	T1C12	42	.130143			
	MFC2	37	.137749	.137749		
	T1C7	45		.151992	.151992	
	T1C10	37			.160979	
	T1C14	19				.204892
	Sig.		.377	.099	.297	1.000

Means for groups in homogeneous subsets are displayed.

a. Uses Harmonic Mean Sample Size = 32.740.

b. The group sizes are unequal. The harmonic mean of the group sizes is used. Type I error levels are not guaranteed.

Fig 56: Duncan's multiple range test of the 1047nm reflectance ANOVA, showing a spread of homogeneous subsets, with T1C14 highest and T1C12 lowest.

2.9 SUMMARY OF THE MAIN POINTS OF THE 1047NM REFLECTANCE ANALYSIS

A lot of data has been presented in numerical, tabular and graphical forms, analysing a series of different parameters within the 1047nm reflectance data set. It is worth producing a summary of the main features of the various analyses before a discussion of the data proceeds.

Qualitative analysis of 1047nm reflectance and core stratigraphy:

- The 1047nm reflectance values often changed in a systematic way with changes in sediment units.
- This change in 1047nm reflectance was often correlated with changes in organic content of the soil. This correlation often was often negative between the two, i.e. where 1047nm reflectance increased soil organic content decreased.
- The changes in 1047nm and organic content did not always identify a change in sediment unit.

1047nm and quantification of relationship to organic matter:

- The individual cores showed weak positive and weak negative relationships between 1047nm reflectance and organic content, although a negative relationship was more common.
- The strength of the relationship varied between cores.
- The all core data set showed a weak negative linear and a weak negative quadratic relationship between 1047nm reflectance and organic content.
- A correlation coefficient between the two variables displayed a highly significant negative relationship at the 0.01 level.
- It is postulated that this relationship is indirect, with neither variable dependent on the other and both variables reflecting changes in sediment architecture.

1047nm and quantification of relationship to carbonate content:

- The individual cores showed weak positive and weak negative relationships between 1047nm reflectance and carbonate content.
- The strength of the relationship varied between cores.
- The all core data set showed a weak negative linear and a weak negative quadratic relationship between 1047nm reflectance and carbonate content.
- A correlation coefficient between the two variables displayed a significant negative relationship at the 0.05 level.
- It is postulated that this relationship is indirect, with neither variable dependent on the other and both variables reflecting changes in sediment architecture.

1047nm and quantification of relationship to magnetic susceptibility:

- The individual cores showed weak positive and weak negative relationships between 1047nm reflectance and magnetic susceptibility.
- The strength of the relationship varied between cores.
- The all core data set showed a weak negative linear and a weak negative quadratic relationship between 1047nm reflectance and magnetic susceptibility.
- A correlation coefficient between the two variables displayed a significant negative relationship at the 0.05 level.
- It is postulated that this relationship is indirect, with neither variable dependent on the other and both variables reflecting changes in sediment architecture.

1047nm and quantification of relationship to pH:

- The individual cores showed weak positive and weak negative relationships between 1047nm reflectance and pH.
- The strength of the relationship varied between cores.
- A correlation coefficient between the two variables displayed no significant relationship at the 0.05 level.

Summary statistics of the global population:

- Variation was seen in the minimum, maximum, mean, range, variance and top value of 1047nm reflectance between the cores.

- The top 1047nm reflectance values showed a lower range than either mean or minimum/maximum values.
- T1C14 had the greatest level of within core variance of 1047nm intensity, potentially a product of its smaller sample size.
- T1C7 had the greatest range in 1047nm reflectance values.
- T1C10 had the highest top 1047nm reflectance value.

Mean organic content and mean 1047nm reflectance of the cores:

- There was no consistent relationship between mean organic content and mean 1047nm intensity.
- Some cores had high organic content and low intensity means, e.g. T1C10.
- Some cores had high organic content and high intensity means, e.g. T1C7.
- There was no consistent relationship between the variance of organic content and the variance of 1047nm intensity.
- Some cores displayed high variance in 1047nm reflectance and low variance in organic content, e.g. T1C14.
- Some cores displayed low variance in intensity and high variance in organic content, e.g. T1C12.
- T1C10 and T1C14 showed more variance in intensity than organic content, whilst the other three cores showed the reverse pattern.
- This randomness in the data set maybe a product of trying to generalise through mean values a range of different sediment units within cores and then comparing between cores.

1047nm reflectance and surface organic content of the cores:

- This population size was small, only five samples.
- There was no consistent relationship between the surface 1047nm value and the surface organic content value.
- T1C10 had the highest 1047nm reflectance value and the lowest organic content.
- T1C7 had the second highest 1047nm reflectance value and the lowest organic content.

Surface to sub surface relationships of the cores:

- This population size was small, only five samples.
- There did appear to be a relationship between surface 1047nm reflectance and sub surface architecture.
- With increasing complexity of sediment units, intensity appears to decrease.
- This suggests that surface sediments are reflecting subsurface architecture, although the small population size suggests care should be taken in extrapolating this data.

Creation of homogeneous subsets of the cores:

- The ANOVA of the 1047nm reflectance and organic content grouped the cores into a series of homogeneous subsets.
- The ranking order of the 1047nm reflectance was almost the opposite of the ranking order of the organic content.

- This analysis suggests that on a between core basis there is a negative correlation between the variables.

2.10 DISCUSSION AND CONCLUSION

The discussion of this data seems to provide contradictory results on a number of levels. Although the qualitative analysis of the 1047nm reflectance against changes in sediment units did show consistency, the changes exhibited in 1047nm were not sufficient to identify each different sediment unit. However, this was the same for the other soil parameters measured such as organic content, carbonate content, etc. The quantitative analysis of the individual core data and all core data sets showed that statistically significant relationships exist between 1047nm reflectance and organic content, carbonate content and magnetic susceptibility. However, these relationships could not be visualised through linear or quadratic lines of best fit.

The further analysis of the all core data set showed that there was no definable relationship between mean 1047nm reflectance and mean organic contents. However, this may not be surprising as each of the cores were different in their sediment composition. The analysis of the top of core values as a proxy for surface Lidar values again showed no definable relationship between the two variables. However, this again may not be surprising, as each core had a relatively shallow A horizon that often differed markedly to the rest of the core, with elevated organic contents within that A horizon.

The relationship of the surface 1047nm reflectance values and the sub surface sediment architecture did indicate that as sediment stratigraphy became more complex surface 1047nm reflectance decreased. However, care must be taken in the analysis of this data due to the very small population size. It maybe that with a more complex depositional history and more sediment units, there is a greater capacity for variation in the surface sediments, promoting an increased cabicity to retain water and also organic matter. The analysis of the cores using ANOVA's showed that on a between core basis there was some indication of a negative relationship between 1047nm reflectance and organic content, with significant differences between the cores. The *post-hoc* ranking of the cores was almost exactly opposite between the two sets, suggesting a two tiered grouping of T1C10 and T1C14 forming one subset and MFC2, T1C7 and T1C12 forming a second subset. This roughly equates within the palaeoecological potential of the cores indicated earlier in the chapter.

Thus from this mass of results what conclusions can be drawn? Primarily, and most importantly, there is a relationship between organic content and 1047nm intensity. Changes in 1047nm reflectance are not dependant on changes in organic content. However, both appear to be reflecting broader changes in sediment architecture within the cores, which is further evidenced through significant correlations being seen with carbonate content and magnetic susceptibility. Therefore, model A is accepted (Fig. 2.13) that many soil parameters are influencing 1047nm intensity. The relationship between organic content and 1047nm reflectance is incidental and this does limit the predictive capacity of air borne Lidar to identify organic rich deposits.

From these results the following statements are made, regarding the predictive capacity of 1047nm reflectance to identify sediments of high organic potential:

- There is a strong correlation between 1047nm reflectance and organic content.
- Within this correlation 1047nm reflectance is not dependant on organic content.
- Both of these variables are interpreted as reflecting broader changes in sediment architecture within the cores, thus their correlation is casual not causal.
- The relationship between 1047nm reflectance and organic content is not linear or quadratic.
- 1047nm reflectance can be used to help identify changes in sediment architecture along palaeoenvironmental samples.
- When different cores are analysed using 1047nm reflectance it is likely that significant differences between the cores will be evident.
- It is interpreted that 1047nm reflectance has greater application in identifying/predicting different sediment types within a sample, rather than between samples.
- When this is translated to spatial airborne Lidar survey, it is suggested that the predictive capacity of 1047nm reflectance is limited by any dominant factor that defines a discrete sample, i.e., in scenario A the dominant factor is land use and the predictive capacity of intensity can only be used within a sample of land use type, e.g. discrete sample 1 = bare earth fields, discrete sample 2 = pasture fields, etc.

2.11 LIMITATIONS OF THE DATA

Within this analysis there needs to be awareness of the analytical approach followed and the limitations of the interpretations drawn. Primarily, and most importantly, all of the sample cores entered into this analysis came from one type of geomorphological unit, namely palaeochannels. This one fact may have significantly skewed the data set. If a range of cores had been seen from other geomorphological units, e.g. terrace units, then a larger data set, with a higher level of contrast may have produced more tangible results. By using only palaeochannel samples the variation in the data set may have been extremely limited, with greater contrast being expected between geomorphological units.

Secondly and equally importantly only a limited number of soil parameters were measured in this analysis, a product of time available for processing the data. It is suggested that measuring the moisture content of the cores and also the particle size distribution of the samples would have increased the understanding of this data set. Whilst the results of this survey have produced limited results it is suggested that this is a profitable line for future research and should be investigated further, potentially using more samples, from a greater range of study areas, incorporating a wider range of geomorphological units.

3 GROUND BASED LASER SCANNING

3 GROUND BASED LASER SCANNING

3.1 INVESTIGATING LIDAR INTENSITY WITH GROUND BASED SURVEY

This stage of the project investigated the land cover and properties influencing backscattered laser intensity. Since mobilisation of an airborne system is both costly and time consuming, with no guarantee that data can be collected to suit specific soil and vegetation conditions, work on this stage of the project made use of a NIR terrestrial lidar with appropriate deployment and data manipulation to simulate airborne lidar.

The aims of this stage of the project were:

- to investigate the extent to which intensity data might allow identification of buried archaeological remains through their physical expression at the earth surface as crop or soil marks (including those not otherwise evident in the visible portion of the spectrum).
- to examine and quantify the aspects of land cover, soil and sediment properties affecting intensity values.

To address these aims ground based lidar survey was undertaken at two test sites, Port Meadow, Oxford and Lockington, Leicestershire. Both sites were surveyed on two separate occasions and on a variety of land covers, including pasture, bare earth and crop. Work considered both anthropogenic and natural features. The method devised for ground based laser scanning and data manipulation and analysis protocols are set out below (section 3.2). The results for Port Meadow are discussed in section 3.3 and those for Lockington in section 3.4

3.2 METHOD STATEMENT: COLLECTION OF TERRESTRIAL LIDAR DATA

3.2.1 Field Survey Technique

Terrestrial lidar data was collected using a Measurement Devices Ltd (MDL) LaserAce scanner (Fig. 57). The MDL scanner combines a reflectorless total station with an automatic scanning function that can record up to 250 points per second. The LaserAce operates at 950nm providing an effective analogue of the Optech airborne lidar. Survey areas were set up at each site using 20 x 20m survey grids. Lidar data for each grid was collected using the LaserAce 'Polygon' scan option: this requires the user to define a survey area boundary encompassing each grid. The scanner was then set to Fast Scan mode to record points at a fixed interval on both the horizontal and vertical axis. During the course of the survey it was found that a denser concentration of points were recorded for the area closest to the tripod, where the machine was near-perpendicular to the ground (Fig. 58). In order to compensate for this, and obtain a relatively even spread of points for each grid, the machine had to be set up at a distance of approximately 15m from each 20 x 20m survey grid. The LaserAce was set to Total Station mode to record the position of the four corners of

each grid in relation to each scan. A differential GPS was used to log each grids geographic location.

Fig 57: The LaserAce scanner was mounted on a 'giant' tripod (extendable to a maximum height of 4m) fitted with a 500mm telescopic elevator. For safety reasons, and ease of access and operation, the machine was set up to a height of c.3.0m.

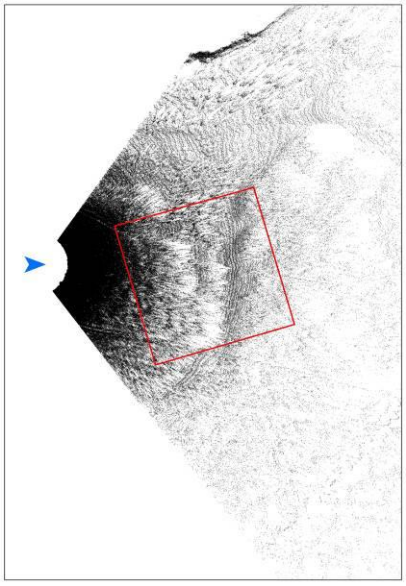

Fig 58: Scan data collected using the LaserAce Polygon scan option. The survey grid is shown in red. The position of the scanner is indicated by the arrow. Note the denser concentration of data points collected adjacent to the scanner.

3.2.2 Processing of Point Cloud Data

Data from the scanner, which was stored (as an FSC file) on Compact Flash card, and was downloaded into MDL's proprietary Model ACE post-processing and data visualisation software (Fig. 59).

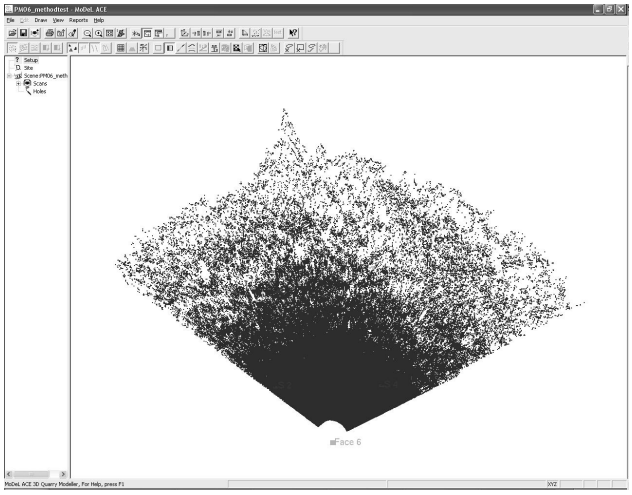

Fig 59: Scan data imported into MDL's proprietary Model ACE post-processing and data visualisation software.

Model ACE provides a facility for exporting the data for each scan as a csv file. However, data exported in this way only includes x,y,z,i observations - angle and range data are excluded from the process. In order to export all of the recorded data for each scan, the angle/range data and coordinate/intensity values for each horizontal and vertical scan had to be exported as separate csv files. UltraEdit32 text editing software was then used to merge the resulting files for each horizontal and vertical scan. The x,y,z coordinates for the four corners of each 20 x 20 m grid were exported as a separate csv file.

The vertical (Fig. 60) and horizontal (Fig. 61) scan data from each survey was then imported into ArcGIS/ArcMap and displayed using the tabular X,Y coordinate information. The data was then exported to shapefile format. The horizontal and vertical readings for each 20 x 20m grid were extracted from the point cloud using ArcMap's Select by Location and Export Data functions. The horizontal/vertical scan data was then merged to create a layer containing all of the data for each grid square (Fig. 62).

The shapefile point data was used to create raster grids from the elevation values (Fig. 63) and intensity values (Fig. 64) for each 20 x 20m study area. Raster grids were also created for the vertical angle and range attributes of the point cloud. In order to directly compare intensity and moisture values, a low resolution vector grid was created, the spacing of which corresponded with that chosen for the collection of soil moisture data in the field (Fig. 65).

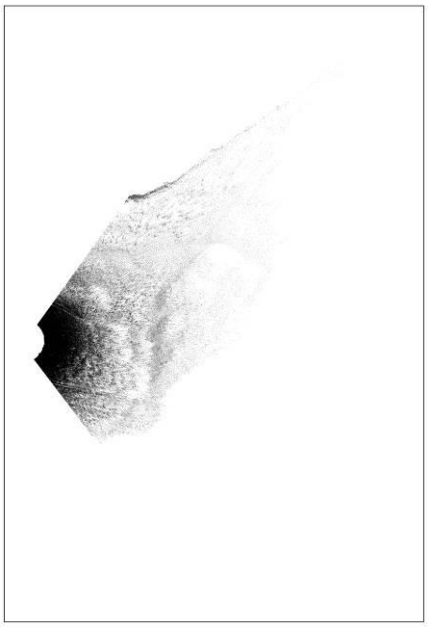

Fig 60: Vertical scan data.

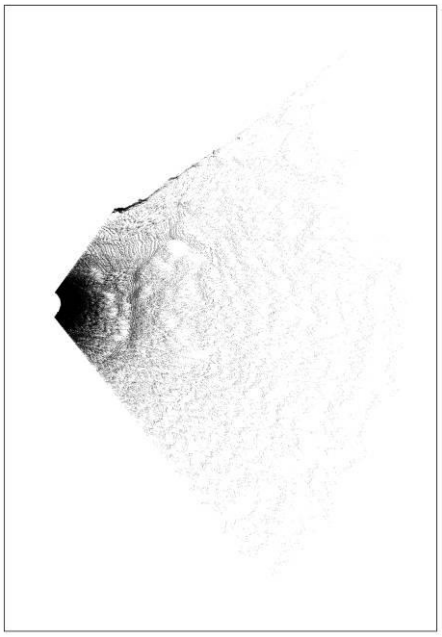

Fig 61: Horizontal scan data.

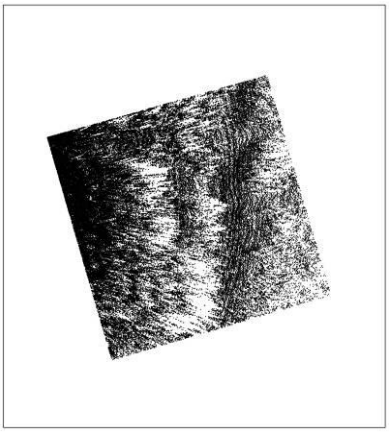

Fig 62: Combined horizontal and vertical readings for single grid.

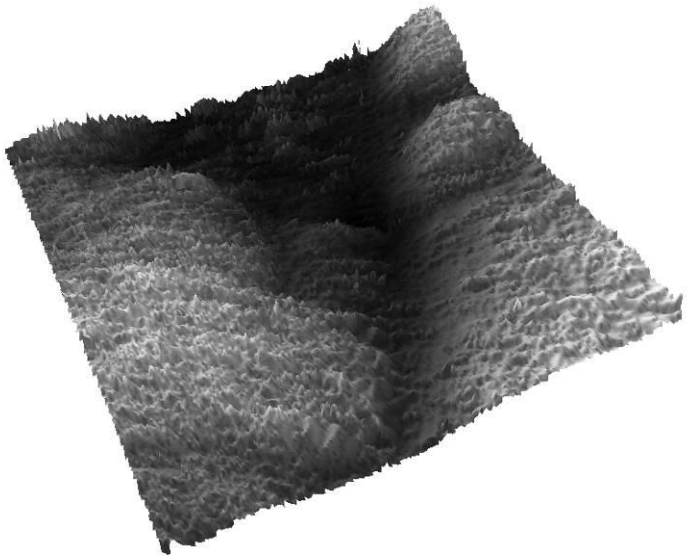

Fig 63: Elevation raster grid displayed in ArcScene.

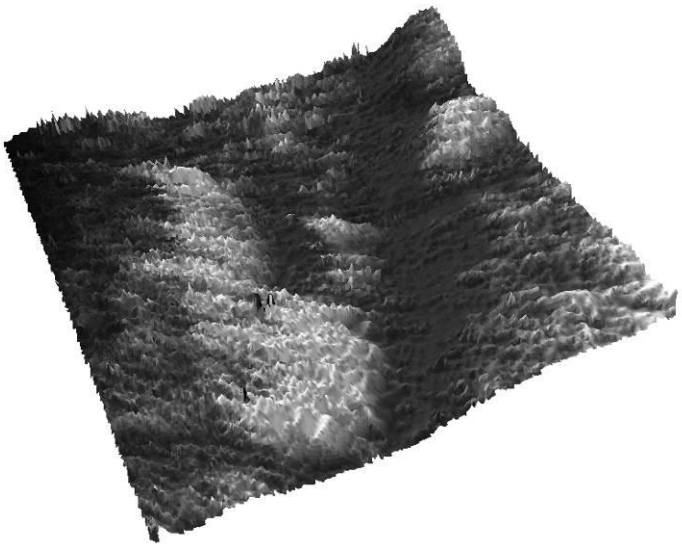

Fig 64: Intensity raster grid displayed in ArcScene.

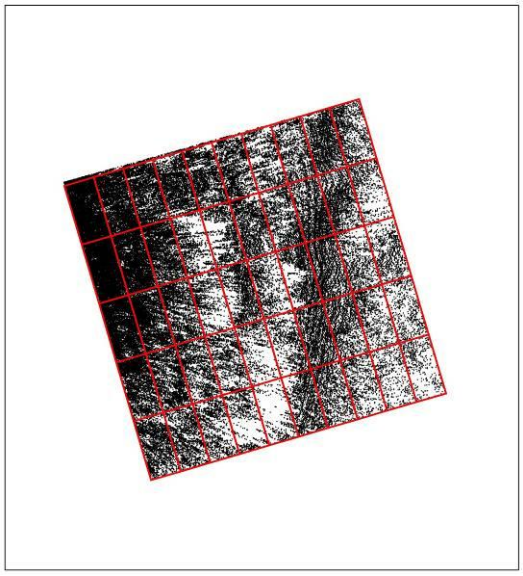

Fig 65: Low resolution vector grid overlaid onto point cloud data.

A new point shapefile was created from the central point (centroid) within each polygon of the vector grid. This centroid point file represented the location at which the soil moisture data were collected in the field. The 'intersect point tool' was then used to attach the pixel values from the raster grids that corresponded with the centroid points. The soil moisture and percentage organics values were manually entered into the attribute tables of the centroid files.

3.2.3 Soil Moisture Data Collection and Processing

Topsoil moisture readings were taken using a Delta T Devices Theta probe. Measurements were obtained at a 4 metre interval (25 readings per 20 x 20m) for most of the grids. For one of the grids at Port Meadow (PM07) the number of moisture readings taken was increased to 50 by changing the sampling interval to 2 metres on the axis perpendicular to the feature that was being investigated by the survey. The soil moisture readings were manually entered into the centroid shapefiles for each study area (see above) and a raster grid created across the points using a spline interpolation function (Fig. 66).

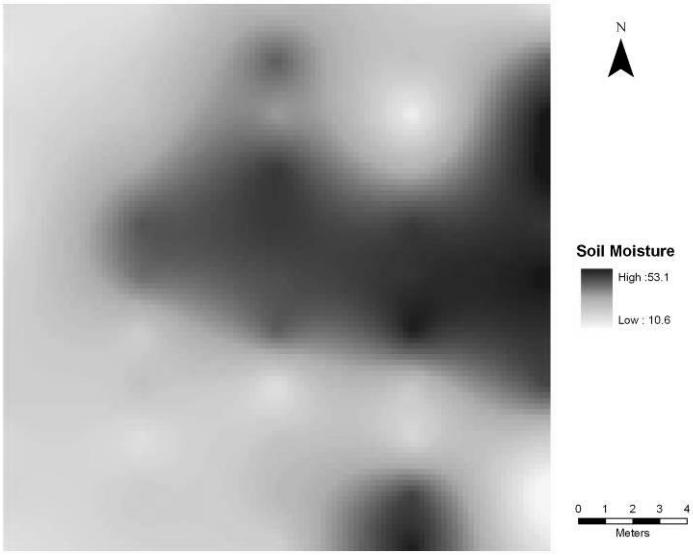

Fig 66: ArcGIS moisture data raster grid.

3.2.4 Data analysis

The updated attribute tables for the centroid files were exported from ArcGIS as .dbf files, before being opened in Microsoft Excel and saved as .xls files and exported into SPSS for data analysis. SPSS allowed graphs and correlation coefficients to be computed, comparing the correlation between different variables, for example backscattered intensity against soil moisture (Fig. 67).

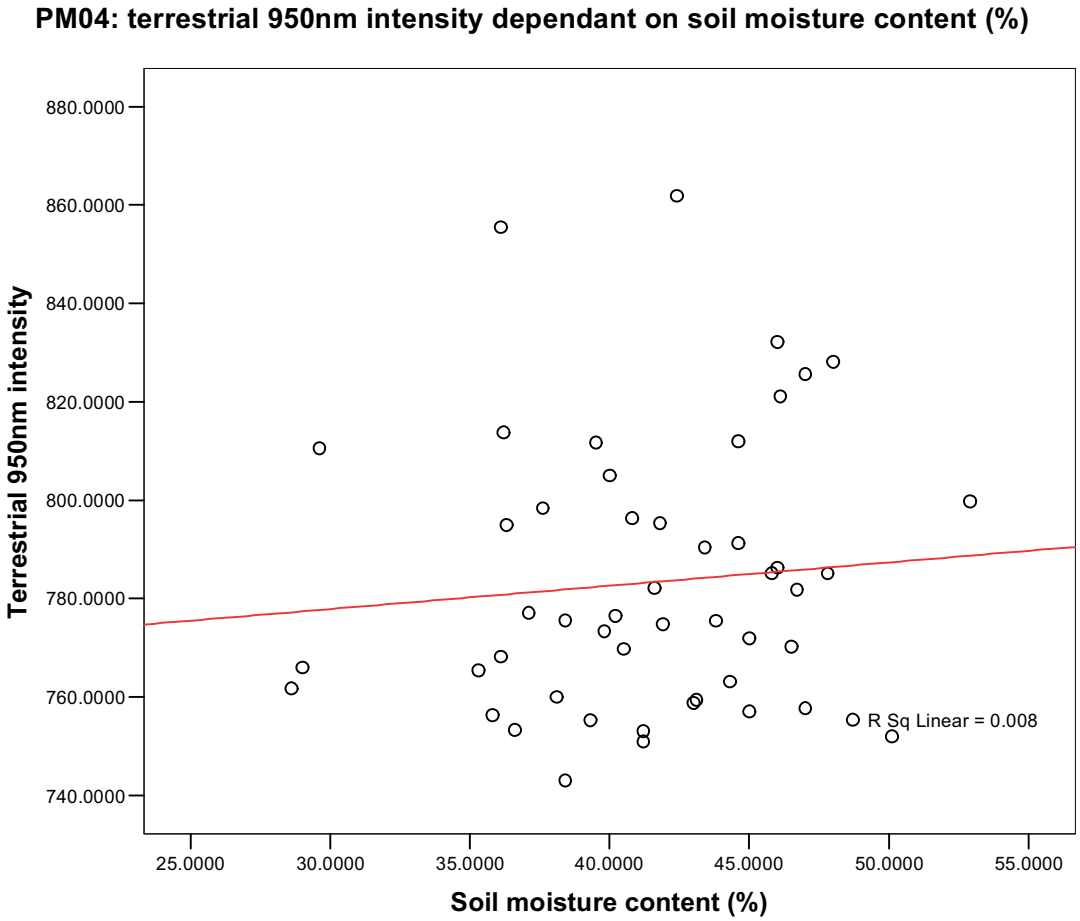

Fig 67: Scattergraph showing relationship between backscattered intensity and soil moisture.

3.2.5 Correction models

After initial examination the data were found to contain a significant variance in intensity values caused by the data collection parameters of range and vertical angle. In order to minimise this unwanted variance in the data set a correction file was created. Intensity values were recorded running from the grid edge closest to the machine to the grid edge furthest from the machine at 4 metre intervals. A line graph was created of this data plot showing a near linear relationship (Fig. 68). The overall difference from the first to last data point intensity value was 126 units.

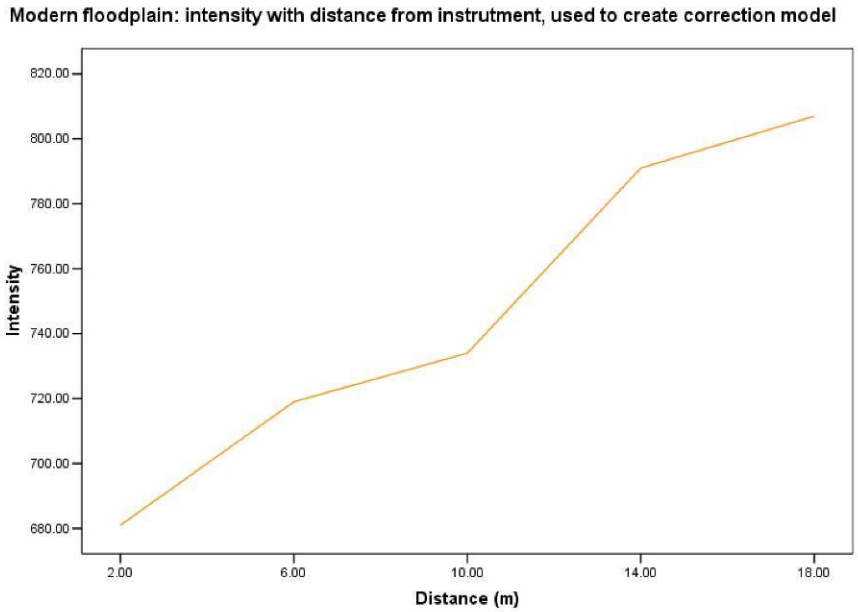

Fig 68: Line graph showing the increase in intensity with increasing distance from the scanner location.

From these data a correction was created using a simple model, where:

$$\frac{\textit{difference in intensity}}{\textit{distance}} = \frac{126}{20} = 6.3 \text{ units}$$

From this a correction model was created for the intensity, where a spreadsheet was produced with an increase in distance of 0.5m resulting in an increase in intensity of 3.15 units. In order to make the calibration more realistic, a stagger effect was placed in the correction model, to mimic the arc effect that occurs in the terrestrial lidar data collection. Each 0.5m line was staggered 0.5m further away from the machine (Tab. 3).

Line 1 = 0.5 metres		Line 2 = 1.0 metres		Line 3 = 1.5 metres	
Distance	Intensity	Distance	Intensity	Distance	Intensity
0.5	10	0.5	3.7	0.5	3.7
1	13.15	1	10	1	6.85
1.5	16.3	1.5	13.15	1.5	10
2	19.45	2	16.3	2	13.42
2.5	22.6	2.5	19.45	2.5	16.3

Tab 3: Staggering of intensity correction model.

The spreadsheet data were imported into ArcGIS and a raster grid created by interpolating between the points. The raster calculator tool in Spatial Analyst was used to subtract the correction model from the intensity surface, to create a new intensity surface with a reduced influence due to range (Fig. 69).

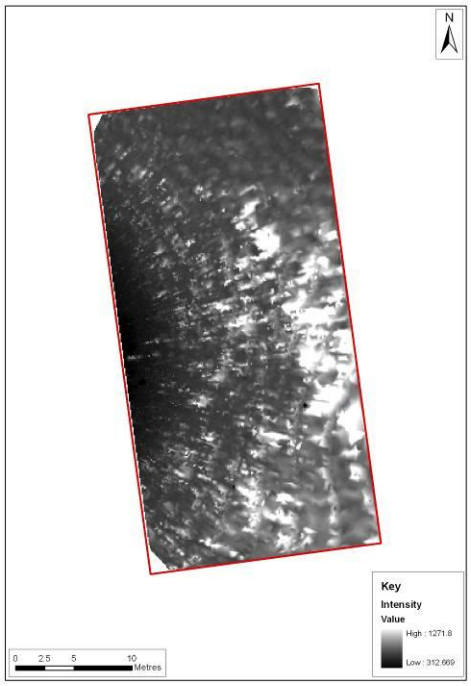

Fig 69: (a) MF intensity raster.

Fig 69: (c) MF intensity minus correction surface.

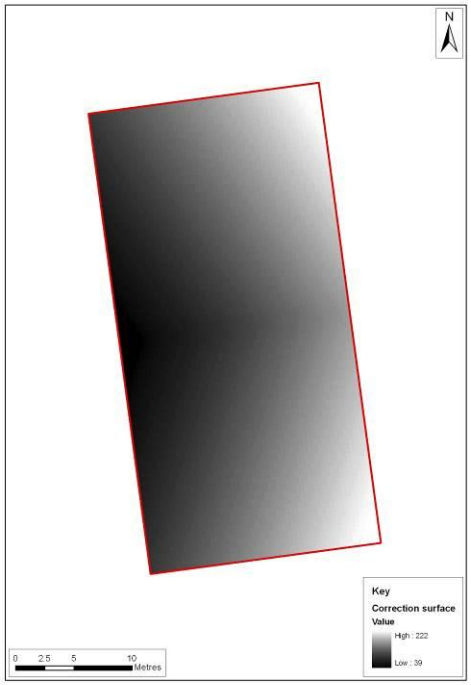

Fig 69: (b) MF correction surface.

A second attempt was made at removing the influence of range on the backscattered intensity values by separately analysing data points that were all equidistant from the scanner. The raster created from the range attribute was used in the GIS to create three polyline arcs passing along areas which were all equally spaced from the scanner location. Each polyline arc was divided into 0.5 metre lengths and a point digitised at these subdivisions. The intersect point tool was used to attach the cell values for each scan attribute, as well as soil moisture and organics, at each point location (Fig. 70). The updated attribute tables for the arc point files were exported and were again examined for significant relationships between variables.

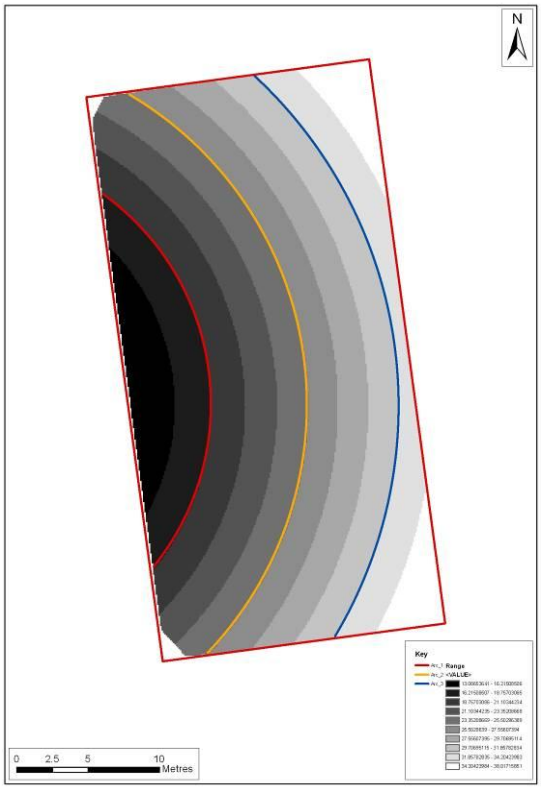

Fig 70: (a) Arcs positioned based on range from scanner.

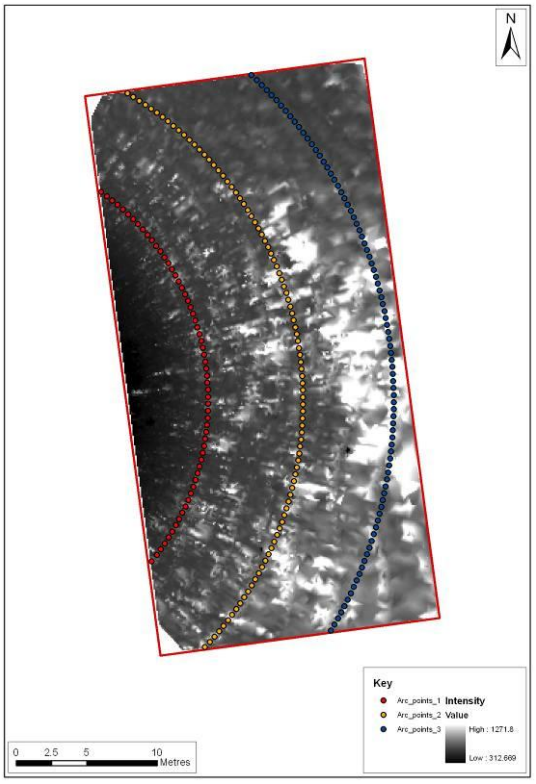

Fig 70: (b) 0.5 metre spaced points along arcs.

3.3 PORT MEADOW, OXFORD

3.3.1 Geology and Topography of the Study Area

The Port Meadow study area focussed on a section of the River Thames around four kilometres north of its confluence with the River Cherwell in Oxford. The study area was located on the floodplain of the river, with the lidar elevation model revealing little large-scale topographic change across the site. Microtopographic variations due to relict river channels and cultural archaeological earthworks were, however, easily identifiable. The BGS drift geology map of the area indicates that the vast majority of the study area is covered by alluvium from the River Thames, although with isolated deposits of Northmoor Member sand and gravel and Summertown-Radley Member sand and gravel. These terrace deposits are concentrated through the centre of the study area, either side of the modern river channel, and correspond with slight topographic rises visible on the lidar DTM.

3.3.2 Locations of Terrestrial Laser Scanning Test Areas

Five test sites were selected for detailed analysis within the Port Meadow study area (Fig. 71). Of these sites, two were across palaeochannels (PM02 and PM04), one across a natural depression at the edge of the modern Thames floodplain (PM07) and two across anthropogenic earthwork features (PM06 and PM09). The test areas differed in size from 20 x 20m grids up to a 40 x 40m grid, depending on the scale and form of the feature being investigated. These sites had been selected through the preliminary analysis of the airborne last pulse lidar surface, combined with on-site field inspection, to provide a range of sites for suitable comparative analysis between airborne and terrestrial laser scanning. By analysing a variety of natural and cultural features it was hoped that the capabilities of terrestrial laser scanning for acting as a proxy for airborne lidar could be demonstrated.

3.3.3 Analysis and Discussion of Results

The analysis of the results of the terrestrial scanning survey for Port Meadow followed the methodology outlined in section 3.2 of this report. The results from each of the five Port Meadow surveys will be discussed in turn below, providing details of the features that were targeted, the survey parameters employed and the results obtained.

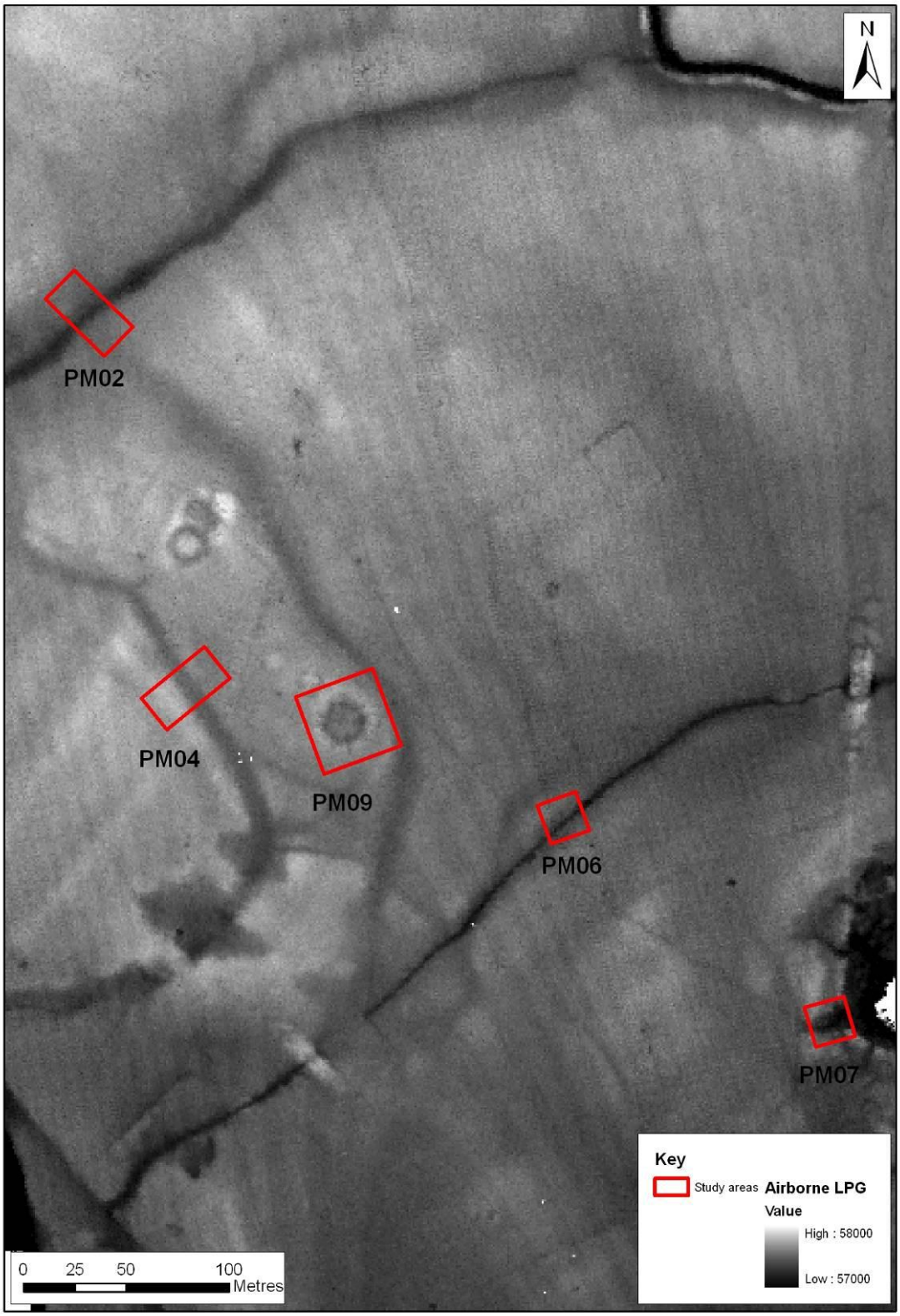

Fig 71: Port Meadow, Oxford. Lidar digital surface model showing the locations of the areas of ground based laser scanning outlined in red.

3.3.4 Area PM02

Survey area PM02 was a 40m x 20m grid across a palaeochannel located to the northwest of the Port Meadow study area. The palaeochannel was oriented west-southwest to east-northeast and was clearly visible on the airborne lidar last pulse surface as a sinuous linear depression measuring c.10m in width, and c.0.4m lower than the surrounding floodplain. The survey grid was aligned so the palaeochannel ran perpendicular to the maximum length of the scanned area. The scanner was located to the southwest of the PM02 grid, oriented east-northeast along the line of the palaeochannel. At the time of the survey the site was under relatively dense damp pasture/meadow grass (>c. 0.4m in height), with cold but clear weather conditions. The grass was notably shorter on the surface of the palaeochannel, with patches of bare soil.

The elevation surface model from the terrestrial laser scanning revealed the line of the palaeochannel as a linear depression running through the centre of the survey grid, matching the location of the feature on the airborne lidar elevation model (Fig. 72). The palaeochannel was also apparent on the 950nm reflectance surface produced from the terrestrial scanning and on the surface produced from the soil moisture readings taken in the field, although on both of these data sets the feature was less clear than in the elevation model. The 950nm reflectance surface demonstrated a general correlation of lower intensity readings in the palaeochannel when compared to the adjacent northwest and southeast terrace. In addition, the surface model produced from the soil moisture readings demonstrated that the highest soil moisture contents were concentrated in the palaeochannel. However, there was a clear effect of the range of the laser pulse from the scanner on the backscattered intensity values. The arc pattern of the laser scanner is visible within the interpolated intensity surface, with a clear trend of increasing 950nm reflectance with increased range from the scanner (Fig. 73). The scanner was positioned 10 metres away from the survey grid to provide a more even resolution of data points, but the influence of range was unavoidable.

Although both the terrestrial 950nm reflectance and the soil moisture measurements appeared to visibly record the location and general form of the palaeochannel, there was not a statistically significant relationship between the two variables. A scattergraph produced from the 4 metre grid centroid values across the survey area only indicated a very weak positive relationship ($R^2 = 0.004$) between backscattered intensity and soil moisture content and the correlation coefficient showed that this relationship was not significant at the 0.05 level (Figs. 74 and 75). The attributes of the 4 metre grid centroid points were also used to test the significance of the relationship between backscattered intensity against range and demonstrated a positive relationship with an R^2 value of 0.556 (Fig. 76). The correlation coefficient for this relationship indicated that it is significant at the 0.01 level (Fig. 77). The backscattered intensity values clearly increase with increasing distance from the scanner. This masks any significant relationships between intensity and other variables such as soil moisture.

A further complicating factor was found to be the relationship between the backscattered laser intensity and the vertical angle of the scanner head. The scattergraph produced from the 4 metre grid centroids from PM02 indicated a positive relationship between the two variables with an R^2 value of 0.554 and the correlation coefficient showed that this relationship was significant at the 0.01 level (Figs. 78 and 79). Therefore, as the vertical angle increases (i.e. the angle between the scanner head and the ground becomes more oblique) the backscattered intensity value increases. Although the scanner was mounted on a tall tripod to provide as vertical a scan as possible, the nature of the terrestrial scanning equipment meant that the

effect of this variable could not be avoided. The reason for this correlation is unclear but it may be another factor that prevents other significant relationships being identified.

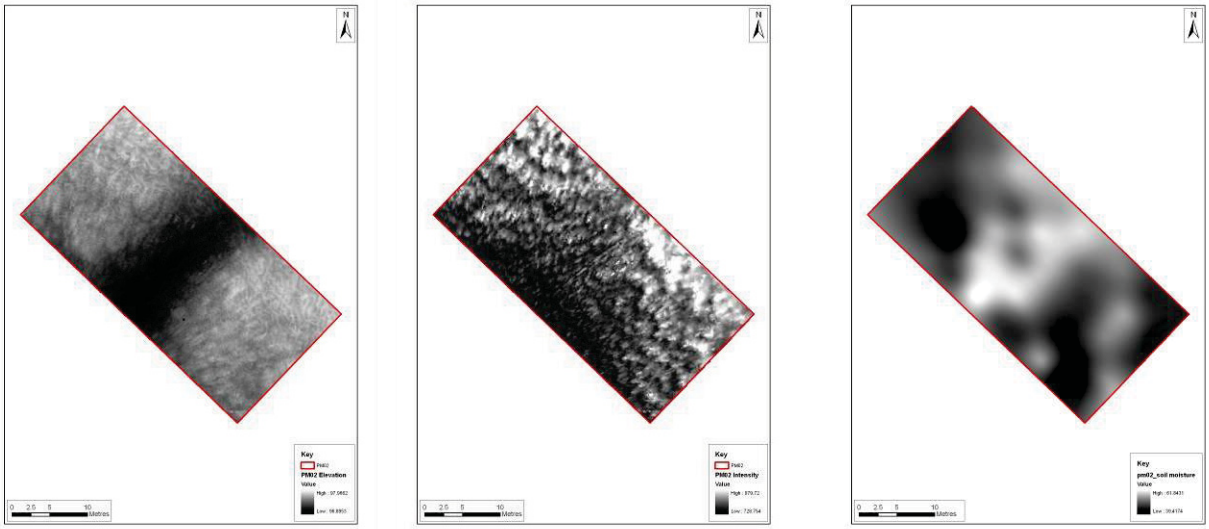

Fig 72: Port Meadow area PM02 terrestrial laser scanning showing from left to right elevation, 950nm reflectance and volumetric soil moisture.

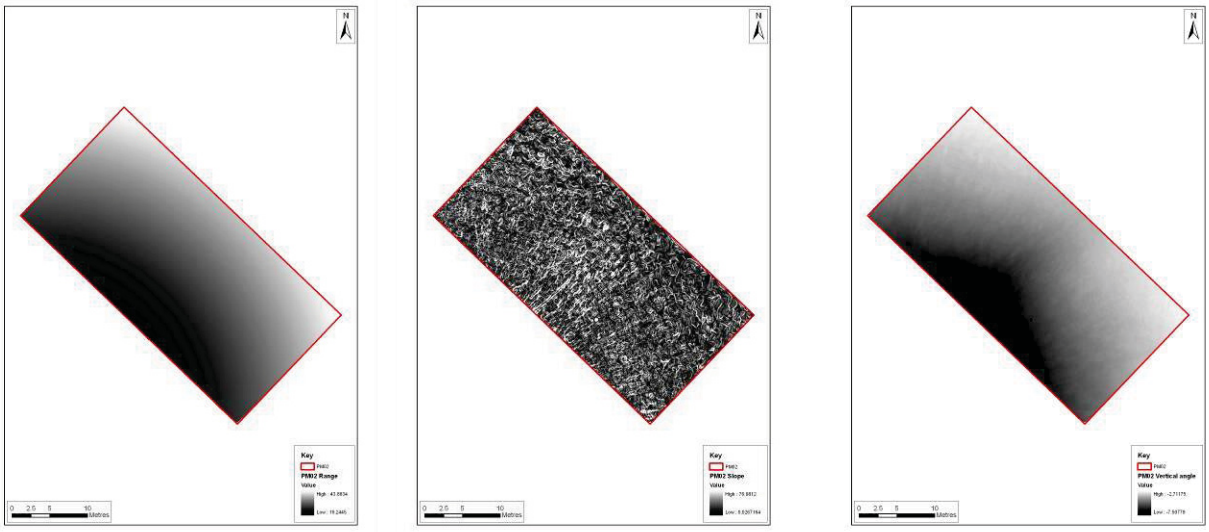

Fig 73: Port Meadow area PM02 terrestrial laser scanning showing from left to right, range, slope severity and vertical angle.

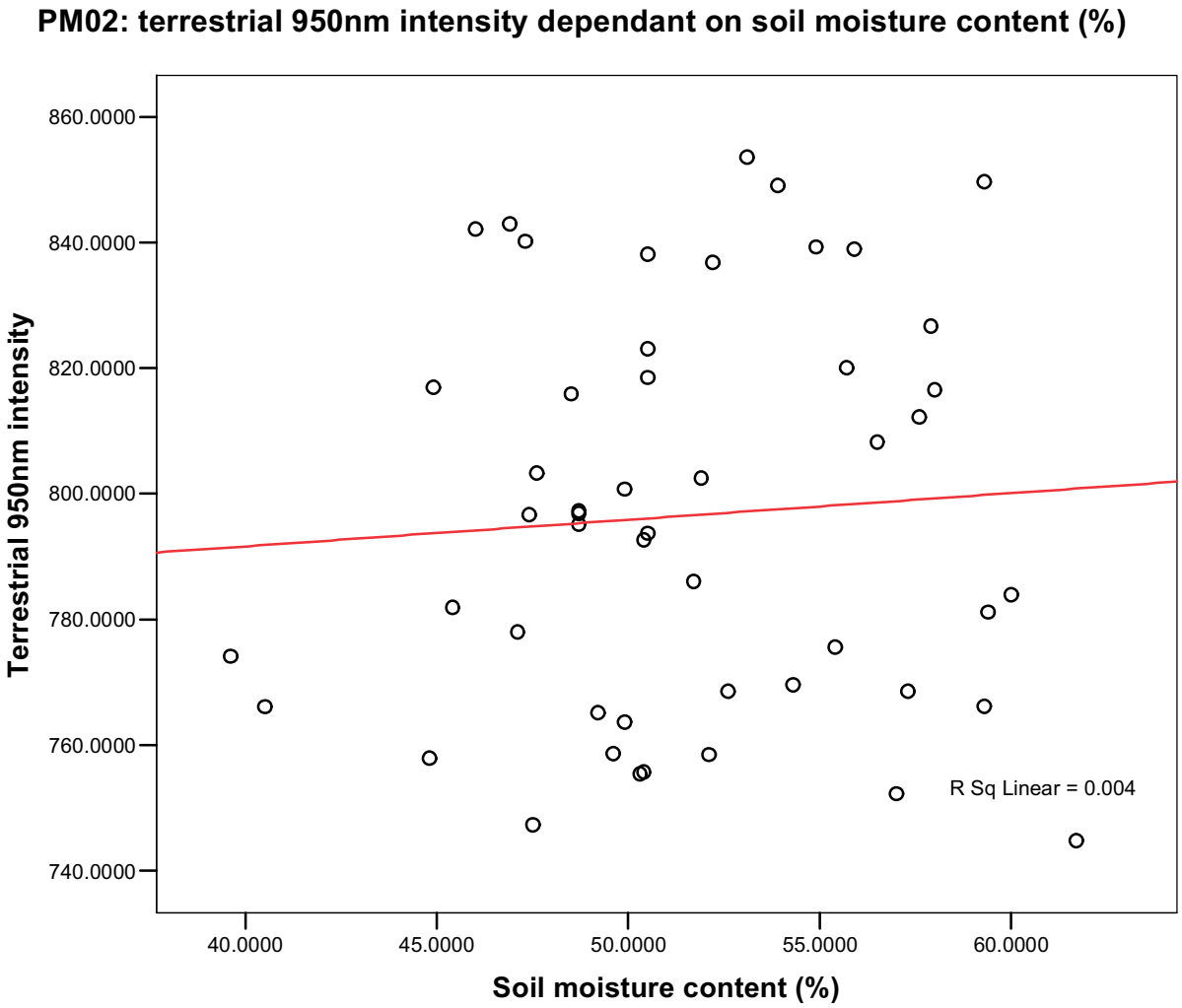

Fig 74: Port Meadow area PM02. Scatter plot showing 950nm reflectance and soil moisture content.

Correlations

		Terrestrial 950nm intensity	Soil moisture content (%)
Terrestrial 950nm intensity	Pearson Correlation	1	.067
	Sig. (2-tailed)		.644
	N	50	50
Soil moisture content (%)	Pearson Correlation	.067	1
	Sig. (2-tailed)	.644	
	N	50	50

Fig 75: Port Meadow area PM02. Correlation coefficient of 950nm reflectance against soil moisture content.

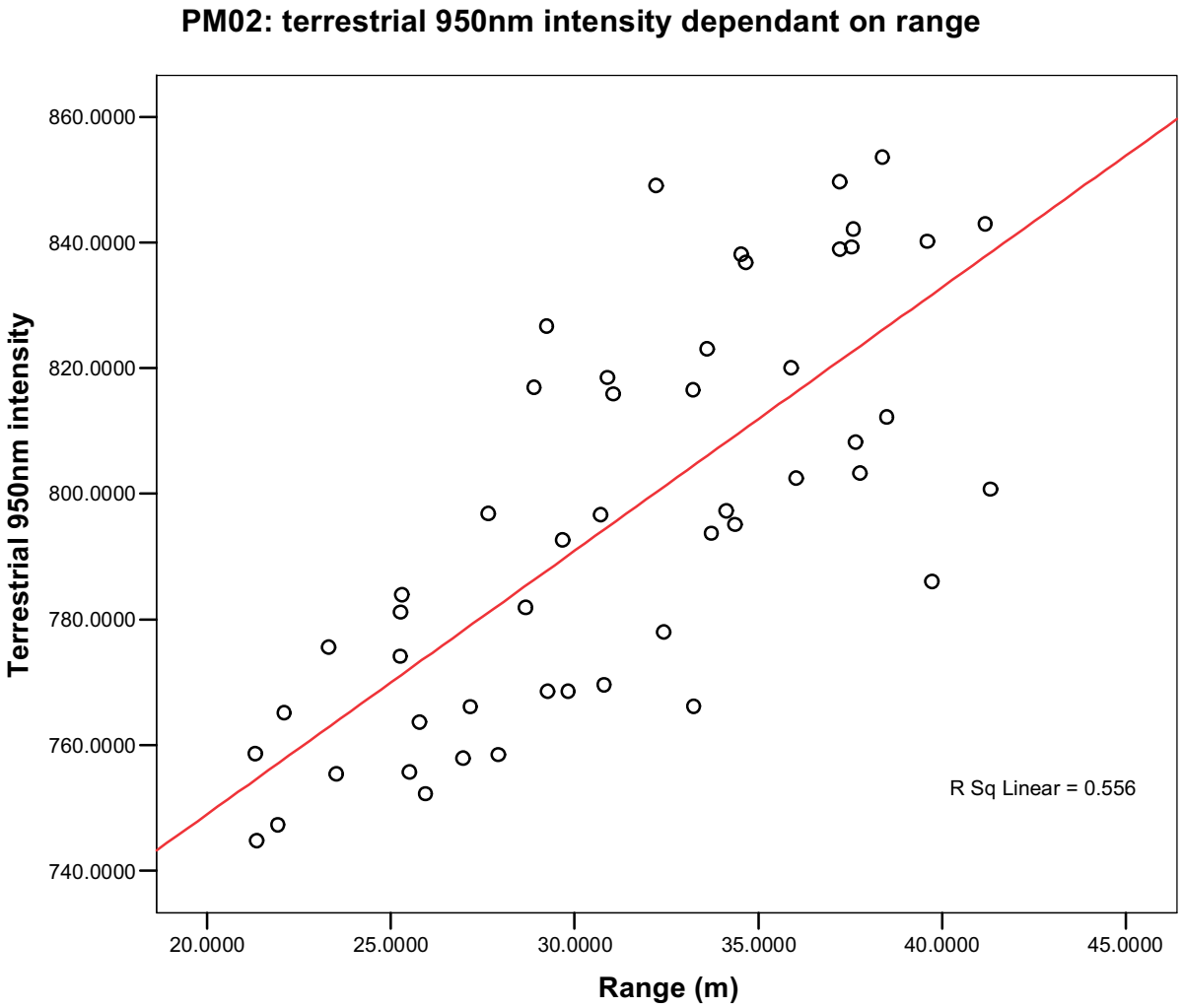

Fig 76: Port Meadow area PM02. Scatter plot showing 950nm reflectance against range.

Correlations

		Terrestrial 950nm intensity	Range (m)
Terrestrial 950nm intensity	Pearson Correlation	1	.745**
	Sig. (2-tailed)		.000
	N	50	50
Range (m)	Pearson Correlation	.745**	1
	Sig. (2-tailed)	.000	
	N	50	50

**. Correlation is significant at the 0.01 level (2-tailed).

Fig 77: Port Meadow area PM02. Correlation coefficient of 950nm reflectance against range (m).

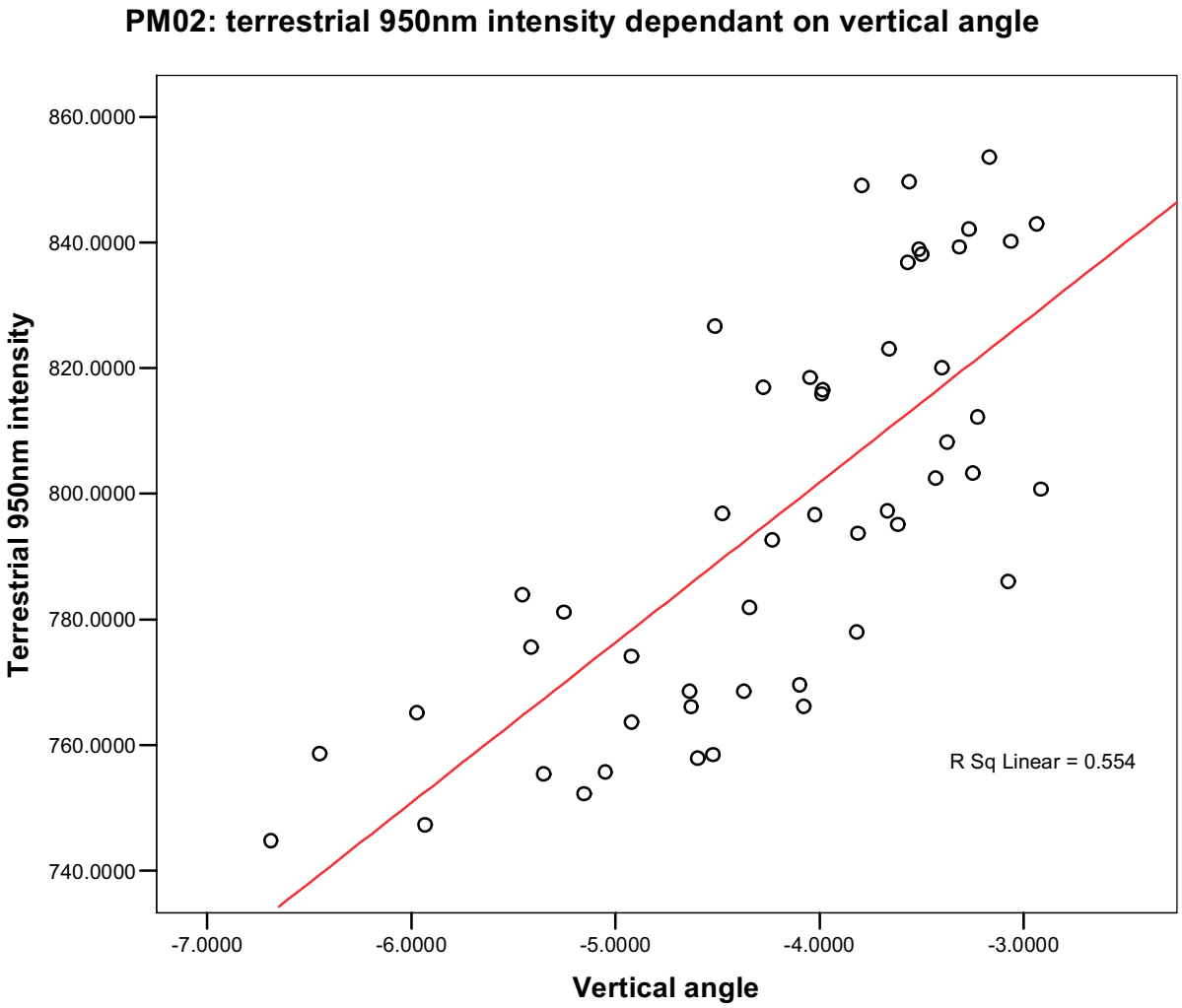

Fig 78: Port Meadow area PM02. Scatter plot showing 950nm reflectance against vertical angle.

Correlations

		Terrestrial 950nm intensity	Vertical angle
Terrestrial 950nm intensity	Pearson Correlation	1	.744**
	Sig. (2-tailed)		.000
	N	50	50
Vertical angle	Pearson Correlation	.744**	1
	Sig. (2-tailed)	.000	
	N	50	50

**. Correlation is significant at the 0.01 level (2-tailed).

Fig 79: Port Meadow area PM02. Correlation coefficient of 950nm reflectance against vertical angle.

3.3.5 Area PM 04

Survey area PM04 was a 40m x 20m grid centred across a palaeochannel feature located to the west of the Port Meadow study area. The palaeochannel was oriented north-northwest to south-southeast and was clearly visible on the airborne lidar last pulse surface as a linear depression measuring c.10m in width, and c.0.4m lower than the surrounding floodplain. The survey grid was aligned so that the palaeochannel ran perpendicular to the maximum length of the scanned area. The scanner was located to the north of the PM04 grid, oriented south-southeast along the line of the palaeochannel. At the time of the survey, the site was under relatively dense damp pasture/meadow grass (>c. 0.4m in height), with cold but clear weather conditions.

The elevation surface produced from the terrestrial laser scanning of PM04 clearly shows a linear depression along the line of the palaeochannel also visible on the airborne lidar last pulse surface (Fig. 80). This channel is flanked by terraces to the west and east, with the terrace to the west being notably higher in elevation. Minor topographic irregularities are also visible within the different geomorphological units. The surface generated from the backscattered 950nm reflectance values revealed a general concentration of low 950nm reflectance values within the area occupied by the palaeochannel. The surface model of the soil moisture readings indicated relatively high percentage moisture contents within the palaeochannel, although there were also areas on the adjacent terraces with equally high moisture contents. The range of the laser pulse from the scanner was found to significantly affect the backscattered laser intensity values for the PM04 survey area. The interpolated surface model produced from the intensity values displayed a general trend towards increasing intensity with increased range from the scanner (Fig. 81).

The terrestrial 950nm reflectance and the soil moisture measurements appeared to visually record the location and form of the PM04 palaeochannel. The values from the various surface models were again attached to the 4 metre grid centroids and scattergraphs produced from the different variables. The scattergraph comparing the backscattered 950nm reflectance with the volumetric soil moisture values indicated a very weak positive relationship with an R^2 value of only 0.008 and the correlation coefficient indicated that this relationship was not significant at the 0.05 level (Figs. 82 and 83).

In addition, the scattergraph comparing the range values and backscattered 950nm reflectance revealed a positive relationship with an R^2 value of 0.509 (Fig. 84). The correlation coefficient for the variables indicated that this relationship was significant at the 0.01 level (Fig. 85). The backscattered 950nm reflectance values again clearly increased with increasing distance from the scanner, masking any other significant relationships between intensity and other variables such as soil moisture. The vertical angle of the scanner head was also found to significantly affect the backscattered laser intensity values, as with the PM02 survey area. The scattergraph produced from the 4 metre grid centroids from PM04 indicated a positive relationship between the vertical scanner angle and the backscattered intensity with an R^2 value of 0.502 (Fig. 86). The correlation coefficient for the laser intensity and vertical scanner angle indicated that the relationship is significant at the 0.01 level (Fig. 87). This value suggests that as the vertical angle of the scanner becomes more oblique the backscattered intensity value increases. Along with the effect of the laser range, this instrumentation factor significantly influenced the intensity values, preventing other significant relationship being identified.

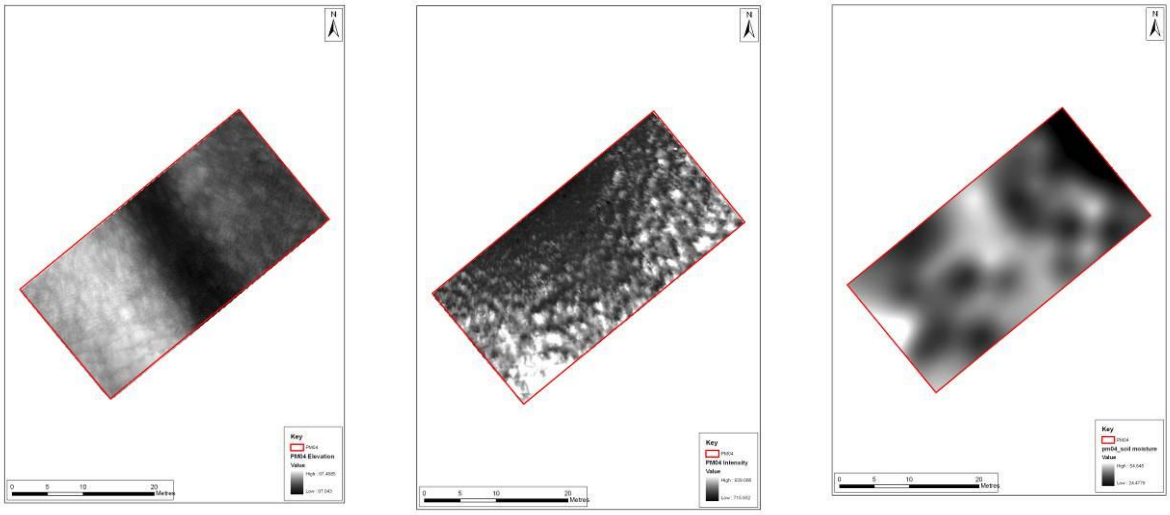

Fig 80: Port Meadow area PM04 terrestrial laser scanning showing from left to right elevation, 950nm reflectance and volumetric soil moisture.

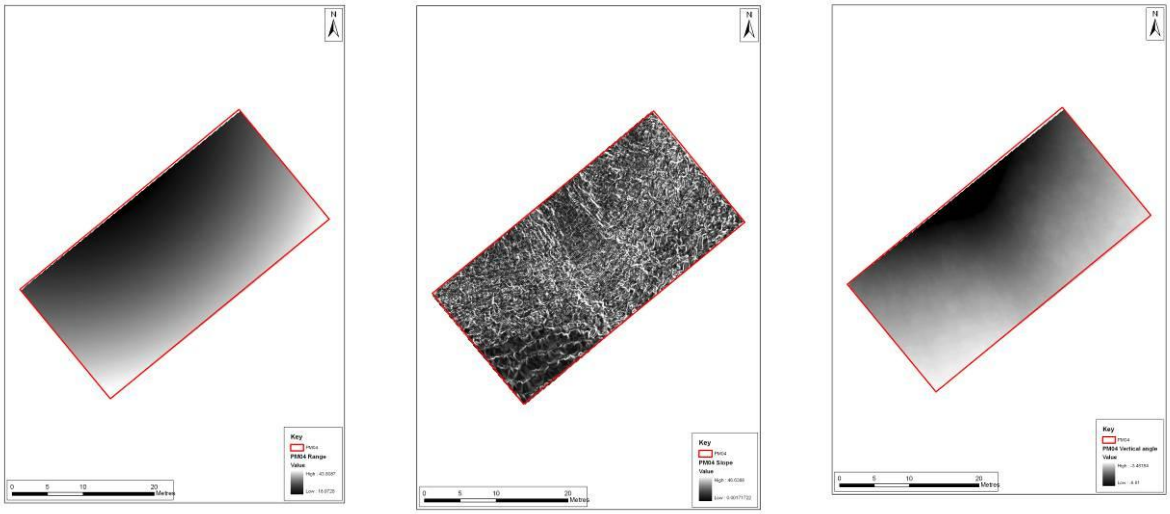

Fig 81: Port Meadow area PM04 terrestrial laser scanning showing from left to right range, slope severity and vertical angle.

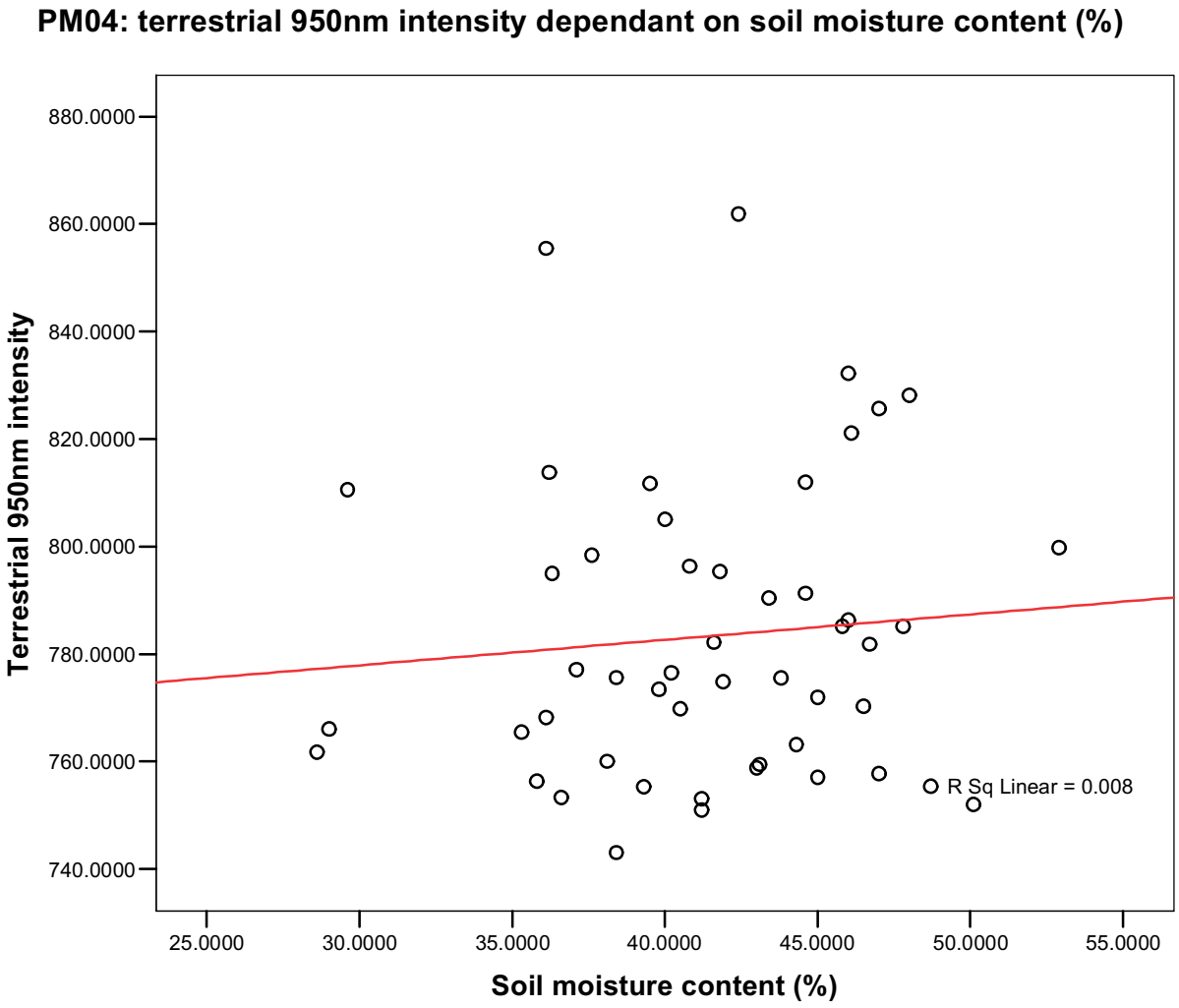

Fig 82: Port Meadow area PM04. Scatter plot showing 950nm reflectance and soil moisture content.

Correlations

		Terrestrial 950nm intensity	Soil moisture content (%)
Terrestrial 950nm intensity	Pearson Correlation	1	.090
	Sig. (2-tailed)		.533
	N	50	50
Soil moisture content (%)	Pearson Correlation	.090	1
	Sig. (2-tailed)	.533	
	N	50	50

Fig 83: Port Meadow area PM04. Correlation coefficient of 950nm reflectance against soil moisture content.

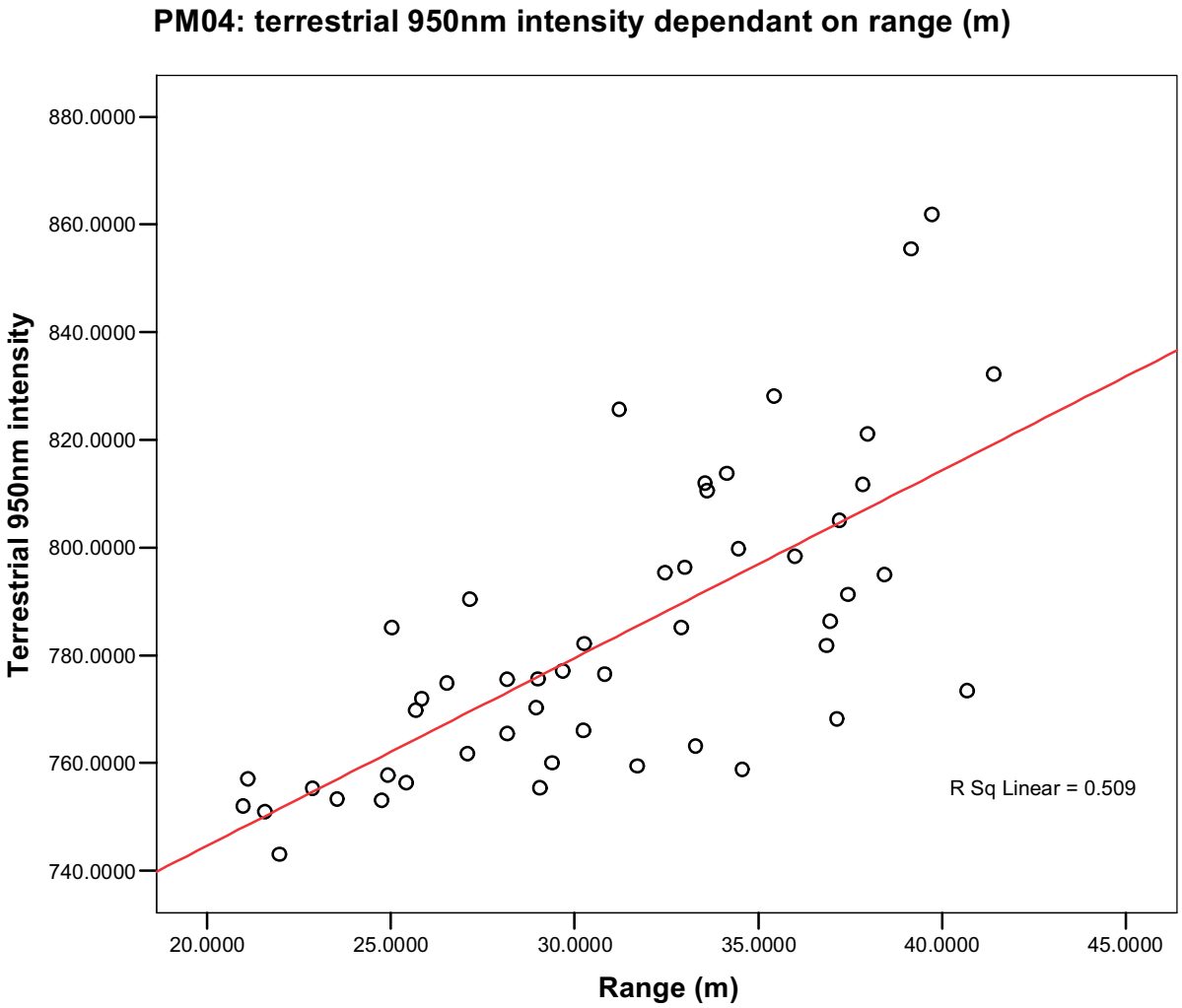

Fig 84: Port Meadow area PM04. Scatter plot showing 950nm reflectance against range (m).

Correlations

		Range (m)	Terrestrial 950nm intensity
Range (m)	Pearson Correlation	1	.714**
	Sig. (2-tailed)		.000
	N	50	50
Terrestrial 950nm intensity	Pearson Correlation	.714**	1
	Sig. (2-tailed)	.000	
	N	50	50

**. Correlation is significant at the 0.01 level (2-tailed).

Fig 85: Port meadow area PM04. Correlation coefficient of 950nm reflectance against range (m).

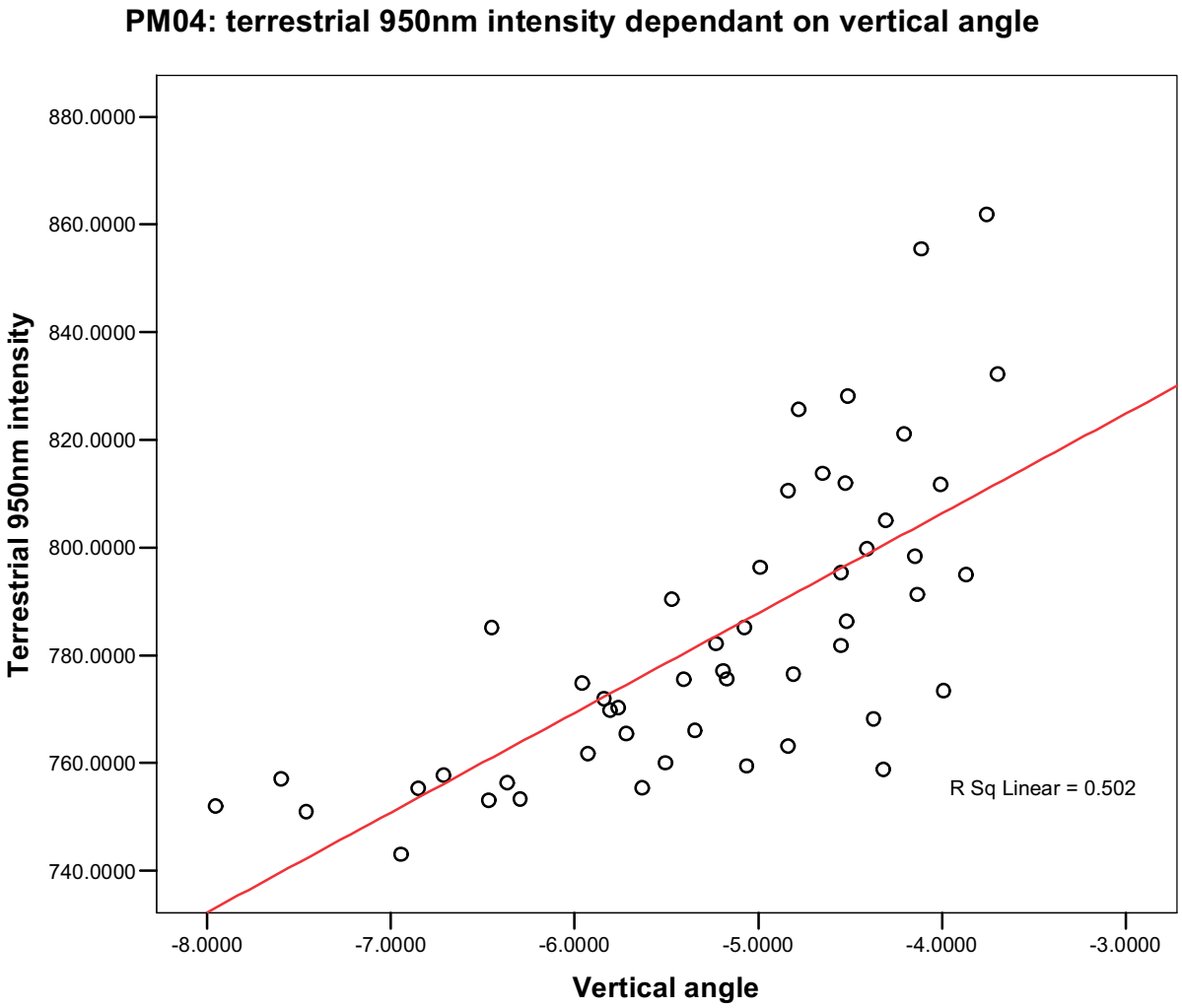

Fig 86: Port Meadow area PM04. Scatter plot showing 950nm reflectance against vertical angle.

.

Correlations

		Terrestrial 950nm intensity	Vertical angle
Terrestrial 950nm intensity	Pearson Correlation	1	.708**
	Sig. (2-tailed)		.000
	N	50	50
Vertical angle	Pearson Correlation	.708**	1
	Sig. (2-tailed)	.000	
	N	50	50

**. Correlation is significant at the 0.01 level (2-tailed).

Fig 87: Port meadow area PM04. Correlation coefficient of 950nm reflectance against vertical angle.

3.3.6 Area PM 06

Survey area PM06 was a 20m x 20m grid across an anthropogenic linear earthwork ditch located to the southwest of the Port Meadow study area. The ditch was oriented southwest-northeast and was visible on the airborne lidar last pulse surface as a linear depression, extending from the eastern extent of the lidar image as far west as a meander of the Thames. The ditch measured c. 4m in width and was c. 0.4 metres below the level of the surrounding floodplain. The survey grid was aligned southwest-northeast, parallel to the earthwork feature, with the scanner located to the west and oriented northeast. At the time of survey the site was under relatively dense damp pasture/meadow grass, with cold but clear weather conditions.

The elevation surface produced from the terrestrial laser scanning of PM06 recorded the location and form of the linear ditch with a high degree of clarity and matched the location of the feature on the airborne lidar elevation model (Fig. 88). The 950nm reflectance surface also highlighted the position of the linear ditch, especially towards the northeast edge of the survey grid, with notably higher 950nm reflectance readings being located within the ditch when compared with the surrounding floodplain. However, the surface produced from the volumetric soil moisture readings was less clear. Although the northeastern portion of the ditch could be clearly distinguished by an area of high soil moisture content, the western half was only just perceptible against the background moisture values of the rest of the survey grid, but this could be a product of the coarse sample interval used. Surfaces were again produced from the other possible variables that could have affected the backscattered 950nm intensity, and the values from these surfaces were attached to the 4 metre grid centroid points (Fig. 89). Again significant distortion of the data is seen through factors such as vertical angle, slope and range.

A scattergraph produced from the centroid points indicated a weak positive relationship between the backscattered 950nm reflectance and the soil moisture content with an R^2 value of 0.04 (Fig. 90). The correlation coefficient between these variables indicated that no significant correlation exists at the 0.05 level, suggesting that another factor(s) was responsible for the changing intensity readings (Fig. 91). The scattergraphs produced from the other variables revealed that the range of the laser pulse and vertical angle of the scanner head were again considerably influencing the 950nm reflectance values. The scattergraph comparing range to 950nm reflectance clearly showed that as the range from the scanner increased, the intensity value also increased (Fig. 92). This relationship was visible as a general background arc pattern on the intensity surface model but was also shown to have an R^2 value of 0.236 and a correlation coefficient that is significant at the 0.05 level (Fig. 93). The same relationship between the vertical angle of the scanner head and the backscattered 950nm reflectance that had been noted in the other survey areas was again recorded. As the angle of the scanner head increased (i.e. the laser-ground angle became more oblique), the 950nm reflectance also increased. The scattergraph comparing these variables demonstrated a positive relationship with an R^2 value of 0.199 (Fig. 94) and the correlation coefficient indicated that the relationship is significant at the 0.05 level (Fig. 95). Although both of these instrumentation variables were clearly influencing the 950nm reflectance values within the PM06 survey area, the scale of the influence was appreciably lower than the R^2 values obtained from the PM02 and PM04 survey areas.

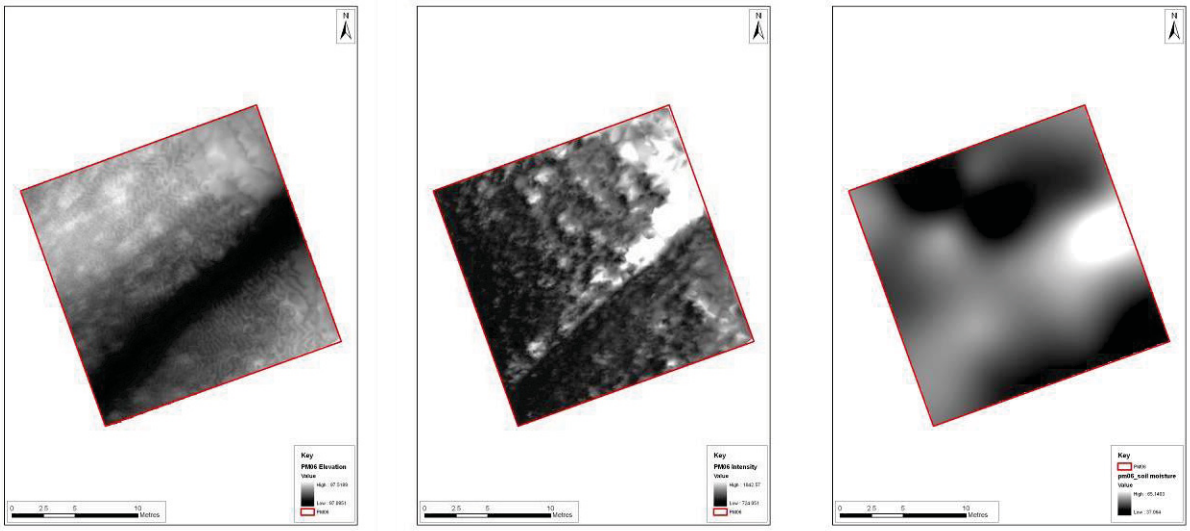

Fig 88: Port Meadow area PM06 terrestrial laser scanning showing from left to right elevation, intensity and volumetric soil moisture.

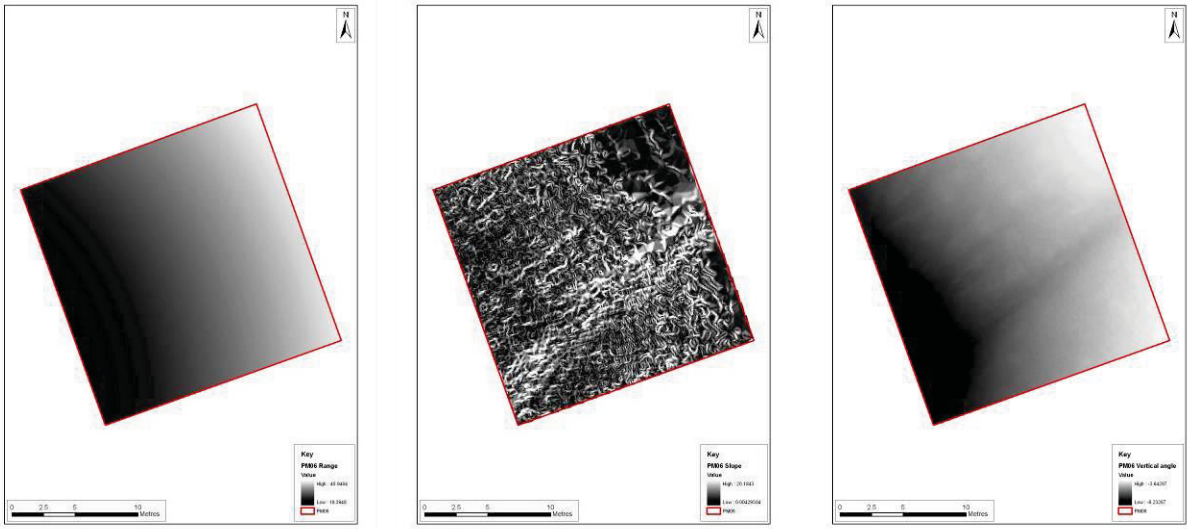

Fig 89: Port Meadow area PM06 terrestrial laser scanning showing from left to right slope severity, range and vertical angle.

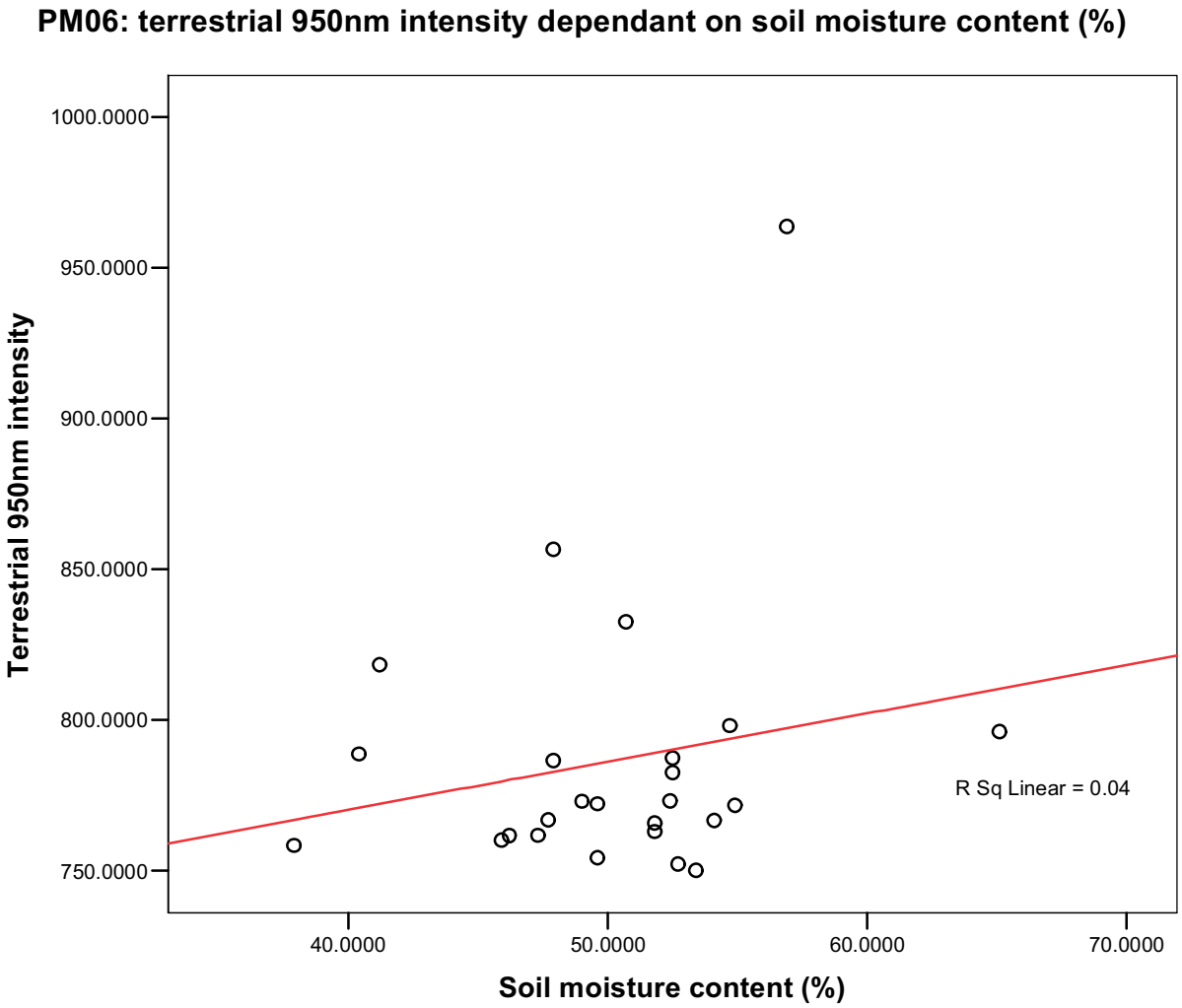

Fig 90: Port Meadow area PM06. Scatter plot showing 950nm reflectance against soil moisture content.

Correlations

		Terrestrial 950nm intensity	Soil moisture content (%)
Terrestrial 950nm intensity	Pearson Correlation	1	.199
	Sig. (2-tailed)		.340
	N	25	25
Soil moisture content (%)	Pearson Correlation	.199	1
	Sig. (2-tailed)	.340	
	N	25	25

Fig 91: Port meadow area PM06. Correlation coefficient of 950nm reflectance against soil moisture content.

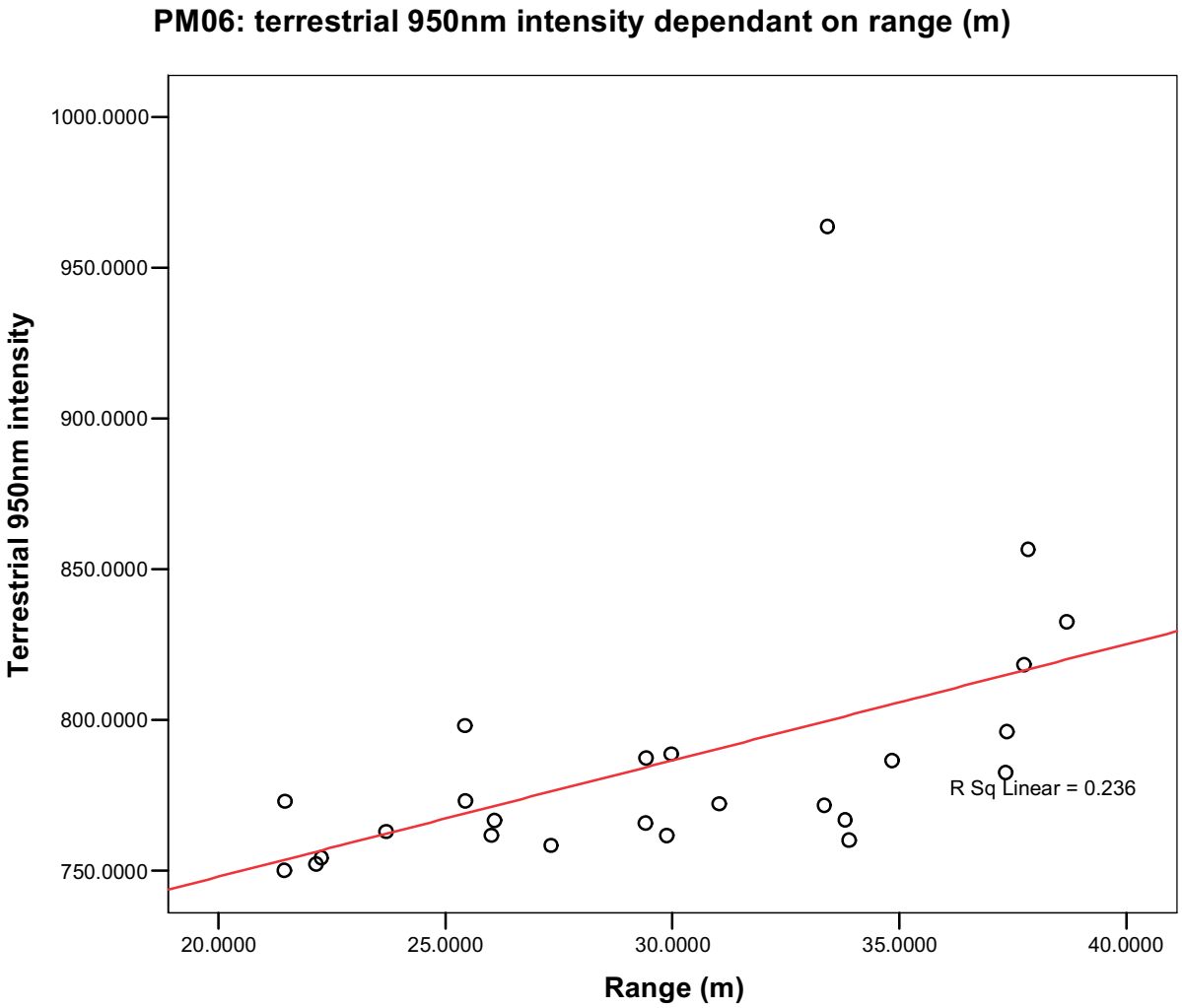

Fig 92: Port Meadow area PM06. Scatter plot showing 950nm reflectance against range (m).

Correlations

		Terrestrial 950nm intensity	Range (m)
Terrestrial 950nm intensity	Pearson Correlation	1	.486*
	Sig. (2-tailed)		.014
	N	25	25
Range (m)	Pearson Correlation	.486*	1
	Sig. (2-tailed)	.014	
	N	25	25

*. Correlation is significant at the 0.05 level (2-tailed).

Fig 93: Port meadow area PM06. Correlation coefficient of 950nm reflectance against range (m).

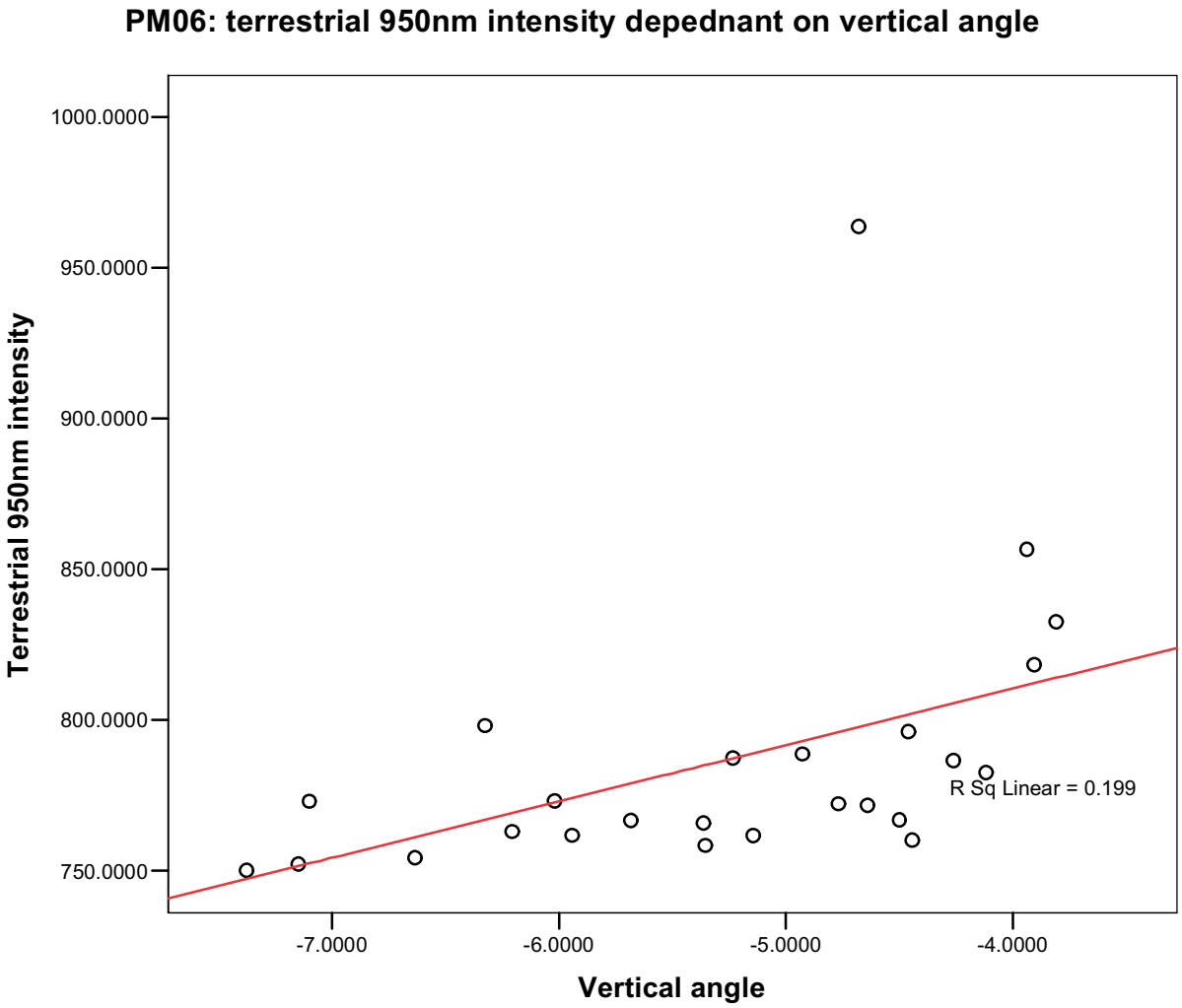

Fig 94: Port Meadow area PM06. Scatter plot showing 950nm reflectance against vertical angle.

Correlations

		Terrestrial 950nm intensity	Vertical angle
Terrestrial 950nm intensity	Pearson Correlation	1	.446*
	Sig. (2-tailed)		.026
	N	25	25
Vertical angle	Pearson Correlation	.446*	1
	Sig. (2-tailed)	.026	
	N	25	25

*. Correlation is significant at the 0.05 level (2-tailed).

Fig 95: Port meadow area PM06. Correlation coefficient of 950nm reflectance against vertical angle.

3.3.7 Area PM 07

Survey area PM07 was a 20m x 20m grid across a natural depression at the edge of the Thames floodplain, to the southeast of the Port Meadow study area. The irregular depression was oriented broadly southwest-northeast, with the survey grid being positioned perpendicular to the feature. The depression measured approximately 10-13 metres in width and reached a maximum depth of c.0.5 metres below the level of the surrounding floodplain. The scanner was located to the north/northeast of the survey grid, oriented south/southwest perpendicular to the line of the feature. At the time of the survey the site was under short pasture/meadow grass with patches of exposed soil within the depression. The weather conditions were warm and sunny with light cloud cover.

The elevation surface produced from the terrestrial laser scanning of PM07 revealed an irregular depression extending southwest-northeast through the centre of the grid (Fig. 96). This surface corresponded with the airborne lidar elevation model, adding clarity and detail to the form of the feature. A visual inspection of the 950nm reflectance surface produced from the pointcloud data appears to indicate a relationship between the location of the depression and the backscattered 950nm reflectance readings, with low 950nm reflectance readings being concentrated within the depression. In addition, the volumetric soil moisture readings recorded for the soil within the depression are markedly higher than for the raised terraces surrounding it, although more obviously towards the eastern edge of the survey area than the western edge. Unlike in the other study areas at Port Meadow, the range of the laser pulse from the scanner does not appear to have been one of the dominant factors affecting the intensity readings for PM07, although vertical angle and slope severity are still having a large influence on the data (Fig. 97).

Both the soil moisture survey and the backscattered 950nm reflectance appeared to record the location of the natural depression in PM07 but a scattergraph comparing these two variables revealed a very weak positive correlation with an R^2 value of only 0.002 (Fig. 98). The correlation coefficient for the variables confirms that no significant relationship exists at the 0.05 level (Fig. 99). This again suggests that other factors were influencing the 950nm reflectance of the laser pulse.

Unlike in the other study areas at Port Meadow, the range of the laser pulse from the scanner does not appear to have been one of the dominant factors affecting the intensity readings for PM07. A scattergraph produced from the intensity and range values for the centroid points provided a weak positive relationship with an R^2 value of only 0.025 and the correlation coefficient confirmed there was no significant statistical relationship at the 0.05 level (Figs. 100 and 101). However, the vertical angle of the scanner head was found to have a far more significant impact on the intensity readings, with a positive relationship between these variables with an R^2 value of 0.119 and a correlation coefficient confirming the relationship was significant at the 0.05 level (Figs. 102 and 103). Although this is noticeably less than the equivalent correlation value for the other Port Meadow study areas, it does again suggest that as the angle between the scanner head and the ground becomes more oblique, the backscattered 950nm reflectance value increases. Furthermore, the slope angle of the ground surface (as generated from the elevation model) was also found to have a significant positive relationship with the backscattered intensity ($R^2 = 0.117$) and a statistically significant correlation coefficient at the 0.05 level (Figs. 104 and 105). These relationships appear to have masked any significant correlation between the terrestrial intensity and other variables.

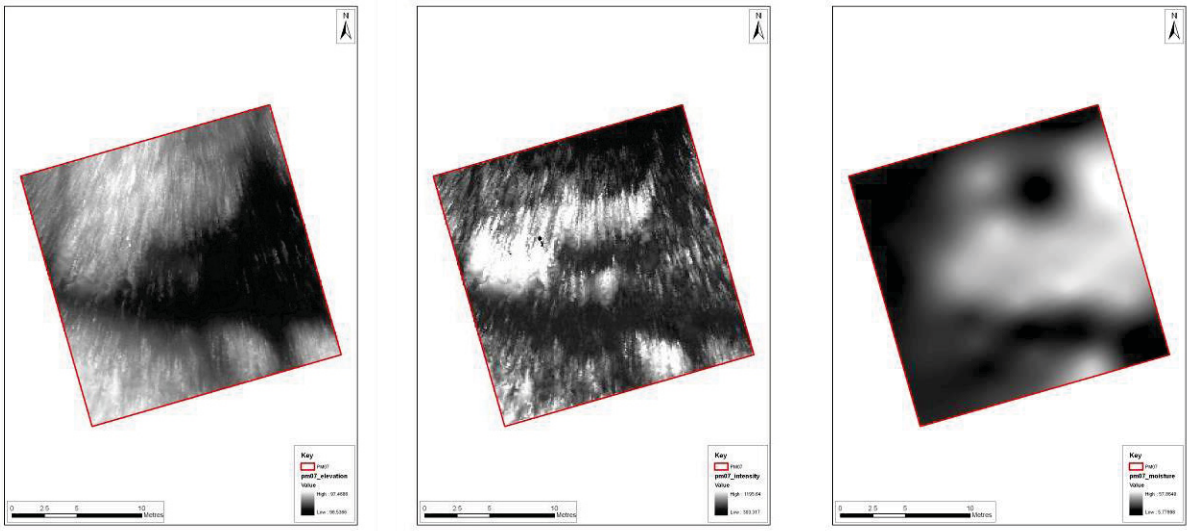

Fig 96: Port Meadow area PM07 terrestrial laser scanning showing from left to right elevation, intensity and volumetric soil moisture.

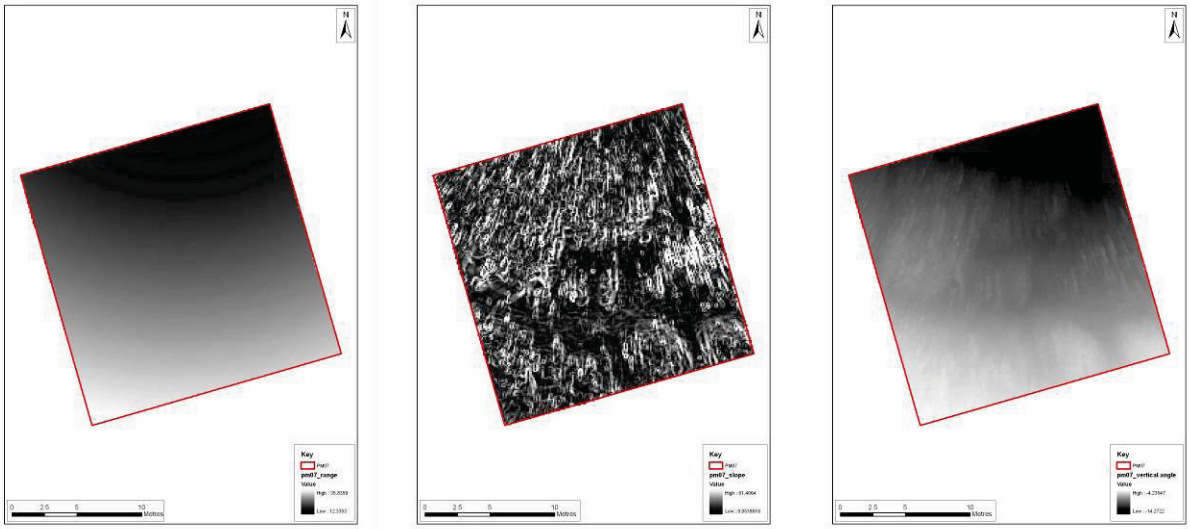

Fig 97: Port Meadow area PM07 terrestrial laser scanning showing from left to right slope severity, range and vertical angle.

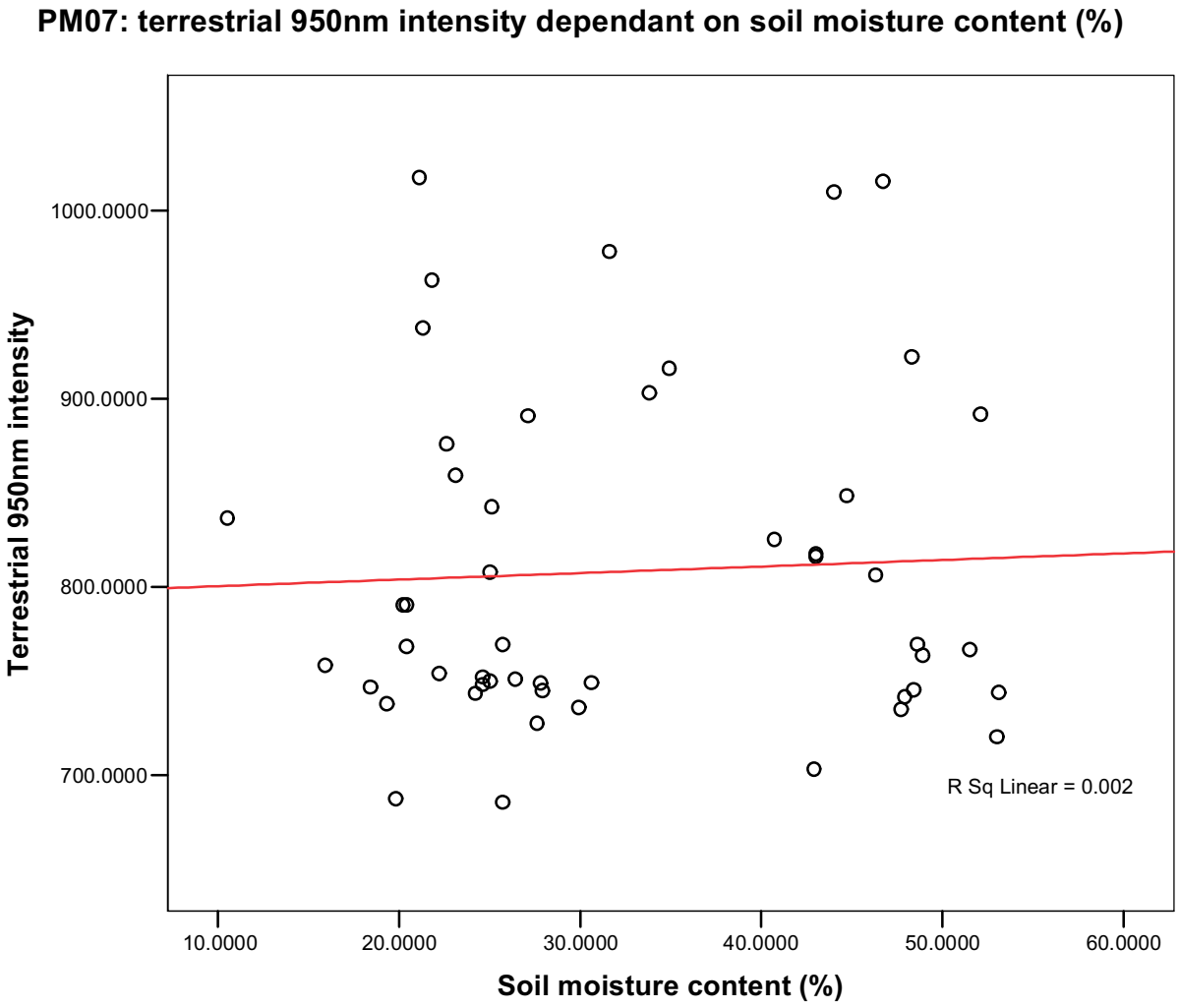

Fig 98: Port Meadow area PM07. Scatter plot showing 950nm reflectance against soil moisture content.

Correlations

		Terrestrial 950nm intensity	Soil moisture content (%)
Terrestrial 950nm intensity	Pearson Correlation	1	.047
	Sig. (2-tailed)		.743
	N	50	50
Soil moisture content (%)	Pearson Correlation	.047	1
	Sig. (2-tailed)	.743	
	N	50	50

Fig 99: Port meadow area PM07. Correlation coefficient of 950nm reflectance against soil moisture content.

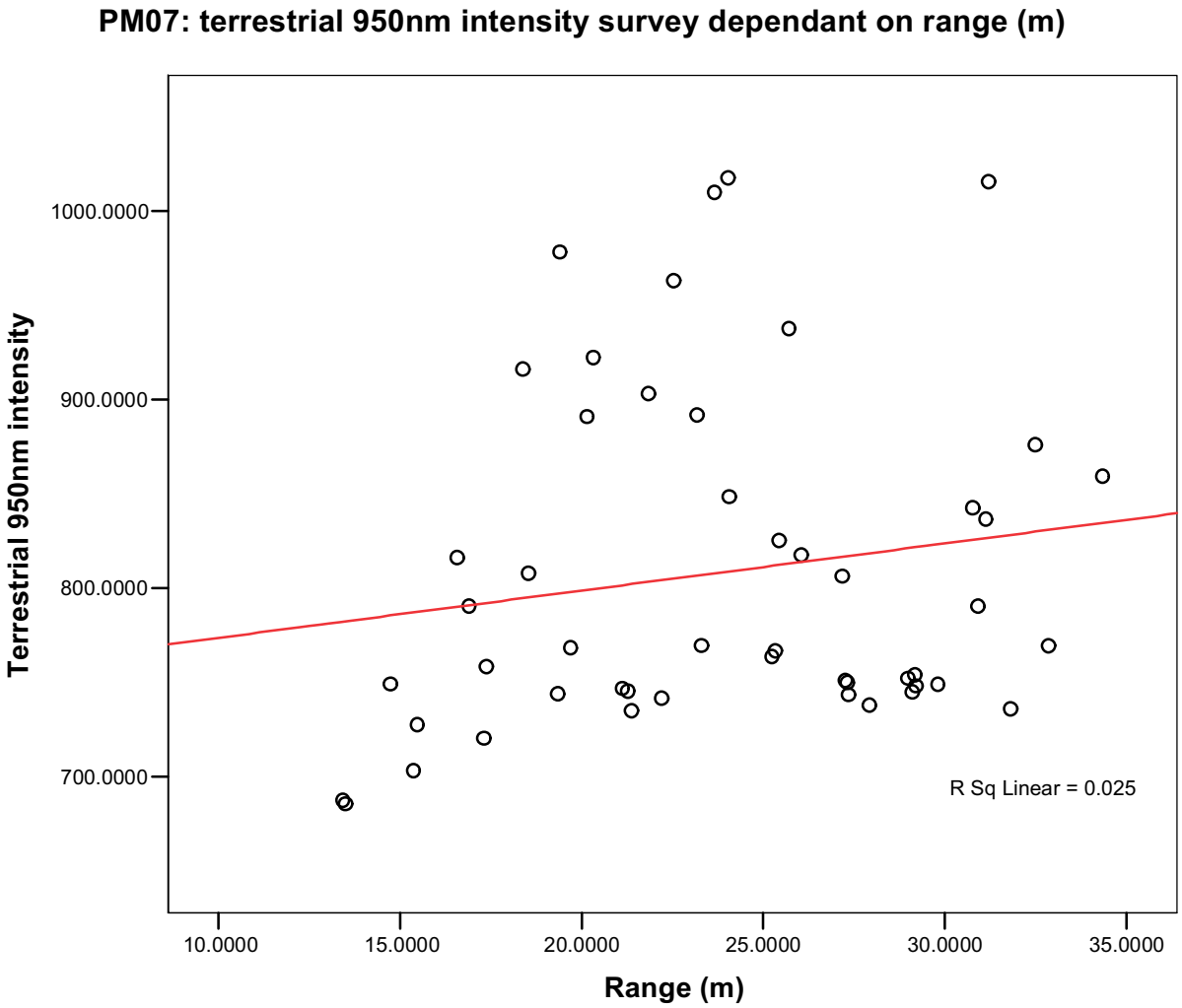

Fig 100: Port Meadow area PM07. Scatter plot showing 950nm reflectance against range (m).

Correlations

		Terrestrial 950nm intensity	Range (m)
Terrestrial 950nm intensity	Pearson Correlation	1	.159
	Sig. (2-tailed)		.270
	N	50	50
Range (m)	Pearson Correlation	.159	1
	Sig. (2-tailed)	.270	
	N	50	50

Fig 101: Port meadow area PM07. Correlation coefficient of 950nm reflectance against range (m).

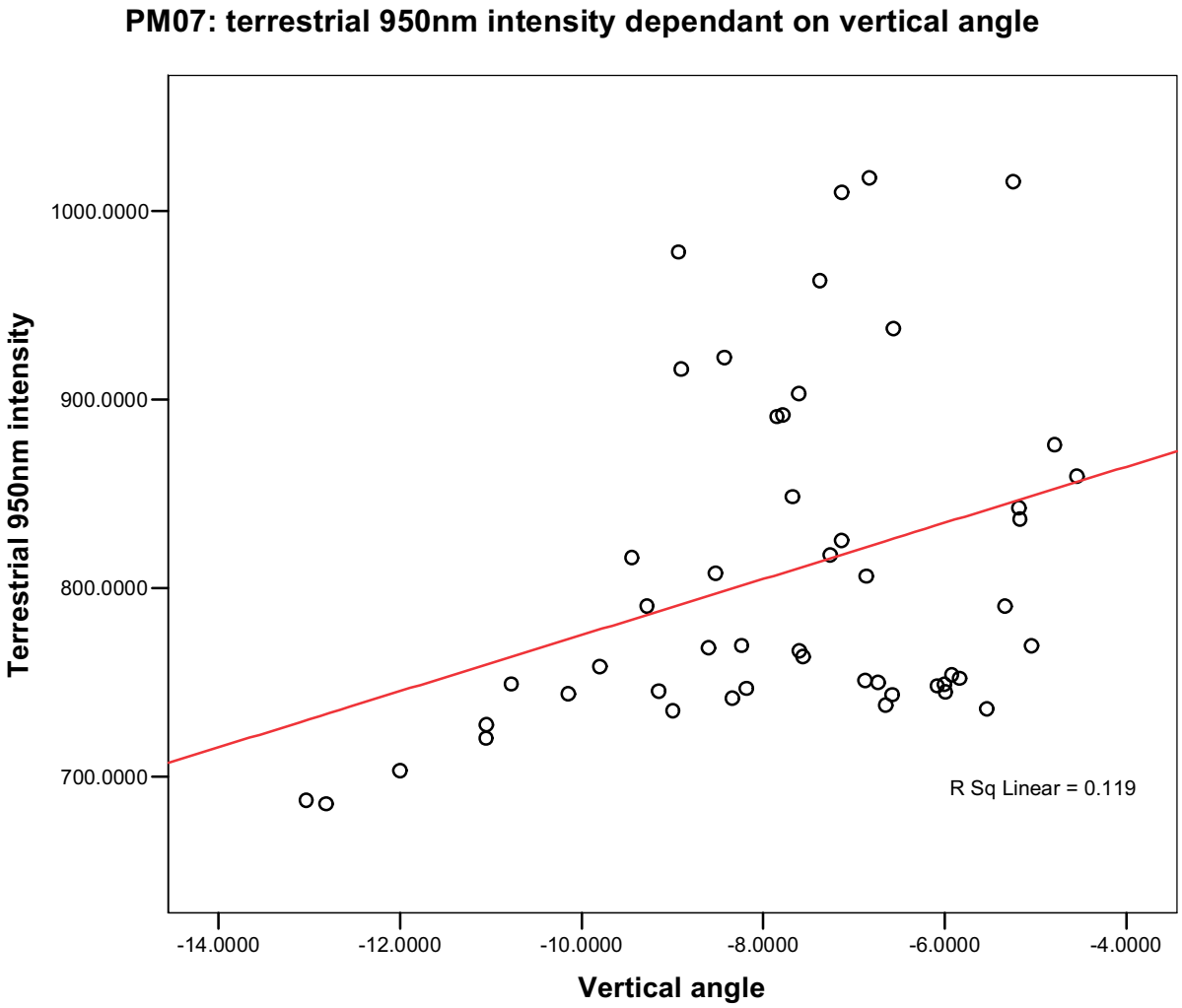

Fig 102: Port Meadow area PM07. Scatter plot showing 950nm reflectance against vertical angle.

Correlations

		Terrestrial 950nm intensity	Vertical angle
Terrestrial 950nm intensity	Pearson Correlation	1	.345*
	Sig. (2-tailed)		.014
	N	50	50
Vertical angle	Pearson Correlation	.345*	1
	Sig. (2-tailed)	.014	
	N	50	50

*. Correlation is significant at the 0.05 level (2-tailed).

Fig 103: Port meadow area PM07. Correlation coefficient of 950nm reflectance against vertical angle.

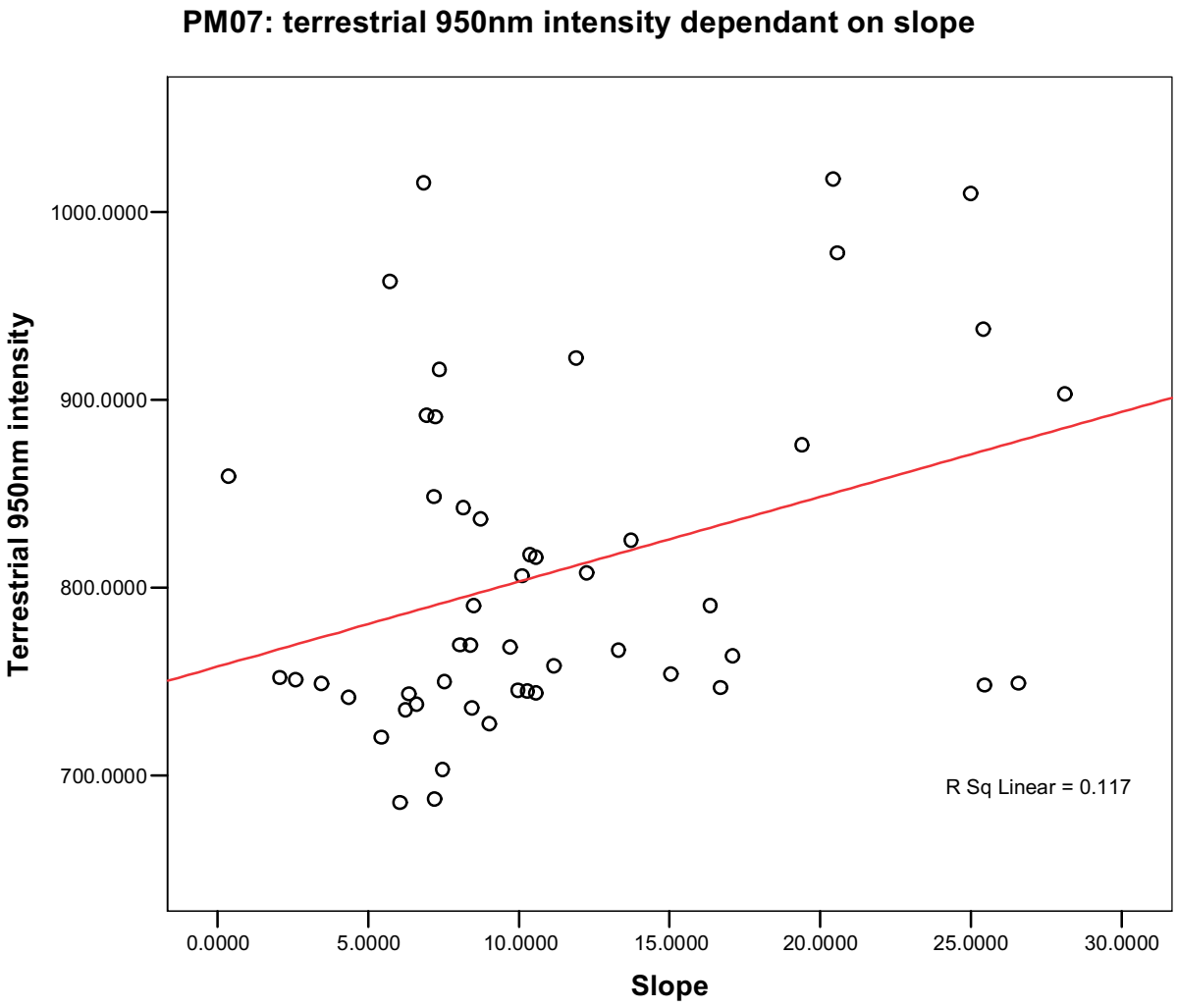

Fig 104: Port Meadow area PM07. Scatter plot showing 950nm reflectance against slope.

Correlations

		Terrestrial 950nm intensity	Slope
Terrestrial 950nm intensity	Pearson Correlation	1	.342*
	Sig. (2-tailed)		.015
	N	50	50
Slope	Pearson Correlation	.342*	1
	Sig. (2-tailed)	.015	
	N	50	50

*. Correlation is significant at the 0.05 level (2-tailed).

Fig 105: Port meadow area PM07. Correlation coefficient of 950nm reflectance against slope.

3.3.8 Area PM 09

Survey area PM09 was a 40m x 40m grid centred over a large anthropogenic ring-ditch in the centre of the Port Meadow study area. The feature consisted of a large earthen bank measuring approximately 34 metres in diameter, 7 metres in width and surviving to a maximum height of c. 0.3 metres above the surrounding floodplain. The bank appeared to be interrupted by narrow perpendicular ditches in three equally-spaced locations; to the west, east and south. A shallow ditch was located around the interior of the bank with a relatively flat central platform. The survey grid was oriented southwest-northeast in order to fully cover the extant earthwork remains. The scanner was located to the southwest of the survey grid and oriented northeast. At the time of the survey the site was under relatively dense damp pasture/meadow grass (c.0.4m in height), with cold but clear weather conditions.

The terrestrial laser scanning of PM09 produced a detailed elevation surface that accurately recorded the topography of the earthworks (Fig. 106). The airborne lidar elevation model had recorded the location and general form of the ring-ditch but in less detail than the terrestrial scan. The general form of the earthwork was also recorded on the 950nm reflectance surface produced from the pointcloud data, as well as the interpolated volumetric soil moisture readings. The surface revealed the bank as a high 950nm reflectance ring and the ditched areas as low 950nm intensity, although with other factors such as range clearly influencing the data set. The surface interpolated from the soil moisture readings highlighted the earthwork bank as an interrupted ring of low percentage moisture values, with the centre of the earthwork and the ditched areas being marked by relatively high moisture values. The range from the scanner again appeared to be a dominant factor affecting the backscattered 950nm reflectance of the terrestrial laser, indicating that as the range increased the 950nm reflectance value also increased (Fig. 107). As aforementioned, the scanner had been positioned over 10 metres away from the survey grid to provide a more even resolution of data points, but the influence of the range was again unavoidable. Slope and vertical angle also appeared to be distorting the 950nm intensity.

Although the earthwork was visible on both the backscattered 950nm reflectance and the volumetric soil moisture surface models, a scattergraph produced from these variables revealed a weak negative visual relationship between them with an R^2 value of only 0.0104 (Fig. 108). The correlation coefficient for these variables indicated no significant relationship at the 0.05 level (Fig. 109). However, a scattergraph produced comparing the 950nm reflectance values to the range of the laser pulse from the scanner revealed a strong positive relationship with an R^2 value of 0.6879 and the correlation coefficient indicated that the relationship was significant at the 0.01 level (Figs. 110 and 111).

A series of other scattergraphs were again produced from the 4 metre grid centroid points to test if any other variables were having a significant influence on the intensity values. For PM09 it was found that the impact of the slope angle ($R^2 = 0.101$) (Figs. 112 and 113) and the vertical angle of the scanner head ($R^2 = 0.0448$) (Figs. 114 and 115) were both significant at the 0.01 level. At PM09 the main factor influencing the backscattered 950nm reflectance values was found to be the range of the reflective target away from the scanning instrument itself.

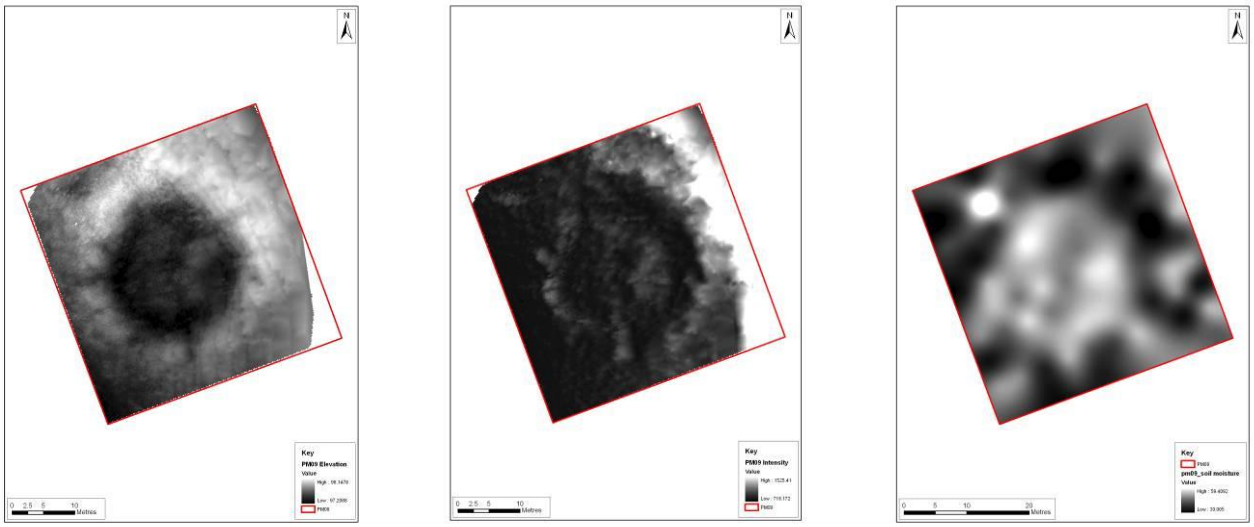

Fig 106: Port Meadow area PM09 terrestrial laser scanning showing from left to right elevation, intensity and volumetric soil moisture.

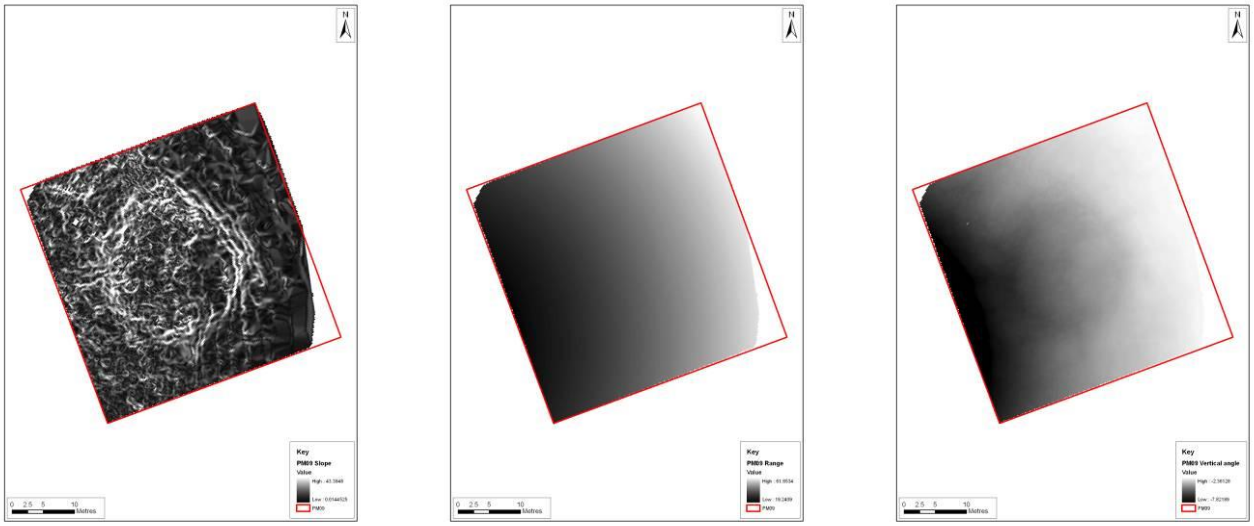

Fig 107: Port Meadow area PM09 terrestrial laser scanning showing from left to right slope severity, range and vertical angle.

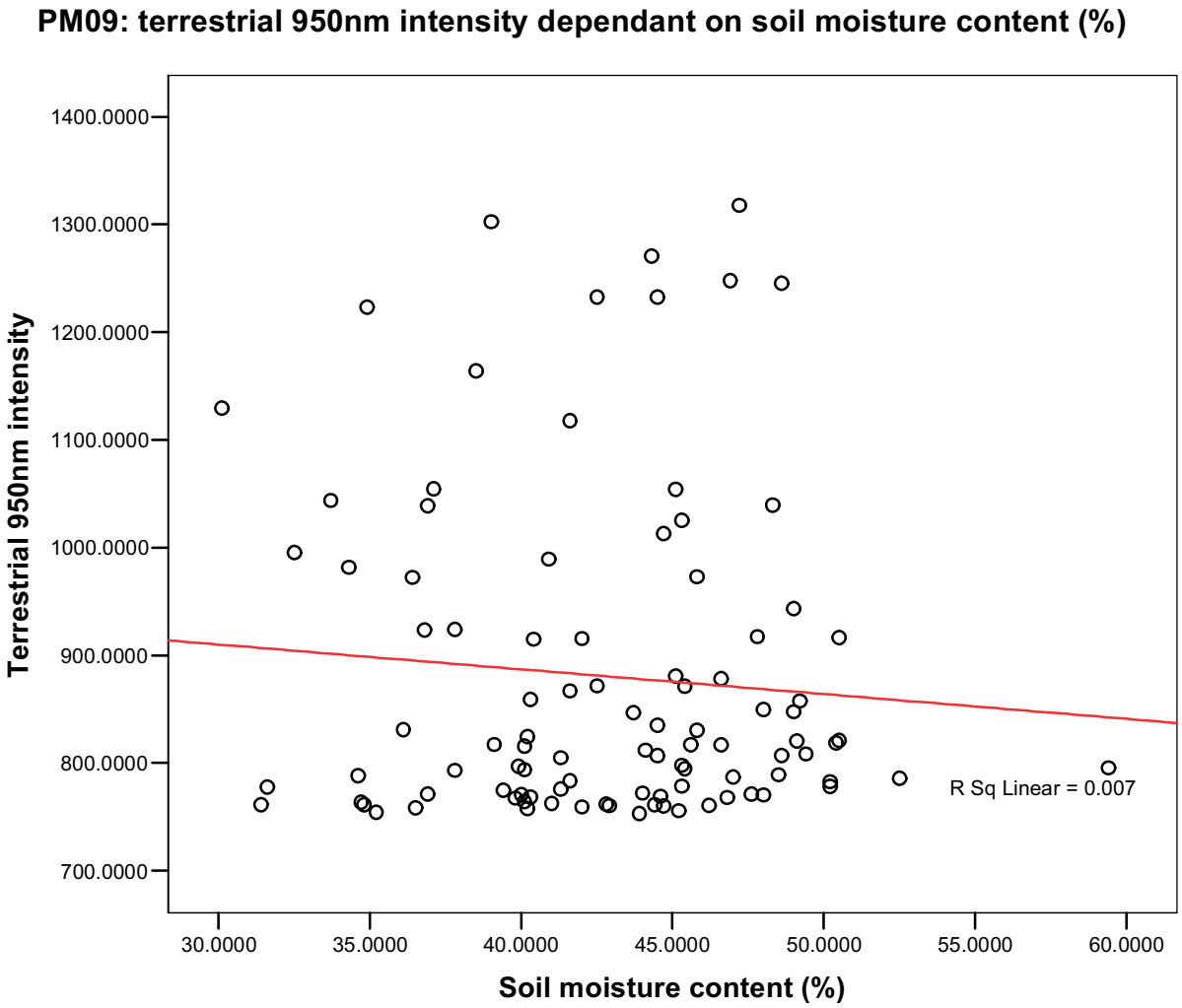

Fig 108: Port Meadow area PM09. Scatter plot showing 950nm reflectance against soil moisture content.

Correlations

		Terrestrial 950nm intensity	Soil moisture content (%)
Terrestrial 950nm intensity	Pearson Correlation	1	-.082
	Sig. (2-tailed)		.421
	N	98	98
Soil moisture content (%)	Pearson Correlation	-.082	1
	Sig. (2-tailed)	.421	
	N	98	98

Fig 109: Port meadow area PM09. Correlation coefficient of 950nm reflectance against soil moisture content.

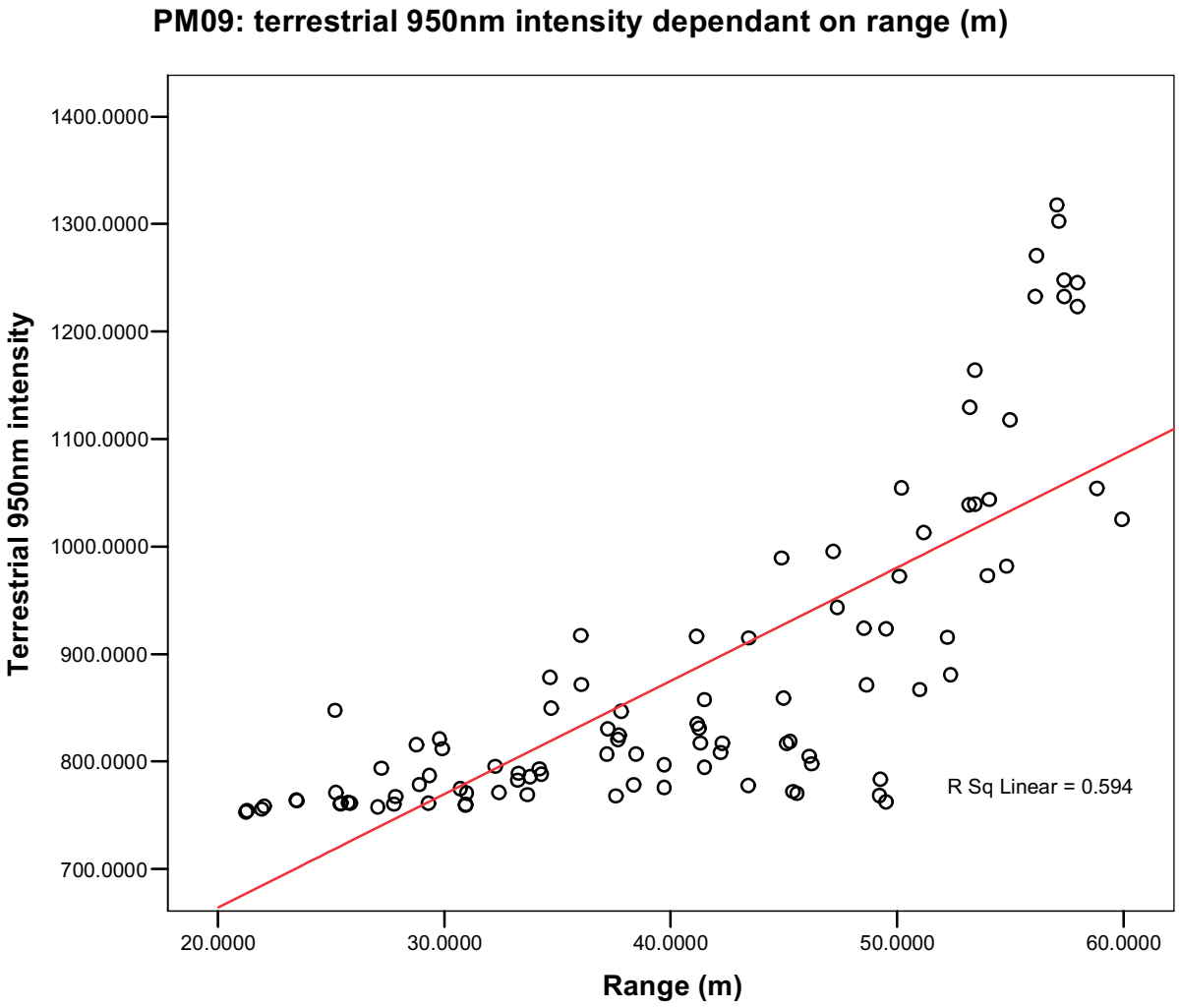

Fig 110: Port Meadow area PM09. Scatter plot showing 950nm reflectance against range (m).

Correlations

		Terrestrial 950nm intensity	Range (m)
Terrestrial 950nm intensity	Pearson Correlation	1	.771**
	Sig. (2-tailed)		.000
	N	98	98
Range (m)	Pearson Correlation	.771**	1
	Sig. (2-tailed)	.000	
	N	98	98

**. Correlation is significant at the 0.01 level (2-tailed).

Fig 111: Port meadow area PM09. Correlation coefficient of 950nm reflectance against range (m).

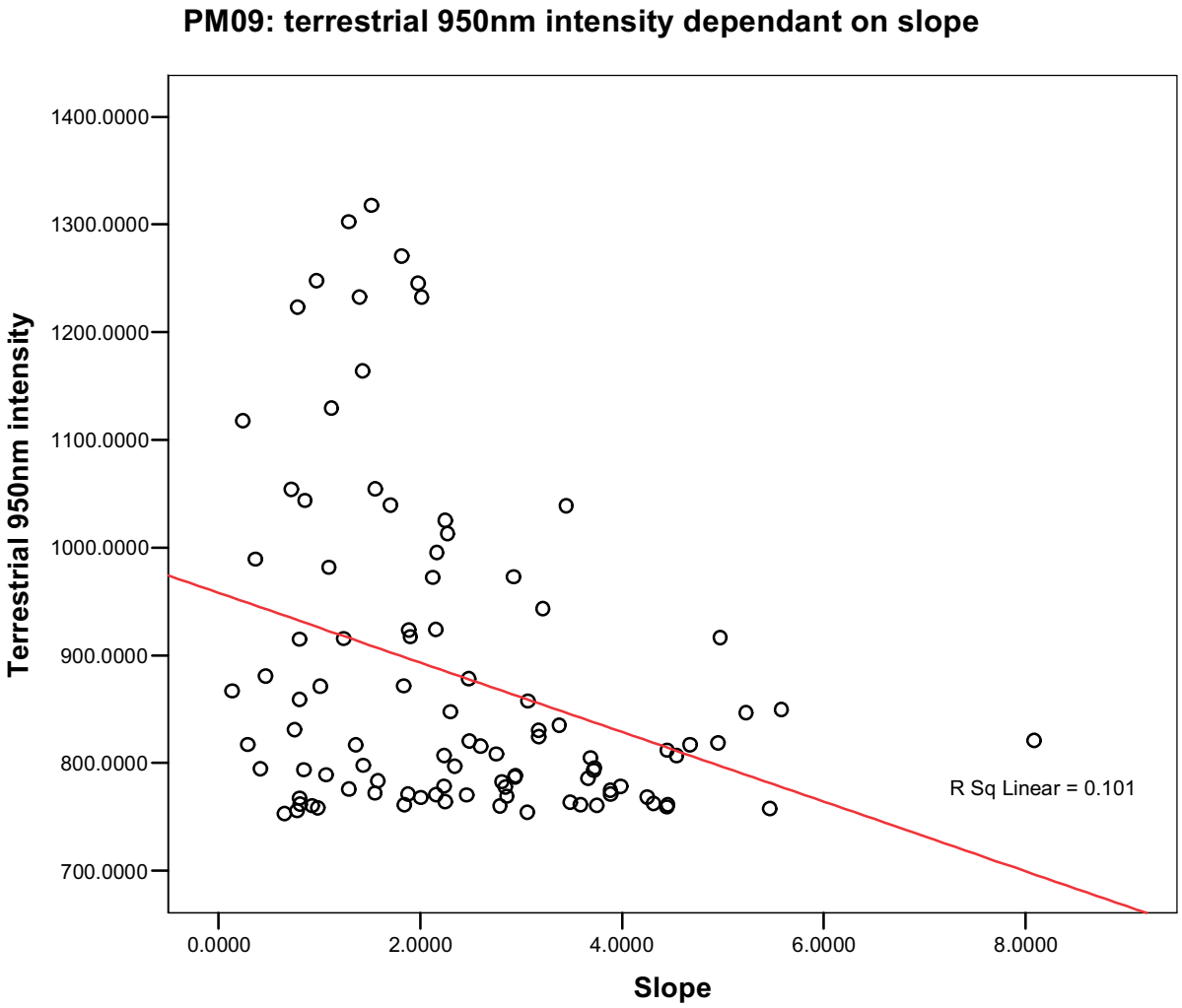

Fig 112: Port Meadow area PM09. Scatter plot showing 950nm reflectance against slope.

Correlations

		Terrestrial 950nm intensity	Slope
Terrestrial 950nm intensity	Pearson Correlation	1	-.318**
	Sig. (2-tailed)		.001
	N	98	98
Slope	Pearson Correlation	-.318**	1
	Sig. (2-tailed)	.001	
	N	98	98

**. Correlation is significant at the 0.01 level (2-tailed).

Fig 113: Port meadow area PM09. Correlation coefficient of 950nm reflectance against slope.

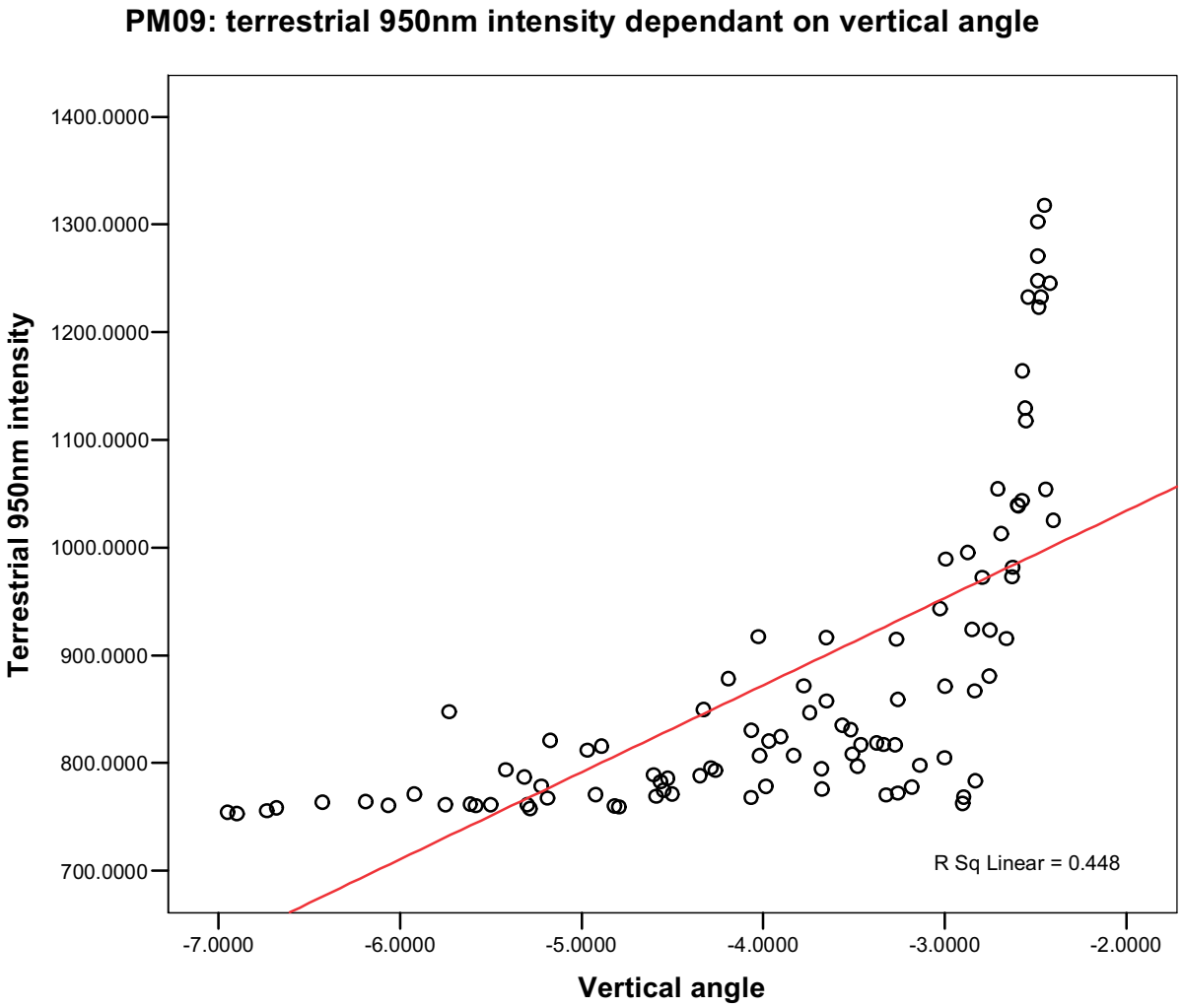

Fig 114: Port Meadow area PM09. Scatter plot showing 950nm reflectance against vertical angle.

.

Correlations

		Terrestrial 950nm intensity	Vertical angle
Terrestrial 950nm intensity	Pearson Correlation	1	.670**
	Sig. (2-tailed)		.000
	N	98	98
Vertical angle	Pearson Correlation	.670**	1
	Sig. (2-tailed)	.000	
	N	98	98

**. Correlation is significant at the 0.01 level (2-tailed).

Fig 115: Port meadow area PM09. Correlation coefficient of 950nm reflectance against vertical angle.

3.4 LOCKINGTON MARSHES, LEICESTERSHIRE

Three test scanning areas were undertaken on the Trent Soar confluence at Lockington marshes in Leicestershire, East Midlands, U.K. The surveys used terrestrial 950nm reflectance scanning combined with soil moisture, soil organic and earth resistance survey, over both geomorphological and cultural features. Not all data sets were recovered in all survey areas.

3.4.1 Geology and Topography of the Study Area

The study area is the confluence of the rivers Trent/Soar. The BGS drift geology map provides an overview of the study area, showing a two fold dating distribution of alluvial geomorphology, dividing the study area into Holocene and Devensian periods (116). The Lidar LP DTM provides a detailed topographic model of the study area, with the known HER (Historic Environment Record) plotted (Fig. 117). From the Lidar LP DTM it is clear that the there is an area of upper Devensian terrace (brown colour), containing the majority of the known archaeological resource. Then there is an area of intermediate/lower terrace, containing a wealth of geomorphological features such as palaeochannels, but little in the way of a visible cultural archaeological resource.

The ALSF funded project 'Predictive modelling of multi-period geoarchaeological resources at a river confluence' (PNUM 3351, Brown *et al.* 2005; 2007), showed the confluence zone below the Devensian terrace to have evolved primarily from avulsion events over a braid plain of reworked Devensian gravels, with little floodplain development through meander migration in the Holocene. This has produced a series of well defined palaeochannels and terraces segments with typically 1-2m of above gravel alluvium in the lower Holocene terraces. In contrast the upper Devensian terrace has very thin soils (c. 40cm) covering terrace Devensian gravels, with little in the way of preserved palaeochannels or other geomorphological features, but a very visible cultural archaeological resource due to thin soils.

3.4.2 Locations of Terrestrial Laser Scanning Test Areas

With the study area three locations were selected for terrestrial 950nm reflectance scanning. They were selected to provide a test for a series of different geoarchaeological features (Fig. 118). The survey locations were:

A) Fort Field (FF survey): This survey was conducted on an area of Holocene terrace, where a palaeochannel bisects an area of terrace. Four 30m x 30m grids were surveyed. Data collection involved 950nm intensity, soil organic content, soil moisture content and earth resistance survey.
B) Modern floodplain survey (MF survey): This survey was on the lowest part of the study area, surveying an area of terrace and an area of palaeochannel. Two 30m x 30m grid were used. Data collection involved 950nm intensity, soil organic content and soil moisture content.
C) Villa Field survey (VF Survey): This survey was conducted on an area of Devensian terrace 2, surveying over some cropmark locations. Data collection was 950nm reflectance data only.

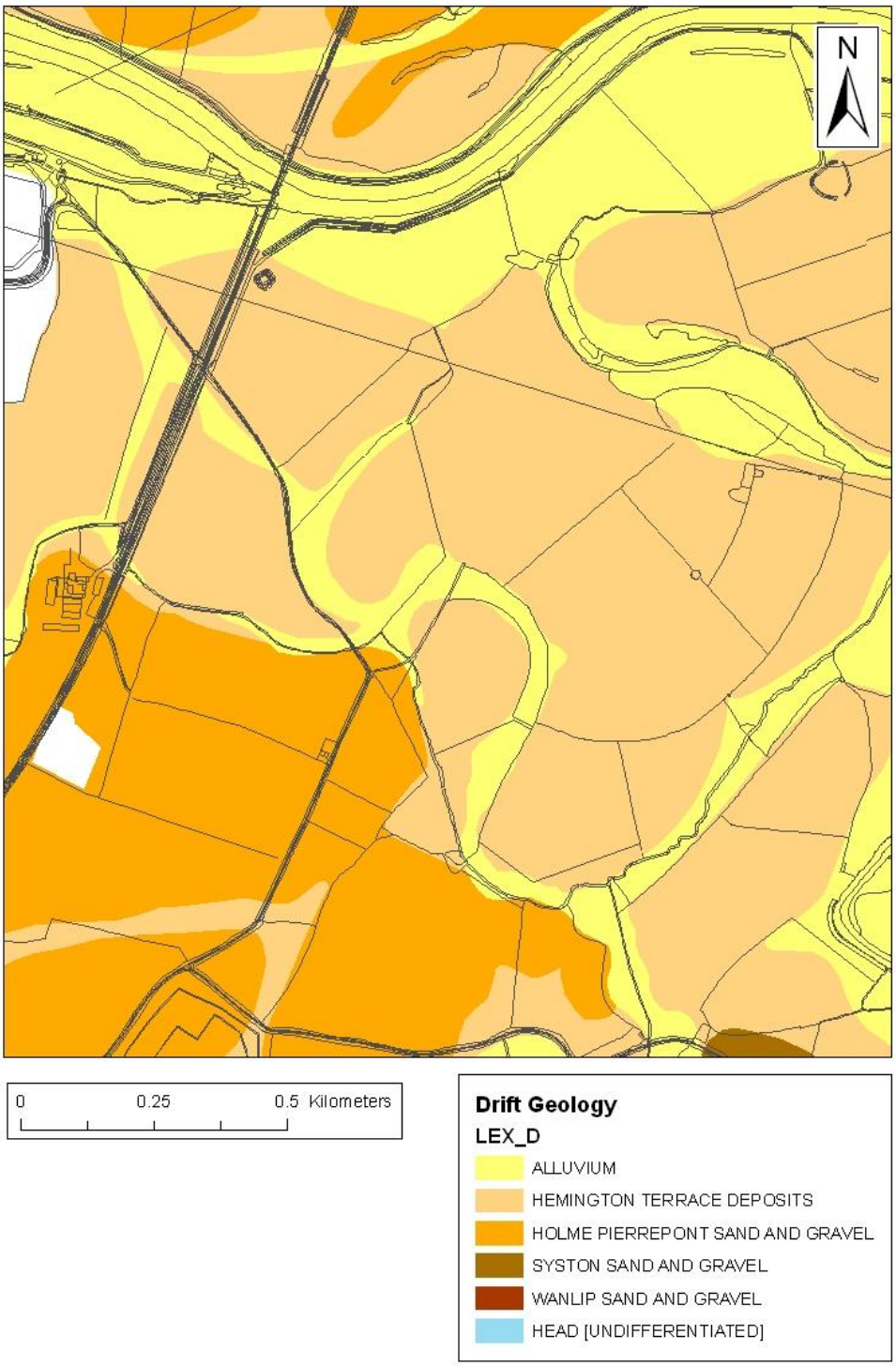

Fig 116: The BGS drift geology map of the study area.

Fig 117: The study area with HER recorded sites shown.

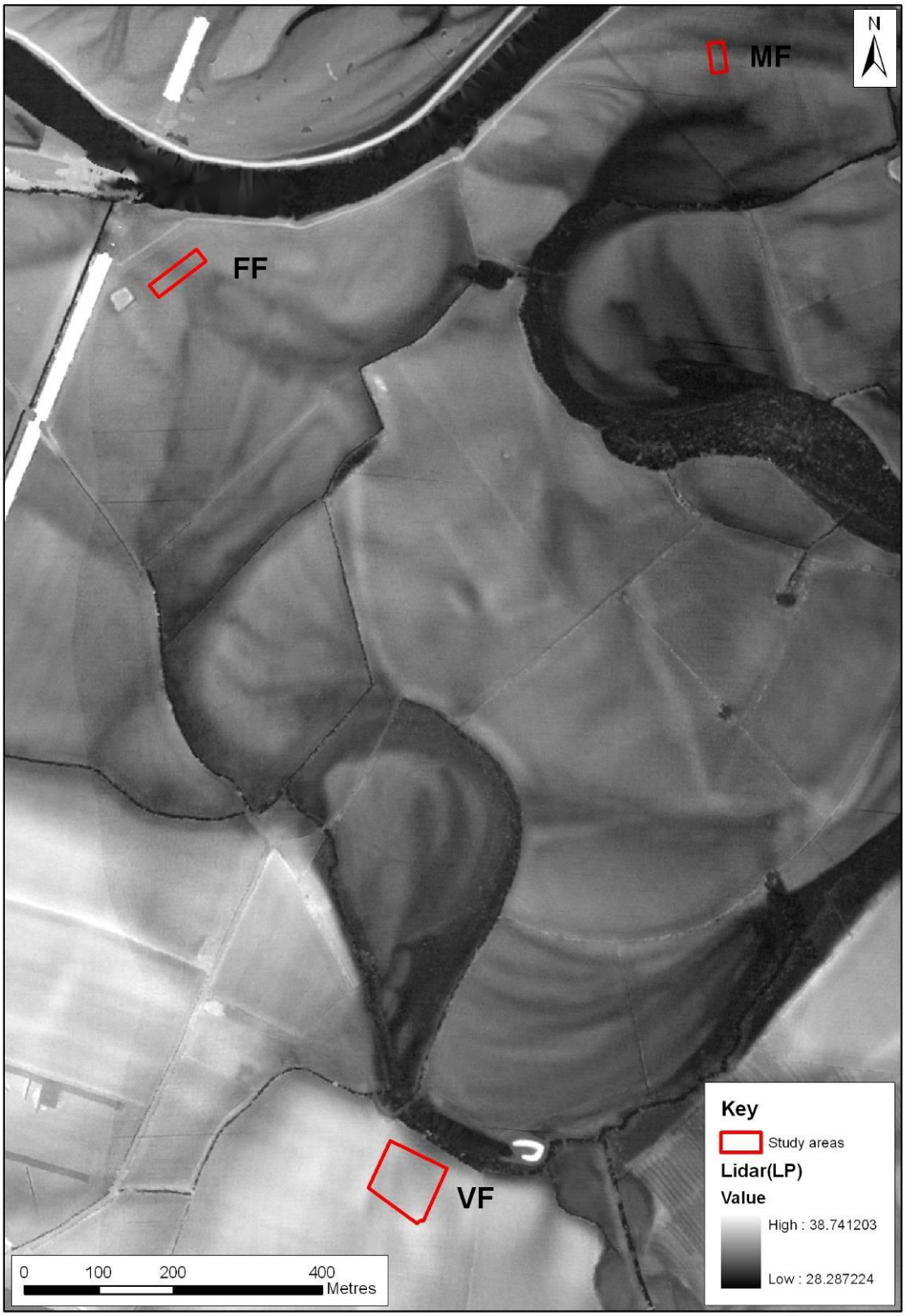

Fig 118: Lockington, Leicestershire. Lidar digital surface model showing areas of terrestrial laser scanning outlined in red.

3.4.3 Area FF

The survey used four 30 x 30m grids set out in a line, moving from an area of terrace, over a palaeochannel and back on to an area of terrace (Fig. 118). The survey aimed to investigate the difference in 950nm spectral reflectance between the palaeochannel and terrace deposits. Soil organic samples were taken from the topsoil at 4m intervals within each grid, using a centroid method, and soil moisture was also recorded at each sample location. The scanner had two separate survey locations, each survey location being 20m from the grid edge. Survey point one was 20m behind the junction between grids 1and 2 and survey point 2 was 20m behind the junction between grids 3 and 4. The scanner locations were to the southeast of the grid. In addition to the soil organic and moisture measurements, an earth resistance survey was also undertaken using a 1m sample interval over the grids, as a proxy for variation in soil moisture/soil organic content. The field condition was short pasture.

Within the FF survey area the palaeochannel and areas of terrace are not evident as a surface topographic feature from the terrestrial scanning (Fig. 119). The 950nm reflectance produces an even less clear image, with a distinct range effect. It is apparent that the 950nm reflectance values increase with increasing distance from the scanner, and this effect significantly distorts the data. Neither the palaeochannel nor the areas of terrace are recognisable as areas of higher intensity. The variation in the topographic and intensity data sets appears, through visual examination, to be the product of instrumentation.

The soil moisture data does not define any of the geomorphology in the survey area (Fig. 120). The area of higher terrace to the northeast of the survey area clearly has low moisture values and the palaeochannel does record some high surface moisture values. However, the surface generated from the soil moisture point cloud does not clearly define either the palaeochannel or the areas of terrace. The soil organic data provides a contrast to the soil moisture data with the palaeochannel and the areas of terrace clearly definable (Fig. 120). Surprisingly, the palaeochannel is evident through having low soil organic content relative to the areas of terrace with higher organic content. The earth resistance survey clearly defines the geomorphology of the survey area, with the palaeochannel and areas of terrace interpretable (Fig. 120). As expected the palaeochannel is evident as a low resistance feature and the areas of terrace are visible as areas of higher resistance.

The 950nm reflectance response was investigated through the properties of slope, range and vertical angle, which are all properties of the scanning instrument (Fig. 121). It is clear that there are factors other than soil conditions affecting the backscatter of 950nm intensity. The slope, which decreases with increasing distance from the scanning instrument, shows two defined arches, one from each scanning location. The range also shows the same arcing pattern from each scanner location, as does the vertical angle. It is clear that the dominant forms of variance within the data set are a product of instrumentation and the relationship of intensity to vertical angle demonstrates this (Fig. 122), with a positive relationship of 49% between the two variables and a highly significant relationship (Fig. 123). Likewise, the range of the scanner has a positive relationship with 950nm reflectance (Fig. 124) and also displays a highly significant relationship (Fig. 125). The slope reveals a weak negative relationship with 950nm reflectance and this relationship is not significant (Figs. 126 and 127). The fact that the dominant form of variance in the data set is instrumentation means that any relationships between soil parameters and the 950nm reflectance are liable to only account for a very small part of the variance in the data set.

However, there is a weak negative linear relationship between soil moisture and 950nm reflectance (Fig. 128). This is shown as significant at the 0.05 level (Fig. 129). The relationship of 950nm reflectance dependant on organic content reveals a weak positive linear relationship (Fig. 130), but this is shown as a highly significant positive correlation at the 0.01 level (Fig. 131). The correlation coefficient also displays a positive relationship, as did the graphical analysis and the surface models earlier in the chapter. This positive relationship between 950nm reflectance and organic content of the soil relates to the curious distribution of organics within the survey area, with the areas of terrace adjacent to the palaeochannel having a higher organic content than the surface sediments of the palaeochannel. The reverse situation would normally be expected, with a negative relationship between the two variables, with palaeochannels (areas of higher moisture content) having higher organic contents.

The 950nm reflectance against earth resistance survey shows a moderate positive relationship (Fig. 132), but is again shown to statistically significant at the 0.01 level (Fig. 133). Again the correlation between the two variables is positive, as ohms increases (higher resistance, lower water, e.g. areas of terrace) then 950nm reflectance increases. This is what is expected, i.e. the opposite of the relationship to soil moisture content.

It is surprising that the soil parameters show statistically significant relationships to 950nm intensity, when the strongest linear relationships seen have been vertical angle and range; variance in the data caused by instrumentation. However, like with the laboratory 1047nm reflectance data set, it is interpreted that 950nm reflectance is not dependant on any of the soil parameters, e.g. organic content. Merely 950nm and the other soil variables are representing variations in the sediment architecture. Further to this, as the organic content distribution produced a surface model contrary to that expected (higher organic contents in the terrace deposits compared to the palaeochannel), it aptly demonstrates that 950nm was not dependant on organic content, otherwise a reversed distribution in 950nm would have been detected.

The soil parameters do show significant relationships to each other, demonstrating consistency with the results obtained from the 950nm intensity. Surprisingly there is a moderate linear negative relationship between soil moisture and soil organic contents (Fig. 134). Although this would not be anticipated in normal conditions, the organic content showed a surface distribution model opposite to that expected, with the palaeochannel having a lower organic content than the surrounding terrace. Thus the negative relationship reflects that witnessed in the surface distribution models and is significant at the 0.05 level (Fig. 135). This relationship is again apparent between earth resistance survey and organic soil content (Fig. 136) with a moderate positive relationship between the two variables (as earth resistance increases, e.g. gravel units, organic content increases). This is again shown to be a highly significant positive correlation at the 0.01 level (Fig. 137) and is in agreement with the interpretations made earlier in the chapter. The relationship between soil moisture and earth resistance is shown to be a moderate negative linear relationship (Fig. 138) and is again highly significant at the 0.01 level (Fig. 139).

From this analysis there are several key points:

- The main cause of variance in the data set was the scanning instrument.
- This variance caused a linear increase in intensity with increasing distance from the scanner.

- The soil organic distribution produced a surface model with higher organic contents on the terrace than in the palaeochannel. It was originally expected that the palaeochannel surface sediments would have the highest organic content, but this model proved to be incorrect in this instance.
- The soil organic content revealed a highly significant positive relationship with 950nm intensity.
- The positive relationship between soil organic content and 950nm reflectance is the opposite of that expected. However, the soil organic contents were lower in the palaeochannel than in the terrace.
- The soil moisture content and 950nm reflectance revealed a significant negative relationship.
- The earth resistance survey and 950nm reflectance showed a highly significant positive relationship.
- The visual relationship of 950nm reflectance to each of the soil parameters appears to be non linear. However, this maybe a function of variance caused by the instrument distorting the analysis.
- The soil parameters showed a high level of inter-variable correlation.
- Soil moisture and soil organic contents displayed a negative relationship, i.e. as soil moisture increased organic content decreased. This is the opposite of the expected relationship.
- Soil moisture content and earth resistance survey revealed a significant negative relationship.
- Soil organic content and earth resistance survey revealed a significant positive relationship.
- It is interpreted from this data that 950nm reflectance is not dependant on any of the single soil parameters. Instead the soil parameters and 950nm reflectance are all reflecting underlying changes in sediment architecture.

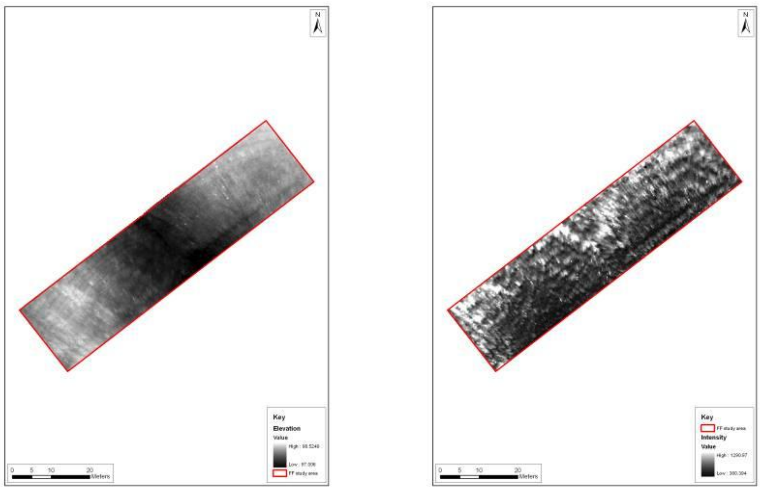

Fig 119: Lockington area FF terrestrial laser scanning showing from left to right elevation and intensity.

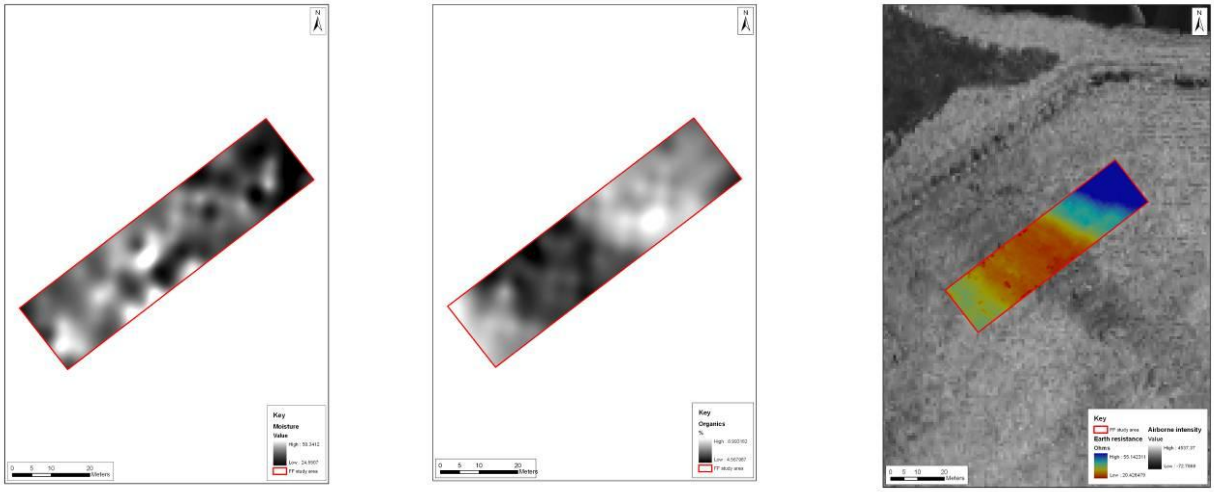

Fig 120: Lockington area FF showing from left to right volumetric soil moisture, organic content and earth resistance survey (ohms).

Fig 121: Lockington area FF terrestrial laser scanning showing from left to right slope severity, range and vertical angle.

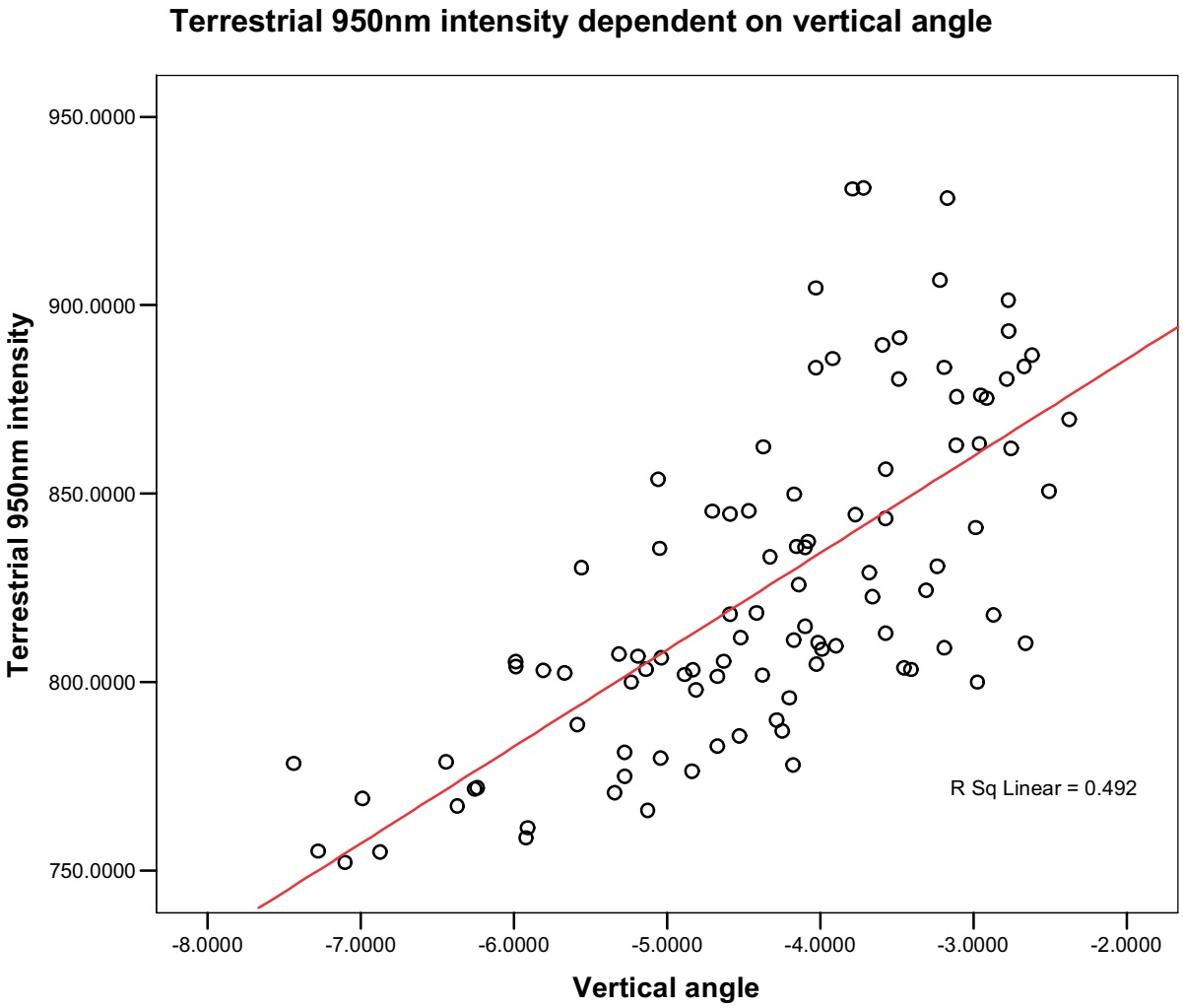

Fig 122: Scattergraph of 950nm reflectance against vertical angle of the scanner head. There is a relatively strong positive relationship between the two variables, with 49% of the variance in the data set explained by the relationship of the two variables.

Correlations

		Terrestrial 950nm intensity	Vertical angle
Terrestrial 950nm intensity	Pearson Correlation	1	.701**
	Sig. (2-tailed)		.000
	N	100	100
Vertical angle	Pearson Correlation	.701**	1
	Sig. (2-tailed)	.000	
	N	100	100

**. Correlation is significant at the 0.01 level (2-tailed).

Fig 123: The positive relationship between 950nm reflectance and vertical angle is highly significant at the 0.01 level (two tailed).

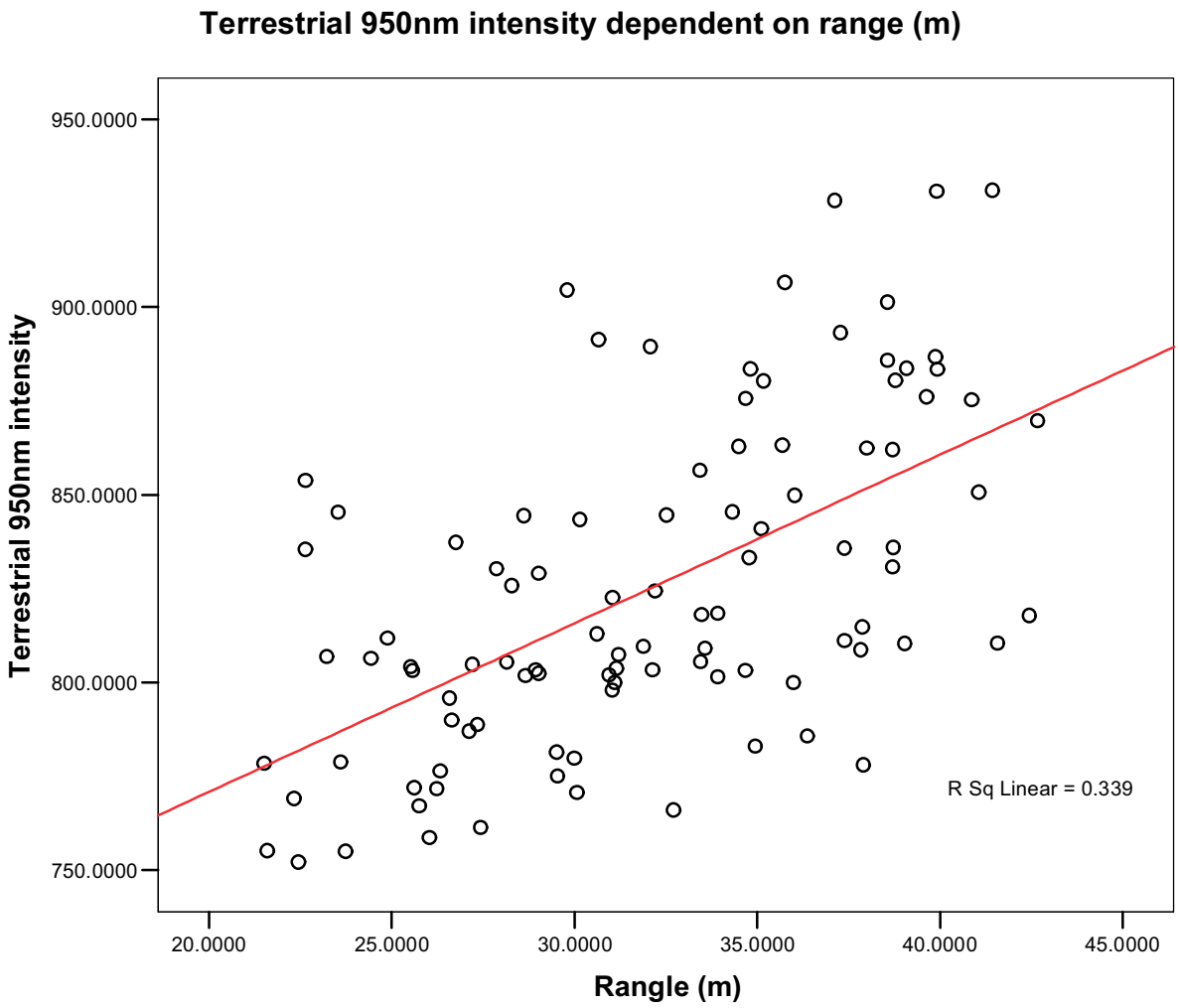

Fig 124: Scattergraph of 950nm reflectance against range (the distance of measurement from the scanner). There is a relatively strong positive relationship between the two variables.

Correlations

		Terrestrial 950nm intensity	Rangle (m)
Terrestrial 950nm intensity	Pearson Correlation	1	.582**
	Sig. (2-tailed)		.000
	N	100	100
Rangle (m)	Pearson Correlation	.582**	1
	Sig. (2-tailed)	.000	
	N	100	100

**. Correlation is significant at the 0.01 level (2-tailed).

Fig 125: The relationship between 950nm reflectance and range is highly significant at the 0.01 level (two tailed). This is hardly surprising as vertical angle is a function of range.

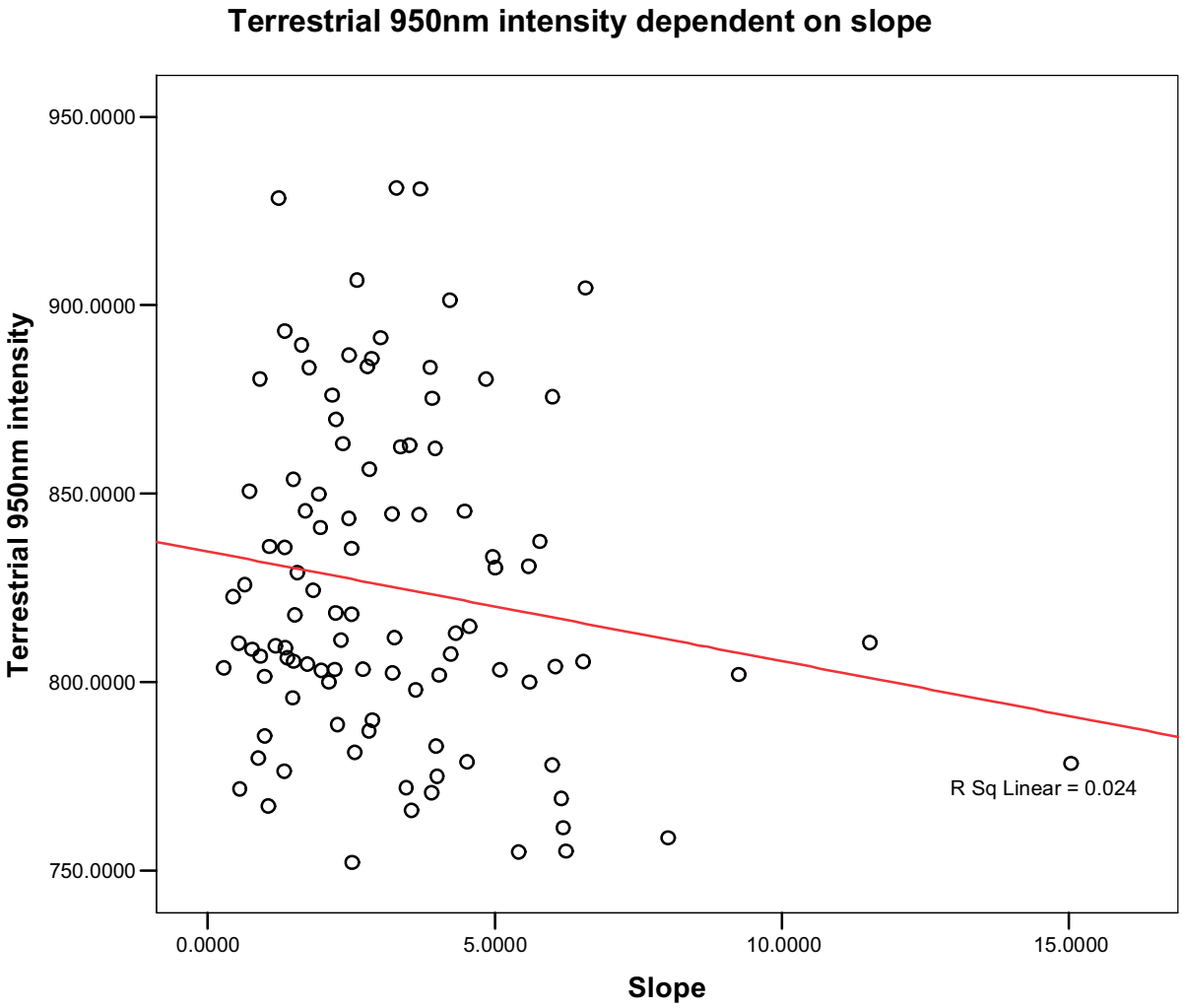

Fig 126: Scattergraph of 950nm reflectance against slope. There is a weak negative linear relationship between the two variables.

Correlations

		Terrestrial 950nm intensity	Slope
Terrestrial 950nm intensity	Pearson Correlation	1	-.156
	Sig. (2-tailed)		.120
	N	100	100
Slope	Pearson Correlation	-.156	1
	Sig. (2-tailed)	.120	
	N	100	100

Fig 127: There is no systematic relationship between the two variables.

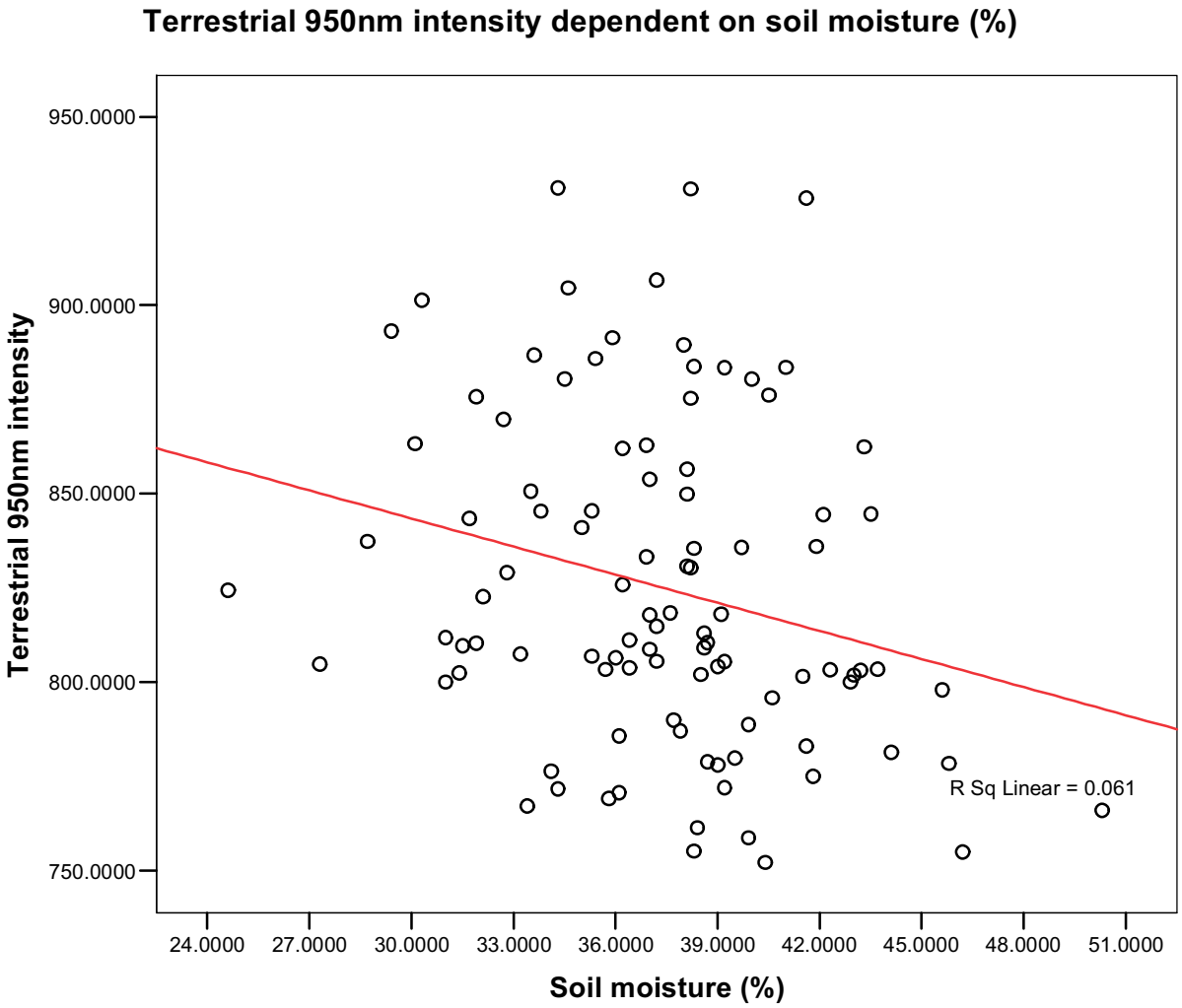

Fig 128: Scattergraph of 950nm reflectance dependant on soil moisture. A weak negative linear relationship is apparent.

Correlations

		Terrestrial 950nm intensity	Soil moisture (%)
Terrestrial 950nm intensity	Pearson Correlation	1	-.248*
	Sig. (2-tailed)		.013
	N	100	100
Soil moisture (%)	Pearson Correlation	-.248*	1
	Sig. (2-tailed)	.013	
	N	100	100

*. Correlation is significant at the 0.05 level (2-tailed).

Fig 129: There is a significant negative relationship between 950nm reflectance and soil moisture at the 0.05 level.

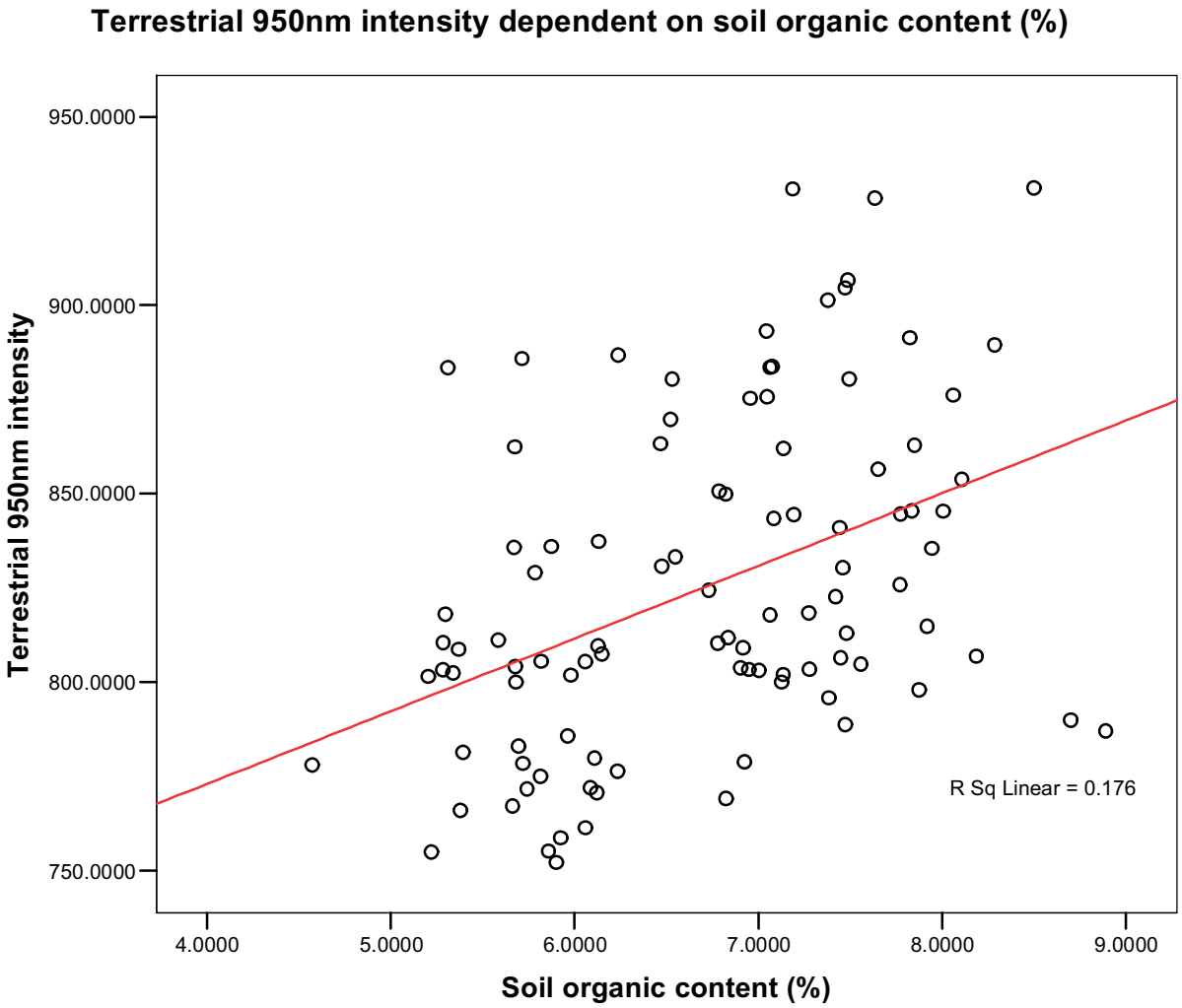

Fig 130: Scattergraph of 950nm reflectance dependant on soil organic content. There is a positive relationship between these two variables.

Correlations

		Soil organic content (%)	Terrestrial 950nm intensity
Soil organic content (%)	Pearson Correlation	1	.419**
	Sig. (2-tailed)		.000
	N	100	100
Terrestrial 950nm intensity	Pearson Correlation	.419**	1
	Sig. (2-tailed)	.000	
	N	100	100

**. Correlation is significant at the 0.01 level (2-tailed).

Fig 131: There is a highly significant positive relationship between 950nm reflectance and soil organic content at the 0.01 level.

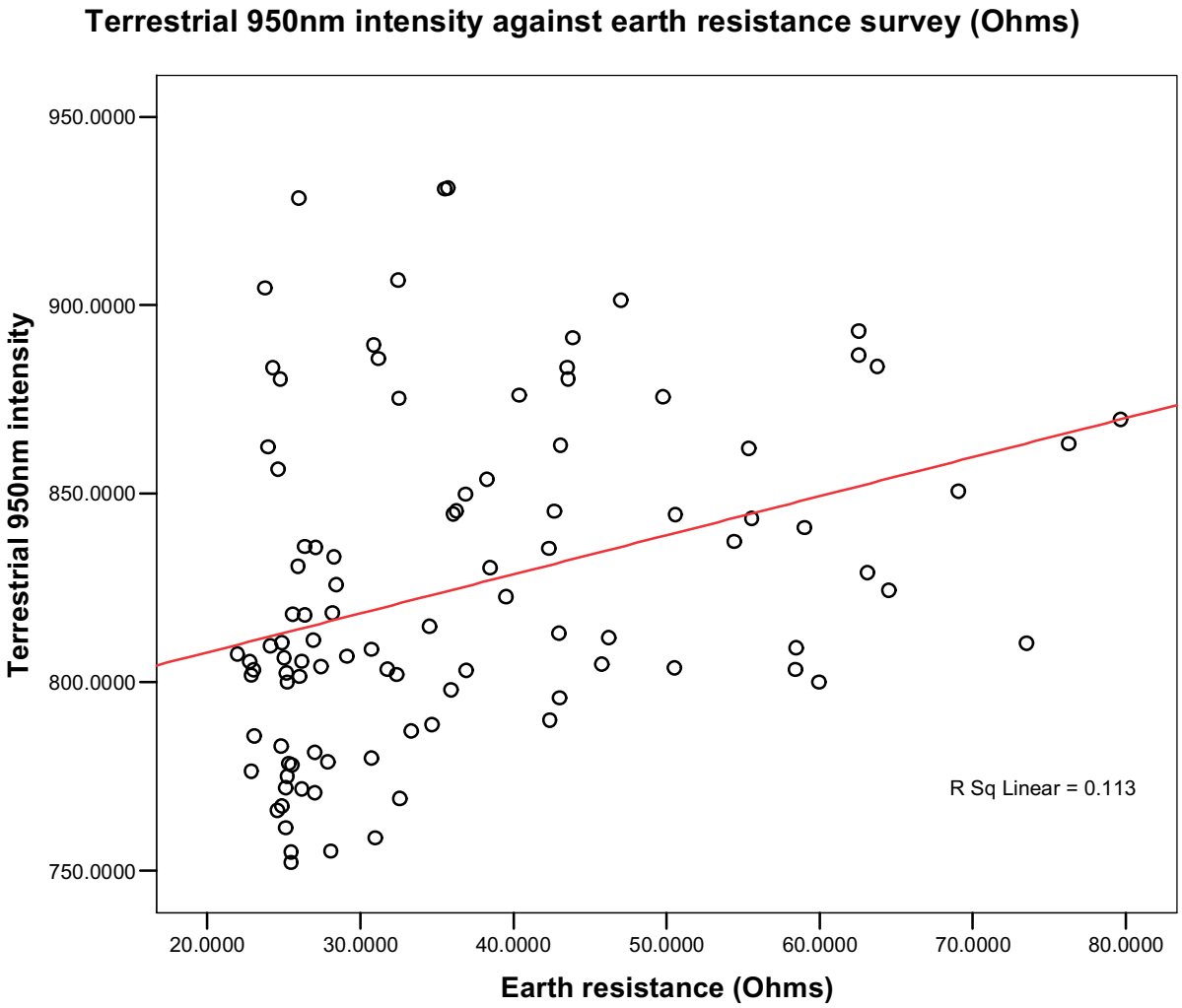

Fig 132: 950nm reflectance against earth resistance survey (Ohms), showing a moderate positive relationship.

Correlations

		Terrestrial 950nm intensity	Earth resistance (Ohms)
Terrestrial 950nm intensity	Pearson Correlation	1	.336**
	Sig. (2-tailed)		.001
	N	100	100
Earth resistance (Ohms)	Pearson Correlation	.336**	1
	Sig. (2-tailed)	.001	
	N	100	100

**. Correlation is significant at the 0.01 level (2-tailed).

Fig 133: There is a highly significant positive relationship between the two variables at the 0.01 level.

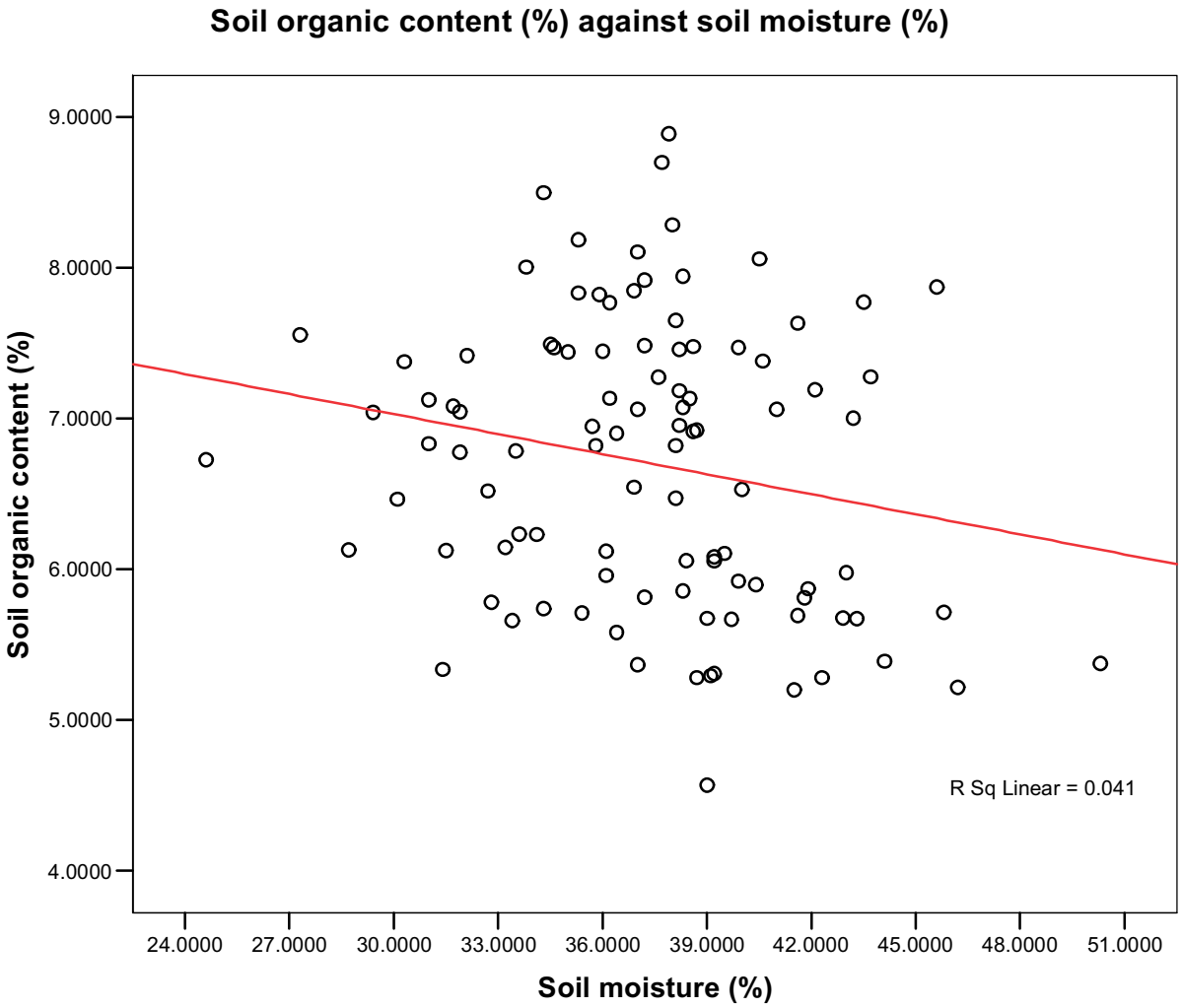

Fig 134: Scattergraph of soil organic content against soil moisture content. There is weak negative relationship between the two variables.

Correlations

		Soil organic content (%)	Soil moisture (%)
Soil organic content (%)	Pearson Correlation	1	-.203*
	Sig. (2-tailed)		.043
	N	100	100
Soil moisture (%)	Pearson Correlation	-.203*	1
	Sig. (2-tailed)	.043	
	N	100	100

*. Correlation is significant at the 0.05 level (2-tailed).

Fig 135: The negative relationship between soil organic content and soil moisture is significant at the 0.05 level.

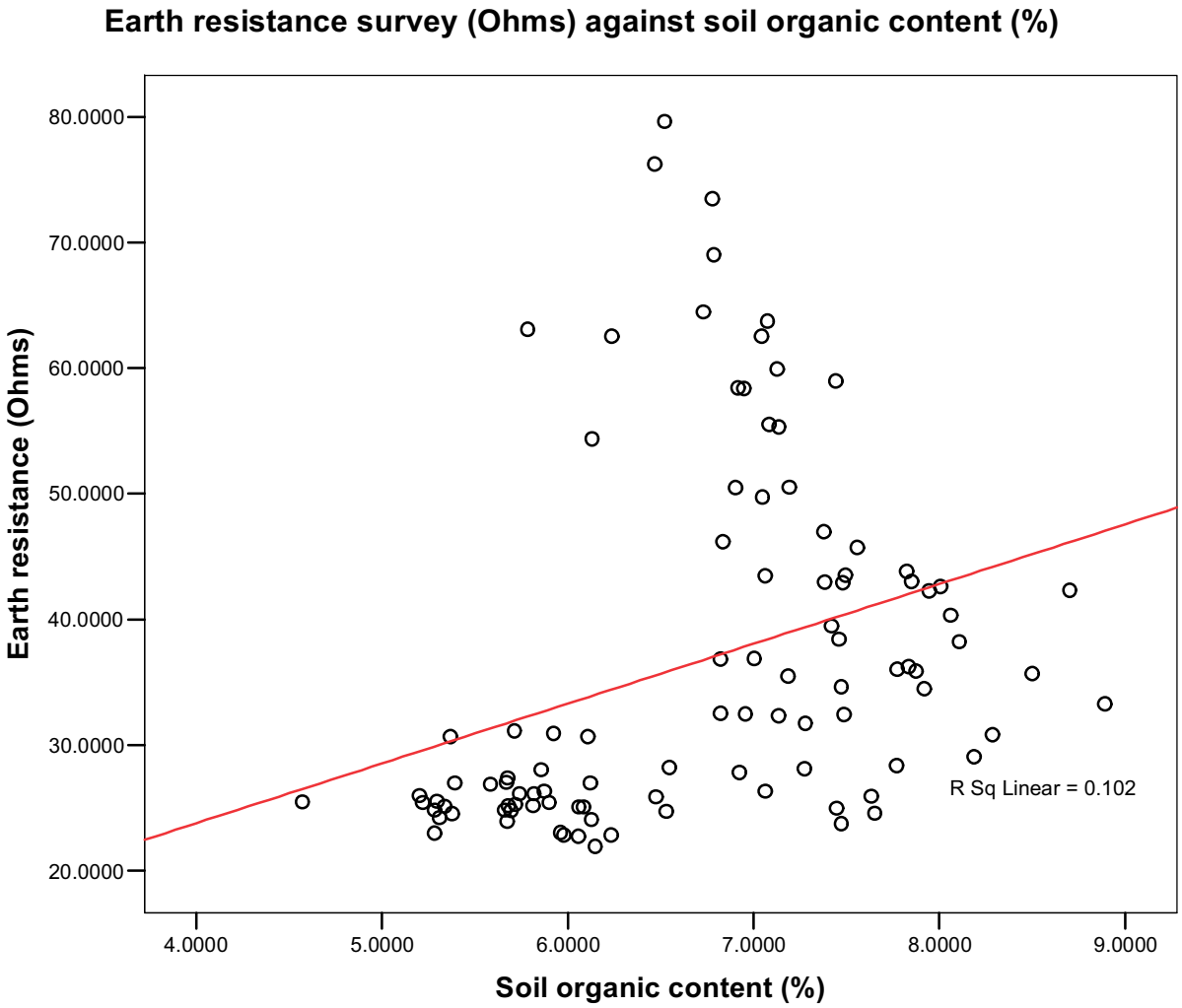

Fig 136: Scattergraph of earth resistance survey (Ohms) against soil organic content (%), showing a moderate positive relationship.

Correlations

		Earth resistance (Ohms)	Soil organic content (%)
Earth resistance (Ohms)	Pearson Correlation	1	.319**
	Sig. (2-tailed)		.001
	N	100	100
Soil organic content (%)	Pearson Correlation	.319**	1
	Sig. (2-tailed)	.001	
	N	100	100

**. Correlation is significant at the 0.01 level (2-tailed).

Fig 137: There is a highly significant positive correlation between earth resistance survey and soil organic content.

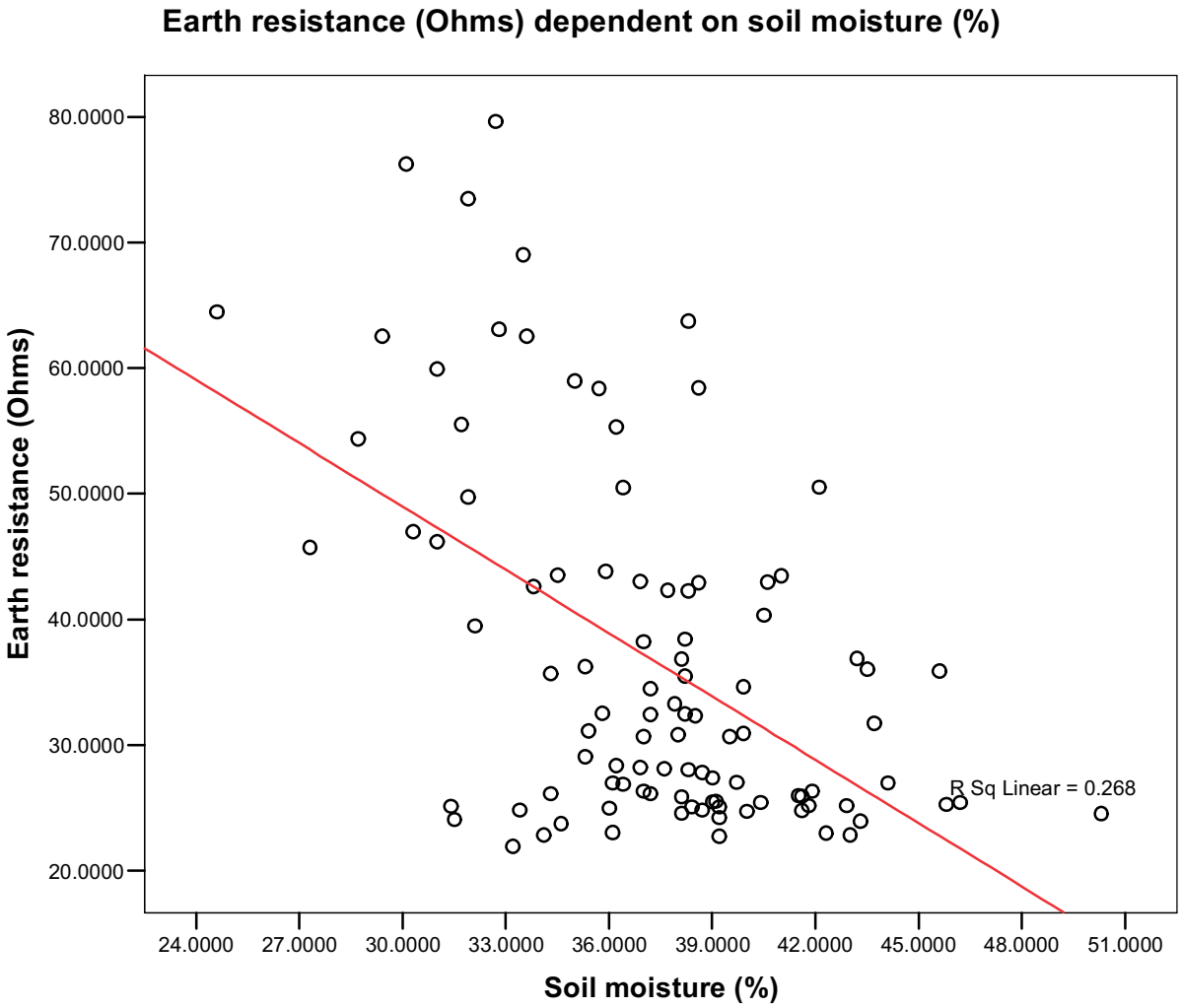

Fig 138: Scattergraph of earth resistance survey (Ohms) against soil moisture showing a moderate negative linear relationship.

Correlations

		Soil moisture (%)	Earth resistance (Ohms)
Soil moisture (%)	Pearson Correlation	1	-.517**
	Sig. (2-tailed)		.000
	N	100	100
Earth resistance (Ohms)	Pearson Correlation	-.517**	1
	Sig. (2-tailed)	.000	
	N	100	100

**. Correlation is significant at the 0.01 level (2-tailed).

Fig 139: There is a highly significant positive correlation between earth resistance survey and soil moisture.

3.4.4 Area MF

The survey used two 30 x 30m grids set out in a line, moving from an area of terrace to a palaeochannel (Fig. 118; Fig. 140). The survey aimed to investigate the difference in 950nm spectral reflectance between the palaeochannel and terrace deposits. Soil organic samples were taken from the topsoil at 4m intervals within each grid, using a centroid method, and soil moisture was recorded at each sample location. The scanner had one survey location, being 20m from the grid edge, at the intersection between grids 1 and 2. The scanner location was to the west of the grid. The site was surveyed over a ground cover of short pasture.

Like with the fort field survey there is a clear effect of the scanner causing variance in the data set. Both the elevation and the intensity data show a clear range effect, with an arcing pattern from the scanner location (Fig. 141). The elevation data does define the location of the palaeochannel as being lower than the terrace, but the 950nm reflectance data produces no definable pattern from which geomorphological features can be recognised. The soil moisture records little difference between the terrace and the palaeochannel (Fig. 142) and neither feature is recognisable based on soil moisture data. The lack of definition in the soil moisture data is potentially a product of sampling during the month of July, when the dry ground conditions meant there was a limited contrast in soil moisture between the two different geomorphological features. The soil organic content defines the palaeochannel as an area of higher organic content compared to an area of lower organics on the terrace. This distribution of soil organics is expected on a *pre-hoc* basis, and stands out in contrast to the FF survey area.

The instrumentation can be shown to be having a large affect on the data, like with the FF survey (Fig. 143). The slope, range and vertical angle can all be seen to have a large effect on the data, with an arcing pattern with movement away from the scanner location. These parameters are clearly having an affect on the elevation and 950nm reflectance values. The analysis of the data shows a clear relationship between 950nm reflectance and range (Fig. 144), with a highly significant positive relationship at the 0.01 level (Fig. 145). There is a strong positive relationship between 950nm reflectance and vertical angle of the scanner head (Fig. 146), again with a highly significant correlation (Fig. 147). A positive relationship is also seen between 950nm reflectance and slope (Fig. 148) and this relationship is also significant at the 0.01 level (Fig. 149).

In contrast the soil parameters can only be accounting for a small level of the residual variance in the intensity data set, after the effects of range, slope and vertical angle have been accounted for. The 950nm reflectance shows virtually no graphical relationship to soil organic content (Fig. 150) and this is confirmed by the correlation coefficient showing no systematic relationship between these two variables (Fig. 151). Likewise, 950nm reflectance dependant on soil moisture shows a weak negative relationship (Fig. 152) and this is not statistically significant (Fig. 153).

In contrast the soil parameters of soil organic content dependent on soil moisture does show a positive linear relationship (Fig. 154) and the correlation between the two variables is highly significant (Fig. 155). The relationship is positive and with increasing soil moisture content there is increasing soil organic content. This relationship does show that there are differences in sediment composition between the palaeochannel and the area of terrace, but this difference has not been detected by the 950nm reflectance values. It is interesting how the

relationship of 950nm reflectance to soil moisture shows a weak positive relationship in this survey, but a weak negative relationship in the FF survey.

The main points of the MF survey can be summarised as:

- The main cause of variance in the data set was the scanning instrument.
- This variance caused a linear increase in intensity with increasing distance from the scanner.
- The soil organic distribution produced a surface model with higher organic contents in the palaeochannel than on the terrace.
- The relationship of 950nm reflectance dependent on soil organic content produced a very weak positive linear relationship.
- The soil organic content did not reveal a statistically significant relationship to 950nm intensity.
- The soil moisture distribution produced a surface model that did not identify the palaeochannel or the terrace features.
- The 950nm reflectance dependant on soil moisture revealed a weak positive relationship, which was not statistically significant.
- The visual relationship of 950nm reflectance to each of the soil parameters appears to be non linear. However, this maybe a function of variance caused by the instrument distorting the analysis.
- The soil moisture and soil organic contents displayed a positive relationship. This proves there are differences in sediment architecture between the terrace and the palaeochannel, which the 950nm reflectance does not define.
- From this data it is again interpreted that 950nm reflectance is not dependant on any of the single soil parameters.

Fig 140: The MF study area, showing the palaeochannel grid to the left (north) and the terrace grid to the right (south) of the photograph.

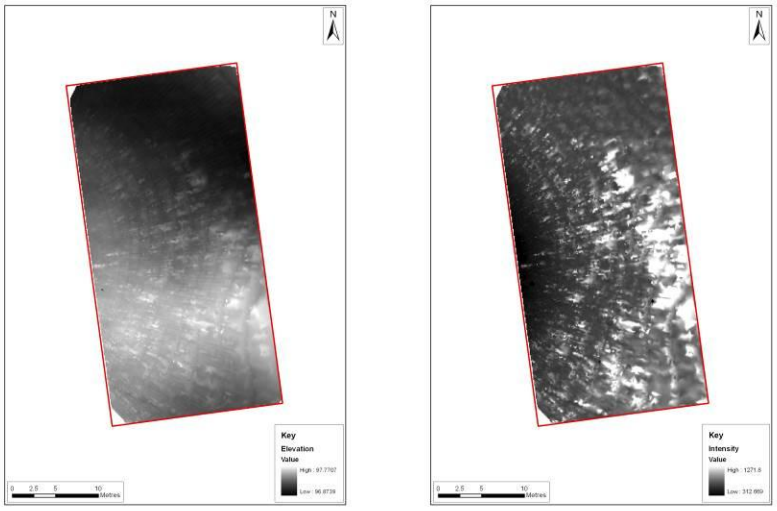

Fig 141: Lockington area MF terrestrial laser scanning showing from left to right elevation and intensity.

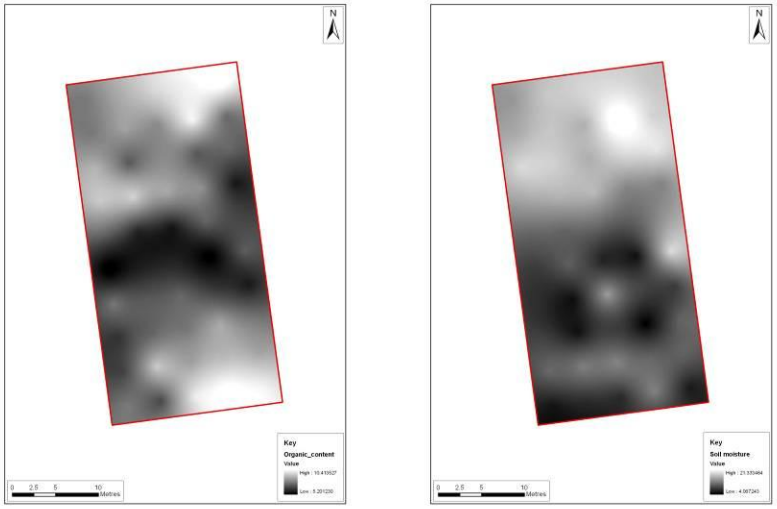

Fig 142: Lockington area MF showing from left to right volumetric soil moisture and organic content.

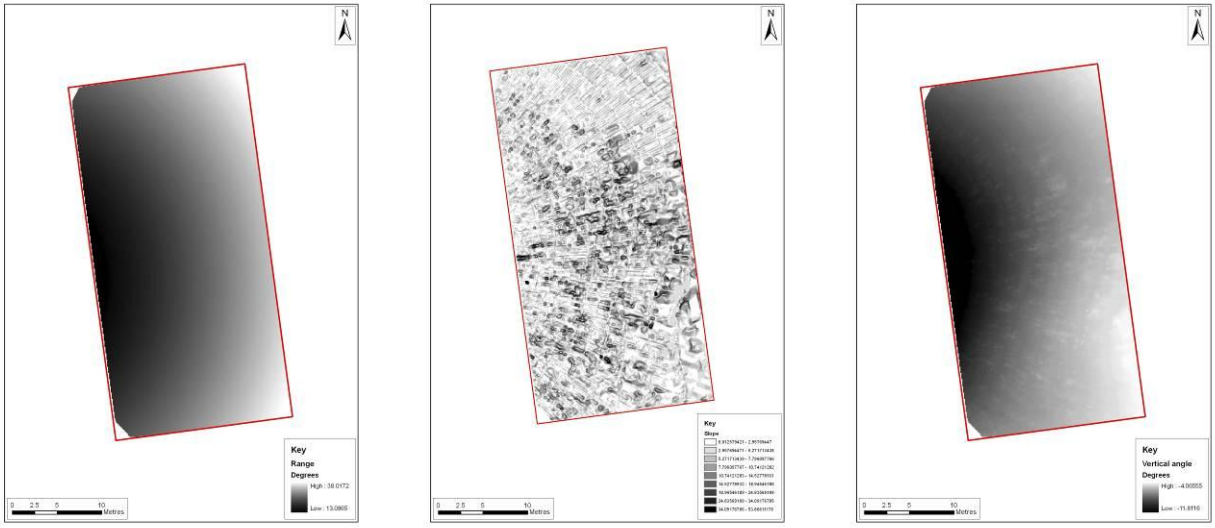

Fig 143: Lockington area MF terrestrial laser scanning showing from left to right slope severity, range and vertical angle.

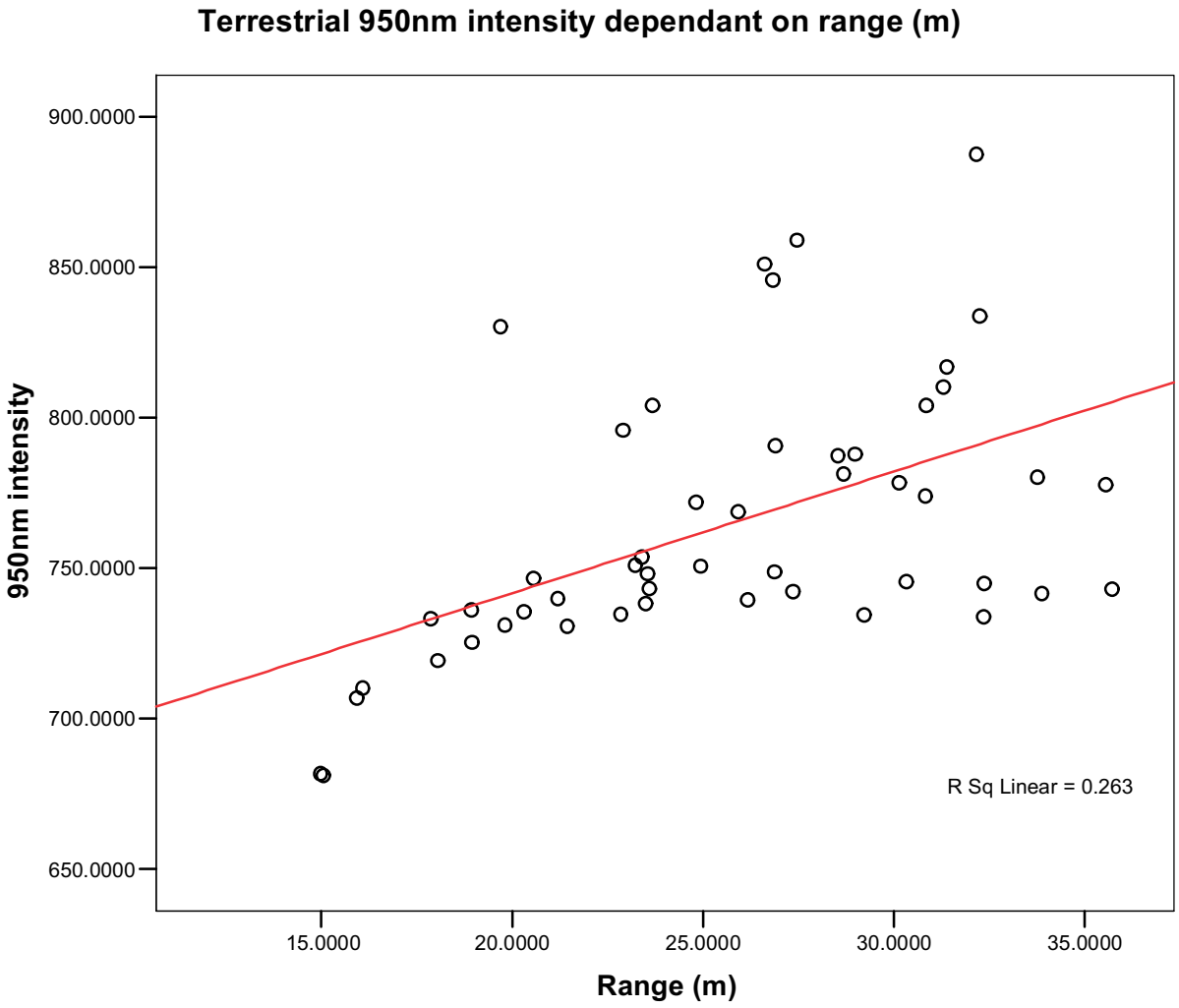

Fig 144: Scattergraph of 950nm reflectance dependant on range (m). Clearly range is having a significant affect on the data.

Correlations

		950nm intensity	Range (m)
950nm intensity	Pearson Correlation	1	.513**
	Sig. (2-tailed)		.000
	N	50	50
Range (m)	Pearson Correlation	.513**	1
	Sig. (2-tailed)	.000	
	N	50	50

**. Correlation is significant at the 0.01 level (2-tailed).

Fig 145: There is a significant positive relationship between 950nm reflectance and range (m).

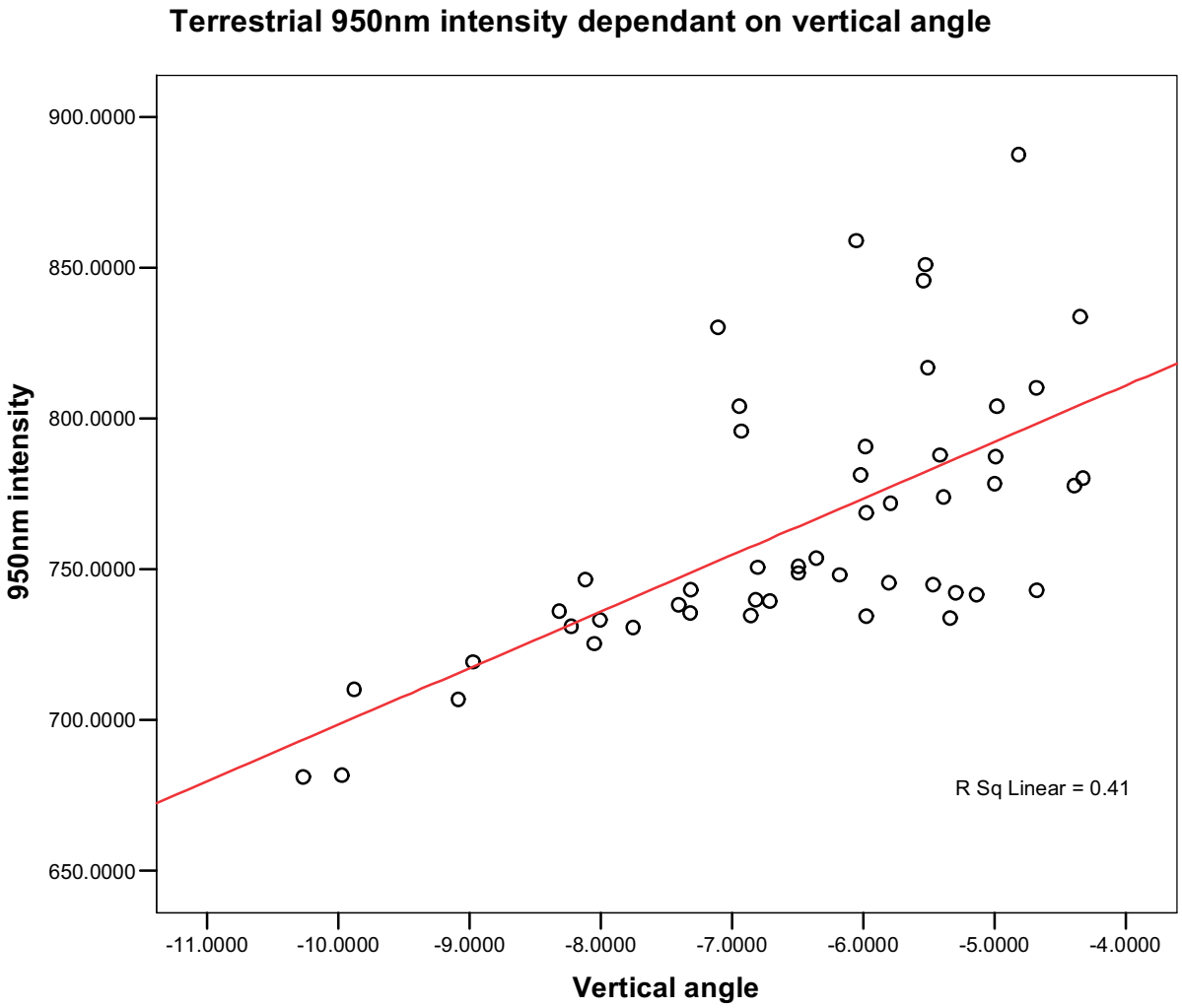

Fig 146: Scattergraph of 950nm reflectance dependant on vertical angle.

Correlations

		950nm intensity	Vertical angle
950nm intensity	Pearson Correlation	1	.641**
	Sig. (2-tailed)		.000
	N	50	50
Vertical angle	Pearson Correlation	.641**	1
	Sig. (2-tailed)	.000	
	N	50	50

**. Correlation is significant at the 0.01 level (2-tailed).

Fig 147: There is a highly significant positive correlation between 950nm reflectance and vertical angle.

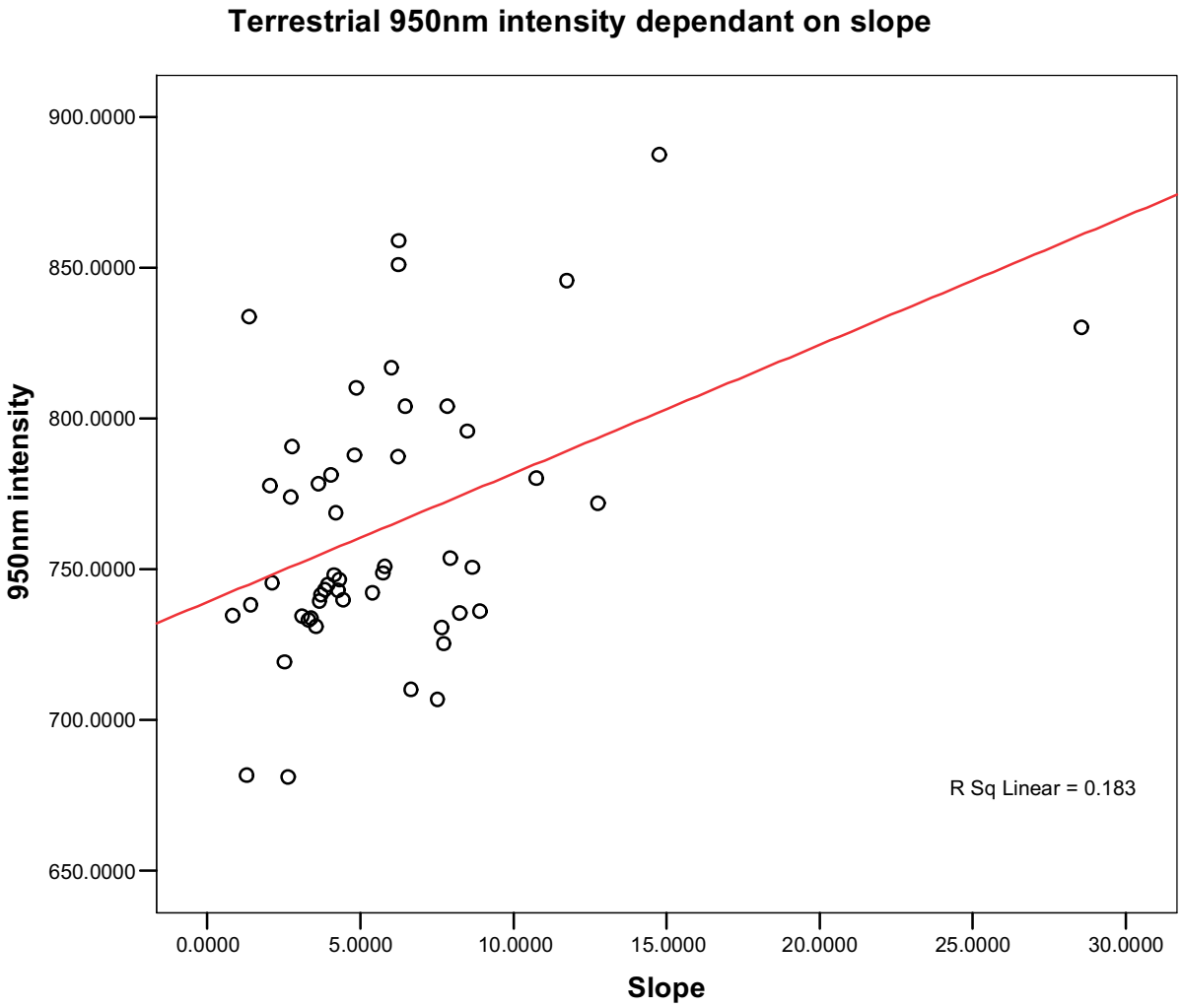

Fig 148: Scattergraph of 950nm dependant on slope.

Correlations

		950nm intensity	Slope
950nm intensity	Pearson Correlation	1	.428**
	Sig. (2-tailed)		.002
	N	50	50
Slope	Pearson Correlation	.428**	1
	Sig. (2-tailed)	.002	
	N	50	50

**. Correlation is significant at the 0.01 level (2-tailed).

Fig 149: There is a highly significant positive correlation between 950nm reflectance and slope.

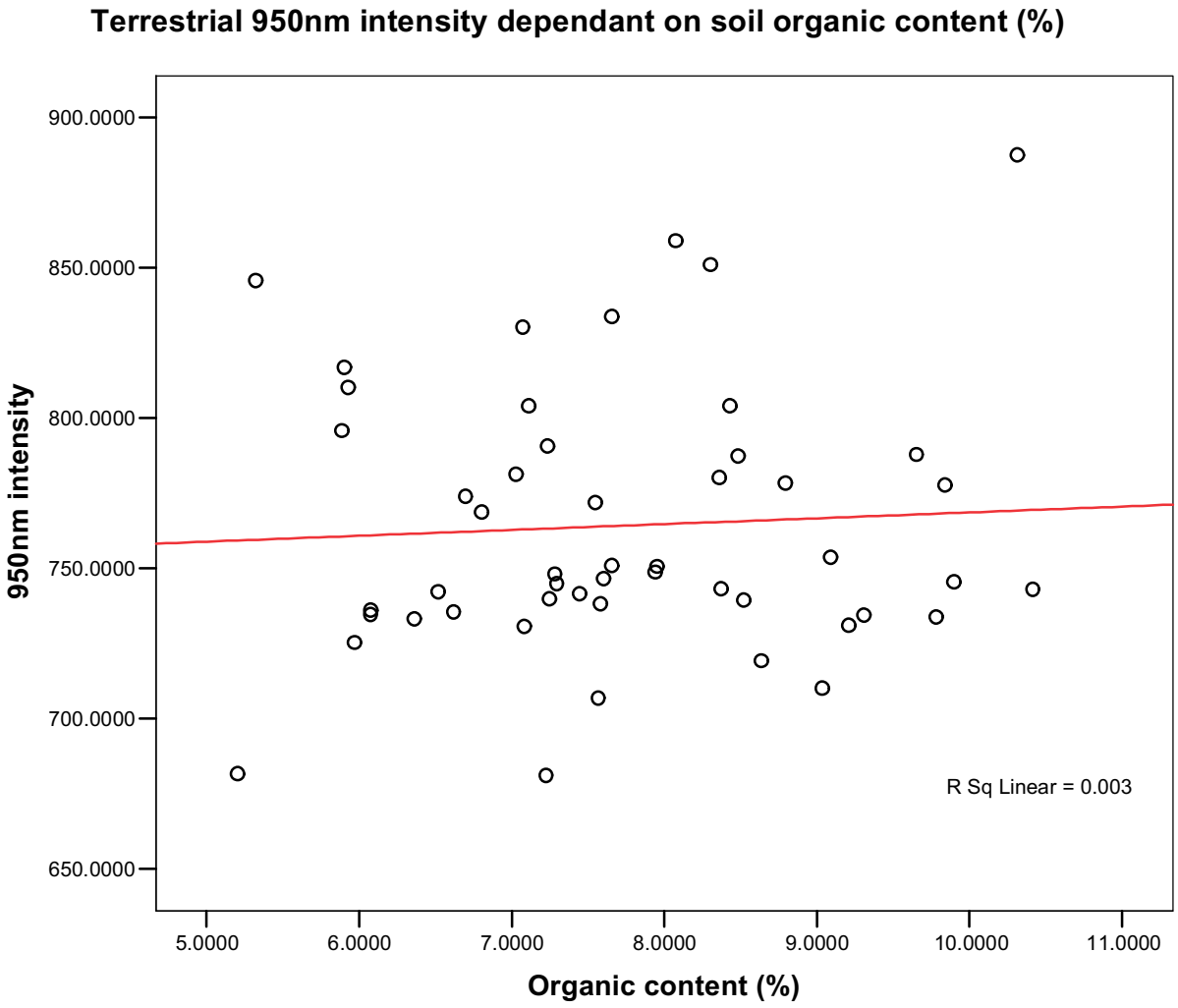

Fig 150: Scattergraph of 950nm reflectance dependant on soil organic content.

Correlations

		950nm intensity	Organic content (%)
950nm intensity	Pearson Correlation	1	.058
	Sig. (2-tailed)		.692
	N	50	50
Organic content (%)	Pearson Correlation	.058	1
	Sig. (2-tailed)	.692	
	N	50	50

Fig 151: The correlation coefficient shows there is no systematic relationship between 950nm reflectance and soil organic content in this survey.

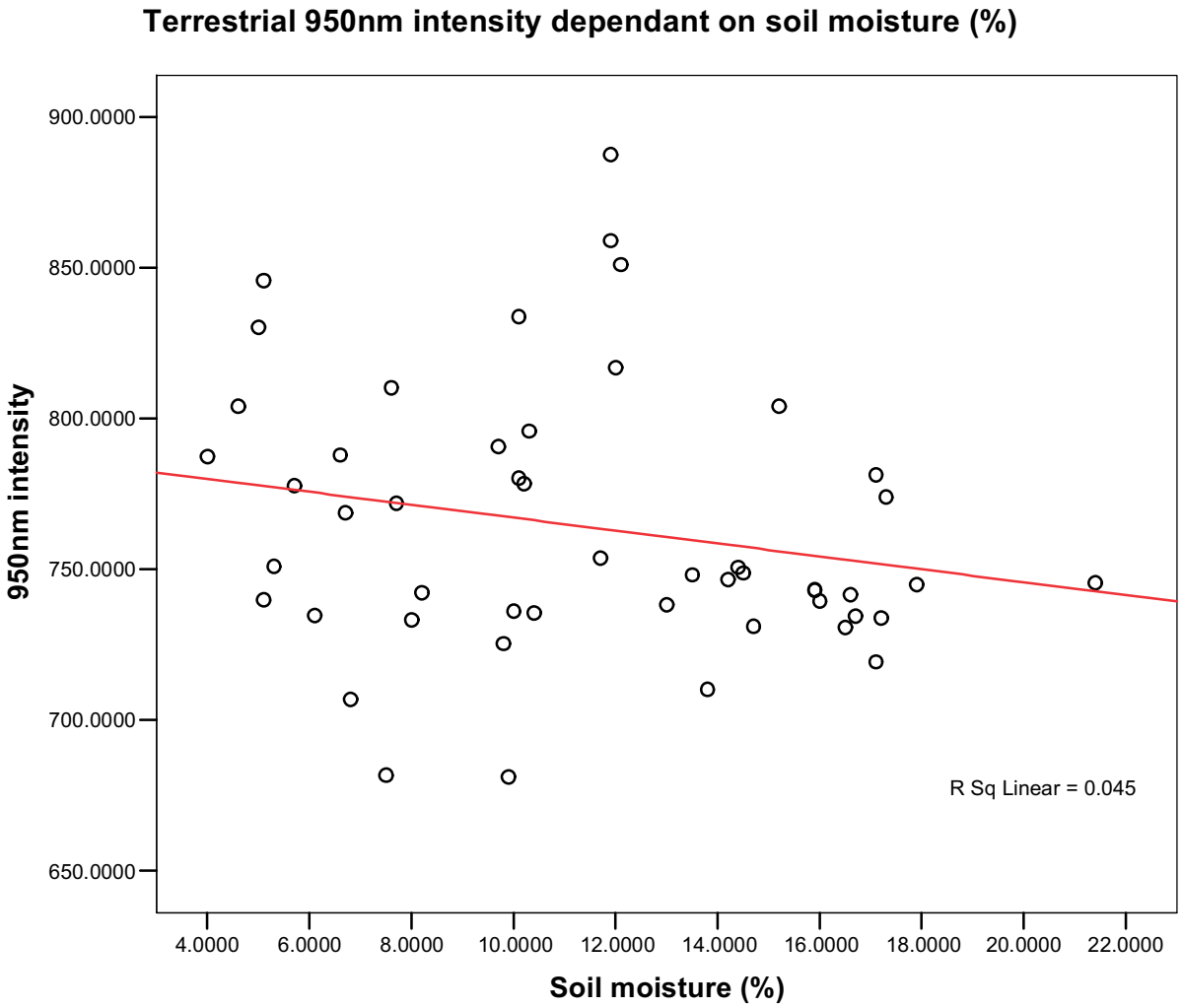

Fig 152: Scattergraph of 950nm reflectance dependant on soil moisture.

Correlations

		950nm intensity	Soil moisture (%)
950nm intensity	Pearson Correlation	1	-.213
	Sig. (2-tailed)		.138
	N	50	50
Soil moisture (%)	Pearson Correlation	-.213	1
	Sig. (2-tailed)	.138	
	N	50	50

Fig 153: There is no significant relationship between 950nm reflectance and soil moisture in the MF survey area.

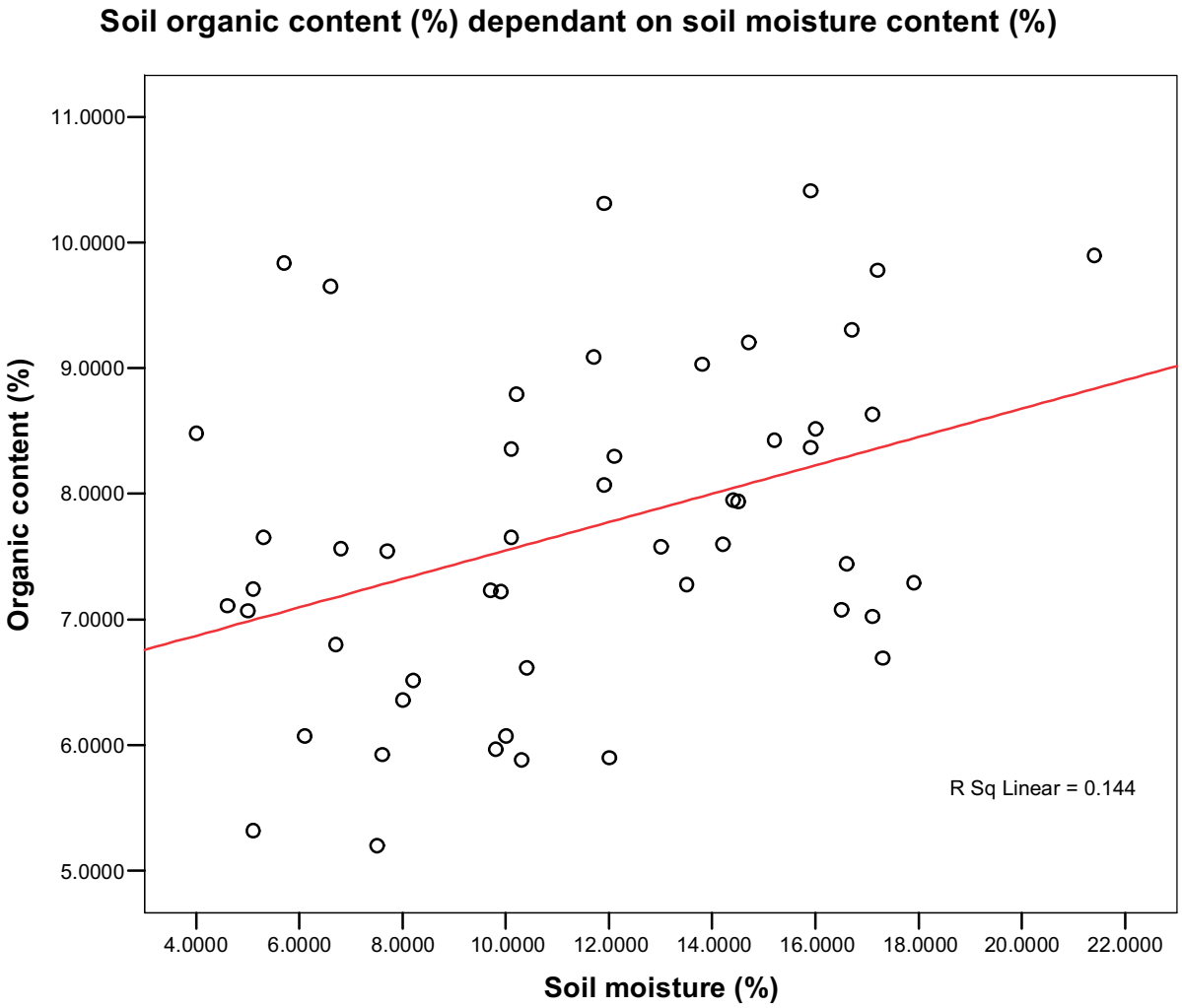

Fig 154: Scattergraph of soil organic content dependant on soil moisture. A positive relationship is seen, showing there are differences in the sediment composition of the terrace/palaeochannel.

Correlations

		Organic content (%)	Soil moisture (%)
Organic content (%)	Pearson Correlation	1	.379**
	Sig. (2-tailed)		.007
	N	50	50
Soil moisture (%)	Pearson Correlation	.379**	1
	Sig. (2-tailed)	.007	
	N	50	50

**. Correlation is significant at the 0.01 level (2-tailed).

Fig 155: There is significant positive relationship between soil organic content dependent on soil moisture at the 0.01 level.

3.4.5 Area VF

The VF survey aimed to investigate the pattern of 950nm reflectance in a survey area where significant cropmarks existed produced from archaeological remains. The VF survey covered part of an area of cropmarks related to a presumed Romano-British settlement (Fig. 156), although it is likely that the archaeological features within the field span a range of periods. The survey only investigated 950nm reflectance against potential cropmarks, with no other data being collected. The data was collected when the site was under an arable crop, excluding access to the survey area, other than the scanner location. The survey was scanned from a public footpath.

The results show that no archaeological or geomorphological features are present from either the elevation data or the 950nm reflectance data (Fig. 157). Again there is an arcing pattern with increasing distance from the scanner location, with 950nm reflectance increasing with range. When the 950nm reflectance data is shown against the transcribed cropmarks within the survey area it is clear that the 950nm reflectance data shows no correlation to the cropmarks (Fig. 158). The intensity data does reveal the lines of the crop arable crop planting, running north/south over the image. It is interpreted that the scanner intensity as well as having a significant range, vertical angle and slope effect, is only reflecting variation in the crop structure. It is presumed that only a very small level of intensity is being reflected from the soil surface.

Fig 156: The 'Lockington Villa' complex within the study area. The complex contains a wealth of archaeological features, which are interpreted as dating from a range of periods, from the later prehistoric through to the Romano-British and possibly, post Romano-British periods. The complex is located on the Devensian terrace 2.

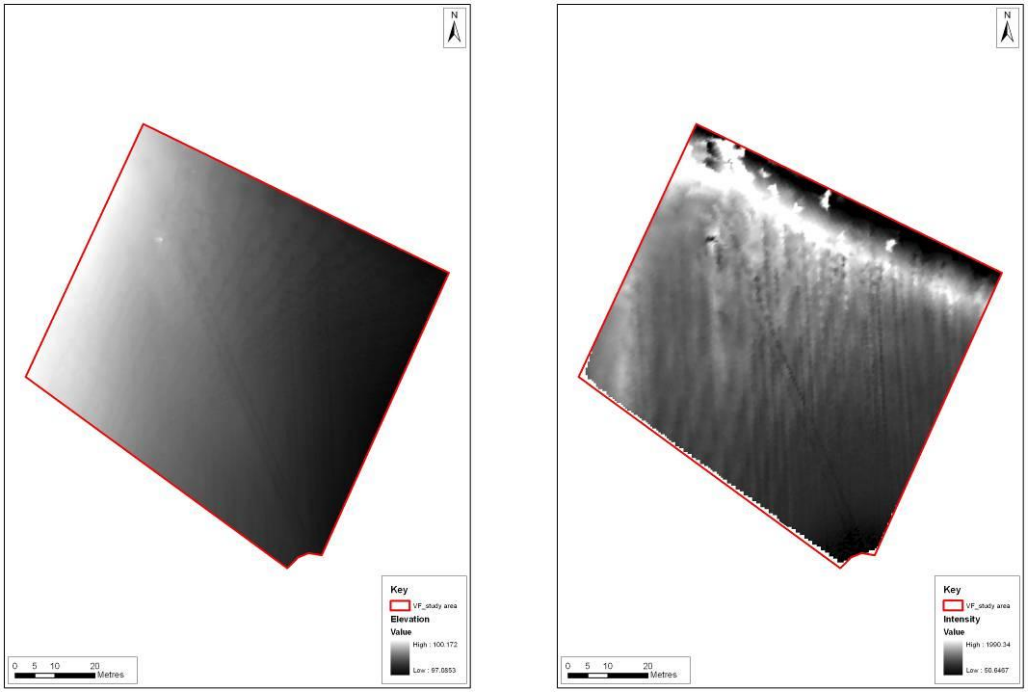

Fig 157: Lockington area VF terrestrial laser scanning showing from left to right elevation and intensity.

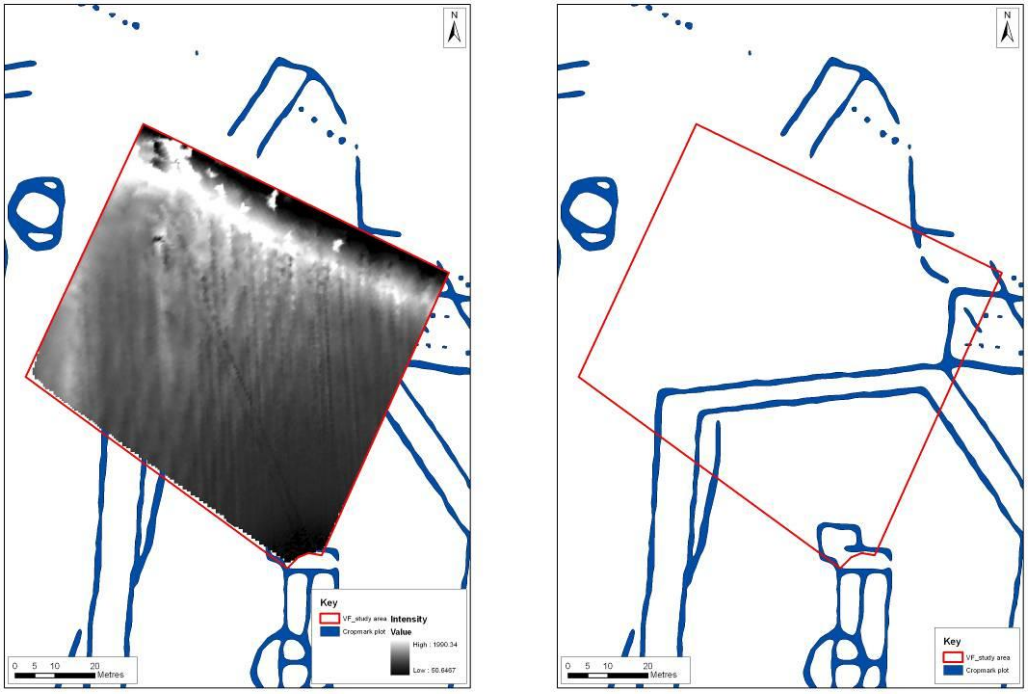

Fig 158: Lockington area VF terrestrial laser scanning showing from left to right intensity and cropmarks.

3.4.6 Results: comparison of 950nm reflectance from terrestrial scanning compared to 1047nm reflectance from Lidar survey.

Although the application of terrestrial 950nm reflectance as a proxy for air borne Lidar 1047nm reflectance was complicated by the level of variance introduced into the data set by the instrument, it is still possible to compare the two data sets from the Lockington survey areas. The comparison of the Fort Field data set shows the terrestrial 950nm reflectance grids superimposed on the Lidar 1047nm reflectance survey (Fig. 159). The striking feature in this comparison is the difference between the two data sets.

The Lidar 1047nm reflectance produces a surface model that clearly defines the palaeochannel and the terrace. In comparison the terrestrial 950nm reflectance data is extremely messy and does not define the main geomorphological units within the survey grid. Not surprising a scattergraph of the two data sets shows no linear relationship (Fig. 160) and the computed correlation coefficient is not significant at the 0.05 level (Fig. 161). Based on this data there is no relationship between 950nm reflectance and 1047nm reflectance and this would appear to be a product of the variance introduced into the 950nm data set through the terrestrial scanner.

The MF survey produces a similar result. Again the terrestrial 950nm reflectance survey is shown superimposed on the 10417nm intensity surface model (Fig. 162). The palaeochannel and the terrace are both evident as features on the Lidar 1047nm reflectance data set. Although the range effect is strong in the 950nm reflectance data set, the palaeochannel is still evident as an area of lower intensity, with the terrace partially defined as an area of higher intensity. The scattergraph between terrestrial 950nm reflectance and air borne 1047nm reflectance shows no linear relationship between the two variables (Fig. 163). This is confirmed by the correlation coefficient, which produces no statistically significant correlation between 950nm reflectance and 1047nm reflectance at the 0.05 level (Fig. 164). Again the variance introduced into the 950nm reflectance data set by the terrestrial scanner has meant that any real structure to the data set has been obscured.

Lastly, the VF survey is shown with the 950nm reflectance data superimposed on the air borne 1047nm reflectance surface model (Fig. 165). There is little visual correlation between the two data sets. The air borne 1047nm reflectance clearly shows the field boundaries but no real variation in the survey area. The 950nm reflectance data again shows a clear range effect, but the plough/crop lines are visible in the image trending north-northeast/south-southwest. The 950nm reflectance data is also shown superimposed on a rectified aerial photograph of the survey area (Fig. 166). Although a wealth of cropmarks are visible in the photograph none of these are visible in the 950nm reflectance data, nor in the air borne 1047nm reflectance data.

Fig 159: The FF survey 950nm reflectance survey superimposed on the 1047nm reflectance surface model. The range effect in the 950nm reflectance data caused by the scanner is clearly evident.

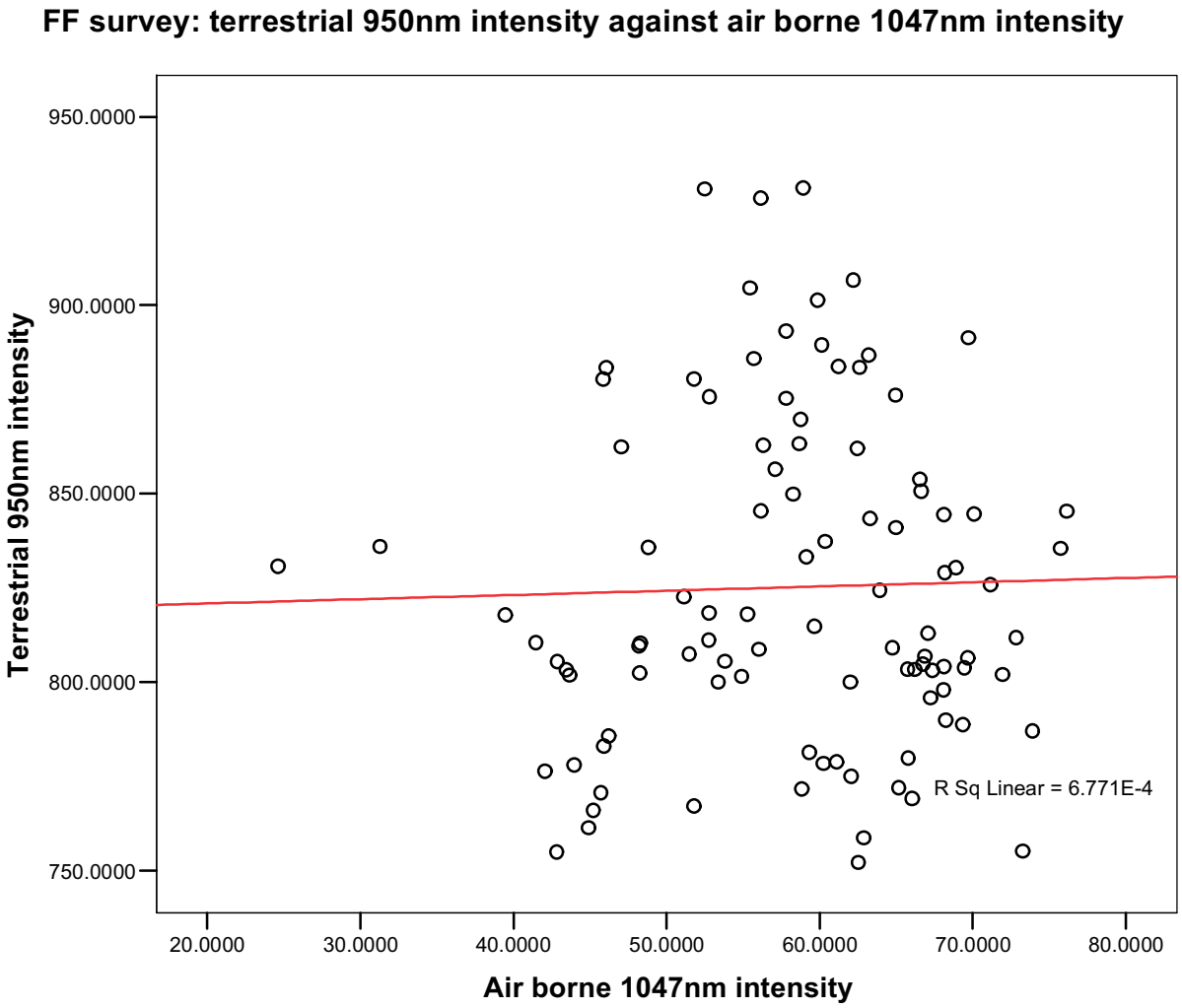

Fig 160: Scattergraph of the FF terrestrial 950nm reflectance against air borne 1047nm intensity. Visually there is no relationship between the two data sets.

Correlations

		Terrestrial 950nm intensity	Air borne 1047nm intensity
Terrestrial 950nm intensity	Pearson Correlation	1	.026
	Sig. (2-tailed)		.797
	N	100	100
Air borne 1047nm intensity	Pearson Correlation	.026	1
	Sig. (2-tailed)	.797	
	N	100	100

Fig 161: On the FF survey the correlation coefficient shows no significant relationship between the two variables at the 0.05 level.

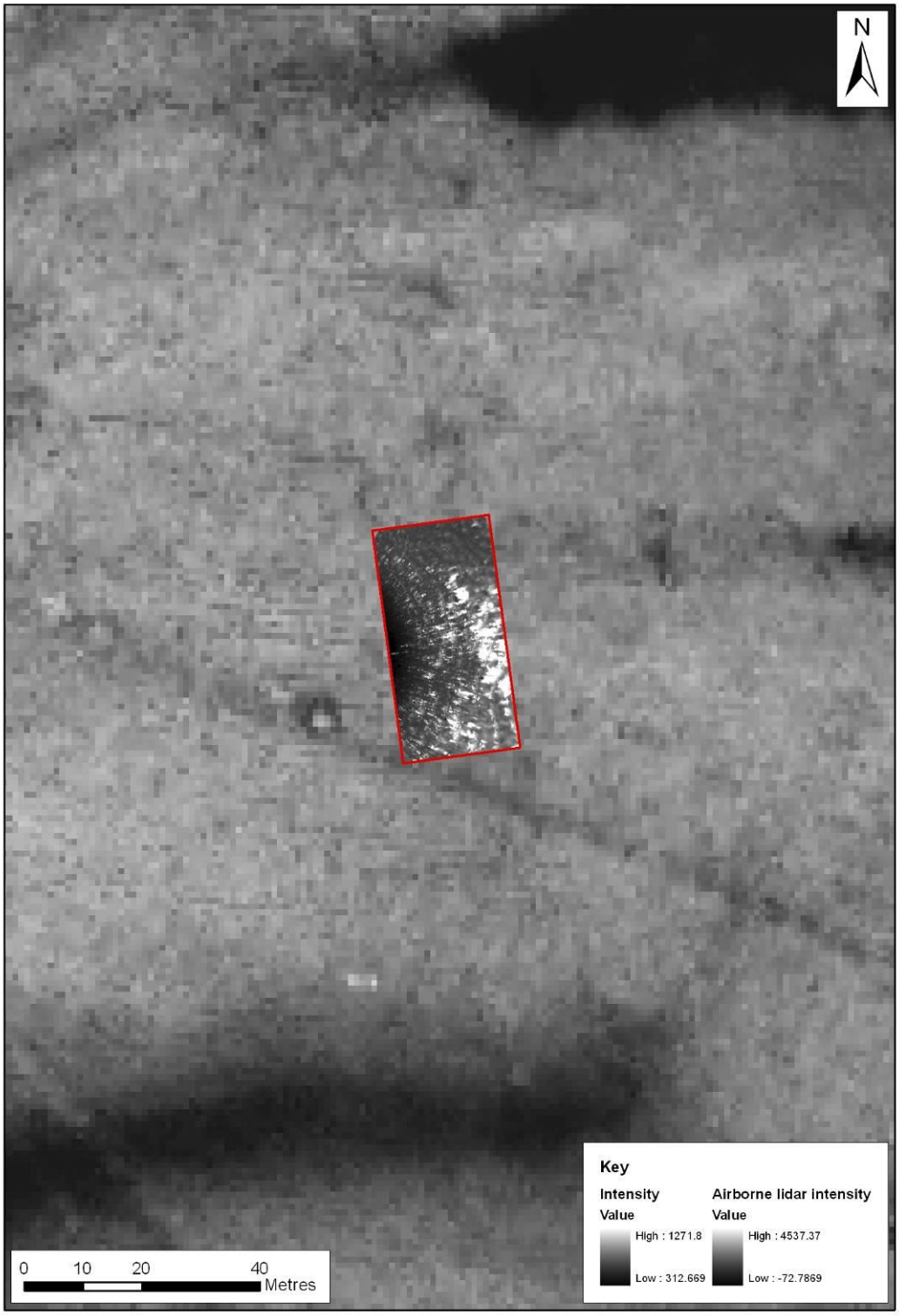

Fig 162: The MF survey terrestrial 950nm reflectance survey superimposed on the air borne Lidar 1047nm reflectance model.

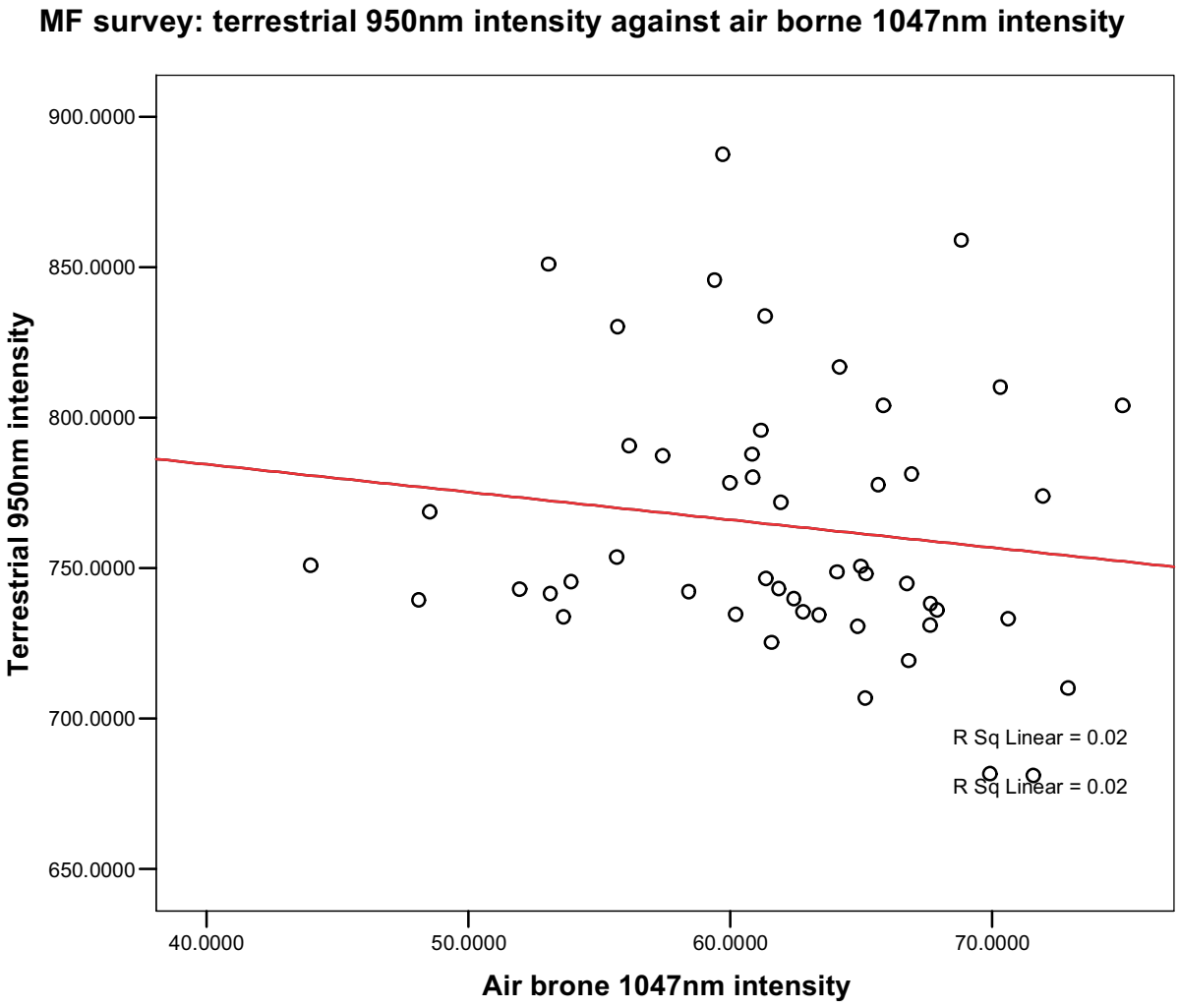

Fig 163: MF survey: terrestrial 950nm reflectance against air borne 1047nm intensity. Visually there is no definable relationship between the two variables.

Correlations

		Air borne 1047nm intensity	Terrestrial 950nm intensity
Air borne 1047nm intensity	Pearson Correlation	1	-.141
	Sig. (2-tailed)		.330
	N	50	50
Terrestrial 950nm intensity	Pearson Correlation	-.141	1
	Sig. (2-tailed)	.330	
	N	50	50

Fig 164: MF survey: the correlation coefficient shows there is no systematic relationship between 950nm reflectance and 1047nm intensity.

Fig 165: VF survey terrestrial 950nm reflectance superimposed on the air borne 1047nm intensity.

Fig 166: VF survey terrestrial 950nm reflectance superimposed on aerial photograph showing cropmarks.

3.5 DISCUSSION

The results from the terrestrial 950nm scanning have been disappointing, due to the high level of variance introduced into all of the data sets through the terrestrial scanning instrument. This variance from the instrument has made it difficult for any other structure within the data to become apparent. The terrestrial 950nm shows a clear effect, with increasing distance from the scanner, intensity increases. However, there are still some results within the surveys that hint at the potential of NIR scanning to identify deposits of organic content. Any conclusions reached during this section must be treated with caution, due to the level of variance introduced into the data by the scanner.

3.5.1 Terrestrial 950nm reflectance and organic content

The FF survey produced a highly significant positive correlation (0.01 level) between terrestrial 950nm reflectance and soil organic content, whilst the MF survey produced a weak negative not significant (0.05 level) relationship between 950nm reflectance and organic content. The distribution of organics within the FF survey was unexpected, with lower organic contents in the palaeochannel samples compared to the terrace deposits. However, the intensity values still decreased within the palaeochannel measurements. The opposite distribution of organics was seen in the organic deposits on the MF survey and here a very weak negative relationship was seen.

These results clearly define that 950nm reflectance is not dependent on soil organic content. If it were the opposite distribution of 950nm reflectance would have been seen in the FF survey, with lower 950nm reflectance readings on the terrace deposits compared to the palaeochannel. Therefore, the correlation between these two variables, although highly significant in the FF survey, is incidental. It is interpreted that both variables are reflecting underlying changes in sediment properties.

3.5.2 Terrestrial 950nm reflectance and soil moisture

The FF survey produced a statistically significant negative correlation (0.05) between 950nm reflectance and soil moisture content, whilst the MF survey produced a weak negative relationship that was not statistically significant. Both of these relationships are negative and both palaeochannels from each survey exhibited higher soil moisture levels in the palaeochannels compared to the terrace deposits. This shows there is a relationship between 950nm reflectance and soil moisture but this relationship is incidental. Both variables are highlighting underlying changes in sediment architecture. The Port Meadow data sets produced a similar story. In the Port meadow surveys no statistically significant relationships were realised between 950nm reflectance and soil moisture content. Strangely, four of the five surveys produced a weak positive relationship between 950nm reflectance and soil moisture content (PM02, PM04, Pm06 and PM07), with only PM09 realising a weak negative relationship. The reason for the positive relationship between these two variables in the Port Meadow survey is not understood.

3.5.3 Terrestrial 950nm and earth resistance survey

The FF survey showed there was a significant positive correlation (0.01 level) between 950nm reflectance and earth resistance (Ohms), which is a partially a product of soil moisture. This relationship is not surprising given the significant relationship of soil moisture to 950nm reflectance in the FF survey. However, this does indicate that earth resistance survey could be a good proxy for soil moisture content and hence identifying geoarchaeological potential. In addition it can be used as a good second tier of investigation to ground truth/further investigate Lidar intensity results.

3.5.4 Terrestrial 950nm reflectance compared to air borne1047nm intensity

The relationship of air borne 1047nm reflectance to terrestrial 950nm reflectance showed no definable relationship between the two data sets in either the FF or MF surveys. This should not be considered surprising, due to the different data sets being collected several years apart under different conditions. In addition the variance introduced into the 950nm data set by the scanner means that any structure in the data set is likely to be masked by instrument variance.

3.5.5 Factors that have effected the surveys

It is clear that NIR intensity bears a relationship to various soil parameters. In this sense NIR intensity can have a role to play in prospection of geoarchaeological deposits. However, the specific terrestrial 950nm surveys suffered through the instrument introducing a high level of variance into the data sets. This level of variance was not operator induced and was a product of a twin prism system introducing a greater degree of separation between out going and incoming reflected light pulses with increasing distance from the scanner. This large degree of variance from the instrument is almost certainly masking relationships between 950nm reflectance and soil parameters.

Secondly, it is important to realise that most of the scanner data was not reflecting bare earth conditions, but was recording data mainly from the vegetation. Therefore, if a relationship between 950nm reflectance and various soil parameters is to be realised from this method, the relationship is indirect (Fig. 159). Although it is likely that changes in vegetation will partially be a product of changes in sediment composition in the soil profile, the indirectness of the relationship means further variance is introduced into the data sets. This makes inter-survey comparison between NIR data sets difficult, especially when different land uses are producing different vegetation covers, e.g. arable crop in one survey area compared to pasture cover in another survey area. This suggests that NIR intensity is best interpreted on an intra survey or intra land-use basis.

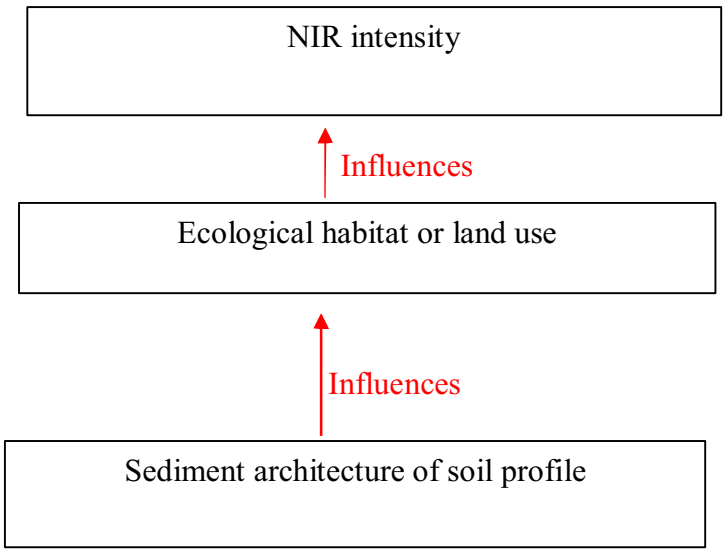

Fig 159: The indirect relationship of NIR intensity data to sediment architecture.

3.5.6 Recommendations based on the terrestrial 950nm reflectance surveys

- Terrestrial scanning using the method described produces intensity results that have an unacceptable of variance caused by instrument operation.

- Earth resistance survey acts a good proxy for sediment composition and moisture contents and should be investigated further in relation to air borne Lidar 1047nm intensity.

- There does appear to be some relationship between soil moisture, soil organics and NIR intensity. This should again be investigated further using air borne Lidar 1047nm intensity.

4 AIRBORNE LIDAR

4 AIRBORNE LIDAR

4.1 INVESTIGATING BACKSCATTERED INTENSITY OF AIRBORNE LIDAR

This stage of the project investigated backscattered 1047nm reflectance against field observations and measurements. In spite of initial assurances there has proven to be no archive 1047nm reflectance data for two of the three study areas highlighted in the original project design (Port Meadow and the Idle Valley around Misterton Carr). In the absence of other data we have focused our study on existing lidar data for Lockington Marshes acquired for PN3357 (Trent-Soar). Airborne lidar 1047nm reflectance data for several contrasting areas within the marshes have been compared to ground based laser scanning, earth resistance survey, soil moisture content and soil organic content. Results show that in some cases airborne intensity has a modest negative correlation with soil moisture and a more marked correlation with soil organic content. There is also a strong correlation between intensity and earth resistance. Intensity 1047nm data was also examined for rivers in the Yorkshire Dales (Rivers Lune, Wenning and Aire), aqquired from Network mapping. Palaeo-drainage features are evident in these valleys in the lidar DSM and are represented in the 1047nm reflectance data. However, since none of these data covers areas of present or predicted aggregate extraction further analysis of this data has not proceeded.

4.2 LOCKINGTON MARSHES

4.2.1 Area FF

Area FF comprises a part of the Hemmington Terrace deposits where a palaeochannel bisects an area of terrace (Fig. 160). The study area is given over to permanent pasture (grassland) and was covered with low closely cropped grass at the time of survey, which took place in November 2006 in dry clear weather conditions. The palaeochannel is evident as a slight topographical feature, approximately 30m wide and 0.5m deep. The palaeochannel is readily apparent in lidar elevation and 1047nm reflectance data (Fig. 161). Samples for soil organic content and moisture were collected at 4m intervals over an 80m x 20m area covering the palaeochannel and its immediate environment and surface models were created from the resulting pointcloud.

The soil organic content varies across the sample area (Fig. 162). The outline of the palaeochannel feature is evident as variation in topsoil organic content, although as discussed earlier in chapter 3, a reverse distribution of soil organic content was witnessed in this survey, with higher organic contents found on the terrace units. The scattergraph of lidar 1047nm reflectance values and topsoil organic content indicates a slight positive relationship (R^2=0.28; Fig. 163), and the computed correlation coefficient shows this relationship to be highly significant at the 0.01 level (Fig. 164).

The volumetric soil moisture varies across the sample area (Fig. 162) from 24% - 50%, giving a heterogeneous surface plot. However, the palaeochannel does contain higher soil moisture levels, although its outline is not discernable from the surface plot. The scattergraph of 1047nm reflectance values and topsoil moisture content indicates a weak negative relationship (R^2=0.016; Fig 165) and the correlation coefficient shows this relationship not to be statistically significant at the 0.05 level (Fig. 166).

In addition to the soil organic and moisture contents, the oppotunity was taken at this site to use earth resistance survey as a proxy for Lidar intensity. Earth resistance survey has the potential to fill in a middle tier between remote sensed data and individual sample points on in the survey area. Changes in earth resistance units (Ohms) are liable to represent variations in sediment architecture, affecting the capacity of the sediment to retain moisture and preserve organics.

The earth resistance survey produced a surface model that clearly and accurately defined the palaeochannel in the survey area. This should not be considered surprising as the earth resistance sample interval was the same as the Lidar sample interval (both 1m spacing) (Fig. 167). The scattergraph indicated a weak positive relationship between air borne 1047nm reflectance and earth resistance survey (Fig. 168), but the correlation coefficient showed this relationship to be significant at the 0.01 level (Fig. 169). This indicates that earth resistance survey maybe a useful proxy for Lidar 1047nm reflectance and this is potentially a future line of research for investigating Lidar intensity data.

Overall the results from the FF survey mimic those seen elsewhere in the project, whereby significant relationships are present between NIR data and various soil parameters, but these relationships cannot be visualised in linear two dimensional forms. The fact that relationships can still be seen when the data collection between the air borne 1047nm reflectance and the ground measurements were several years apart suggests that these relationships are real and should be investigated further.

Fig 160: A photograph showing the Lockington study area FF.

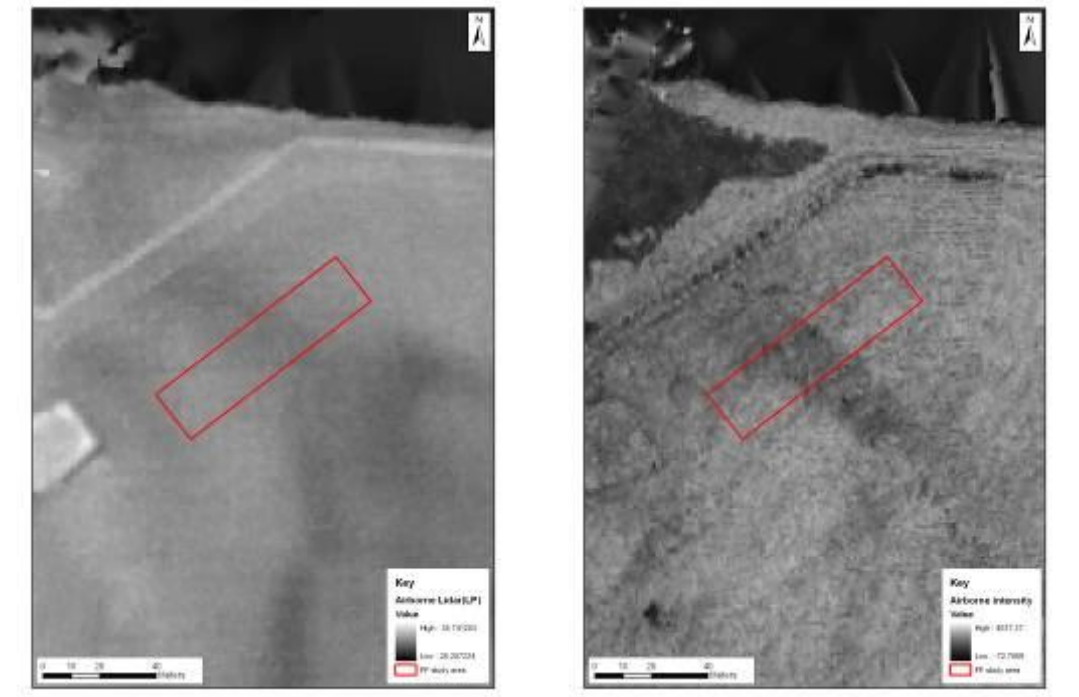

Fig 161: Lockington area FF showing left airborne lidar DSM and right airborne lidar intensity.

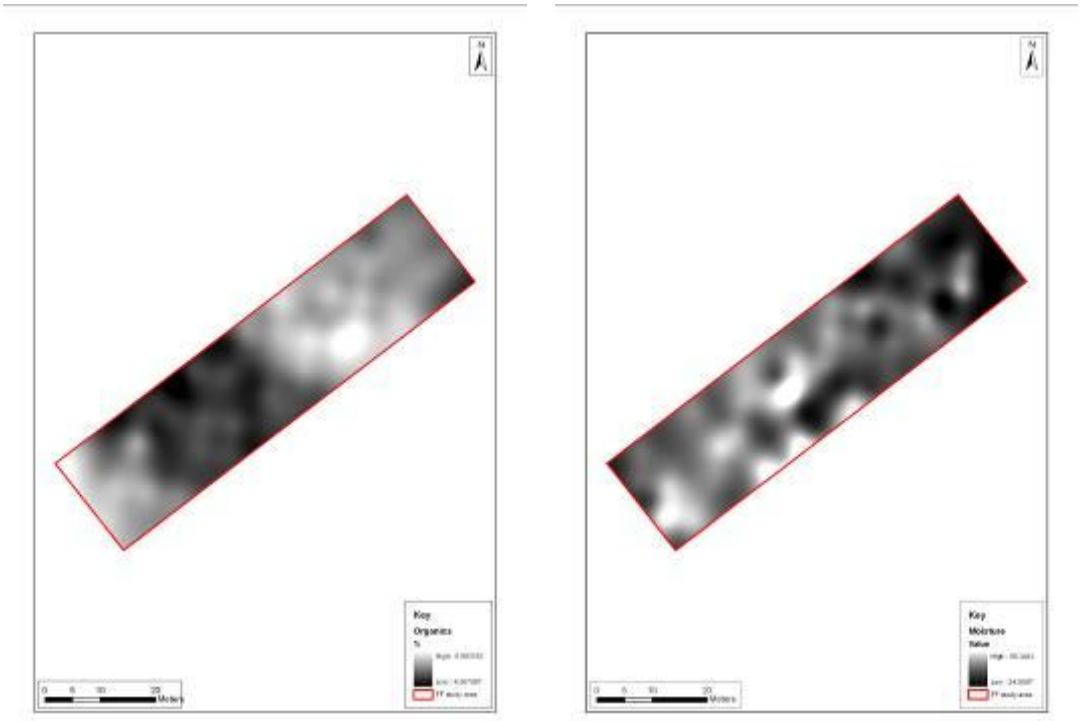

Fig 162: Lockington area FF showing left topsoil organic content and right volumetric soil moisture of topsoil.

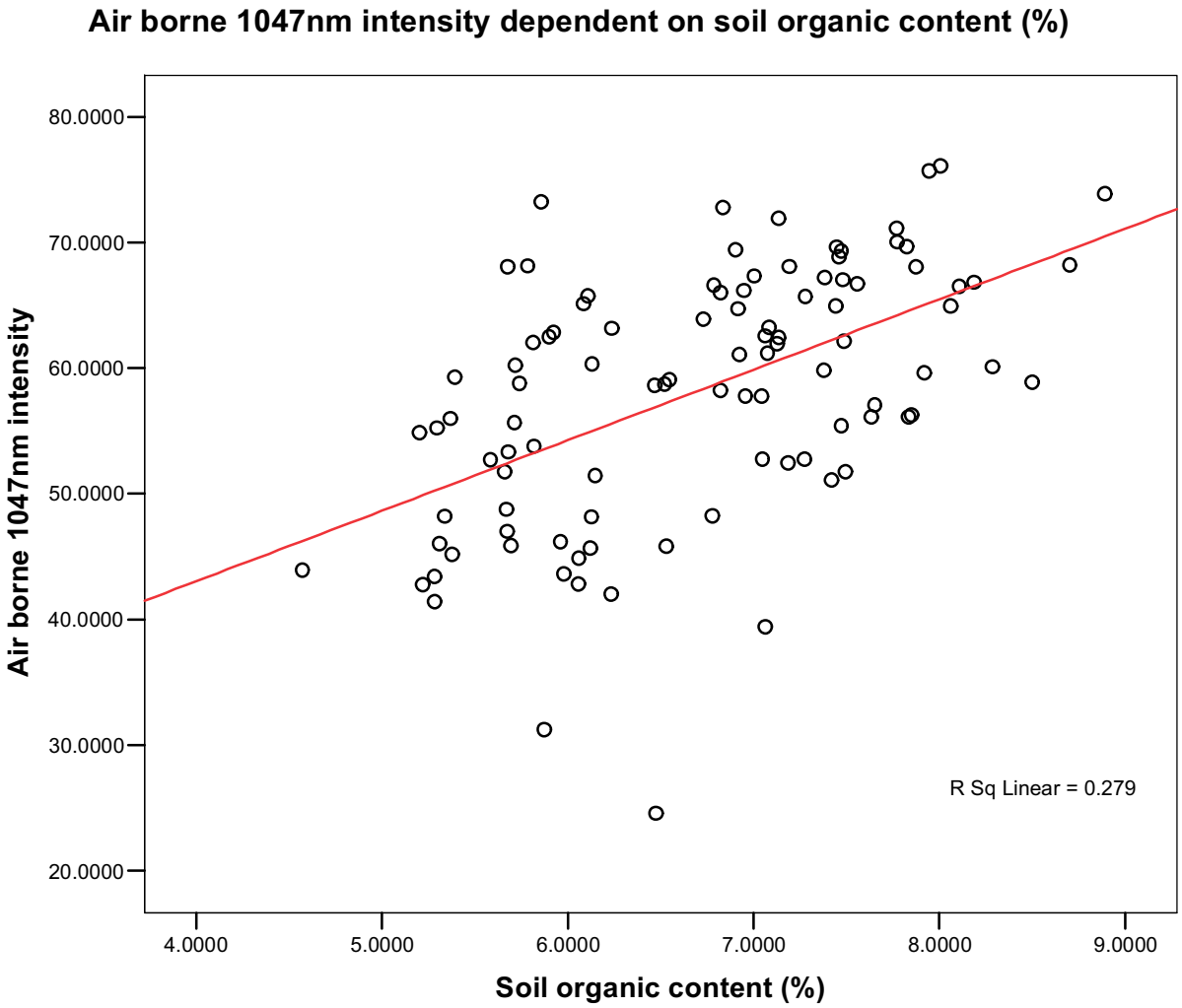

Fig 163: FF survey. Scattergraph of 1047nm reflectance against soil organic content.

Correlations

		Air borne 1047nm intensity	Soil organic content (%)
Air borne 1047nm intensity	Pearson Correlation	1	.528**
	Sig. (2-tailed)		.000
	N	100	100
Soil organic content (%)	Pearson Correlation	.528**	1
	Sig. (2-tailed)	.000	
	N	100	100

**. Correlation is significant at the 0.01 level (2-tailed).

Fig 164: FF survey. There is a highly significant correlation between 1047nm reflectance and soil organic content.

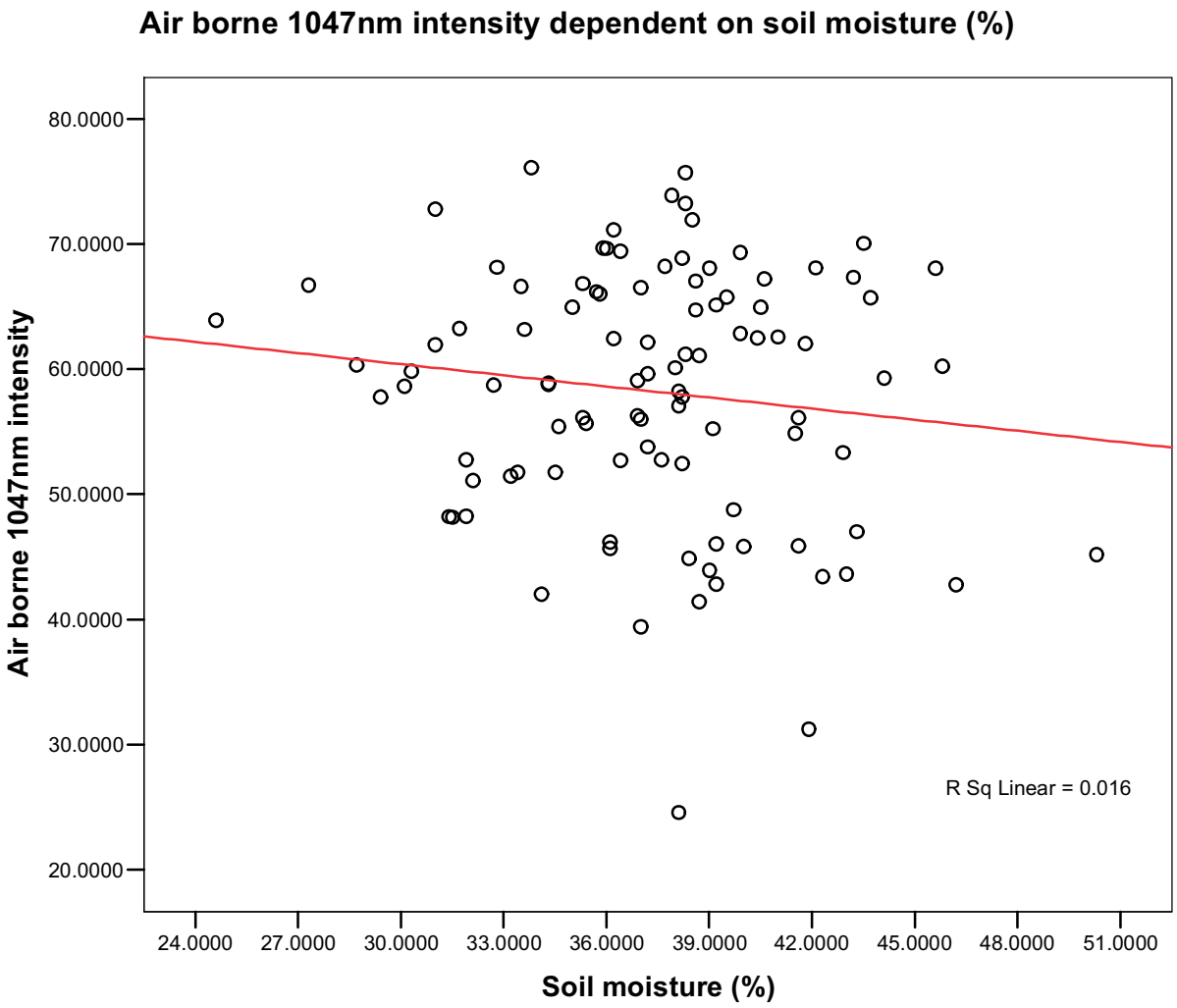

Fig 165: FF survey. Scattergraph of 1047nm reflectance against soil moisture.

Correlations

		Air borne 1047nm intensity	Soil moisture (%)
Air borne 1047nm intensity	Pearson Correlation	1	-.128
	Sig. (2-tailed)		.205
	N	100	100
Soil moisture (%)	Pearson Correlation	-.128	1
	Sig. (2-tailed)	.205	
	N	100	100

Fig 166: FF survey. There is no significant relationship between 1047nmintensity and soil moisture content.

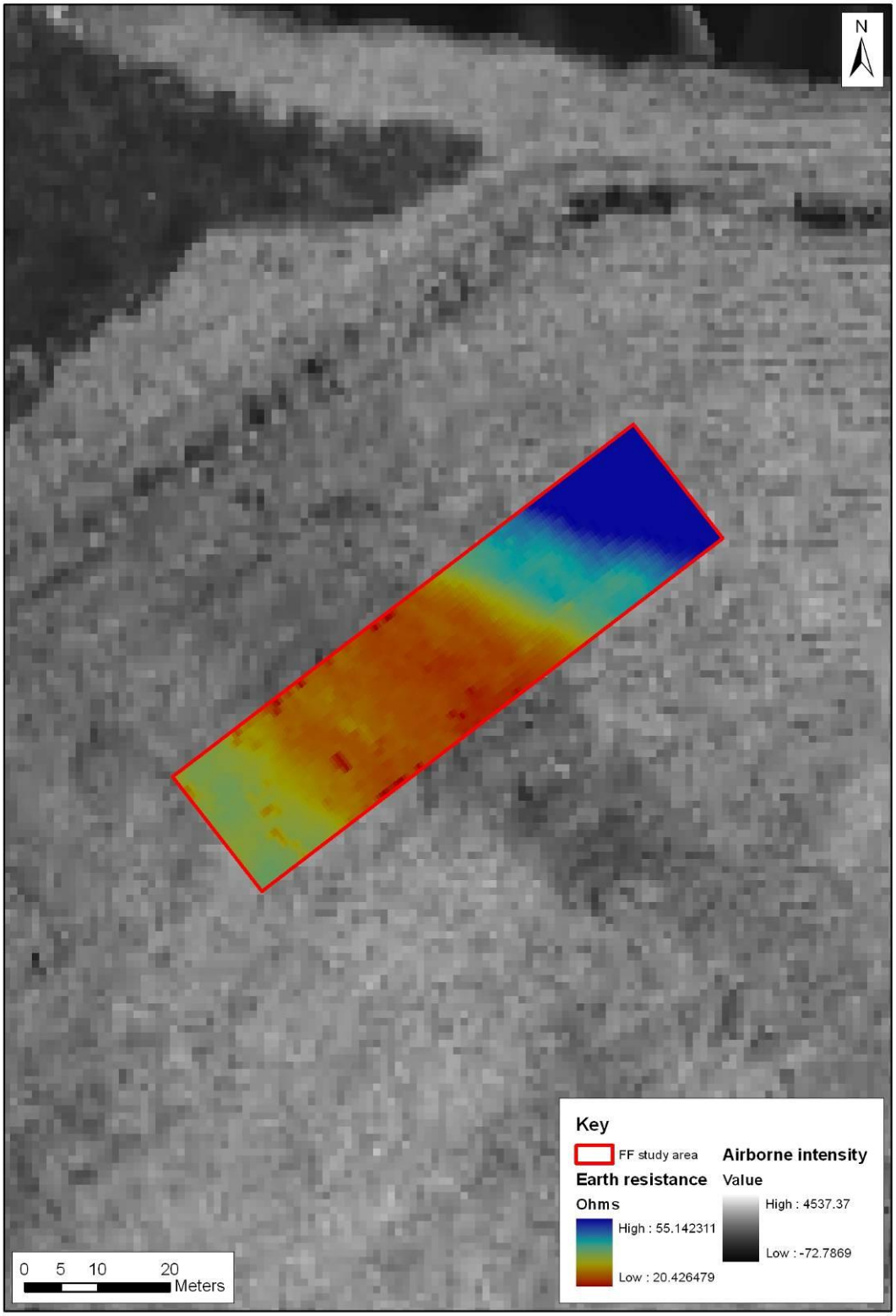

Fig 167: FF survey: The earth resistance survey superimposed on the 1047nm reflectance data. The palaeochannel is clearly definable within the earth resistance data and there is a geranerally good correlation between the two data types.

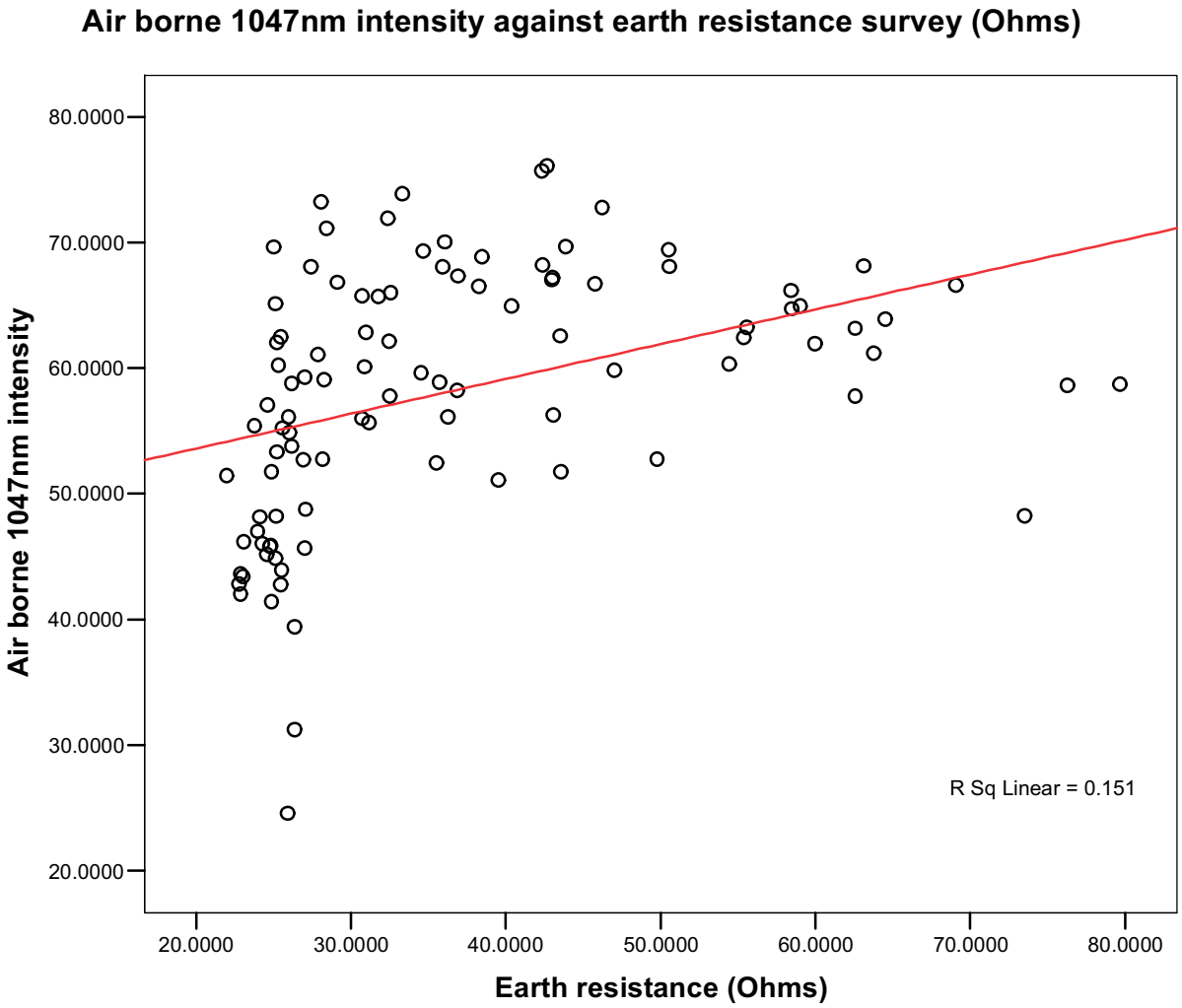

Fig 168: FF survey: Scattergraph of 1047nm reflectance against earth resistance survey (Ohms).

Correlations

		Air borne 1047nm intensity	Earth resistance (Ohms)
Air borne 1047nm intensity	Pearson Correlation	1	.388**
	Sig. (2-tailed)		.000
	N	100	100
Earth resistance (Ohms)	Pearson Correlation	.388**	1
	Sig. (2-tailed)	.000	
	N	100	100

**. Correlation is significant at the 0.01 level (2-tailed).

Fig 169: FF survey. There is a highly significant positive correlation between 1047nm reflectance and earth resistance survey (Ohms).

4.2.2 Area MTF

The MTF survey investigated a fragment of the Hemington Terrace at the western edge of palaeochannel (Fig. 170). Auger survey showed the palaeochannel to have a fill of 1.5m of above gravel silty clay interspersed by clayey medium sands and up to 1.5m of above gravel silt clay alluvium on the terrace. The palaeochannel is evident as a topographical feature, up to 75m wide and 0.7m deep and is readily apparent in lidar elevation data (Fig. 169). The palaeochannel is also a significant feature in the 1047nm reflectance data and this surface model potentially has greater geomorphological value than the topographic model. The study area was pasture (grassland) at the time of field survey in November 2006, in dry clear weather conditions. Samples for volumetric soil moisture were collected at c 4m intervals over two 20 x 20m area one (MTF1) focused on the palaeochannel and the other (MTF2) the terrace.

The soil organic content showed little difference in surface distribution between the terrace (MTF2) and the palaeochannel (MTF1) (Fig. 171). However, the data is spikey and with only 25 data points in each grid high data points are having a larger effect on the interpolation process. A scatter graph of air borne 1047nm reflectance against soil organics produced a linear response, with a moderate hegative relationship (R2 = 36.7%; Fig. 172). The computed correlation coefficient showed this relationship to be significant at the 0.01 level (Fig. 173). This graph hints at the potential of using 1047nm reflectance as a proxy for sediments of high organic content.

The soil moisture content varies across the sample areas (Fig. 174), producing a heterogeneous surface plot. The data is again spikey due to the lower number of samples in each surface interpolation (only 25 readings per grid), although areas of higher soil moisture are visible within the palaeochannel. Overall, based on the surface models produced from the two grids, it is not possible to differentiate between the terrace deposit and palaeochannel based on soil moisture content. The scattergraph of 1047nm reflectance against soil moisture reveals a weak positive relationship (Fig. 175) and no significant correlation between the two variables is witnessed (Fig. 176). It is possible that the palaeochannel and the terrace deposits in this instance have similar soil moisture contents, but different soil organic contents, primarily due to their mechanism of formation. The high clay content in both the palaeochannel and terrace deposits is potentially causing soil moisture retention in both floodplain components.

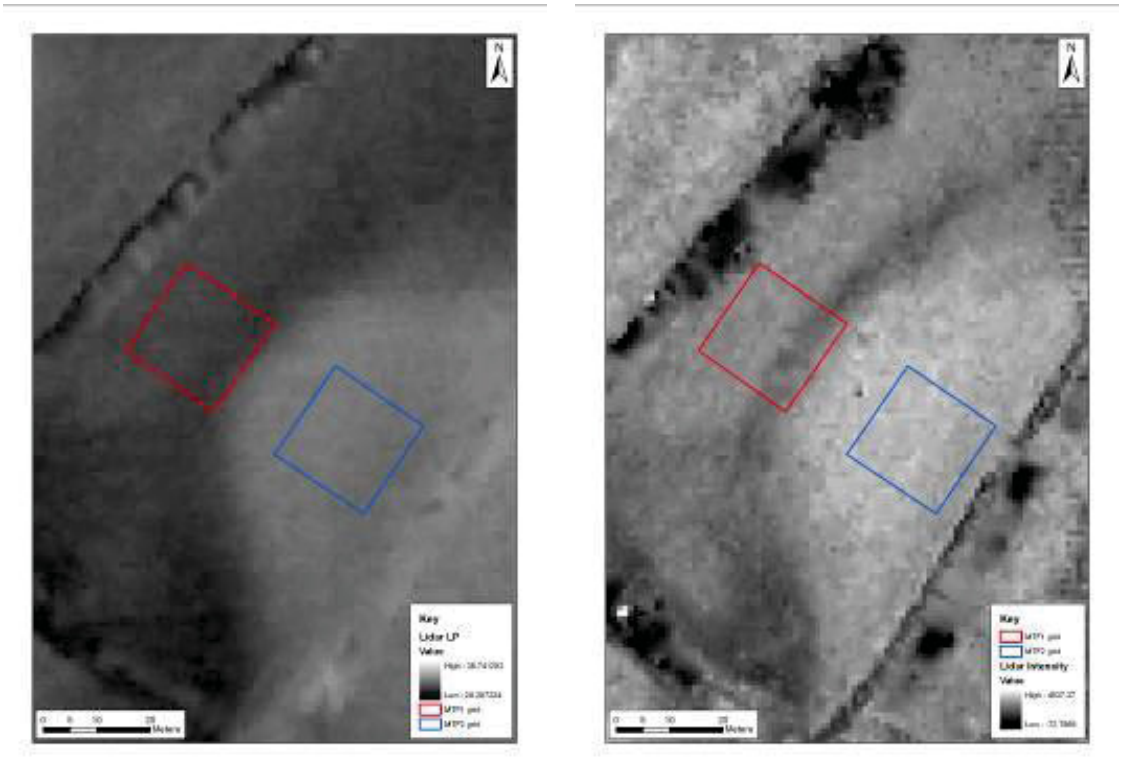

Fig 170: MTF survey. Left, lidar elevation data and right lidar intensity values.

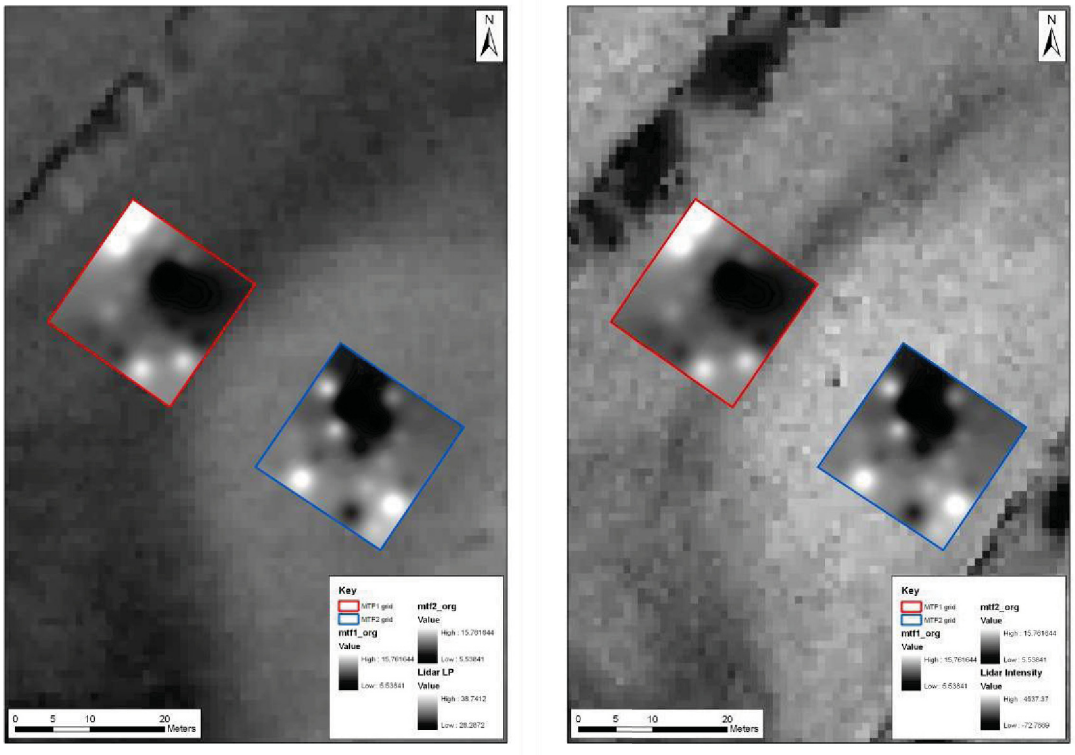

Fig 171: MTF survey. Left, soil organic content superimposed on 1047nm topography and right soil organic content superimposed on 1047nm intensity.

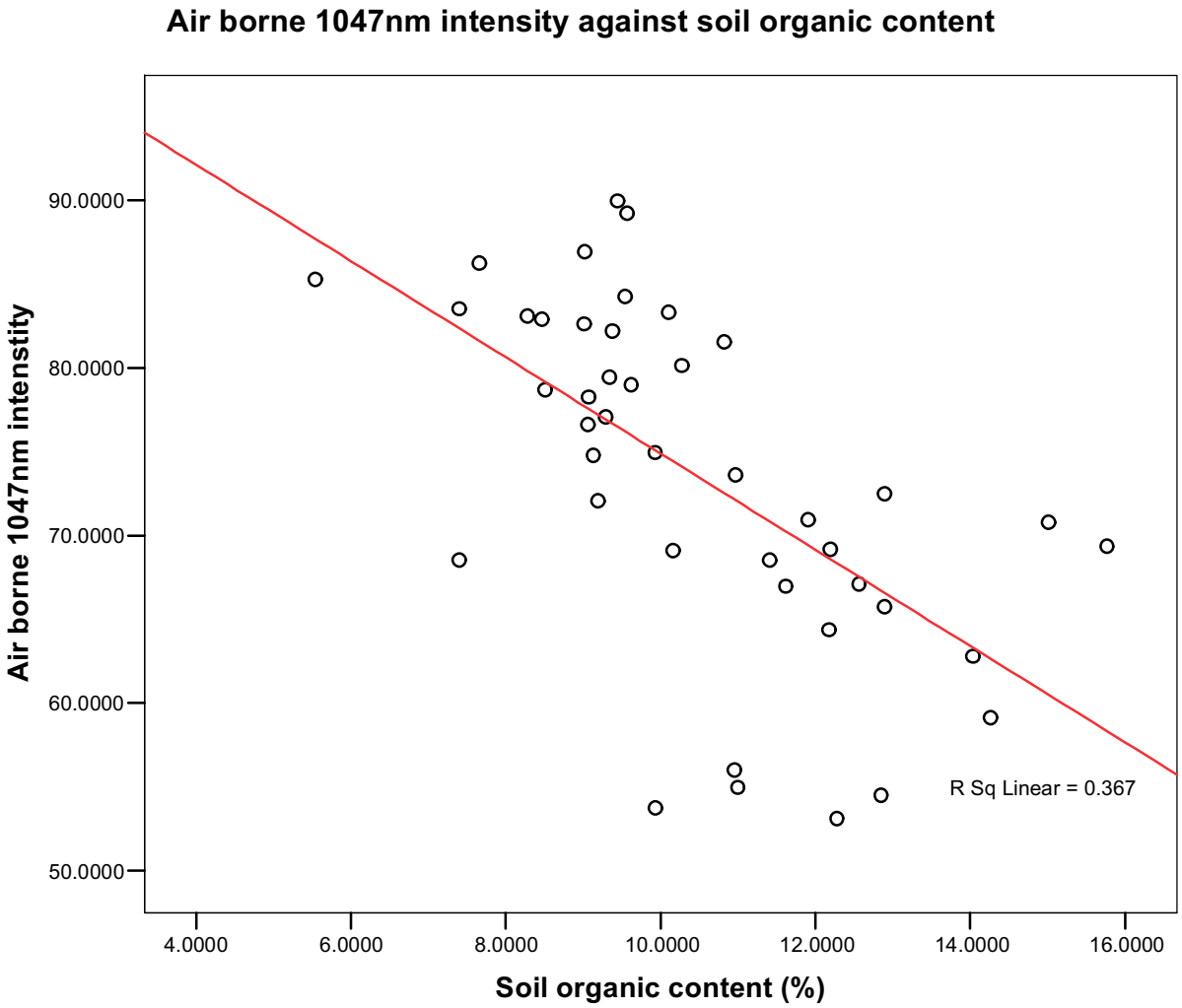

Fig 172: MTF survey. 1047nm reflectance against soil organic content. A moderate negative relationship between the variables is visible.

Correlations

		Soil organic content (%)	Air brone 1047nm intenstity
Soil organic content (%)	Pearson Correlation	1	-.606**
	Sig. (2-tailed)		.000
	N	43	43
Air brone 1047nm intenstity	Pearson Correlation	-.606**	1
	Sig. (2-tailed)	.000	
	N	43	49

**. Correlation is significant at the 0.01 level (2-tailed).

Fig 173: MTF survey: There is a highly significant negative relationship between air borne 1047nmintensity and soil organic content.

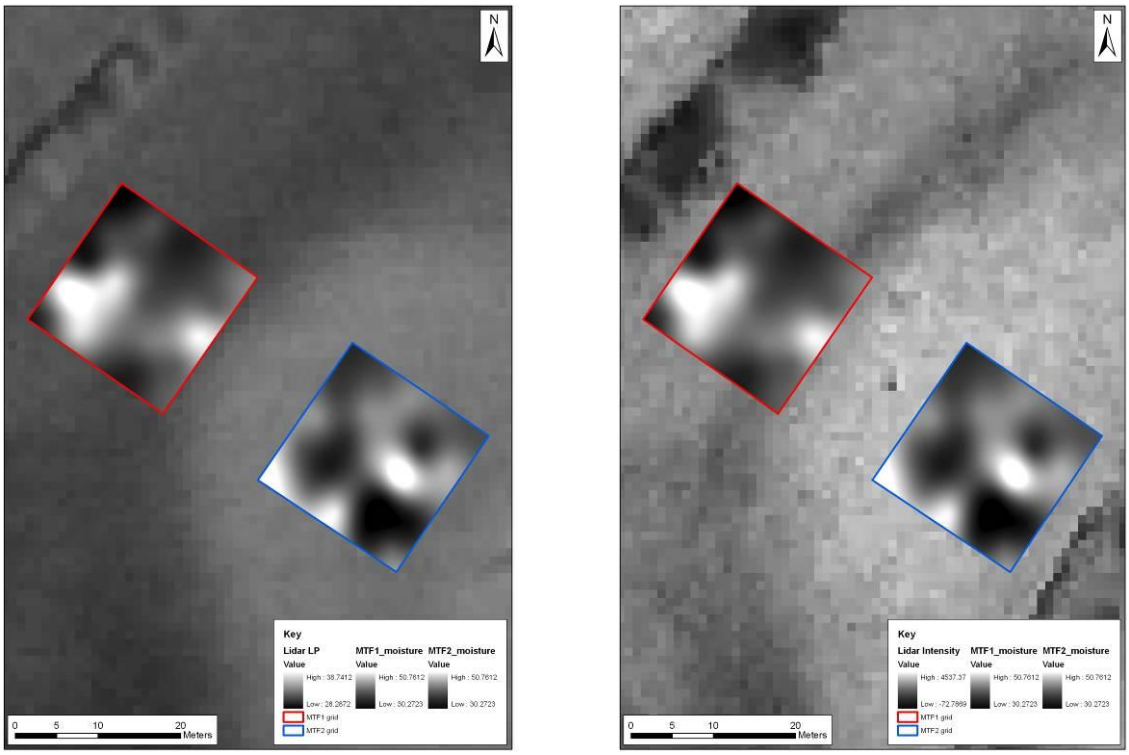

Fig 174: MTF survey. Left, soil moisture content superimposed on 1047nm topography and right, soil moisture content superimposed on 1047nm intensity.

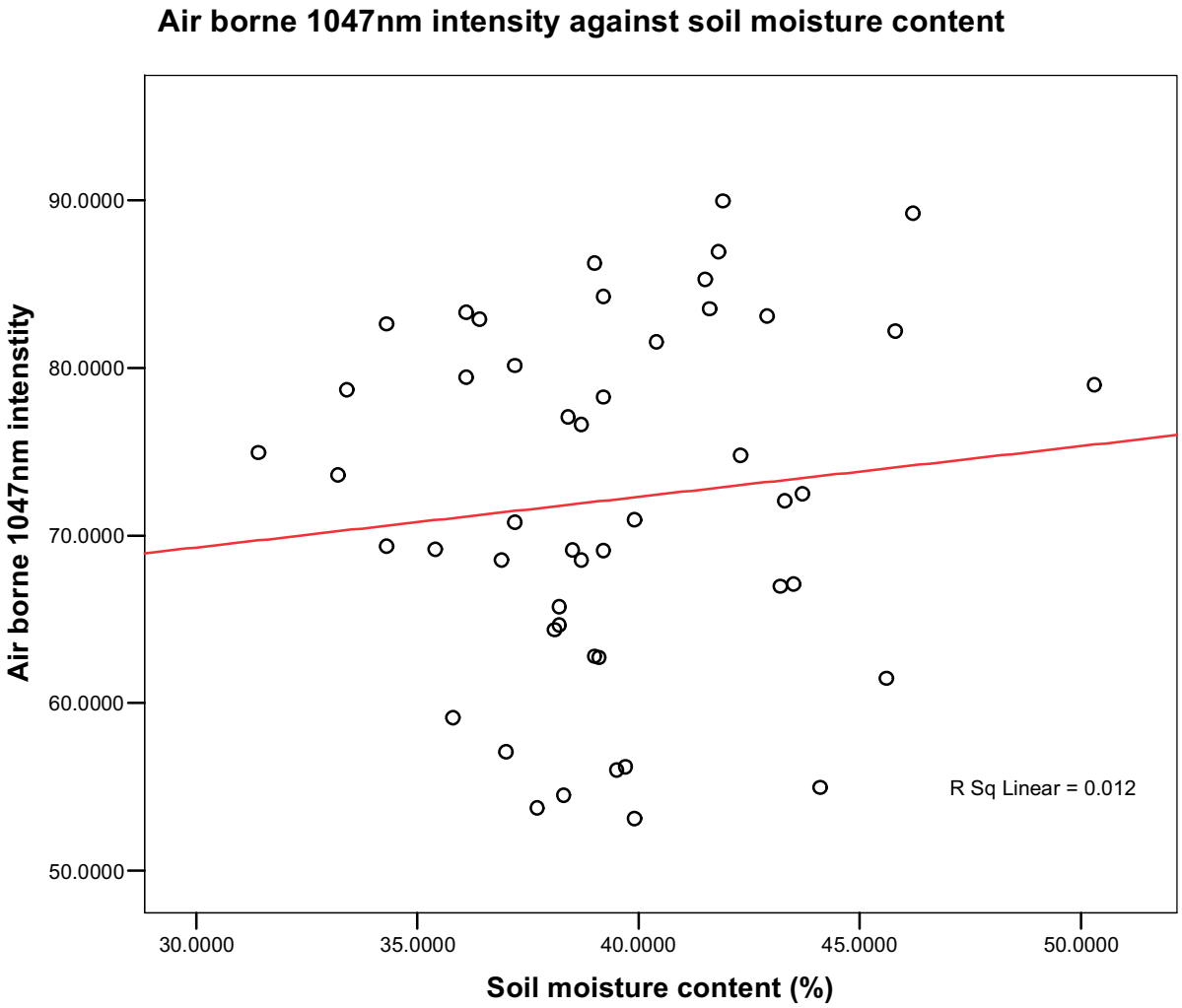

Fig 175: MTF survey. Air borne 1047nm reflectance against soil moisture content. There is a very weak positive relationship between the two variables.

Correlations

		Air brone 1047nm intenstity	Soil moisture content (%)
Air brone 1047nm intenstity	Pearson Correlation	1	.107
	Sig. (2-tailed)		.463
	N	49	49
Soil moisture content (%)	Pearson Correlation	.107	1
	Sig. (2-tailed)	.463	
	N	49	49

Fig 176: MTF survey. There is no significant correlation between air borne 1047nm reflectance and soil moisture content.

4.2.3 Area MF

Area MF comprises a part of the modern floodplain of the River Trent where a palaeochannel lies parallel to a raised linear ride of sand and gravel, probably a channel bar (Fig. 177). The palaeochannel shows as a slight topographical feature, approximately 20m wide and 0.5m deep the bar as a broader c 40m wide c 0.4m high feature. Both palaeochannel and bar show clearly in lidar elevation data, whilst the palaeochannel is just evident in the lidar 1047nm reflectance surface (Fig. 178). The study area is given over to permanent pasture and was covered with low cropped grass at the time of survey in July 2006, in exceptionally dry weather conditions. At the time of the survey the linear gravel bar was clearly apparent as a well-defined parchmark in the grass. Samples for soil organic content and moisture were collected at c 4m intervals over a 40 x 20m area covering the channel and adjacent bar.

Fig 177: Lockington study area MF showing palaeochannel (left) and bar feature (right).

The soil organic content clearly defines the palaeochannel and bar (Fig. 179). Soils within the palaeochannel feature have a higher organic content than those associated with the bar feature. Surprisingly the scattergaph shows only a weak negative relationship between soil organic content and air brone 1047nm reflectance (Fig. 180) and this is confirmed by the correlation coefficient showing no significant relationship between the two variables (Fig. 181). However, visually there does appear to be a strong correlation between these two variables.

The soil moisture content (Fig. 179) shows some heterogeniety in its surface distribution, but the palaeochannel and bar are both evident as variation in soil moisture content. However, the scattergraph of 1047nm reflectance dependant on soil moisture reveals practically no visual linear relationship between the two variables (Fig. 182) and this is confirmed by the correlation coefficient (Fig. 183). The separation in time between the Lidar survey and the soil moisture survey could be interpreted as the reason for the lack of correlation between these variables and simultaneous sampling is recommended for future ground truthing research.

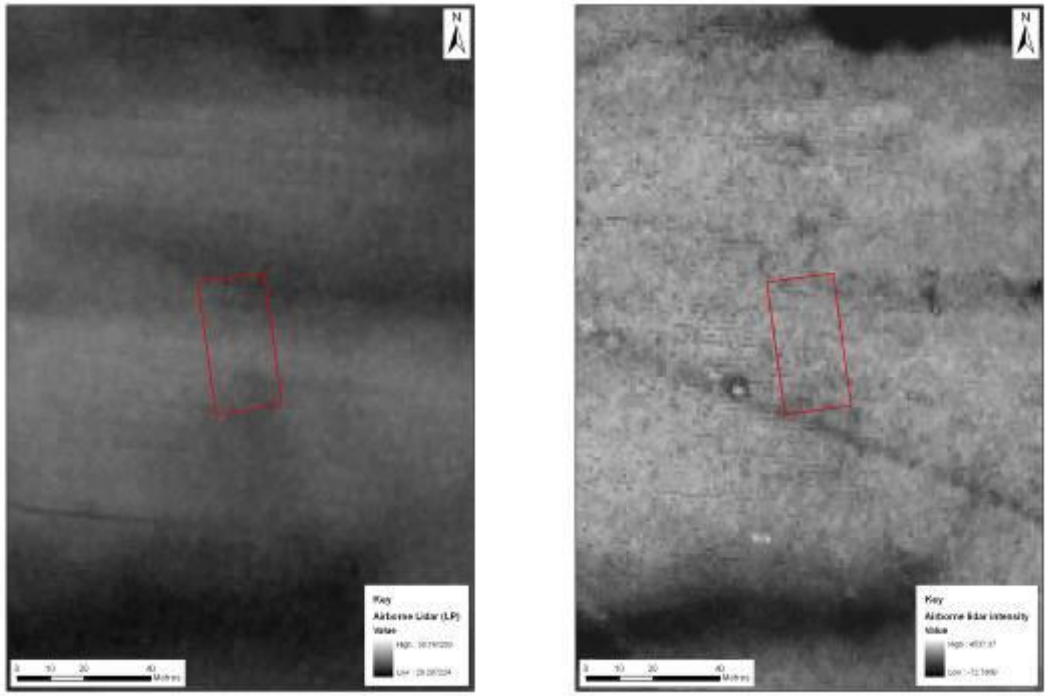

Fig 178: MF survey. Lidar elevation (left) and intensity (right).

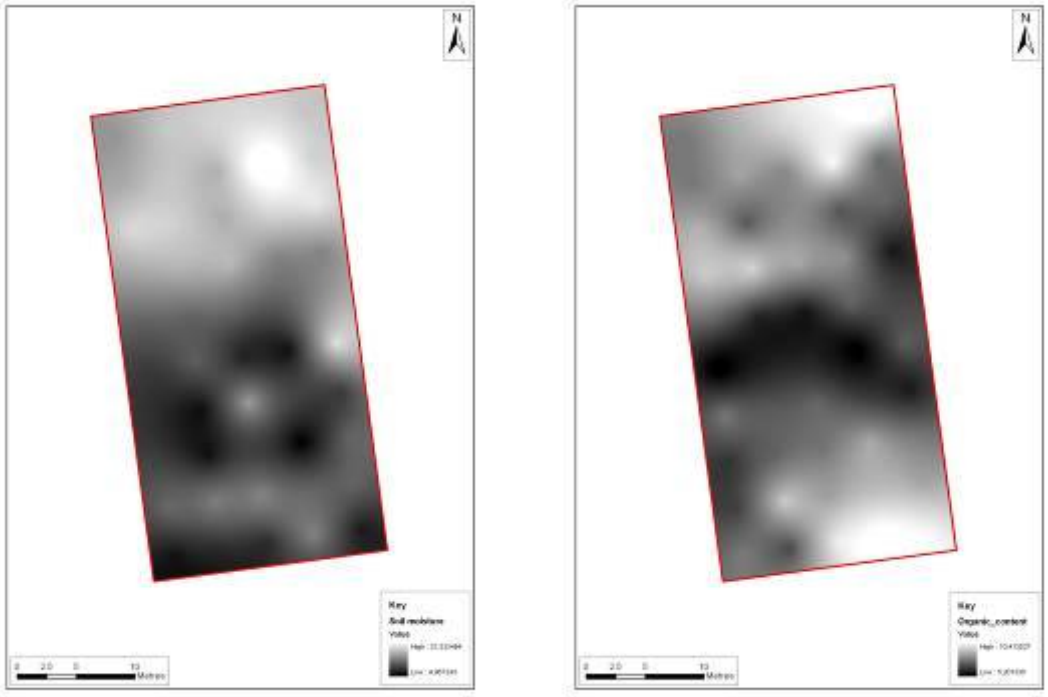

Fig 179: MF survey. Volumetric soil moisture (left) and topsoil organic content (right).

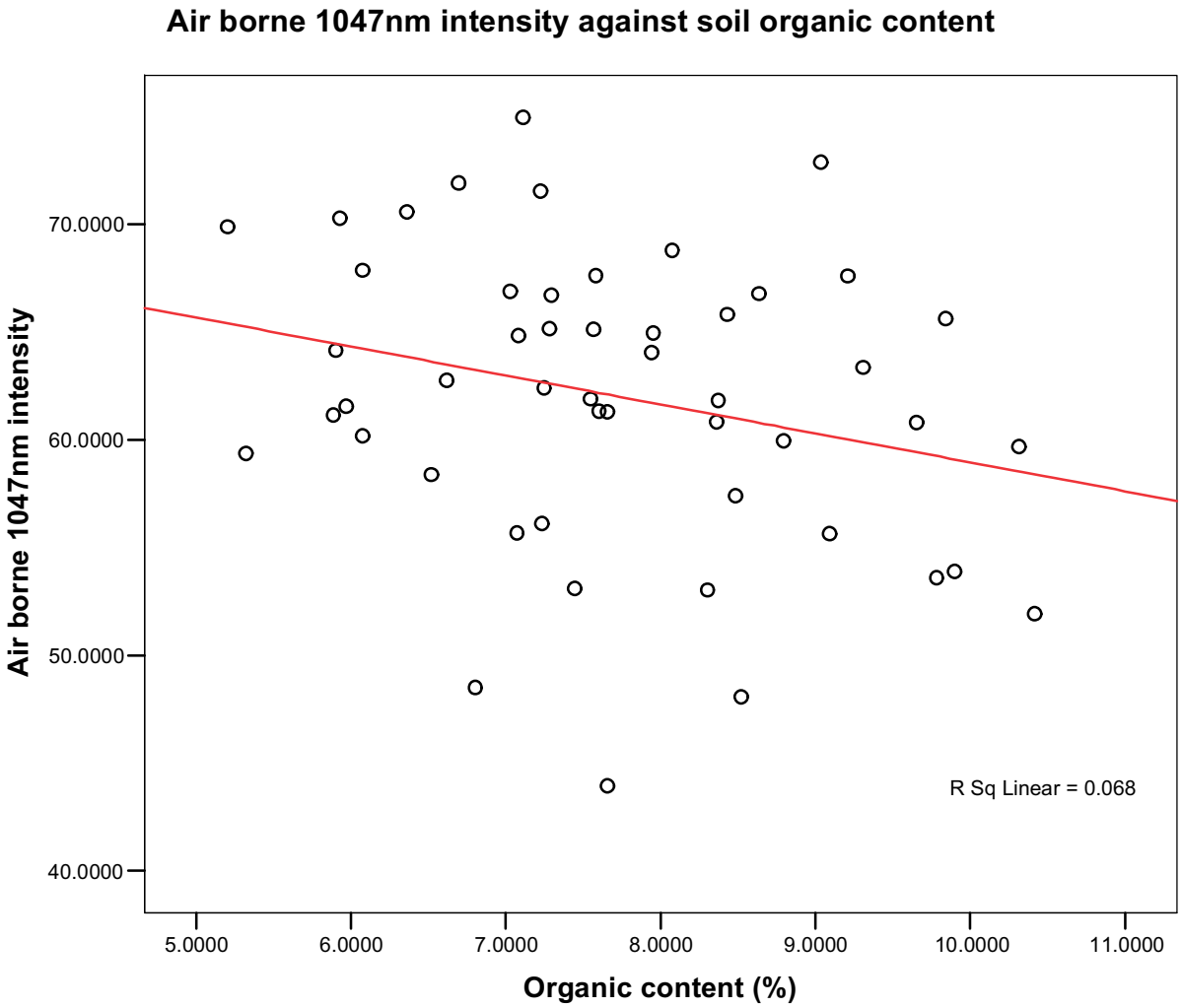

Fig 180: MF survey. Air borne 10747nm intensity against soil organic content. Only a weak negative relationship is seen.

Correlations

		Organic content (%)	Air borne 1047nm intensity
Organic content (%)	Pearson Correlation	1	-.261
	Sig. (2-tailed)		.067
	N	50	50
Air borne 1047nm intensity	Pearson Correlation	-.261	1
	Sig. (2-tailed)	.067	
	N	50	50

Fig 181: MF survey. There is no significant correlation between air borne 1047nm reflectance and soil organic content.

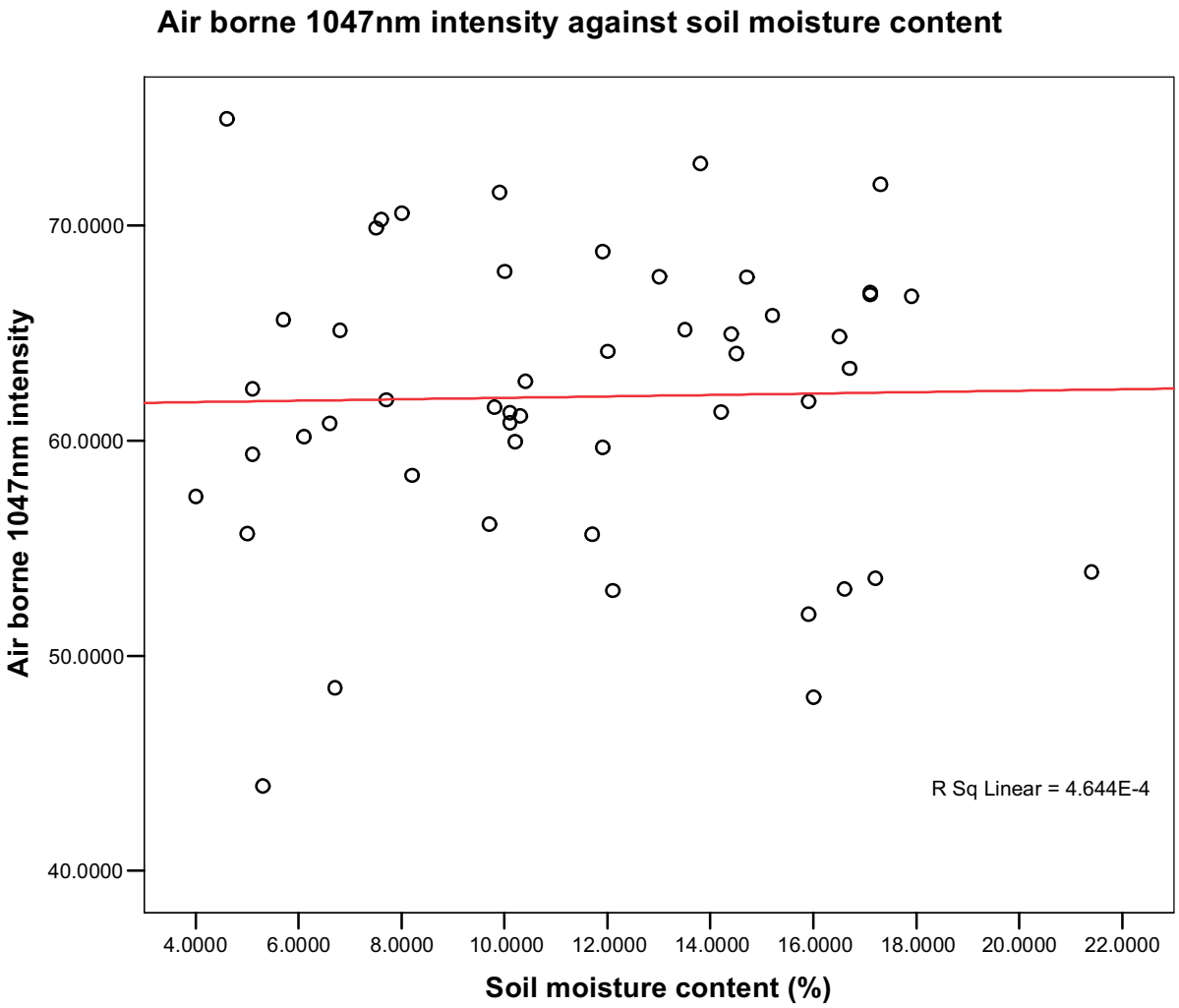

Fig 182: MF survey. Air borne 10747nm intensity against soil moisture content. There is virtually no definable visual linear relationship between the two variables.

Correlations

		Air borne 1047nm intensity	Soil moisture (%)
Air borne 1047nm intensity	Pearson Correlation	1	.022
	Sig. (2-tailed)		.882
	N	50	50
Soil moisture (%)	Pearson Correlation	.022	1
	Sig. (2-tailed)	.882	
	N	50	50

Fig 183: MF survey. There is no significant correlation between air borne 1047nm reflectance and soil moisture content.

4.3 YORKSHIRE DALES

4.3.1 Introduction

The landscape between Nether Kellet and Pannal consists of relict glacial deposits that developed during the Devensian glaciation (Last Glacial Maximum, 22,000 yrs BP). The drainage network that evolved in response to postglacial climatic amelioration incised into the glacial till deposits, developing the catchments of Rivers Lune, Wenning, Ribble, Aire and Wharfe. Repeated phases of incision and aggredation during the postglacial period are likely to have resulted in the gradual erosion and re-deposition of glacial till within each catchment area and the subsequent development of river floodplains over time. Consequently, the topography of the region consists of areas of higher relief composed predominantly of glacial till and lowland river floodplains.

From analysis of the Lidar data it is interpreted that the river floodplains have the highest palaeoenvironmental potential. The areas of higher ground bordering each river catchment have developed drainage systems that are composed of relatively steeply incised channels. Consequently, there is limited potential for channel movement, which would normally encourage palaeochannel development and subsequent organic accumulation. The floodplains of the Rivers Lune, Wenning and Aire contained an abundance of possible palaeochannel features. The floodplains of the rivers Ribble and Wharfe contained limited evidence for palaeochannel development. This is suggestive of anastomosing sedimentary systems, in which minimal channel migration took place and floodplain development occurred primarily through vertical accretion. Utilising the information created through Lidar analysis, a summary of each area of interest is provided, including images identifying the regions in which palaeoenvironmental potential has been identified (Fig. 184).

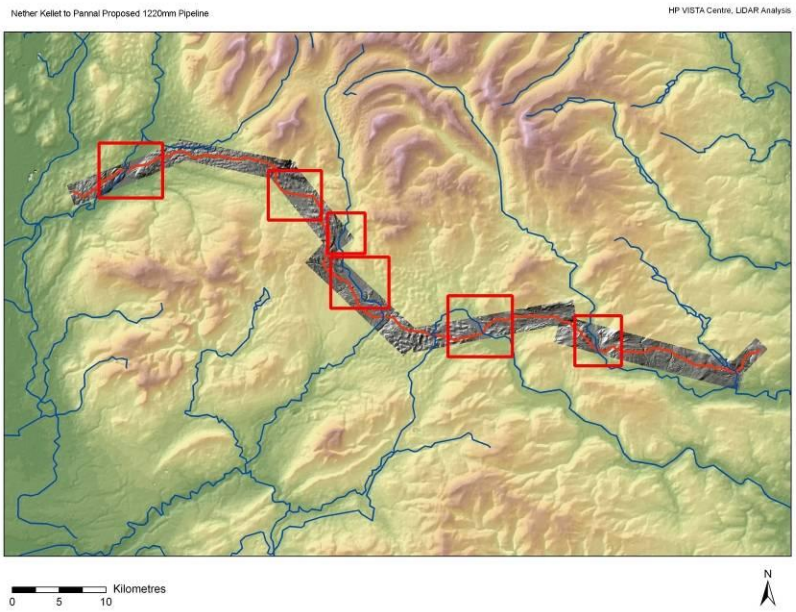

Fig 184: The Yorkshire Dales between Nether Kellet and Pannal showing the extent of the lidar DSM and intensity data in grey and selected study areas outlined in red. Base elevation data is Space Shuttle Radar (SRTM).

4.3.2 River Lune Floodplain at Hornby

Along the floodplain of the River Lune, analysis of the hillshade last pulse ground (hslpg) layer identified an abundance of topographic features indicative of palaeochannel development and preservation. Figure 185 shows the 'hslpg' layer of the River Lune proximal to Hornby, with the 1047nm reflectance data highlights the palaeochannel features evident within the floodplain. Upon analysis, it seems clear that the 'hslpg' layer provides a detailed assessment of the variations in surface altitude that have resulted from channel migration over time. Cross-sections traversing the valley floodplain have been created, confirming that the visual anomalies present across the floodplain are indeed areas of lower relief relative to the floodplain (Fig. 186). The majority of the topographic features identified run broadly parallel with the contemporary River Lune. Palaeochannel development is therefore suggested to have occurred primarily through lateral channel migration across the floodplain, with former channels being abandoned when alternative routes for the river have developed (possibly in response to flooding episodes). The 1047nm reflectance readings do show some correlation with palaeochannels identified through topographic expression, however, the intensity data is noisy and maybe reflecting a host of other features such as hedges, roads, etc.

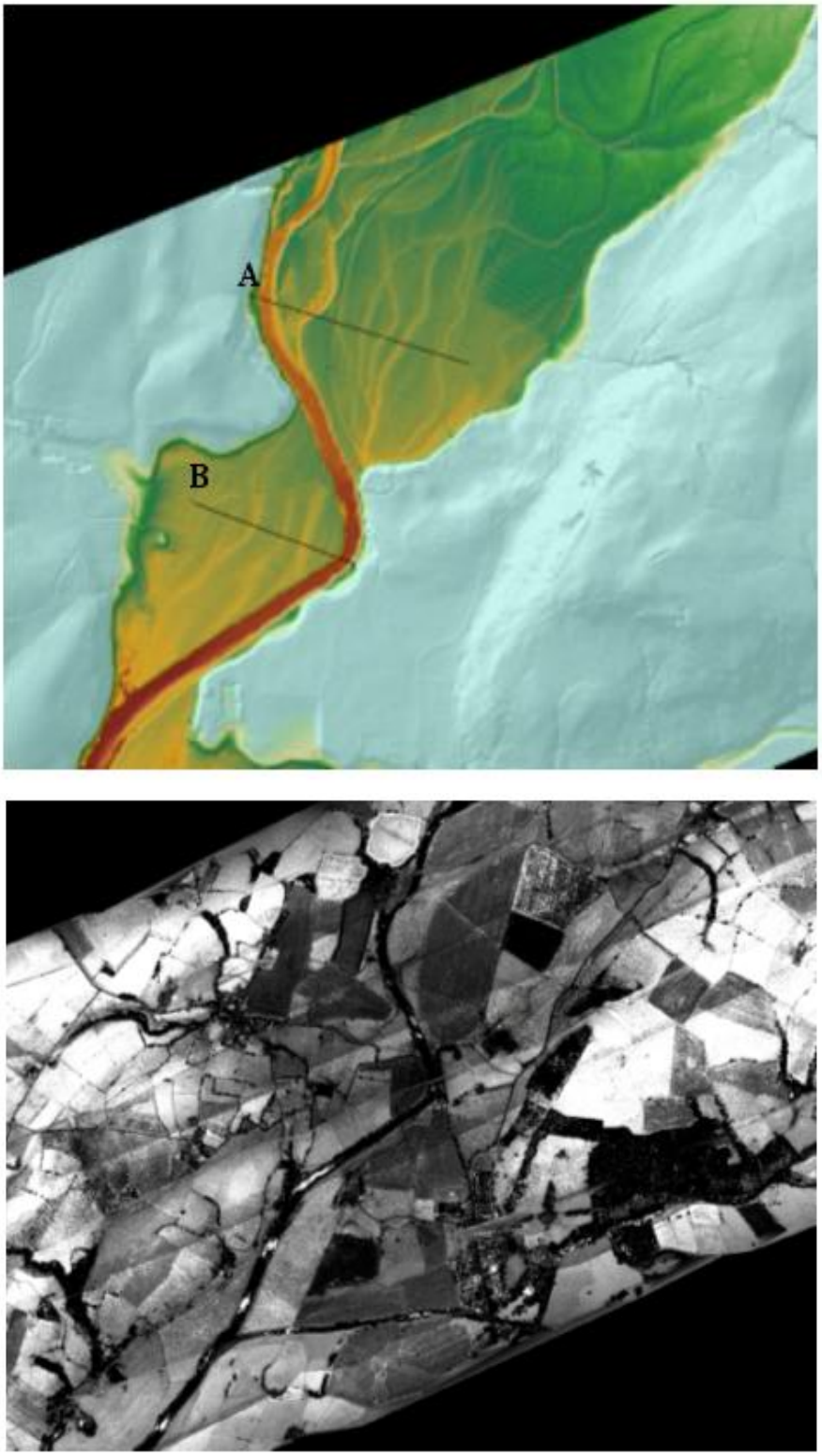

Fig 185: River Lune at Hornby, Top lidar LPG DSM showing profile locations, bottom lidar LPG intensity.

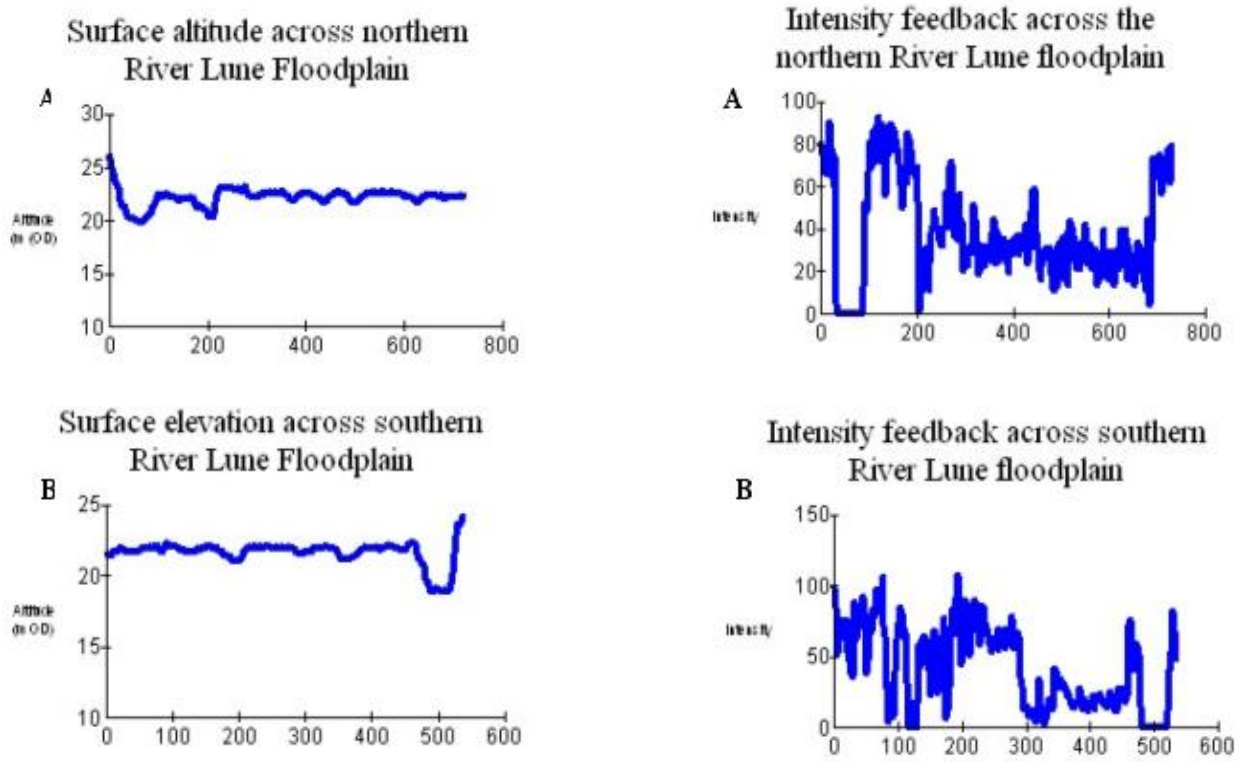

Fig 186: Profiles through lidar LPG DSM and Intensity Data for the River Lune study reach.

4.3.3 River Wenning at Clapham

Approximately 15km east of Hornby, within the catchment of the River Wenning, evidence of further palaeoenvironmental resources has been identified through Lidar data (Fig. 187), through both topographic and intensity data types. In contrast to the River Lune, the majority of the features identified along the floodplain of the River Wenning appear to be former ox-bow lakes. It is therefore likely that such features developed when the river channel was much more sinuous than that present today. The nature of the former river channel would have encouraged meander bends to become cut-off from the main channel as the drainage system developed over time. This could have been in response to variations in catchment stability, palaeohydrology and sediment supply. Once such meander bends had become disconnected, they would develop a stagnant water body known as an ox-bow lake. The feature would experience *in-situ* biogenic sedimentation through vegetation development within the ox-bow lake and around its margins. Eventually the depositional basin would become infilled with peat to prevent its identification from the ground.

The intensity results for the site were assessed and, as with the floodplain of the River Lune, were found to provide limited evidence for archaeological or palaeoenvironmental potential (Fig. 188). Whilst some areas within the floodplain provided low intensity readings that corresponded to areas of low relief identified through standard Lidar analysis (transect A), the majority of the intensity anomalies related to areas of dense vegetation, field boundaries etc. Transect B shows little relationship between the intensity response and topographic data. It is possible that floodplain sedimentation had capped much of the organic sediments that have accumulated within the former ox-bow lakes, potentially resulting in similar readings between areas of floodplain and areas of ox bow lake.

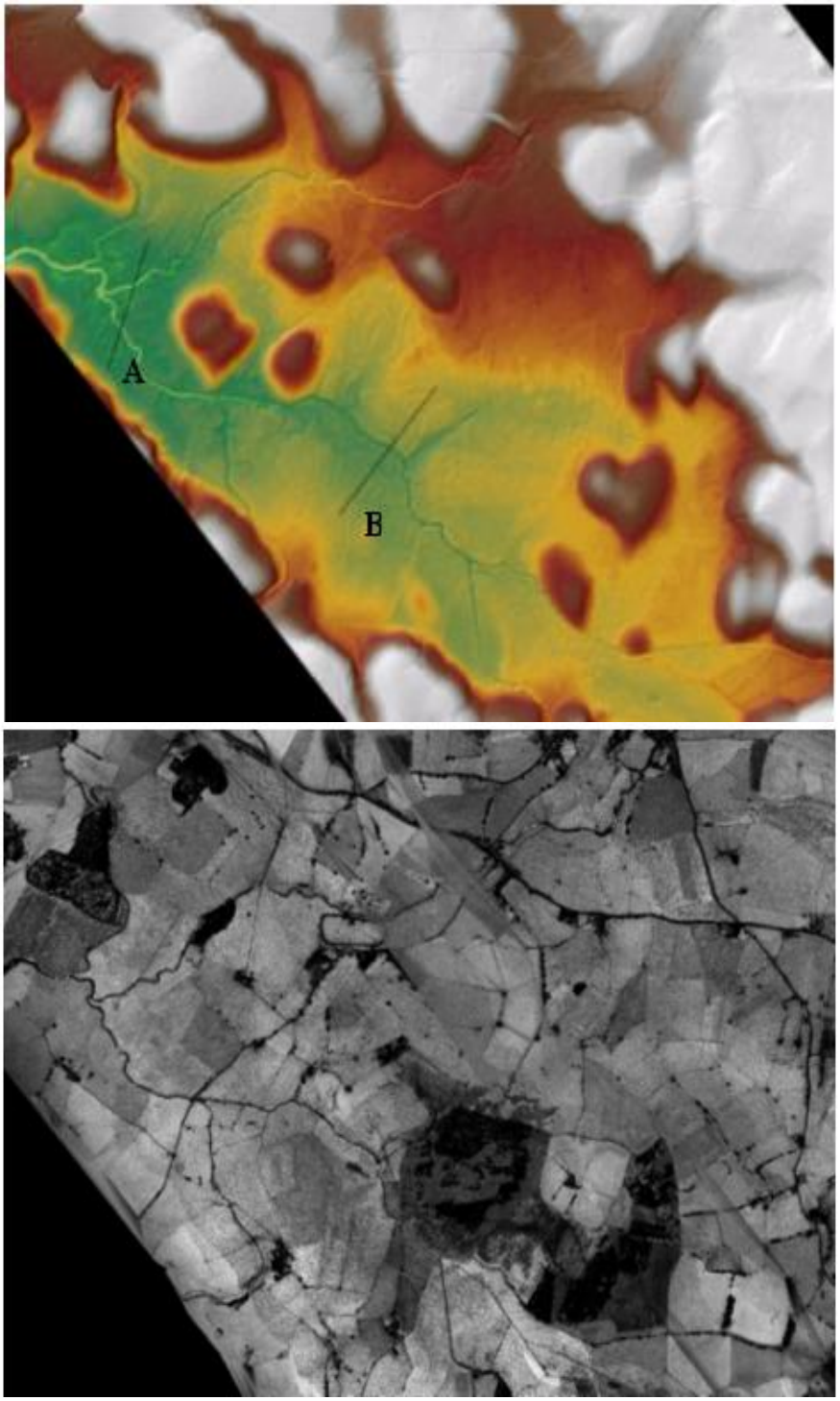

Fig 187: River Wenning at Clapham, Top lidar LPG DSM showing profile locations, bottom lidar LPG intensity.

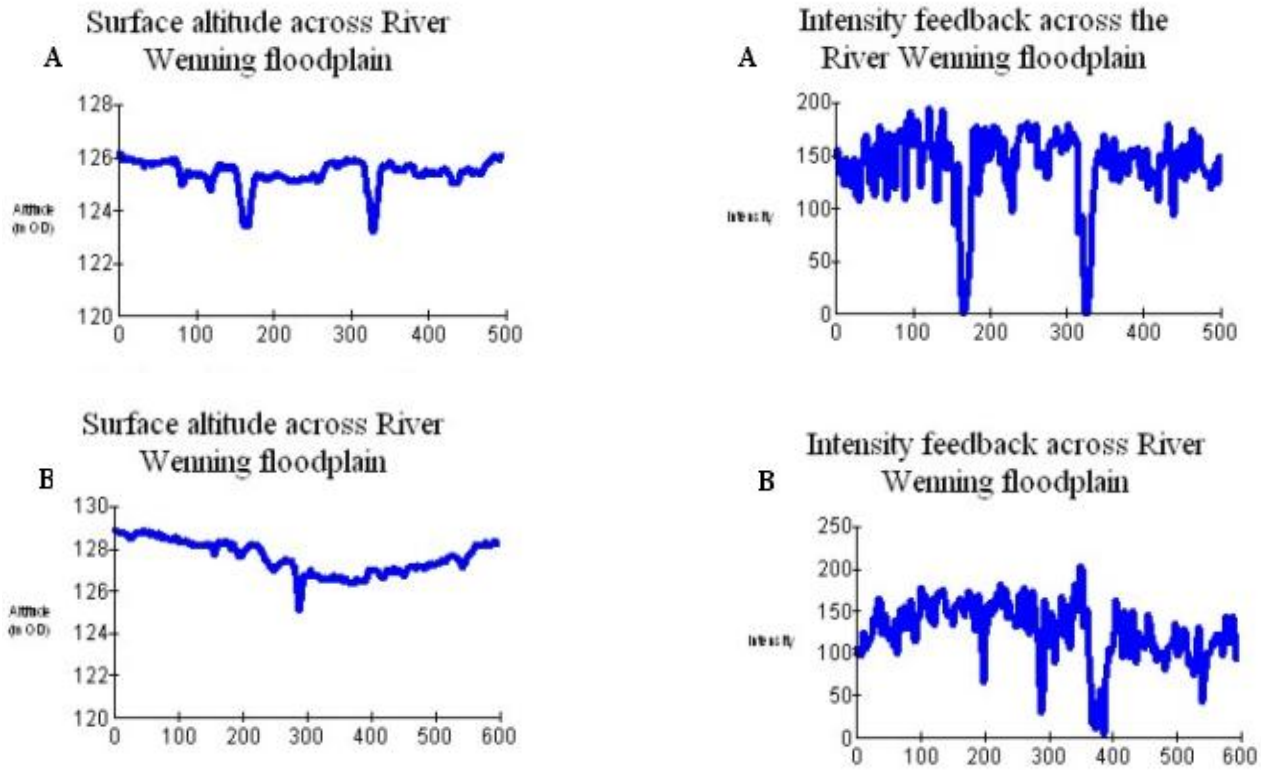

Fig 188: Profiles through lidar LPG DSM and Intensity Data for the River Wenning study reach.

4.3.4 River Aire at Gargrave

A third site was identified during the assessment of the Nether Kellet to Pannal Lidar data, located along the floodplain of the River Aire, proximal to Gargrave. A series of palaeochannels were identified using the last pulse ground elevation data (Fig. 189). As with the palaeochannel features from the River Wenning floodplain, the majority of the topographic anomalies appear to be in the form of meander cut-offs, having developed over time in response to channel evolution. A distinctive potential palaeochannel is evident immediately west of the railway line that runs northwest-southeast through the floodplain. This is likely to have formed as a result of human activity, possibly diverting the river to simplify railway line construction. Analysis of historical maps would confirm whether this. A second meander cut-off is also evident to the northeast, which appears as a distinctive topographic anomaly.

The cross valley transects provide some curious visual correlation between lidar topographic and intensity data (Fig. 190). On transect A, where there are lower topographic values lower intensity readings are also seen, especially between 200 – 400m along the transect. In contrast on transect B areas of higher topographic values at c. 200 – 300m are also seen as lower intensity values, the opposite of transect A. The low points with low intensity values in transect A could easily be identifying organic rich sediments in palaeochannels. The reasons for the high intensity readings in transect B are unknown.

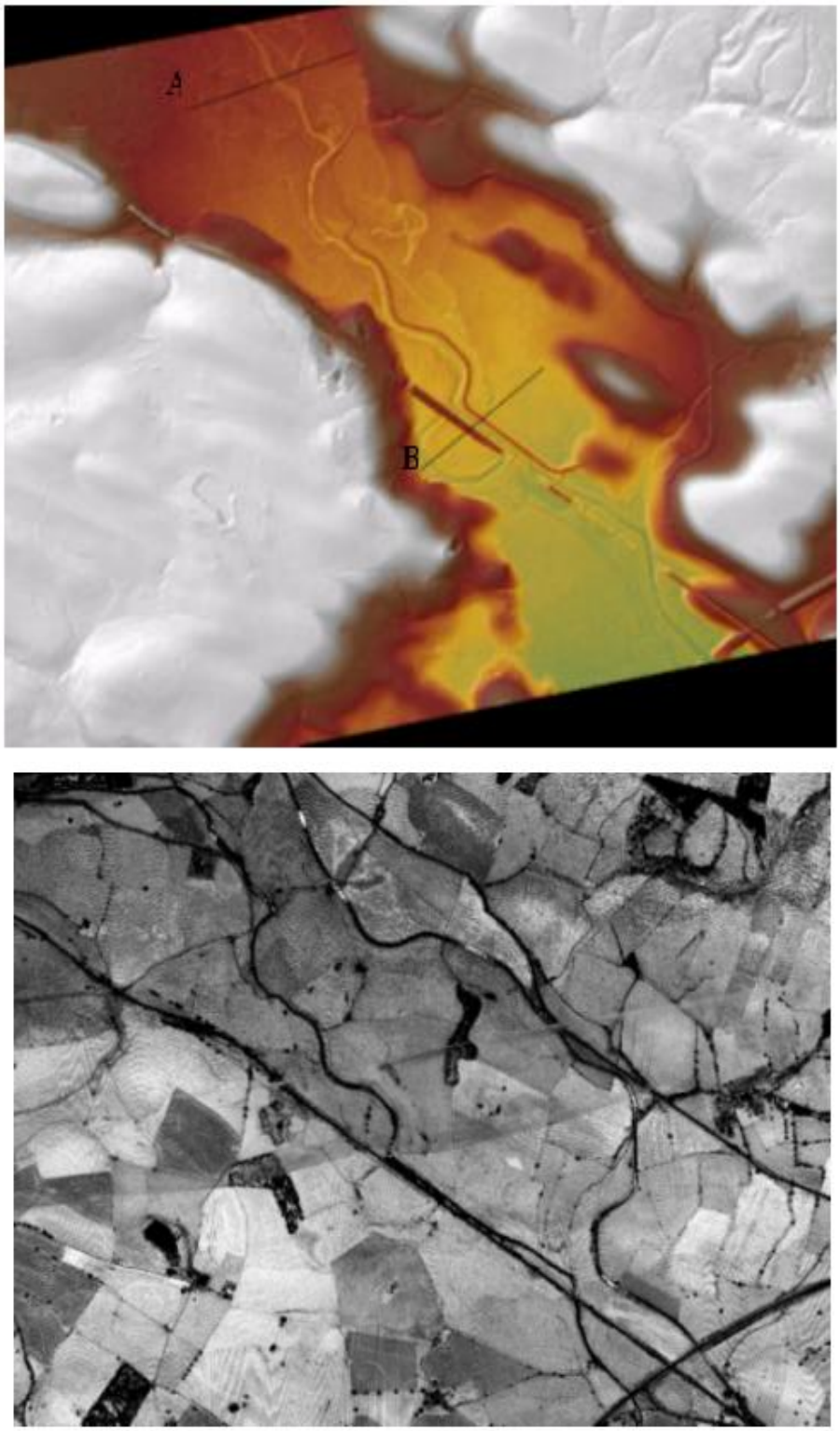

Fig 189: River Aire, at Gargrave, Top lidar LPG DSM showing profile locations, bottom lidar LPG intensity.

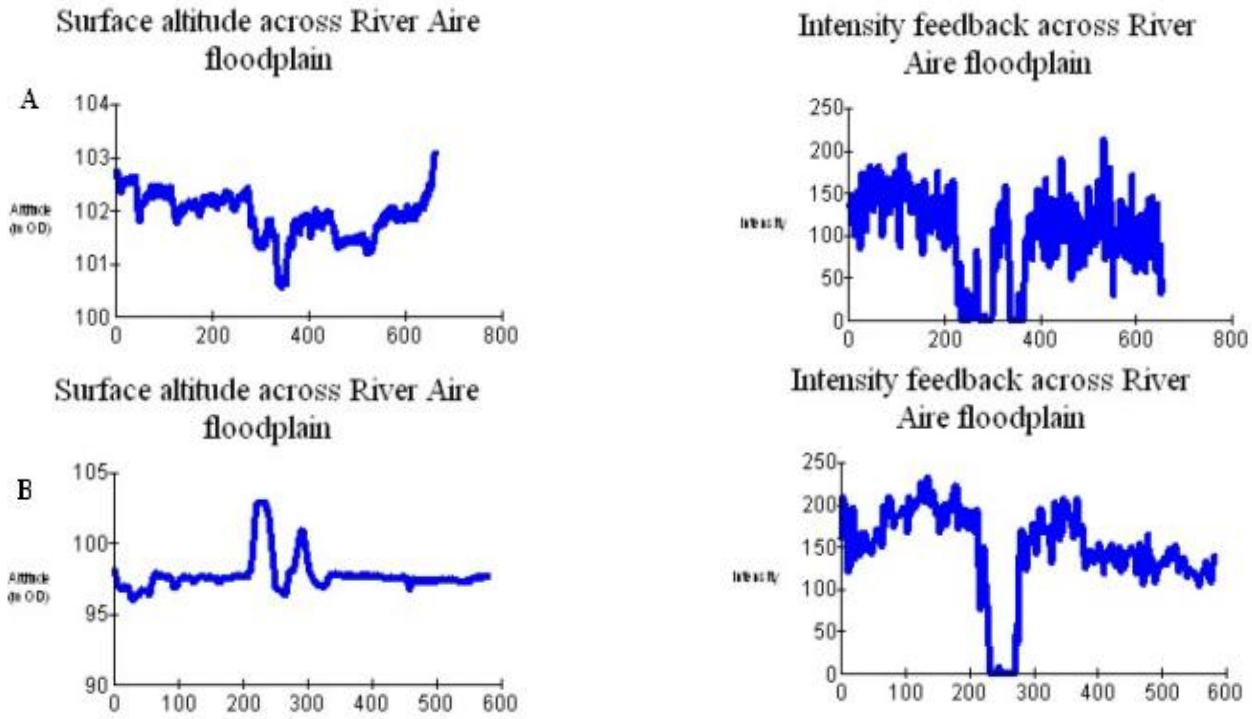

Fig 190: Profiles through lidar LPG DSM and Intensity Data for the River Aire study reach.

4.3.5 Hesley Hill at Rathmell

A final site was located on the western valley side of the River Ribble, located some 4.5km southwest of Settle and to the west of the village of Rathmell. Analysis of the Lidar data provided restricted results. This is typical for such upland regions, primarily due to the steep gradients of the valley sides hiding any subtle topographic hollows that would be suggestive of organic accumulation. Consequently, no assessment of the topographic LPG data is provided. However, on analysis of the intensity data, the upland catchment around the Hesley Hill area yielded potentially promising results. A number of upland valley basins, fed by small streams running east towards the River Ribble, provided an abundance of low intensity readings (Fig. 191). The results may be explained by areas of peat accumulation within the higher ground.

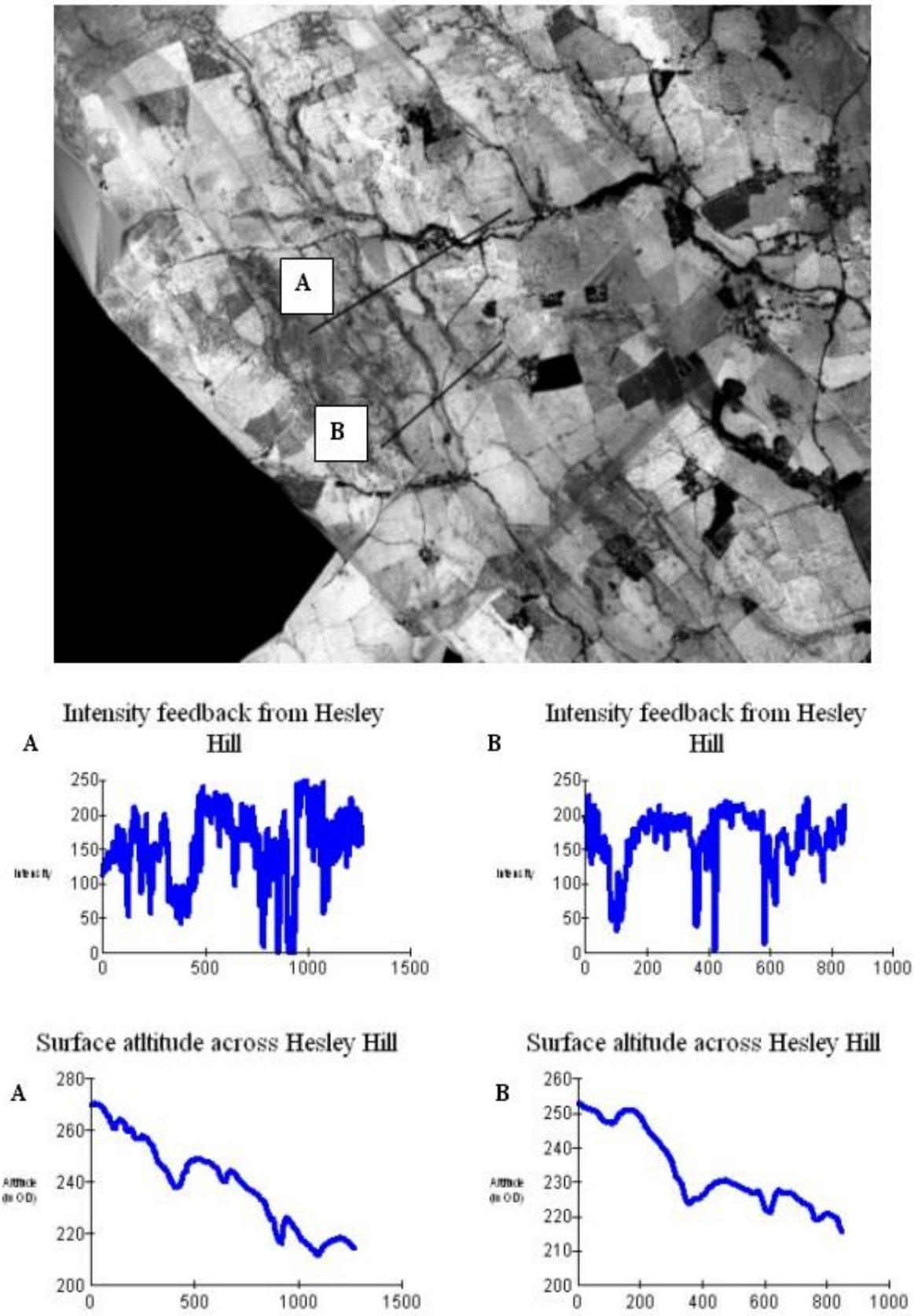

Fig 191: Hesley Hill, Lidar LPG Intensity and profiles through DSM and Intensity data.

5 CONCLUSIONS

5 CONCLUDING COMMENTS AND FUTURE DIRECTIONS

This section will attempt to provide a coherent overview of the results, with recommendations for future research as well as awareness of limitations. Data has been analysed from a large number of sources to assess the predictive capacity of lidar intnsity data to identify waterlogged organic rich deposits. The analysed data sets can be summarised as:

- Laboratory collected NIR data.
- Ground based assessment of terrestrial Lidar.
- Correlation of air borne Lidar with soil parameters.
- Assessment of air borne 1047nm topographic/intensity data in isolation.

The laboratory analysis of the NIR data did qualify a visual relationship between 1047nm reflectance and sediment stratigraphy. When changes in sediment architecture of the cores were witnessed NIR reflectance also changed. Significant correlations were proven to exist between 1047nm reflectance and soil organic content, soil carbonate content and magnetic susceptability, although these relationships were hard to assess visually. Eventually a model was accepted where 1047nm was not dependant on any of the single variables, but the soil parameters and 1047nm reflectance were all reflecting larger changes in sediment architecture.

The ground based assessment of lidar reflectance using a terrestrial 950nm scanner proved to be extremely problematic, due to a range effect induced into the reflectance readings. With increasing distance from the scanner reflectance readings increased. A series of correction factors were applied to the resultant data sets but these failed to correct the data. Although detailed measurements were taken of soil organic contents, soil moisture contents and 950nm intensity, no significant relationships were realised due to the range effect dominating the data sets.

The correlation of airborne Lidar with ground based measurements of soil parameters was more successful and hinted at the potential of this approach in order to understand intensity. On the limited study areas undertaken, significant visual and mathematical relationships were seen between 1047nm reflectance and soil organic content. However, the results did vary enormously, partly due to variance introduced into these data sets through the survey times between the 1047nm intensity and soil parameters being several years apart. It is suggested that this is a profitable line of future research and should be explored further. Lastly, the analysis of the 1047nm reflectance data in the Yorkshire dales again proved somewhat frustrating. However, features evident as topographic palaeochannels were identifiable through generally lower 1047nm reflectance readings.

It is suggested that further Lidar flights are undertaken to assess 1047nm intensity. At the same point in time sample areas should be selected that reflect a series of different geomorphological and cultural features, which should be surveyed simultaneously with the 1047nm reflectance data. In addition, it is suggested that larger survey areas are undertaken, providing a greater resolution of soil organic content, soil moisture data and earth resistance survey. It is suggested that more earth resistance survey in particular is undertaken, providing a proxy between 1047nm reflectance and volumetric soil moisture content.

6 REFERENCES

6 REFERENCES

Baker, S. (2003). *The Trent Valley: Palaeochannel Mapping from Aerial Photographs*. Trent Valley Geoarchaeology Research Report. Nottingham: Trent & Peak Archaeological Unit.

Bewley, R.H. Crutchley, S.P and Shell, C.A. (2005). New light on an ancient landscape: lidar survey in the Stonehenge World Heritage Site. *Antiquity* Volume: 79 Number 305: 636–647

Bewley, R. H. (2003). Aerial survey for archaeology. *The Photogrammetric Record* 18 (104): 273-292.

Bishop, M. (2003). Issues and agenda in archaeological research and management: a case study from the Trent Valley, UK. In Howard, A.J., Macklin, M.G. and Passmore, D.G. (eds) *Alluvial Archaeology in Europe.* Lisse: Balkema: 123-131.

Brown, A. G., Carey, C. J., Howard, A. H., Challis, K. C., Kincey, M. K., Tetlow, E. and Cooper, L. 2007. Predictive modelling of multi-period geoarchaeological resources at a river confluence phase II. Unpublished report for English Heritage, funded through the ALSF scheme. PNUM 3357.

Brown, A.G., Carey, C. J., Howard, A. H., Challis, K. C. and Cooper, L. 2005. Predictive modelling of multi-period geoarchaeological resources at a river confluence phase I. Unpublished report for English Heritage, funded through the ALSF scheme. PNUM 3357.

Brown, A.G. (1997). *Alluvial Geoarchaeology. Floodplain archaeology and environmental change.* Cambridge: Cambridge University Press.

Brown, K., Duncan, A., O'Dwyer, C., Davison, B., Hogarth, P,. Butler, D. & Sampson, E. (2003). Integrated airborne data collection by the Environment Agency. In Aplin P. and Mather, P.M. (eds) *Proceedings of RSPSoc 2003: Scales and Dynamics in Observing the Environment, Nottingham, 10-12 September 2003*. Nottingham: The Remote Sensing and Photogrammetry Society.

Challis, K. (2006). Airborne laser altimetry in alluviated landscapes. *Archaeological Prospection.* Vo 13.

Challis, K. 2005a. *Predictive Modelling of Multi-Period Geoarchaeological Resources at a River Confluence Airborne Remote Sensing. Analysis of the Effectiveness of Aerial Photography, Lidar and IFSAR.* English Heritage PNUM3357.

Challis, K. 2005b. Airborne Lidar: A Tool for Geoarchaeological Prospection in Riverine Landscapes. in Stoepker, H. (ed) *Archaeological Heritage Management in Riverine Landscapes.* Rapporten Archeologische Monumentenzorg, 126: 11-24

Devereux, B.J. Amable, G.S. Crow, P. and Cliff, A.D. (2005) The potential of airborne lidar for detection of archaeological features under woodland canopies. *Antiquity*, Volume: 79 Number: 305: 648–660

Garton, D. & Malone, S. (1998). Geomorphology from aerial photographs in the Trent Valley. In Challis, K. (ed) Fieldwork by Trent & Peak Archaeological Trust in

Nottinghamshire, 1996-7. *Transactions of the Thoroton Society of Nottinghamshire* 102: 139-141.

Kenward, H.K. and Large, F. 1998. Recording the preservation condition of archaeological insect fossils. *Environmental Archaeology* 2, 49-60.

Lambrick, G., 1992. Alluvial archaeology of the Holocene in the Upper Thames basin 1971-1991: a review, in Needham, S., and Macklin, M.G., eds., *Alluvial Archaeology in Britain*: London, The Society of Antiquaries of London, 209-225

Murphy, P.L. and Wiltshire, P.E.J. 1994. A proposed scheme for evaluating plant macrofossil preservation in some archaeological deposits. *Circaea* 11 (1), 1-7.

Riley, D.N. (1980). *Early Landscape from the Air. Studies of cropmark sites in South Yorkshire and North Nottinghamshire.* Sheffield: Department of Archaeology and Prehistory, University of Sheffield.

Robinson, M., and Lambrick, G., 1984, Holocene alluviation and hydrology in the Upper Thames basin: *Nature* (London), v. 308, 809-814.

Wehr, A. and Lohr, U. (1999). Airborne laser scanning – an introduction and overview. *ISPRS Journal of Photogrammetry & Remote Sensing* 54: 68-82.


birmingham
archaeology